Charles University in Prague
Faculty of Mathematics and Physics

DOCTORAL THESIS

Adam Kosík

Fluid-structure interaction

Department of Numerical Mathematics

Supervisor: Prof. RNDr. Miloslav Feistauer, DrSc., Dr.h.c.
Study programme: Mathematics
Study branch: Scientific and Technical Calculations

Prague 2016

I would like to express my gratitude to Prof. RNDr. Miloslav Feistauer, DrSc., Dr.h.c., for his patient guidance throughout my studies. He was always well-minded and open for discussion and his support during the time was exceptional. I am very grateful to Ing. Jaromír Horáček, DrSc., for the opportunity to be a member of his working group and for providing information and practical advices touching the problem of fluid-structure interaction in human vocal tract. I am also obliged to Martin Hadrava for a great cooperation in our working group. He was significantly concerned in the implementation of the proposed methods. Many thanks to all my colleagues and co-workers, namely Prof. RNDr. Vít Dolejší, Ph.D., DSc., Monika Balázsová, Jaroslava Hasnedlová, Petr Sváček and Petr Šimánek. I would also like to thank Prof. Dr. Dmitri Kuzmin who invited me to join his research group in Germany and Univ.-Prof. Dr. Olaf Steinbach for his support during my stay in Austria. Finally, the greatest appreciation goes to my family, my friends and my girlfriend for their support during the last few years.

My thanks also go to institutions that provided financial support for my research work. Through my doctoral study, my work was partially supported by the grants GAChU 549912, SVV-2011-263316, SVV-2012-267316, SVV-2013-265316, and SVV-2014-260106 of the Charles University in Prague and by the projects 13-00522S and P101/11/0207 of the Czech Science Foundation.

I declare that I carried out this doctoral thesis independently, and only with the cited sources, literature and other professional sources.

I understand that my work relates to the rights and obligations under the Act No. 121/2000 Sb., the Copyright Act, as amended, in particular the fact that the Charles University in Prague has the right to conclude a license agreement on the use of this work as a school work pursuant to Section 60 paragraph 1 of the Copyright Act.

In Prague on May 5, 2016 signature of the author

Název práce: Interakce proudící tekutiny a elastického tělesa
Autor: Adam Kosík
Katedra: Katedra numerické matematiky
Vedoucí disertační práce: Prof. RNDr. Miloslav Feistauer, DrSc., Dr.h.c.

Abstrakt: V této práci se zabýváme numerickou simulací interakce proudící stlačitelné vazké tekutiny a elastického tělesa ve 2D. Deformace obtékaného elastického tělesa jsou popsány pomocí 2D lineárního modelu pružnosti a nelineárního St. Venantova-Kirchhoffova a neo-Hookeova modelu pružnosti. Proudění tekutiny je popsáno stlačitelnými Navierovými-Stokesovými rovnicemi, které jsou formulovány v ALE (arbitrary Lagrangian-Eulerian) tvaru. Pomocí ALE metody bereme v potaz časovou závislost oblasti vyplněné tekutinou. Diskretizace problému proudění i problému pružnosti je provedena pomocí nespojité Galerkinovy metody konečných prvků (DGM). Svoji pozornost věnujeme testování DGM aplikované na řešení problémů proudění tekutiny a pružnosti. Dále popisujeme algoritmus interakce a způsobu, jak vyřešit problém deformace oblasti vyplněné proudící tekutinou. Motivací naší práce jsou aplikace v biomedicíně. Numerické experimenty zahrnují numerickou simulaci kmitání lidských hlasivek vyvolané působením stlačitelného vazkého proudění.

Klíčová slova: interakce proudící tekutiny a elastického tělesa, nespojitá Galerkinova metoda, lineární a nelineární pružnost, stlačitelné Navierovy-Stokesovy rovnice, ALE metoda

Title: Fluid-structure interaction
Author: Adam Kosík
Department: Department of Numerical Mathematics
Supervisor: Prof. RNDr. Miloslav Feistauer, DrSc., Dr.h.c.

Abstract: In this thesis we are concerned with the numerical simulation of the interaction of compressible viscous flow and an elastic structure in 2D. For the elastic deformation we use a 2D linear model and nonlinear St. Venant-Kirchhoff and neo-Hookean models. The flow is described by the compressible Navier-Stokes equations written in the arbitrary Lagrangian-Eulerian (ALE) form in order to take into account the time-dependence of the flow domain. The discretization of both the flow problem and the elasticity problem is realized by the discontinuous Galerkin finite element method (DGM). We focus on testing the DGM applied to the solution of the flow and elasticity problems. Furthermore, we discuss the coupling algorithm and the technique, how to deal with the deformation of the computational domain for the fluid flow problem. Our work is motivated by the biomedical applications. Numerical experiments include numerical simulation of vibrations of human vocal folds induced by the compressible viscous flow.

Keywords: fluid-structure interaction, discontinuous Galerkin method, linear and nonlinear elasticity, compressible Navier-Stokes equations, ALE method

Contents

Introduction

Fluid-structure interaction (FSI) problems are solved in various aerospace, civil and mechanical engineering applications for many years, see e.g. the monographs [23] and [54] and the proceedings [7] and [8], where various aspects of FSI modeling and simulation are treated. To the best of our knowledge, mostly the model of incompressible fluid is used and the numerical techniques for the FSI simulation are based on the application of the finite volume method or conforming finite elements. Recently the methods for solution of such problems have also been quickly developed in the field of biomechanics. We are particularly interested in biomechanics of voice, see the model of the voice production in Figure 1, where the methods of numerical simulation of human vocal folds self-oscillation are currently in an intensive development. These self-oscillations, which originate in the interaction of airflow coming from the human lungs with the compliant biological tissue of the vocal folds, produce primary sound enabling voicing (phonation, speech, singing), see e.g. [51]. One of the latest papers published by Tian et al. [63] considers an interaction of incompressible viscous airflow described by the Navier-Stokes equations with nonlinear elastic structure of the human vocal folds. For large vibration amplitudes the authors are solving the problem by using the so-called immersed boundary method for flow and finite element method for the viscoelastic tissue with large shape changes of the biological structure modeling the vocal folds. For further models and aspects of the numerical simulation of vocal folds vibrations we refer to the works [1, 32, 41, 55, 56, 67, 68].

A nonlinear benchmark problem on FSI was proposed in [64], where a beam vibrating in incompressible laminar flow is modeled as a linear elastic structure with the geometrical nonlinearity. However, until now not many papers on FSI deal with dynamics of a nonlinear continuum. Even very few static problems using the model of nonlinear continuum are analyzed, see e.g. [6]. Especially, models of biological viscoelastic tissues subjected to large deformations are still unresolved.

In this thesis we are concerned with the numerical simulation of the interaction of compressible flow and a nonlinear elastic structure in 2D using the discontinuous Galerkin method (DGM). The DGM was originally introduced in [57] and first analysed in [50] and improved in [45]. The particular issue of nonlinear elasticity, compressible flow and the use of the DGM is the last result of our employment in FSI problems in recent years. In [48] the problem of the linear elastic structure and viscous incompressible flow was numerically solved by the conforming finite element methods. This is followed by the work [40], which is concerned with FSI problem of compressible flow and linear elastic structure, where the elasticity problem was solved by conforming finite element method in space and by the Newmark method in time and the flow problem was solved by the DGM in space and finite difference method of second order in time. We continue in this work on the numerical solutions of FSI problems. Mainly, this work closely relates to [12] using the implementation of the viscous compressible fluid flow in time-dependent domains. However, unlike the approach in [48] and [40], both the structure and fluid flow problem are discretized by the DGM and the nonlinear elasticity problem is included. Furthermore, we discuss the cou-

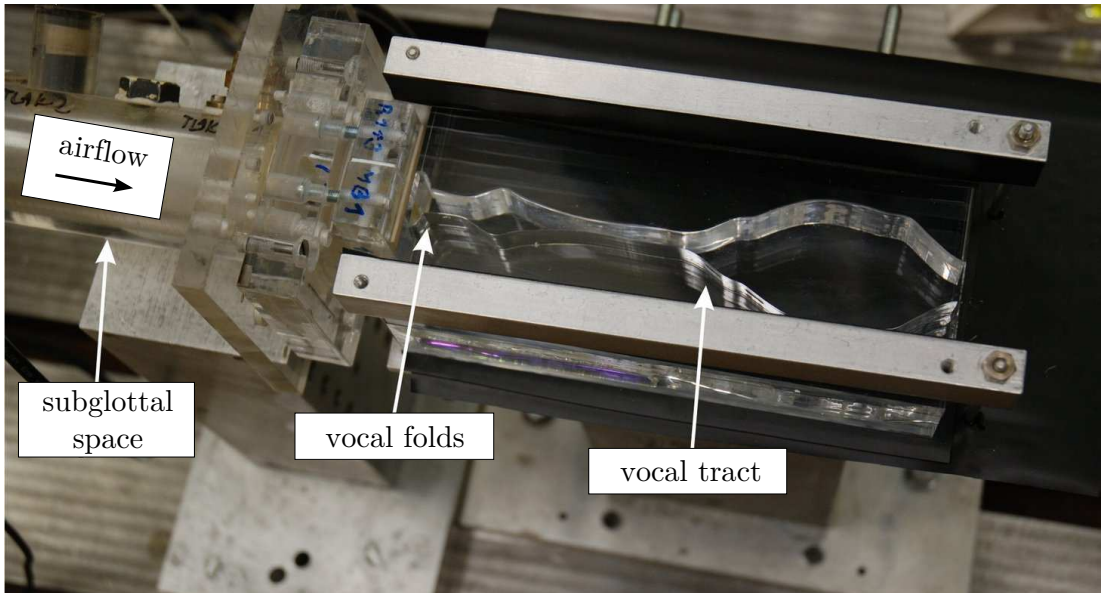

Figure 1: Model of the voice production in humans, measurement set-up, see [42].

pling algorithm and the technique how to deal with the large deformation of the computational domain of the fluid flow problem.

As already mentioned, the problem is formulated in 2D. By the assumption that the field variable is independent of the third dimension we reduce the complexity of the problem. It makes the implementation simpler and even the cases with more complicated geometries and finer mesh are computable in the conditions of our research. However we keep the principle of the problem and it should be possible to extend it in 3D. Especially nowadays by the large offer of open-source tools for numerical simulation the development of the 3D implementation of the problem should not be so hard challenge. Except of the technical difficulties our description of the discretization could be followed for the 3D case as well.

Since the main interest of the thesis, the FSI problem in 2D, contains many particular problems, we attend to them successively. We can split them in two groups. Chapters 1–3 are devoted to the numerical simulation of the elastic structure with deformations induced by the acting force by the DGM. Both the linear and nonlinear problems are included. In Chapter 1 we provide an introduction to the mathematical theory of nonlinear elasticity and formulate the respective elasticity equations. The final result is the formulation of the dynamic nonlinear elasticity problem, even though we describe also the static case and the linear elasticity problem. For all of them we present the use of the DGM for the discretization in space and the use of finite difference schemes for the discretization in time. For the description of the deformation of the elastic structure the nonlinear St. Venant-Kirchhoff and neo-Hookean model is used, see e.g. [10].

In Chapter 2 we introduce the numerical method for the simulation of stationary and nonstationary elasticity problem considering both linear and nonlinear material characteristics. We employ the discontinuous Galerkin method (DGM) as high-order piecewise polynomial discontinuous approximation on arbitrary meshes in space. For the time discretization we apply the backward

difference formula (BDF) method based on finite-difference approximations in time. We describe the discretization in detail according to its implementation. Since, we developed the .NET library written in C# for the numerical solution of the 2D dynamic linear and nonlinear elasticity problem with mixed boundary conditions.

Chapter 3 is concluding the part of the thesis, which is devoted just to the elasticity problem. In this chapter we present several numerical experiments in order to demonstrate the applicability of the developed method. Particularly, these are numerical experiments for the simulation of the deformation of an elastic beam, which is inspired by the benchmark described by Turek and Hron, see [64]. First, we are concerned with the numerical solution of the particular elasticity problems. Further we focus on the choice of the optional penalty coefficient and the comparison with the standard conform finite element method. Finally, we present the numerical experiments for the solution of the elasticity problem with the nonhomogeneous material characteristics.

The other part of the thesis is devoted to the numerical solution of the interaction of the compressible viscous flow and the dynamic elasticity problem. In Chapter 4 we deal with the viscous compressible fluid flow problem in a time-dependent domain. We introduce the compressible Navier-Stokes equations with appropriate initial and boundary equations. The compressible Navier-Stokes equations are formulated in the arbitrary Lagrangian-Eulerian (ALE) form in order to take the time-dependence of the flow domain into account. The problem is solved by the DGM using piecewise polynomial approximations of the exact solution on a finite element mesh without the requirement of the continuity on interfaces between neighboring elements. Several works (e.g. [3, 22, 29]) prove that this method is suitable for numerical approximations of nonlinear convection-diffusion problems and compressible flow, when the solutions contain discontinuities and/or internal and boundary layers. DGM was employed in many papers for the discretization of compressible fluid flow problems, see, e.g., [3, 4, 5, 16, 19, 20, 22, 24, 25, 29, 37, 38, 39, 46, 47]. For the time discretization we employ the backward difference formula (BDF) method or the full space-time discontinuos Galerkin method (STDGM). The BDF method is a suitable high order time discretization method, which is unconditionally stable. In the later approach the DGM is employed for the discretization in space and also in time. Using this numerical scheme we obtain high order results both in space and in time. The algorithmization of the problem is briefly described in the end of this chapter. It is corresponding to the C library developed by Česenek, see [11], which was embedded in the .NET library for the numerical solution of the elasticity problem and used for the numerical solution of the fluid-structure interaction (FSI) problem.

Chapter 5 is devoted to the numerical solution of the FSI problem, which is the main result of the thesis. At first we define the coupled problem of the compressible viscous flow and the linear or nonlinear elasticity problem. The coupling is realized via transmission conditions, which are implemented in the numerical process with the aid of a strong coupling algorithm. The coupling algorithm is described in detail and in particular we explain, how are the transmission conditions fulfilled and how is derived the ALE mapping. According to the proposed algorithmization the described method was implemented. We modified the C li-

brary for the numerical solution of the fluid flow problem and it was coupled with the numerical solution of the elasticity problem. The developed method can be applied to problems of biomechanics, aerodynamics and aerospace engineering. As already mentioned our work is particularly motivated by the simulation of airflow in a simplified model of human airways created by the trachea, a glottal region with vibrating vocal folds and the vocal tract channel. The applicability and robustness with respect to low Mach number flows and a suitable nonlinear elastic structure of the developed method are shown on the example representing approximate human vocal folds region with a realistic model of an elastic part. Except of the numerical simulation of vocal folds in more complicated domain, we also present the results obtained in a simplified computational domain.

Chapter 6 is the last chapter of the thesis. It contains some technical details of the implementation and few remaining numerical topics as mesh generation and numerical integration.

1. Nonlinear elasticity problem

In this chapter we provide an introduction to the mathematical theory of nonlinear elasticity and formulate the respective elasticity equations. The general problem in nonlinear elasticity is to find the equilibrium of an elastic body subjected to applied forces. The equations of nonlinear elasticity are based on the relationship between stress and strain. Therefore first we introduce the basic concepts of stress and strain and other basic quantities in the elasticity theory. Stress is defined as the force applied to a unit area of a deformable body, while strain is the dimensionless measure of the deformation the body has undergone. Stress and strain are second order tensor functions of space and the constitutive law for materials describes the complex relationship between them. Our goal is to assign the dynamic elasticity problem and also the equations of static equilibrium of an elastic body. The elasticity theory contains the nonlinear model of elasticity and the classical linear model of elasticity. We attend to both of them, but partly in different sections.

Section 1.2 is devoted to the definition, characteristics and measures of a mapping describing the deformation of an elastic body. Accordingly the definition of strain tensor is included. Further we continue in the Section 1.3 with the formulation of the quantities used in dynamic elasticity and finally with the formulation of the nonlinear elastic problem. We obtain the definition of the governing elasticity equations including the initial and boundary conditions. In order to solve the nonlinear elasticity problem, we need to add in Section 1.4 the relationship between stress and strain. One of our modelling assumptions is the hyperelasticity. We define the strain-energy function, which is a function of strain only, and from which stress is computed. Tissues for which a strain-energy function exists are known as hyperelastic. The last Section 1.5 of this chapter is concerned with the linear elasticity. The linear and nonlinear problem described in this chapter needs to be solved by suitable numerical technique. In Chapter 2 we discuss the numerical solution of the elasticity problem by the discontinuous Galerkin finite element method (DGM).

We formulate the problem in 2D. It can be extended to the 3D theory of elasticity following [10, 53]. By the assumption that the field variable is independent of the third dimension, we reduce the complexity of the problem. However we keep the principle of the problem. The basic concept of nonlinear elasticity is mainly taken from the already mentioned books [10, 53]. Nevertheless just the parts needed for the formulation of the initial-boundary-value problem have been described. Finally let us note that we distinguish the notation used for elasticity problems by upper index b (body).

1.1 Preliminaries

The space of real n-vectors is denoted by $\mathbb{R}^n$, with canonical basis $e_1, \ldots, e_n$. The vector product of two vectors $\boldsymbol{x}$ and $\boldsymbol{y}$ is defined by the formula

$$\boldsymbol{x} \times \boldsymbol{y} = \|\boldsymbol{x}\| \, \|\boldsymbol{y}\| \sin\theta \boldsymbol{n}, \tag{1.1}$$

where θ is the angle between $\boldsymbol{x}$ and $\boldsymbol{y}$ in the plane containing them, $\|.\|$ denotes the magnitude of a vector, and $\boldsymbol{n}$ is the unit vector perpendicular to the plane containing $\boldsymbol{x}$ and $\boldsymbol{y}$ in the direction given by the right-hand rule.

The space of real $m \times n$-matrices is denoted by $\mathbb{M}^{m\times n}$ and $\mathbb{M}^n := \mathbb{M}^{n\times n}$. The identity matrix of order n is denoted by $\boldsymbol{I}$. Further let us define the set of all real square matrices of order n whose determinant is positive

$$\mathbb{M}^n_+ := \{\boldsymbol{F} \in \mathbb{M}^n; \det \boldsymbol{F} > 0\}, \tag{1.2}$$

the set of all orthogonal matrices of order n

$$\mathbb{O}^n := \left\{\boldsymbol{P} \in \mathbb{M}^n; \boldsymbol{P}\boldsymbol{P}^T = \boldsymbol{P}^T\boldsymbol{P} = \boldsymbol{I}\right\}, \tag{1.3}$$

and the set of all rotations in $\mathbb{R}^n$

$$\mathbb{O}^n_+ := \{\boldsymbol{P} \in \mathbb{O}^n; \det \boldsymbol{F} > 0\} = \{\boldsymbol{P} \in \mathbb{O}^n; \det \boldsymbol{F} = 1\}. \tag{1.4}$$

For $\boldsymbol{A} \in \mathbb{M}^n$ and $\boldsymbol{B} \in \mathbb{M}^n$ we set $\boldsymbol{A} : \boldsymbol{B} = \sum_{i,j=1}^n A_{ij}B_{ij} = \mathrm{tr}\boldsymbol{A}^T\boldsymbol{B}$, which denotes the *matrix inner product* in $\mathbb{M}^n$.

Let us consider the space $\mathbb{M}^n$ equipped with the matrix inner product $\boldsymbol{A} : \boldsymbol{B}$. If a function $f : \Omega \subset \mathbb{M}^n \to \mathbb{R}$ is differentiable at $\boldsymbol{A} \in \Omega$, we call its gradient the matrix

$$\frac{\partial f}{\partial \boldsymbol{A}}(\boldsymbol{A}) := \begin{pmatrix} \frac{\partial f}{\partial A_{11}}(\boldsymbol{A}) & \ldots & \frac{\partial f}{\partial A_{1n}}(\boldsymbol{A}) \\ \vdots & \ddots & \vdots \\ \frac{\partial f}{\partial A_{n1}}(\boldsymbol{A}) & \ldots & \frac{\partial f}{\partial A_{nn}}(\boldsymbol{A}) \end{pmatrix} \in \mathbb{M}^n, \tag{1.5}$$

whose elements are the partial derivatives of the mapping f.

Let $\boldsymbol{A} = (A_{ij})_{i,j=1}^n$ be a square matrix of order n. For each pair (i, j) of indices, let $\boldsymbol{A}'_{ij}$ be the matrix of order $(n-1)$ obtained by deleting the i-th row and the j-th column in the matrix $\boldsymbol{A}$. The scalar

$$d_{ij} := (-1)^{i+j} \det \boldsymbol{A}'_{ij} \tag{1.6}$$

is called the (i, j) *cofactor* of the matrix $\boldsymbol{A}$, and the matrix

$$\mathrm{Cof}\boldsymbol{A} := (d_{ij})_{i,j=1}^n \tag{1.7}$$

is called the *cofactor matrix* of the matrix $\boldsymbol{A}$. It holds that $\boldsymbol{I} \det \boldsymbol{A} = \boldsymbol{A}(\mathrm{Cof}\boldsymbol{A})^T$. Hence, if $\boldsymbol{A}$ is invertible, then

$$\mathrm{Cof}\boldsymbol{A} = (\det \boldsymbol{A})\boldsymbol{A}^{-T}. \tag{1.8}$$

In the case $n = 2$ one has

$$\mathrm{Cof}\boldsymbol{A} = \begin{pmatrix} a_{22} & -a_{21} \\ -a_{12} & a_{11} \end{pmatrix}. \tag{1.9}$$

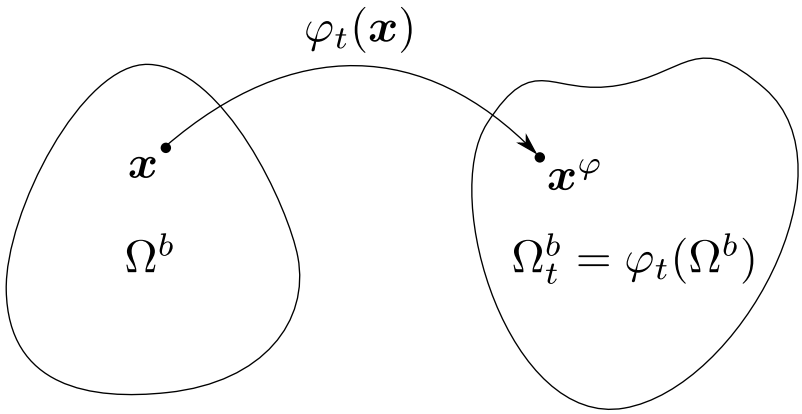

Figure 1.1: Deformation of the body represented by the closure of a domain Ω^b at time t.

1.2 Deformation of an elastic body

Generally a body $B \subset \mathcal{E}$ is a set of points, which are called *material points* or *particles*, occupying a region in some Euclidean space $\mathcal{E}$. A *configuration* of B is a C^2-diffeomorphism $\boldsymbol{\varphi} : B \to \mathcal{E}$ which takes particles of B to the places they occupy in $\mathcal{E}$. We write $\boldsymbol{\varphi}(B) = \{\boldsymbol{\varphi}(x), x \in B\}$ for the set of places occupied by the particles of B. A *motion* of B is a one-parameter family of configurations $\boldsymbol{\varphi}_t : B \to \mathcal{E}$, where the subscript identifies the time t as parameter. In this work let be $\mathcal{E} = \mathbb{R}^2$.

Let us consider a body represented by the closure of a domain $\Omega^b \subset \mathbb{R}^2$ and a time interval $[0, T]$, where $T > 0$. We identify a fixed configuration $\boldsymbol{\varphi}_0$, that the body occupies at time $t = 0$. Configuration $\boldsymbol{\varphi}_0$ is called *reference configuration* and we denote $\Omega_0^b = \boldsymbol{\varphi}_0(\Omega^b)$, which is the region of $\mathbb{R}^2$ occupied by Ω^b in this configuration. We can write

$$\boldsymbol{x} = \boldsymbol{\varphi}_0(x), \quad x = \boldsymbol{\varphi}_0^{-1}(\boldsymbol{x}), \tag{1.10}$$

where $\boldsymbol{x}$ is the place of the particle x in configuration $\boldsymbol{\varphi}_0$. We have identified through (1.10) particle x with its place $\boldsymbol{x}$ in the configuration $\boldsymbol{\varphi}_0$ and therefore we can make no distinction between x and $\boldsymbol{x}$. The coordinates x_1, x_2 of every point $\boldsymbol{x} \in \Omega_0^b$ are known as *Lagrangian coordinates.*

The body is deformed via mapping

$$\boldsymbol{\varphi} : \overline{\Omega}^b \times [0, T] \to \mathbb{R}^2, \tag{1.11}$$

which is smooth enough and injective except possibly on the boundary of the domain Ω^b. It is a mapping from Ω_0^b to the region $\Omega_t^b = \boldsymbol{\varphi}_t(\Omega^b)$ of $\mathbb{R}^2$ occupied by Ω^b in the *actual configuration.* For any fixed t this mapping is called a *deformation* of the reference configuration taking a material point $\boldsymbol{x}$ to a point $\boldsymbol{\varphi}(\boldsymbol{x}, t)$ in space. We write

$$\boldsymbol{x}^{\varphi} = \boldsymbol{\varphi}_t(\boldsymbol{x}) = \boldsymbol{\varphi}(\boldsymbol{x}, t) \tag{1.12}$$

for the place of the particle x at time t. Let us denote the coordinates of the mapped position $\boldsymbol{x}^{\varphi}$ as $(x_1^{\varphi}, x_2^{\varphi})$. They are known as *Eulerian coordinates.* It

is important to distinguish between the Lagrangian coordinate system and the Eulerian coordinate system. Because of the assumption that the reference configuration is known and the deformed configuration needs to be determined, we want to formulate the elasticity problem in Lagrangian coordinates. (The Eulerian approach is usually preferred in fluid dynamics.)

The deformation mapping can be expressed by the use of a displacement function $\boldsymbol{u} : \overline{\Omega}_0^b \times [0,T] \to \mathbb{R}^2$ as

$$\boldsymbol{\varphi}(\boldsymbol{x},t) = \boldsymbol{x} + \boldsymbol{u}(\boldsymbol{x},t). \tag{1.13}$$

For the analysis of the deformation from reference configuration Ω_0^b to actual configuration Ω_t^b we do not require knowledge of the motion so that the time dependence in (1.12) is not needed. We do not consider the dependence on t and replace (1.12) by

$$\boldsymbol{x}^{\boldsymbol{\varphi}} = \boldsymbol{\varphi}(\boldsymbol{x}). \tag{1.14}$$

By $\boldsymbol{F} : \Omega^b \to \mathbb{M}^2_+$,

$$\boldsymbol{F} = \nabla\boldsymbol{\varphi}(\boldsymbol{x}), \tag{1.15}$$

we denote the *deformation gradient*, i.e. $\boldsymbol{F}$ is the Jacobian matrix of the deformation mapping $\boldsymbol{\varphi}$. Further,

$$J = \det \boldsymbol{F} > 0 \tag{1.16}$$

denotes the Jacobian of the deformation. It should be positive, because the orientation of line elements should not change during deformation. We say that the deformation is *orientation preserving*. By δ_{ij} we denote the Kronecker symbol and set $\boldsymbol{I} = (\delta_{ij})_{i,j=1}^2$. If we write $\boldsymbol{x} = (x_1, x_2)^T$ and $\boldsymbol{u}(\boldsymbol{x}) = (u_1(\boldsymbol{x}), u_2(\boldsymbol{x}))^T$, then the deformation gradient can be expressed as

$$\boldsymbol{F} = (F_{ij})_{i,j=1}^2, \quad F_{ij} = \delta_{ij} + \frac{\partial u_i}{\partial x_j}, \quad i,j = 1,2. \tag{1.17}$$

The deformation gradient $\boldsymbol{F}$ can be factorised as $\boldsymbol{F} = \boldsymbol{R}\boldsymbol{U}$, where $\boldsymbol{R} \in \mathbb{O}^2_+$ representing the rotation, and $\boldsymbol{U} \in \mathbb{M}^2_+$ is a tensor representing stretching. $\boldsymbol{R}$ is an orthogonal tensor and $\boldsymbol{U}$ is a symmetric positive-definite tensor. Later we shall introduce different elastic materials and this is usually done by the use of the eigenvalues of $\boldsymbol{U}$, which are strictly positive.

We say the deformation is *homogeneous*, if $\boldsymbol{F}$ does not depend on $\boldsymbol{x}$. It can be described by the affine transformation

$$\boldsymbol{x}^{\boldsymbol{\varphi}} = \boldsymbol{F}\boldsymbol{x} + \boldsymbol{c}, \tag{1.18}$$

where $\boldsymbol{c}$ is the translation. If, on the other hand, $\boldsymbol{F}$ depends on $\boldsymbol{x}$, then the deformation is called *nonhomogeneous*.

1.2.1 Strain tensor

Further we shall define the elasticity strain tensor. The motivation for the definition of the strain is that we want to ignore the rotational part of the deformation. First let us introduce the *right Cauchy-Green tensor*

$$\boldsymbol{C} = \boldsymbol{F}^T \boldsymbol{F}. \tag{1.19}$$

Seeing that $\boldsymbol{C} = \boldsymbol{U}^T \boldsymbol{R}^T \boldsymbol{R} \boldsymbol{U} = \boldsymbol{U}^T \boldsymbol{U}$, $\boldsymbol{C}$ is apparently independent of rotation. If we consider rigid deformation only, $\boldsymbol{C}$ is equal to $\boldsymbol{I}$. This leads us to the definition of the following measure of strain, which vanishes when the material is unstrained. We define the *Green strain tensor* (or also just strain tensor) $\boldsymbol{E} \in \mathbb{R}^{2\times 2}$ by

$$\boldsymbol{E} = \frac{1}{2}\left(\boldsymbol{F}^T \boldsymbol{F} - \boldsymbol{I}\right) = \frac{1}{2}\left(\boldsymbol{C} - \boldsymbol{I}\right), \quad \boldsymbol{E} = (E_{ij})_{i,j=1}^2. \tag{1.20}$$

The strain tensor $\boldsymbol{E} = \boldsymbol{E}(\boldsymbol{u})$ can be written in terms of the displacement function $\boldsymbol{u}$ with the aid of (1.17). We have

$$\begin{aligned}
\left(\boldsymbol{F}^T \boldsymbol{F}\right)_{ij} &= \sum_{k=1}^{2} F_{ik}^T F_{kj} = \sum_{k=1}^{2} F_{ki} F_{kj} = \sum_{k=1}^{2} \left(\delta_{ki} + \frac{\partial u_k}{\partial x_i}\right)\left(\delta_{kj} + \frac{\partial u_k}{\partial x_j}\right) \\
&= \sum_{k=1}^{2} \left(\delta_{ki}\delta_{kj} + \delta_{ki}\frac{\partial u_k}{\partial x_j} + \delta_{kj}\frac{\partial u_k}{\partial x_i} + \frac{\partial u_k}{\partial x_i}\frac{\partial u_k}{\partial x_j}\right) \\
&= \delta_{ij} + \frac{\partial u_i}{\partial x_j} + \frac{\partial u_j}{\partial x_i} + \sum_{k=1}^{2} \frac{\partial u_k}{\partial x_i}\frac{\partial u_k}{\partial x_j},
\end{aligned}$$

and hence

$$E_{ij} = \frac{1}{2}\left(\frac{\partial u_i}{\partial x_j} + \frac{\partial u_j}{\partial x_i}\right) + \frac{1}{2}\sum_{k=1}^{2} \frac{\partial u_k}{\partial x_i}\frac{\partial u_k}{\partial x_j}. \tag{1.21}$$

The trace of the strain tensor $\boldsymbol{E}(\boldsymbol{u})$ can be expressed in the form

$$\mathrm{tr}\boldsymbol{E}(\boldsymbol{u}) = \sum_{l=1}^{2} E_{ll} = \sum_{l=1}^{2} \frac{\partial u_l}{\partial x_l} + \frac{1}{2}\sum_{l=1}^{2}\sum_{k=1}^{2}\left(\frac{\partial u_k}{\partial x_l}\right)^2.$$

1.2.2 Motion and velocity

Let us include again the time dependence of the deformation as expressed in (1.12), i.e.

$$\boldsymbol{x}^{\boldsymbol{\varphi}} = \boldsymbol{\varphi}(\boldsymbol{x}, t). \tag{1.22}$$

The velocity of the material particle $\boldsymbol{v}^b(\boldsymbol{x}, t)$ is defined by

$$\boldsymbol{v}^b(\boldsymbol{x}, t) = \frac{\partial \boldsymbol{\varphi}}{\partial t}(\boldsymbol{x}, t) = \frac{\partial \boldsymbol{u}}{\partial t}(\boldsymbol{x}, t), \tag{1.23}$$

and the acceleration $\boldsymbol{a}^b(\boldsymbol{x}, t)$ by

$$\boldsymbol{a}^b(\boldsymbol{x}, t) = \frac{\partial^2 \boldsymbol{\varphi}}{\partial t^2}(\boldsymbol{x}, t) = \frac{\partial^2 \boldsymbol{u}}{\partial t^2}(\boldsymbol{x}, t). \tag{1.24}$$

1.3 Formulation of the nonlinear elasticity problem

In Section 1.2 we obtained the definition of the deformation of an elastic body and its measure of strain. We can now derive the equation of motion for dynamic problems and equation of equilibrium in static problems using nonlinear elasticity. First we introduce the mass density and applied forces in order to formulate the equilibrium equations over the deformed body. We define the stress tensor and formulate the Cauchy theorem. From the principle of conservation of momentum we can derive the governing equations of nonlinear elasticity. Finally we shall specify the initial and boundary conditions to obtain the complete problem.

1.3.1 Mass density

For any arbitrary body Ω^b by $m(\Omega^b) \geq 0$ we shall denote the *mass* of the body Ω^b. By the principle of *conservation of mass*

$$\frac{\mathrm{d}}{\mathrm{d}t} m(\Omega^b) = 0. \tag{1.25}$$

This means that $m(\Omega^b)$ is independent of the configuration Ω_t^b occupied by Ω^b at time t. We call ρ_t^b mass *density* of the material of the body Ω^b in the configuration Ω_t^b. It is a scalar field defined over Ω_t^b at time t such that

$$m(\Omega^b) = \int_{\Omega_t^b} \rho_t^b(\boldsymbol{x}^{\boldsymbol{\varphi}}, t)\, \mathrm{d}\boldsymbol{x}^{\boldsymbol{\varphi}}. \tag{1.26}$$

It is assumed that ρ_t^b is smooth and non-negative. Let us denote by ρ^b the mass density of Ω^b in the reference configuration Ω_0^b. It can be shown that the densities ρ^b and ρ_t^b are related by the local form of the principle of the conservation of mass

$$\rho_t^b = J^{-1} \rho^b \tag{1.27}$$

and hence

$$\det \boldsymbol{F} = J = \rho^b / \rho_t^b. \tag{1.28}$$

1.3.2 Applied forces

We are concerned with the motion of deforming bodies and we regard to external forces on a given body. We refer to such forces as *applied forces*.

We consider two types of applied forces. The *applied body (volume) forces*

$$\int_{\Omega_t^b} \rho_t^b(\boldsymbol{x}^{\boldsymbol{\varphi}}) \boldsymbol{b}^{\boldsymbol{\varphi}}(\boldsymbol{x}^{\boldsymbol{\varphi}})\, \mathrm{d}\boldsymbol{x}^{\boldsymbol{\varphi}} \tag{1.29}$$

are defined through the density $\boldsymbol{b}^{\boldsymbol{\varphi}} : \Omega_t^b \to \mathbb{R}^2$ per unit of mass in the actual configuration. Example of a body force is gravity, in which $\boldsymbol{b}^{\boldsymbol{\varphi}}$ is acceleration due to gravity. We define also $\boldsymbol{f}^{\boldsymbol{\varphi}} : \Omega_t^b \to \mathbb{R}^2$ by the relation

$$\boldsymbol{f}^{\boldsymbol{\varphi}} = \rho_t^b \boldsymbol{b}^{\boldsymbol{\varphi}}. \tag{1.30}$$

The *applied surface forces*

$$\int_{\Gamma^b_{Nt}} \boldsymbol{g}^{\varphi}(\boldsymbol{x}^{\varphi})\,\mathrm{d}S^{\varphi} \tag{1.31}$$

are defined by the surface traction $\boldsymbol{g}^{\varphi} : \Gamma^b_{Nt} \to \mathbb{R}^2$ on an element $\mathrm{d}S^{\varphi}$ of a subset $\Gamma^b_{Nt} \subset \partial\Omega^b_t$. Then $\boldsymbol{g}^{\varphi}$ is the density per unit length in the actual configuration. Surface traction can be split into a normal and tangential component respectively, acting like a pressure force and friction respectively.

1.3.3 Stress tensor, Cauchy theorem

Stress vector $\boldsymbol{t}^{\varphi}$ is defined as the surface force per unit area on the vector area element.

By the fundamental principles of Euler and Cauchy it is assumed that the stress vector $\boldsymbol{t}^{\varphi}$ at a point $\boldsymbol{x}^{\varphi}$ depends on the surface only through the unit normal $\boldsymbol{n}^{\varphi}$ to the considered surface at $\boldsymbol{x}^{\varphi}$. Hence we can write $\boldsymbol{t}^{\varphi}$ as $\boldsymbol{t}^{\varphi}(\boldsymbol{x}^{\varphi}, \boldsymbol{n}^{\varphi})$. For any subdomain $\mathcal{B}^{\varphi} \subset \Omega^b_t$ the *balance of linear momentum* is written as

$$\int_{\mathcal{B}^{\varphi}} \rho^b_t(\boldsymbol{x}^{\varphi}, t)\boldsymbol{f}^{\varphi}(\boldsymbol{x}^{\varphi}, t)\,\mathrm{d}\boldsymbol{x}^{\varphi} + \int_{\partial\mathcal{B}^{\varphi}} \boldsymbol{t}^{\varphi}(\boldsymbol{x}^{\varphi}, \boldsymbol{n}^{\varphi})\,\mathrm{d}S^{\varphi} = \int_{\mathcal{B}^{\varphi}} \rho^b_t(\boldsymbol{x}^{\varphi}, t)\frac{\partial}{\partial t}\boldsymbol{v}^{\varphi}(\boldsymbol{x}^{\varphi}, t)\,\mathrm{d}\boldsymbol{x}^{\varphi} \tag{1.32}$$

and the *balance of rotational momentum*

$$\int_{\mathcal{B}^{\varphi}} \rho^b_t(\boldsymbol{x}^{\varphi}, t)\boldsymbol{x}^{\varphi} \times \boldsymbol{f}^{\varphi}(\boldsymbol{x}^{\varphi}, t)\,\mathrm{d}\boldsymbol{x}^{\varphi} + \int_{\partial\mathcal{B}^{\varphi}} \boldsymbol{x}^{\varphi} \times \boldsymbol{t}^{\varphi}(\boldsymbol{x}^{\varphi}, \boldsymbol{n}^{\varphi})\,\mathrm{d}S^{\varphi} \tag{1.33}$$

$$= \int_{\mathcal{B}^{\varphi}} \rho^b_t(\boldsymbol{x}^{\varphi}, t)\boldsymbol{x}^{\varphi} \times \frac{\partial}{\partial t}\boldsymbol{v}^{\varphi}(\boldsymbol{x}^{\varphi}, t)\,\mathrm{d}\boldsymbol{x}^{\varphi}, \tag{1.34}$$

where $\boldsymbol{v}^{\varphi}(\boldsymbol{x}^{\varphi}, t) = \boldsymbol{v}^b(\boldsymbol{x}, t)$ is the velocity of the particle which occupies the place $\boldsymbol{x}^{\varphi}$ at time t.

We now formulate the theorem about linear dependence of $\boldsymbol{t}^{\varphi}$ on the normal vector $\boldsymbol{n}^{\varphi}$.

Theorem 1. *(Cauchy Theorem)* Assume that the applied body force density $\boldsymbol{f}^{\varphi} : \overline{\Omega}^b_t \to \mathbb{R}^2$ is continuous, and that the Cauchy stress vector field

$$\boldsymbol{t}^{\varphi} : (\boldsymbol{x}^{\varphi}, \boldsymbol{n}) \in \overline{\Omega}^b_t \times S_1 \to \boldsymbol{t}^{\varphi}(\boldsymbol{x}^{\varphi}, \boldsymbol{n}) \in \mathbb{R}^2$$

is continuously differentiable with respect to the variable $\boldsymbol{x}^{\varphi} \in \overline{\Omega}^b_t$ for each $\boldsymbol{n} \in S_1$ and continuous with respect to the variable $\boldsymbol{n} \in S_1$ for each $\boldsymbol{x}^{\varphi} \in \overline{\Omega}^b_t$. Then the axioms of force and moment balance imply that there exists a continuously differentiable tensor field

$$\boldsymbol{\sigma}^b : \boldsymbol{x}^{\varphi} \in \overline{\Omega}^b_t \to \boldsymbol{\sigma}^b(\boldsymbol{x}^{\varphi}) \in \mathbb{M}^2,$$

such that the Cauchy stress vector satisfies the relation

$$\boldsymbol{t}^{\varphi}(\boldsymbol{x}^{\varphi}, \boldsymbol{n}) = \boldsymbol{\sigma}^b(\boldsymbol{x}^{\varphi})\boldsymbol{n} \quad \forall \boldsymbol{x}^{\varphi} \in \overline{\Omega}^b_t, \forall \boldsymbol{n} \in S_1, \tag{1.35}$$

where for $\boldsymbol{\sigma}^b$ we have

$$-\mathrm{div}^{\boldsymbol{\varphi}}\boldsymbol{\sigma}^b(\boldsymbol{x}^{\boldsymbol{\varphi}}) = \boldsymbol{f}^{\boldsymbol{\varphi}}(\boldsymbol{x}^{\boldsymbol{\varphi}}) \quad \forall \boldsymbol{x}^{\boldsymbol{\varphi}} \in \Omega_t^b, \tag{1.36}$$

$$\boldsymbol{\sigma}^b(\boldsymbol{x}^{\boldsymbol{\varphi}}) = \boldsymbol{\sigma}^b(\boldsymbol{x}^{\boldsymbol{\varphi}})^T \quad \forall \boldsymbol{x}^{\boldsymbol{\varphi}} \in \Omega_t^b, \tag{1.37}$$

$$\boldsymbol{\sigma}^b(\boldsymbol{x}^{\boldsymbol{\varphi}})\boldsymbol{n}^{\boldsymbol{\varphi}} = \boldsymbol{g}^{\boldsymbol{\varphi}}(\boldsymbol{x}^{\boldsymbol{\varphi}}) \quad \forall \boldsymbol{x}^{\boldsymbol{\varphi}} \in \Gamma_{Nt}^b. \tag{1.38}$$

Here $\boldsymbol{n}^{\boldsymbol{\varphi}}$ is the unit outer normal vector along Γ_{Nt}^b.

Proof. See [10]. □

Tensor $\boldsymbol{\sigma}^b$ is a second-order tensor independent of $\boldsymbol{n}$ called the *Cauchy stress tensor*. The equation (1.36) is the *equilibrium equation*.

Taking into account the time-dependence from the equation of linear momentum balance (1.32) using (1.35) and by the application of the divergence theorem to the surface integral we obtain

$$\int_{\mathcal{B}^{\boldsymbol{\varphi}}} \left(\rho_t^b(\boldsymbol{x}^{\boldsymbol{\varphi}}, t)\boldsymbol{f}^{\boldsymbol{\varphi}}(\boldsymbol{x}^{\boldsymbol{\varphi}}, t) + \mathrm{div}^{\boldsymbol{\varphi}}\boldsymbol{\sigma}^{\boldsymbol{\varphi}}(\boldsymbol{x}^{\boldsymbol{\varphi}}, t) - \rho_t^b(\boldsymbol{x}^{\boldsymbol{\varphi}}, t)\frac{\partial}{\partial t}\boldsymbol{v}^{\boldsymbol{\varphi}}(\boldsymbol{x}^{\boldsymbol{\varphi}}, t) \right) \mathrm{d}\boldsymbol{x}^{\boldsymbol{\varphi}} = \boldsymbol{0}. \tag{1.39}$$

This holds for arbitrary body $\mathcal{B}^{\boldsymbol{\varphi}}$. We assume ρ_t^b, $\boldsymbol{f}^{\boldsymbol{\varphi}}$ and $\frac{\partial}{\partial t}\boldsymbol{v}^{\boldsymbol{\varphi}}$ are continuous and $\boldsymbol{\sigma}^{\boldsymbol{\varphi}}$ is once continuously differentiable. Hence, it follows that

$$\rho_t^b(\boldsymbol{x}^{\boldsymbol{\varphi}}, t)\boldsymbol{f}^{\boldsymbol{\varphi}}(\boldsymbol{x}^{\boldsymbol{\varphi}}, t) + \mathrm{div}^{\boldsymbol{\varphi}}\boldsymbol{\sigma}^{\boldsymbol{\varphi}}(\boldsymbol{x}^{\boldsymbol{\varphi}}, t) \tag{1.40}$$

$$= \rho_t^b(\boldsymbol{x}^{\boldsymbol{\varphi}}, t)\frac{\partial}{\partial t}\boldsymbol{v}^{\boldsymbol{\varphi}}(\boldsymbol{x}^{\boldsymbol{\varphi}}, t) \quad \forall \boldsymbol{x}^{\boldsymbol{\varphi}} \in \Omega_t^b, t \in (0, T), \tag{1.41}$$

known as *Cauchy's first law of motion*.

1.3.4 Lagrangian equation of motion

The Cauchy stress tensor is an Eulerian tensor field and it represents the force measured per unit deformed area acting on the deformed body. Although it is the real measure of stress, it is not the most appropriate tensor to use by the formulation of the nonlinear elasticity problems. The problem is that we generally do not know the area in the deformed configuration. Therefore we define also the Piola-Kirchhoff stress tensors, which is mathematically convenient. First we introduce the *nominal stress tensor*

$$\boldsymbol{N}(\boldsymbol{x}) = J(\boldsymbol{x})\left(\boldsymbol{F}(\boldsymbol{x})\right)^{-1}\boldsymbol{\sigma}^b(\boldsymbol{x}^{\boldsymbol{\varphi}}), \quad \boldsymbol{x}^{\boldsymbol{\varphi}} = \boldsymbol{\varphi}(\boldsymbol{x}) \tag{1.42}$$

and its transpose

$$\boldsymbol{P} = \boldsymbol{N}^T = J\boldsymbol{\sigma}^{bT}\boldsymbol{F}^{-T} \tag{1.43}$$

which is called *first Piola-Kirchhoff stress tensor*. First Piola-Kirchhoff stress tensor $\boldsymbol{P}$ represents the force measured per unit undeformed area acting on the deformed body. Because the first Piola-Kirchhoff stress tensor is in general not symmetric, the *second Piola-Kirchhoff stress tensor* $\boldsymbol{S}$ is defined by

$$\boldsymbol{S}(\boldsymbol{x}) = \boldsymbol{F}(\boldsymbol{x})^{-1}\boldsymbol{P}(\boldsymbol{x}) = J(\boldsymbol{x})\left(\boldsymbol{F}(\boldsymbol{x})\right)^{-1}\boldsymbol{\sigma}^b(\boldsymbol{x}^{\boldsymbol{\varphi}})\left(\boldsymbol{F}(\boldsymbol{x})\right)^{-T}. \tag{1.44}$$

$\boldsymbol{S}$ is a Lagrangian tensor field representing the force measured per unit undefromed area acting on a surface in the undeformed body. It is symmetric if (and only if) the Cauchy stress tensor is symmetric.

Next we transform the applied force densities from Ω_t^b to Ω^b. The density of body forces $\boldsymbol{f} : \Omega^b \to \mathbb{R}^2$ in the reference configuration is given by

$$\boldsymbol{f}(\boldsymbol{x}) = \boldsymbol{f}^{\boldsymbol{\varphi}}(\boldsymbol{x}^{\boldsymbol{\varphi}}) \det \boldsymbol{F}(\boldsymbol{x}), \quad \boldsymbol{x}^{\boldsymbol{\varphi}} = \boldsymbol{\varphi}(\boldsymbol{x}), \tag{1.45}$$

where $\boldsymbol{f}^{\boldsymbol{\varphi}}$ is defined in Section 1.3.2. For any subdomain $\mathcal{B} \subset \Omega^b$ and $\mathcal{B}^{\boldsymbol{\varphi}} = \boldsymbol{\varphi}(\mathcal{B})$ it holds that $\int_{\mathcal{B}} \boldsymbol{f}(\boldsymbol{x}) \, \mathrm{d}\boldsymbol{x} = \int_{\mathcal{B}^{\boldsymbol{\varphi}}} \boldsymbol{f}^{\boldsymbol{\varphi}}(\boldsymbol{x}^{\boldsymbol{\varphi}}) \, \mathrm{d}\boldsymbol{x}^{\boldsymbol{\varphi}}$. Similarly we transform the traction force from Ω_t^b to Ω^b. The density of traction force $\boldsymbol{g} : \Gamma_N^b \to \mathbb{R}^2$ in the reference configuration is given by

$$\boldsymbol{g}_N(\boldsymbol{x}) = \boldsymbol{g}^{\boldsymbol{\varphi}}(\boldsymbol{x}^{\boldsymbol{\varphi}}) \left| \mathrm{Cof}(\boldsymbol{F}) \boldsymbol{n}(\boldsymbol{x}) \right|, \quad \boldsymbol{x}^{\boldsymbol{\varphi}} = \boldsymbol{\varphi}(\boldsymbol{x}), \boldsymbol{x} \in \Gamma_N^b, \tag{1.46}$$

where $\boldsymbol{g}^{\boldsymbol{\varphi}}$ is defined in Section 1.3.2. For any subdomain $\mathcal{B} \subset \Omega^b$ and $\mathcal{B}^{\boldsymbol{\varphi}} = \boldsymbol{\varphi}(\mathcal{B})$ it holds that $\int_{\partial\mathcal{B}} \boldsymbol{g}_N(\boldsymbol{x}) \, \mathrm{d}S = \int_{\partial\mathcal{B}^{\boldsymbol{\varphi}}} \boldsymbol{g}^{\boldsymbol{\varphi}}(\boldsymbol{x}^{\boldsymbol{\varphi}}) \, \mathrm{d}S^{\boldsymbol{\varphi}}$.

The linear momentum balance equation (1.32) may be written in terms of integrals over any subdomain $\mathcal{B} \subset \Omega^b$ and its boundary $\partial\mathcal{B}$. We have

$$\int_{\mathcal{B}} \rho^b(\boldsymbol{x}, t) \boldsymbol{f}(\boldsymbol{x}, t) \, \mathrm{d}\boldsymbol{x} + \int_{\partial\mathcal{B}} \boldsymbol{P}(\boldsymbol{x}, t) \boldsymbol{n} \, \mathrm{d}S = \int_{\mathcal{B}} \rho^b(\boldsymbol{x}, t) \frac{\partial^2}{\partial t^2} \boldsymbol{\varphi}(\boldsymbol{x}, t) \, \mathrm{d}\boldsymbol{x}, \tag{1.47}$$

where $\boldsymbol{P}$ is the first Piola-Kirchhoff tensor and $\boldsymbol{f}(\boldsymbol{x}, t) = \boldsymbol{f}^{\boldsymbol{\varphi}}(\boldsymbol{x}^{\boldsymbol{\varphi}}, t)$, where $\boldsymbol{x}^{\boldsymbol{\varphi}} = \boldsymbol{\varphi}(\boldsymbol{x}, t)$. As in Section 1.3.3 we get

$$\rho^b(\boldsymbol{x}, t) \boldsymbol{f}(\boldsymbol{x}, t) + \mathrm{div} \boldsymbol{P}(\boldsymbol{x}, t) = \rho^b(\boldsymbol{x}, t) \frac{\partial^2}{\partial t^2} \boldsymbol{\varphi}(\boldsymbol{x}, t) \quad \forall \boldsymbol{x} \in \Omega^b, t \in (0, T), \tag{1.48}$$

or we can write as an equation for the displacement $\boldsymbol{u}$

$$\rho^b(\boldsymbol{x}, t) \boldsymbol{f}(\boldsymbol{x}, t) + \mathrm{div} \boldsymbol{P}(\boldsymbol{x}, t) = \rho^b(\boldsymbol{x}, t) \frac{\partial^2}{\partial t^2} \boldsymbol{u}(\boldsymbol{x}, t) \quad \forall \boldsymbol{x} \in \Omega^b, t \in (0, T). \tag{1.49}$$

1.3.5 Nonlinear elasticity problem

In order to formulate the initial boundary value problem, the differential equations for the motion need to be supplemented by boundary and initial conditions for the displacement $\boldsymbol{u}(\boldsymbol{x}, t)$.

We consider that the initial condition is given by the initial displacement $\boldsymbol{u}_0$ and initial deformation velocity $\boldsymbol{v}_0^b$. In most of cases they are both set to zero, because we are usually considering some fixed undeformed initial state of the body.

The boundary conditions are of two different types. We usually solve problems which involve both of them. Therefore we consider that the boundary of the domain Ω^b consists of two disjoint parts Γ_D^b and Γ_N^b, see an example in Figure 1.2.

The first boundary condition is called *Dirichlet* or *displacement boundary condition* and we call Γ_D^b as the *Dirichlet* part of the boundary. On the Dirichlet part of the boundary the current position $\boldsymbol{x}^{\boldsymbol{\varphi}} = \boldsymbol{\varphi}(\boldsymbol{x}, t)$ is prescribed. Equivalently it may be specified by the displacement $\boldsymbol{u} = \boldsymbol{x}^{\boldsymbol{\varphi}} - \boldsymbol{x}$. Hence we define the boundary displacement function $\boldsymbol{u}_D : \Gamma_D^b \times [0, T] \to \mathbb{R}^2$ on Γ_D^b. Typically we consider that $\boldsymbol{u}_D$ is zero, which means that the body is fixed on the Dirichlet part of the boundary.

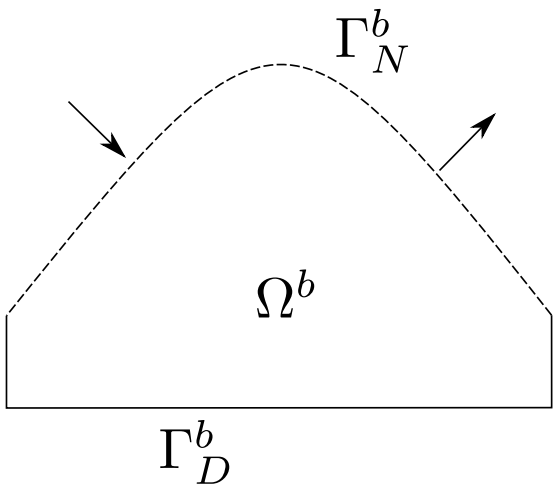

Figure 1.2: Example of the domain Ω^b with the Dirichlet part Γ_D^b and the Neumann part Γ_N^b.

Other type of boundary conditions is a *traction boundary condition* also called as *Neumann boundary condition*. Accordingly we denote the *Neumann* part of the boundary as Γ_N^b. The Neumann boundary condition is given by the surface traction $\boldsymbol{g}^{\varphi}$ as was defined in Section 1.3.2, which is transformed in the reference configuration as $\boldsymbol{g}_N$ defined in (1.46).

In applications to real body motion the dissipative forces are often needed to be taken into account. Therefore to equations (1.48) we add the term

$$C_M \rho^b \frac{\partial \boldsymbol{u}}{\partial t}, \tag{1.50}$$

where C_M is a real constant. This term represents the dissipative structural damping.

Definition 1. *(Dynamic nonlinear elasticity)* Let us consider a bounded domain $\Omega^b \subset \mathbb{R}^2$, with Lipschitz boundary $\partial\Omega^b$ and a time interval $[0,T]$ with $T > 0$. We assume that the boundary of the domain Ω^b consists of two disjoint parts, namely a Dirichlet part Γ_D^b and a Neumann part Γ_N^b. Thus $\partial\Omega^b = \overline{\Gamma}_D^b \cup \overline{\Gamma}_N^b$ and $\Gamma_D^b \cap \Gamma_N^b = \emptyset$. We define the solution of dynamic nonlinear elasticity problem as a displacement function $\boldsymbol{u} : \Omega^b \times [0,T] \to \mathbb{R}^2$ such that

$$\rho^b \frac{\partial^2 \boldsymbol{u}}{\partial t^2} + C_M \rho^b \frac{\partial \boldsymbol{u}}{\partial t} - \mathrm{div}\boldsymbol{P} = \boldsymbol{f} \qquad \text{in } \Omega^b \times [0,T], \tag{1.51}$$

$$\boldsymbol{u} = \boldsymbol{u}_D \quad \text{in } \Gamma_D^b \times [0,T], \tag{1.52}$$

$$\boldsymbol{P} \cdot \boldsymbol{n} = \boldsymbol{g}_N \quad \text{in } \Gamma_N^b \times [0,T], \tag{1.53}$$

$$\boldsymbol{u}(\cdot,0) = \boldsymbol{u}_0, \quad \frac{\partial \boldsymbol{u}}{\partial t}(\cdot,0) = \boldsymbol{v}_0^b \qquad \text{in } \Omega^b, \tag{1.54}$$

where $\boldsymbol{f} : \Omega^b \times [0,T] \to \mathbb{R}^2$ is the density of the acting body force, $\boldsymbol{g}_N : \Gamma_N^b \times [0,T] \to \mathbb{R}^2$ is the surface traction acting on the Neumann part of the boundary Γ_N^b, $\boldsymbol{u}_D : \Gamma_D^b \times [0,T] \to \mathbb{R}^2$ is the prescribed displacement on the Dirichlet part of the boundary Γ_D^b, $\boldsymbol{u}_0 : \Omega^b \to \mathbb{R}^2$ is the initial displacement, $\boldsymbol{v}_0^b : \Omega^b \to \mathbb{R}^2$ is

the initial deformation velocity, $\boldsymbol{n}$ is the unit outer normal, $\rho^b > 0$ is the material density and $C_M \geq 0$ is the damping coefficient. Finally, $\boldsymbol{P} : \Omega^b \to \mathbb{M}^2$ is the first Piola-Kirchhoff stress tensor defined in Section 1.3.4 and specified by the type of the material.

In Section 1.4 are stated the examples of various types of materials used in the implementation. Time-independent steady-state equations can be obtained from dynamic equations by setting all time derivatives to zero.

Definition 2. *(Static nonlinear elasticity)* Let us consider a domain $\Omega^b \subset \mathbb{R}^2$ defined as in Definition 1. We define the solution of static nonlinear elasticity problem as a displacement function $\boldsymbol{u} : \Omega^b \to \mathbb{R}^2$ such that

$$-\mathrm{div}\boldsymbol{P} = \boldsymbol{f} \quad \text{in } \Omega^b, \tag{1.55}$$

$$\boldsymbol{u} = \boldsymbol{u}_D \quad \text{in } \Gamma_D^b, \tag{1.56}$$

$$\boldsymbol{P} \cdot \boldsymbol{n} = \boldsymbol{g}_N \quad \text{in } \Gamma_N^b, \tag{1.57}$$

where $\boldsymbol{f} : \Omega^b \to \mathbb{R}^2$, $\boldsymbol{u}_D : \Gamma_D^b \to \mathbb{R}^2$, $\boldsymbol{g}_N : \Gamma_N^b \to \mathbb{R}^2$, $\boldsymbol{P} : \Omega^b \to \mathbb{M}^2$ and $\boldsymbol{n}$ have the same interpretation as in Definition 1.

1.4 Hyperelastic materials

Equations (1.51)–(1.54) and (1.55)–(1.57) are completed by the use of a *constitutive law* describing the type of the material. We assume hyperelastic materials representing tissues for which a strain-energy function exists. Therefore, at first we need to define the strain-energy function.

1.4.1 Energy

The energy that is stored in the deformed body is referred to as *strain energy* (see [10]). We assume that the strain energy is determined by the deformation mapping of the reference configuration and therefore we use the notation $E^W(\boldsymbol{\varphi}(\boldsymbol{x}))$. We shall only deal with the so-called *hyperelastic materials* where the *first Piola-Kirchhoff stress tensor* $\boldsymbol{P}$ has a potential $W = W(\boldsymbol{F})$ called *stored energy density*, i.e.

$$\boldsymbol{P}(\boldsymbol{F}) = \frac{\partial W(\boldsymbol{F})}{\partial \boldsymbol{F}}. \tag{1.58}$$

The notation $\partial/\partial\boldsymbol{F}$ has been introduced in (1.5). We obtain the strain energy of the deformed body by integrating the energy density function over the entire reference domain Ω^b:

$$E^W(\boldsymbol{\varphi}) = \int_{\Omega^b} W(\nabla\boldsymbol{\varphi}(\boldsymbol{x}))\,\mathrm{d}\boldsymbol{x}. \tag{1.59}$$

By specifying the formula for $W(\boldsymbol{F})$ we define the properties of the modelled material. (For details, see [10].)

Examples of hyperelastic materials are also St. Venant-Kirchhoff material and neo-Hookean material, which are used in our considerations and numerical simulations.

1.4.2 St. Venant-Kirchhoff material

The simplest among the nonlinear models is the *St. Venant-Kirchhoff material*. For its simplicity it is popular in computations. This model is also related to the linear elasticity model by using the nonlinear Green strain tensor $\boldsymbol{E}$ instead of the linearized strain tensor $\boldsymbol{e}$ (see [10]). For the linear elasticity problem we refer to Section 1.5. The energy density function is defined as

$$W(\boldsymbol{F}) = \frac{\lambda}{2}\mathrm{tr}^2(\boldsymbol{E}) + \mu \boldsymbol{E} : \boldsymbol{E}, \tag{1.60}$$

where λ and μ are the *Lamé parameters*. From (1.58) we get the first Piola-Kirchhoff stress tensor in the form

$$\boldsymbol{P}(\boldsymbol{F}) = \boldsymbol{F}\boldsymbol{S}, \tag{1.61}$$

where

$$\boldsymbol{S} = \lambda \mathrm{tr}(\boldsymbol{E})\boldsymbol{I} + 2\mu \boldsymbol{E} \tag{1.62}$$

is the *second Piola-Kirchhoff stress tensor*. Writing $\boldsymbol{S}(\boldsymbol{u}) = (S_{ij})_{i,j=1}^2$, we get

$$S_{ij} = \lambda \left(\sum_{l=1}^{2} \frac{\partial u_l}{\partial x_l} + \frac{1}{2} \sum_{l=1}^{2} \sum_{k=1}^{2} \left(\frac{\partial u_k}{\partial x_l} \right)^2 \right) \delta_{ij} + \mu \left(\frac{\partial u_i}{\partial x_j} + \frac{\partial u_j}{\partial x_i} + \sum_{k=1}^{2} \frac{\partial u_k}{\partial x_i} \frac{\partial u_k}{\partial x_j} \right). \tag{1.63}$$

1.4.3 Neo-Hookean material

As another example of the popular forms of material we take neo-Hookean material, which is given by the energy density function

$$W(\boldsymbol{F}) = \frac{\mu}{2} \left(\mathrm{tr}(\boldsymbol{F}^T \boldsymbol{F}) - 3 \right) - \mu \log(\det \boldsymbol{F}) + \frac{\lambda}{2} \log^2(\det \boldsymbol{F}). \tag{1.64}$$

The corresponding first Piola-Kirchhoff stress tensor has the form

$$\boldsymbol{P}(\boldsymbol{F}) = \mu(\boldsymbol{F} - \boldsymbol{F}^{-T}) + \lambda \log(\det \boldsymbol{F}) \boldsymbol{F}^{-T} \tag{1.65}$$

or equivalently using (1.8)

$$\boldsymbol{P}(\boldsymbol{F}) = \mu \boldsymbol{F} + (\lambda \log(\det \boldsymbol{F}) - \mu) \boldsymbol{F}^{-T} = \mu \boldsymbol{F} + \frac{\lambda \log(\det \boldsymbol{F}) - \mu}{\det \boldsymbol{F}} \mathrm{Cof} \boldsymbol{F}. \tag{1.66}$$

1.5 Linear elasticity

The linear elasticity model is the simplest elasticity model obtained by the assumption of small deformations. By this assumption the second term in (1.21) is neglected and the linear approximation of $\boldsymbol{E}(\boldsymbol{u})$ (linear with respect to the gradient $\boldsymbol{F}$) is denoted by $\boldsymbol{e}(\boldsymbol{u})$ and called the *small strain tensor*, or the *infinitesimal strain tensor*. Then $\boldsymbol{e}(\boldsymbol{u}) = (e_{ij})_{i,j=1}^2$ and

$$e_{ij} = \frac{1}{2} \left(\frac{\partial u_i}{\partial x_j} + \frac{\partial u_j}{\partial x_i} \right). \tag{1.67}$$

Let us assume that the material is isotropic. In terms of the energy density function the linear elasticity material is defined as

$$W(\boldsymbol{F}) = \frac{\lambda}{2}\mathrm{tr}^2(\boldsymbol{e}) + \mu \boldsymbol{e} : \boldsymbol{e}, \tag{1.68}$$

where λ and μ are the *Lamé parameters*. They are related to the material properties of *Young's modulus* E^b and *Poisson's ratio* ν^b, which have a physical interpretation and are often used in experiments:

$$\mu = \frac{E^b}{2(1+\nu^b)}, \quad \lambda = \frac{E^b \nu^b}{(1+\nu^b)(1-2\nu^b)}. \tag{1.69}$$

From (1.58) we get the first Piola-Kirchhoff stress tensor in the form

$$\boldsymbol{P}(\boldsymbol{F}) = \lambda \mathrm{tr}(\boldsymbol{e})\boldsymbol{I} + 2\mu \boldsymbol{e}. \tag{1.70}$$

In linear elasticity, in which the displacement gradients are considered to be small compared to unity, and the nonlinear or second-order terms of the the strain tensor are neglected, the Cauchy and Piola–Kirchhoff tensors are identical. We can write

$$\boldsymbol{\sigma}^b(\boldsymbol{F}) = \boldsymbol{P}(\boldsymbol{F}) = \lambda \mathrm{tr}(\boldsymbol{e})\boldsymbol{I} + 2\mu \boldsymbol{e}. \tag{1.71}$$

Let us note that linear elasticity is not a special case of nonlinear elasticity, but it should be considered as an approximation of model of elasticity that is valid for small displacements. On the basis of the above considerations, we are able to obtain partial differential equations describing the dynamic and static elasticity.

Definition 3. *(Dynamic linear elasticity)* Let us consider a domain $\Omega^b \subset \mathbb{R}^2$ and an interval $[0,T]$ defined as in Definition 1. We define the solution of dynamic linear elasticity problem as a displacement function $\boldsymbol{u} : \Omega^b \times [0,T] \to \mathbb{R}^2$ such that

$$\rho^b \frac{\partial^2 \boldsymbol{u}}{\partial t^2} + C_M \rho^b \frac{\partial \boldsymbol{u}}{\partial t} - \mathrm{div}\, \boldsymbol{\sigma}^b = \boldsymbol{f} \qquad \text{in } \Omega^b \times [0,T], \tag{1.72}$$

$$\boldsymbol{u} = \boldsymbol{u}_D \quad \text{in } \Gamma_D^b \times [0,T], \tag{1.73}$$

$$\boldsymbol{\sigma}^b \cdot \boldsymbol{n} = \boldsymbol{g}_N \quad \text{in } \Gamma_N^b \times [0,T], \tag{1.74}$$

$$\boldsymbol{u}(\cdot,0) = \boldsymbol{u}_0, \quad \frac{\partial \boldsymbol{u}}{\partial t}(\cdot,0) = \boldsymbol{v}_0^b \qquad \text{in } \Omega^b, \tag{1.75}$$

where $\boldsymbol{f}$, $\boldsymbol{u}_D$, $\boldsymbol{g}_N$, $\boldsymbol{u}_0$, $\boldsymbol{v}_0^b$, ρ^b, $\boldsymbol{n}$, C_M, have the same interpretation as in Definition 1 and $\boldsymbol{\sigma}^b$ is given by (1.71).

Definition 4. *(Static linear elasticity)* Let us consider a domain $\Omega^b \subset \mathbb{R}^2$ defined as in Definition 1. We define the solution of the static linear elasticity problem as a displacement function $\boldsymbol{u} : \Omega^b \to \mathbb{R}^2$ such that

$$-\mathrm{div}\, \boldsymbol{\sigma}^b = \boldsymbol{f} \qquad \text{in } \Omega^b, \tag{1.76}$$

$$\boldsymbol{u} = \boldsymbol{u}_D \quad \text{in } \Gamma_D^b, \tag{1.77}$$

$$\boldsymbol{\sigma}^b \cdot \boldsymbol{n} = \boldsymbol{g}_N \quad \text{in } \Gamma_N^b, \tag{1.78}$$

where $\boldsymbol{f}$, $\boldsymbol{u}_D$, $\boldsymbol{g}_N$, ρ^b, $\boldsymbol{n}$ have the same interpretation as in Definition 2 and $\boldsymbol{\sigma}^b$ is given by (1.71).

In this chapter we defined the linear and nonlinear elasticity problem. In order to solve them we need to employ a suitable numerical scheme. In the next chapter we introduce the discontinuous Galerkin finite element method for solving these elasticity problems.

2. Discretization of the elasticity problem by the DGM

Our goal is to develop a sufficiently robust, efficient and accurate numerical method for the simulation of stationary and nonstationary elasticity problem considering both linear and nonlinear material characteristics. We employ the discontinuous Galerkin method (DGM) which has already become popular numerical technique for the solution of the compressible Navier-Stokes equations. In Chapter 4 the use of the DGM for the Navier-Stokes equations is described in detail. Our very good experience with the DGM for the Navier-Stokes equations led us to the idea to choose it also as a discretization method for the elasticity problem. For example the DGM is successfully employed for the elasticity equations in [59, 62]. The DGM is particularly suitable for the numerical solution of hyperbolic conservation laws with discontinuous solutions. This is the motivation for the application of the DGM to dynamic elasticity, where such solution can also appear in some cases. Namely, the nonlinear dynamic elasticity problem is described by nonlinear hyperbolic systems.

In our case the DGM is used as high-order piecewise polynomial discontinuous approximation on arbitrary meshes in space. For the time discretization we apply the backward difference formula (BDF) method. The time discretization could also be carried out by a discontinuous approximation in order to get the space-time discontinuous Galerkin method. It is another technique how to construct a method of high-order accuracy both in space and timediscontinu. The use of this technique for the elasticity problem is briefly described in [36] and [49]. However, we use a backward difference formula method based on finite-difference approximations in time. It is a fully implicit scheme without any restriction of the size of the time step.

The complete discretization leads to a nonlinear algebraic system and in the case of linear elasticity to a linear algebraic system, which should be solved by a suitable solver. In the case of the nonlinear system we apply the iterative Newton method. Then the final linear algebraic system can be solved by a direct solver as Parallel Sparse Direct Solver (PARDISO) and Unsymmetric MultiFrontal method (UMFPACK) or by the use of iterative methods as Bi-Conjugate Gradient Stabilized method (BiCGStab) and Generalized Minimal Residual method (GMRES).

First in this chapter the discretization in space of the linear elasticity problem and also of the nonlinear elasticity problem is described. Further we introduce the discretization in time by the BDF method. In the end the derivatives of the first Piola-Kirchhoff tensor are expressed in detail. They are needed for the solution of the nonlinear elasticity problem by the Newton method. On the basis of the theory of the DGM we developed a .NET library written in C# for the numerical solution of the 2D dynamic linear and nonlinear elasticity problem with mixed boundary conditions. The developed library supports several time discretization techniques, built on top of the DG discretization space.

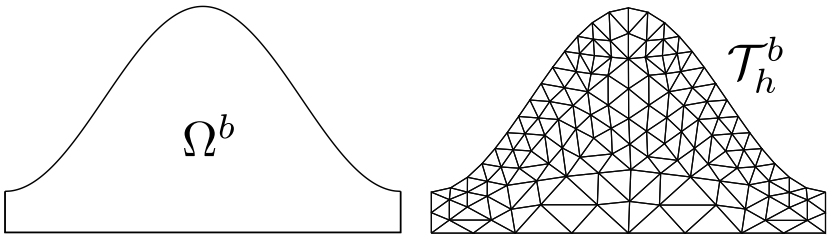

Figure 2.1: Example of a triangulation $\mathcal{T}_h^b$ of a domain Ω^b.

2.1 Preliminaries

Here we introduce the basic concepts of the discontinuous Galerkin method as the definition of triangulation, finite-dimensional spaces and basis functions.

2.1.1 Triangulation

Let Ω_h^b be a polygonal approximation of the domain Ω^b. On the closure $\overline{\Omega}_h^b$ of the domain Ω_h^b we construct a triangulation $\mathcal{T}_h^b$ formed by a finite number of closed triangles K with mutually disjoint interiors such that

$$\overline{\Omega}_h^b = \bigcup_{K \in \mathcal{T}_h^b} K. \tag{2.1}$$

We do not require the standard conforming properties from the finite element method, introduced e.g. in [10]. As we see, in the finite element mesh we admit the so-called hanging nodes. However, in the current implementation hanging nodes are not supported. In general, the discontinuous Galerkin method can handle with more general elements as quadrilaterals and convex or even nonconvex star-shaped polygons. In our further considerations we shall use the following notation. By ∂K we denote the boundary of an element $K \in \mathcal{T}_h^b$ and set

$$h_K = \mathrm{diam}(K), \quad h = \max_{K \in \mathcal{T}_h^b} h_K, \tag{2.2}$$

where $\mathrm{diam}(K)$ is the diameter of the element K. By ρ_K we denote the radius of the largest circle inscribed into K and by $|K|$ we denote the area of K. Let $K,\ K' \in \mathcal{T}_h^b$. We say that K and K' are neighbouring elements (or simply neighbours), if the set $\partial K \cap \partial K'$ has positive onedimensional measure. We say that $\Gamma \subset K$ is a face of K, if it is a maximal connected open subset of either $\partial K \cap \partial K'$, where K' is a neighbour of K, or $\partial K \cap \partial \Gamma_D^b$ or $\partial K \cap \partial \Gamma_N^b$. The symbol $|\Gamma|$ denotes the length of Γ. By $\mathcal{F}_h$ we denote the system of all faces of all elements $K \in \mathcal{T}_h^b$. Further, we define the set of all boundary faces by

$$\mathcal{F}_h^B = \left\{ \Gamma \in \mathcal{F}_h ; \Gamma \subset \partial \Omega_h^b \right\}, \tag{2.3}$$

the set of all *"Dirichlet" boundary faces* by

$$\mathcal{F}_h^D = \left\{ \Gamma \in \mathcal{F}_h ; \Gamma \subset \Gamma_D^b \right\}, \tag{2.4}$$

the set of all *"Neumann" boundary faces* by

$$\mathcal{F}_h^N = \left\{ \Gamma \in \mathcal{F}_h ; \Gamma \subset \Gamma_N^b \right\}, \tag{2.5}$$

and the set of all inner faces

$$\mathcal{F}_h^I = \mathcal{F}_h \setminus \mathcal{F}_h^B. \tag{2.6}$$

Obviously, $\mathcal{F}_h = \mathcal{F}_h^I \cup \mathcal{F}_h^D \cup \mathcal{F}_h^N$ and $\mathcal{F}_h^B = \mathcal{F}_h^D \cup \mathcal{F}_h^N$. For a shorter notation we put

$$\mathcal{F}_h^{ID} = \mathcal{F}_h^I \cup \mathcal{F}_h^D. \tag{2.7}$$

For each $\Gamma \in \mathcal{F}_h$ we define a unit normal vector $\boldsymbol{n}_\Gamma$. We assume that for $\Gamma \in \mathcal{F}_h^B$ the normal $\boldsymbol{n}_\Gamma$ has the same orientation as the outer normal to $\partial\Omega_h^b$. For each face $\Gamma \in \mathcal{F}_h^I$ the orientation of $\boldsymbol{n}_\Gamma$ is arbitrary but fixed. For each $\Gamma \in \mathcal{F}_h^I$ there exist two neighbouring elements $K_\Gamma^{(L)}$, $K_\Gamma^{(R)} \in \mathcal{T}_h^b$ such that $\Gamma \subset \partial K_\Gamma^{(L)} \cap \partial K_\Gamma^{(R)}$. We use the convention that $\boldsymbol{n}_\Gamma$ is the outer normal to $\partial K_\Gamma^{(L)}$ and it is the inner normal to $\partial K_\Gamma^{(R)}$. Moreover, if $\Gamma \in \mathcal{F}_h^B$, then there exists an element $K_\Gamma^{(L)} \in \mathcal{T}_h^b$ such that $\Gamma \subset \partial K_\Gamma^{(L)} \cap \partial\Omega_h^b$.

Let us consider a system $\{\mathcal{T}_h^b\}_{h\in(0,\overline{h})}$, $\overline{h} > 0$, of triangulations of the domain Ω_h^b. We assume that the system $\{\mathcal{T}_h^b\}_{h\in(0,\overline{h})}$ is *shape regular*, i.e. there exists a $c_R > 0$ such that

$$\frac{h_K}{\rho_K} \le c_R \quad \forall K \in \mathcal{T}_h^b \ \forall h \in (0, \overline{h}). \tag{2.8}$$

Further, we define a quantity h_Γ for each face Γ, which is in some way proportional to the length of the face Γ. For $\Gamma \in \mathcal{F}_h$ the three following choices are implemented:

$$\text{mean average} : h_\Gamma = \frac{h_{K_\Gamma^{(L)}} + h_{K_\Gamma^{(R)}}}{2}, \tag{2.9}$$

$$\text{maximum} : h_\Gamma = \max\left(h_{K_\Gamma^{(L)}}, h_{K_\Gamma^{(R)}}\right), \tag{2.10}$$

$$\text{edge length} : h_\Gamma = \text{length of } \Gamma. \tag{2.11}$$

For $\Gamma \in \mathcal{F}_h^B$ we set $h_\Gamma = h_{K_\Gamma^{(L)}}$ in (2.9) and (2.10).

2.1.2 Broken Sobolev space

Since the DGM is based on a discontinuous approximation, the broken Sobolev spaces are naturally appropriate for the purpose of the DGM formulation. These spaces depend on the considered triangulation $\mathcal{T}_h^b$. Hence, for a triangulation $\mathcal{T}_h^b$ of a domain Ω_h^b and for $k \in \mathbb{N}$, we define the so-called *broken Sobolev space*

$$H^k(\Omega_h^b, \mathcal{T}_h^b) = \left\{v \in L^2(\Omega_h^b); v|_K \in H^k(K) \ \forall K \in \mathcal{T}_h^b\right\}, \tag{2.12}$$

which consists of functions, whose restrictions on $K \in \mathcal{T}_h^b$ belong to the Sobolev space $H^k(K)$. We do not require any type of regularity over the faces of $\mathcal{T}_h^b$. The broken Sobolev space is equipped with the *broken Sobolev norm*:

$$\|v\|_{H^k(\Omega_h^b, \mathcal{T}_h^b)} = \left(\sum_{K\in\mathcal{T}_h^b} \|v\|^2_{H^k(K)}\right)^{1/2}, \quad v \in H^k(\Omega_h^b, \mathcal{T}_h^b). \tag{2.13}$$

Further, let $\Gamma \in \mathcal{F}_h^I$ and $K_\Gamma^{(L)}, K_\Gamma^{(R)} \in \mathcal{T}_h^b$ be neighbouring elements such that $\Gamma \subset \partial K_\Gamma^{(L)} \cap \partial K_\Gamma^{(R)}$. For $v \in H^1(\Omega_h^b, \mathcal{T}_h^b)$ we introduce the following notation:

$$\begin{aligned} v|_\Gamma^{(L)} &= \text{the trace of } v|_{K_\Gamma^{(L)}} \text{ on } \Gamma, \\ v|_\Gamma^{(R)} &= \text{the trace of } v|_{K_\Gamma^{(R)}} \text{ on } \Gamma, \\ \langle v \rangle_\Gamma &= \tfrac{1}{2}\left(v|_\Gamma^{(L)} + v|_\Gamma^{(R)}\right), \\ [v]_\Gamma &= v|_\Gamma^{(L)} - v|_\Gamma^{(R)}, \end{aligned} \tag{2.14}$$

where $\Gamma \in \mathcal{F}_h^I$. We say $[v]_\Gamma$ denotes the *jump* of v on Γ. It depends on the orientation of $\boldsymbol{n}_\Gamma$, but the expression $[v]_\Gamma \boldsymbol{n}_\Gamma$ does not. Moreover, let $\Gamma \in \mathcal{F}_h^B$ and $K_\Gamma^{(L)} \in \mathcal{T}_h^b$, $\Gamma \subset K_\Gamma^{(L)} \cap \partial\Omega_h^b$. Then for $v \in H^k\Omega_h^b, \mathcal{T}_h^b$ we introduce the following notation:

$$v|_\Gamma^{(L)} = \text{the trace of } v|_{K_\Gamma^{(L)}} \text{ on } \Gamma, \quad \langle v \rangle_\Gamma = [v]_\Gamma = v|_\Gamma^{(L)}. \tag{2.15}$$

We omit the subscript Γ and simply write $\langle \cdot \rangle$, $[\cdot]$ and $\boldsymbol{n}$ respectively, when $\langle \cdot \rangle_\Gamma$, $[\cdot]_\Gamma$ or $\boldsymbol{n}_\Gamma$ appear in integrals $\int_\Gamma \ldots \, \mathrm{d}S$.

Finally we define the vector broken Sobolev space

$$\boldsymbol{H}^1(\Omega_h^b, \mathcal{T}_h^b) = H^1(\Omega_h^b, \mathcal{T}_h^b) \times H^1(\Omega_h^b, \mathcal{T}_h^b), \tag{2.16}$$

and the vector average and jump as

$$\begin{aligned} \langle \boldsymbol{v} \rangle &= \left(\langle v_1 \rangle, \langle v_2 \rangle\right)^T, \\ [\boldsymbol{v}] &= \left([v_1], [v_2]\right)^T. \end{aligned} \tag{2.17}$$

2.1.3 Finite-dimensional spaces

Let $p \geq 0$ be an integer. The approximate solution obtained by the DGM will be sought in

$$\boldsymbol{S}_{hp} = S_{hp} \times S_{hp}. \tag{2.18}$$

By S_{hp} we denote the space of piecewise polynomial functions on the triangulation $\mathcal{T}_h^b$ defined in Section 2.1.1,

$$S_{hp} = \left\{ v \in L^2(\Omega_h^b); v|_K \in P^p(K), K \in \mathcal{T}_h^b \right\}, \tag{2.19}$$

where $P^p(K)$ denotes the space of polynomial functions of degree $\leq p$ on the finite element K. Obviously, $S_{hp} \subset H^k(\Omega_h^b, \mathcal{T}_h^b)$ for any $k \geq 1$ and its dimension $\dim S_{hp} < \infty$.

Since the space S_{hp} is finite-dimensional, we can construct its finite basis. We have several options, but for each construction method it holds that the support of a basis function is formed by a single element $K \in \mathcal{T}_h^b$. The natural choice is to construct the Lagrange basis: for a given polynomial degree $p \geq 0$, the local dimension on each element is denoted by d_{loc} and equals $\frac{(p+1)(p+2)}{2}$. For each element $K \in \mathcal{T}_h^b$ we can construct d_{loc} points on K, which represent the degrees of freedom, and construct d_{loc} local basis functions such that each basis function equals 1 at a single point and equals 0 at the remaining points representing the degrees of freedom. The global basis of the space S_{hp} is then formed by the union of local bases for each $K \in \mathcal{T}_h^b$. The advantage of the Lagrange basis is that

the coefficients of a given function $u \in S_{hp}$ with respect to the basis are just the function values at the points representing the degrees of freedom.

The second option is to construct the basis such that the mass matrix $\mathbb{M} = (m_{ij})_{i,j=1}^N$, where

$$m_{ij} = \int_{\Omega_h^b} \xi_i \xi_j \, \mathrm{d}\boldsymbol{x}, \tag{2.20}$$

with $\{\xi_i\}_{i=1}^N$, $N = \mathrm{card}\mathcal{T}_h^b \cdot d_{loc}$ forming the basis, is diagonal or even unit, i.e. $\mathbb{M} = \mathbb{I}$. The matrix of the resulting linear algebraic system of equations representing the discrete scheme has then generally a lower condition number than in the case of the Lagrange basis.

The third choice is the simplest: on each element $K \in \mathcal{T}_h^b$ take the functions 1, x, y, x^2, xy, y^2, ... as the local basis (remembering that the basis function equals 0 outside K). This basis is called canonical and yields the fastest computation of the matrix of the system of linear algebraic equations representing the discrete scheme. On the other hand, the condition number is generally so high that the canonical basis is by far the worst option out of the three approaches presented here.

2.2 Discretization of the static elasticity problem

2.2.1 Linear elasticity

We start with the discretization of the static linear elasticity problem by the DGM. We introduce the discretization of the problem with the aid of several variants of the DGM. The primal formulation of the problem is defined by equations (1.76)–(1.78) in the previous chapter. The approximate solution will be sought in the space $\boldsymbol{S}_{hp}$. By the use of the standard conforming finite element method the problem is formulated in the weak form and the solution is sought in the Sobolev space. For the derivation of the DGM we proceed in a similar way. First we introduce a weak form of problem (1.76)–(1.78) in the sense of the broken Sobolev spaces.

We assume that a triangulation $\mathcal{T}_h^b$ of a domain Ω_h^b with elements (triangles) $K \in \mathcal{T}_h^b$ is given and let $\boldsymbol{u} \in H^2(\Omega^b)$ be a sufficiently regular solution of problem (1.76)–(1.78). We multiply equation (1.76) by a test function $\boldsymbol{v} \in \boldsymbol{S}_{hp}$, integrate the resulting equation over a finite element $K \in \mathcal{T}_h^b$, use Green's theorem on the term containing $\boldsymbol{\sigma}^b$ and finally sum the resulting equations over all finite elements $K \in \mathcal{T}_h^b$. We obtain the identity

$$\sum_{K \in \mathcal{T}_h^b} \int_K \boldsymbol{\sigma}^b(\boldsymbol{u}) : \nabla \boldsymbol{v} \, \mathrm{d}\boldsymbol{x} - \sum_{K \in \mathcal{T}_h^b} \int_{\partial K} \left(\boldsymbol{\sigma}^b(\boldsymbol{u}) \cdot \boldsymbol{n}_K\right) \cdot \boldsymbol{v} \, \mathrm{d}S = \sum_{K \in \mathcal{T}_h^b} \int_K \boldsymbol{f} \cdot \boldsymbol{v} \, \mathrm{d}\boldsymbol{x}, \tag{2.21}$$

where $\boldsymbol{n}_K$ denotes the unit outer normal to ∂K. We rewrite the integrals over ∂K according to the type of the faces $\Gamma \in \mathcal{F}_h$ that form the boundary of the

element $K \in \mathcal{T}_h^b$:

$$\sum_{K\in\mathcal{T}_h^b} \int_{\partial K} \big(\boldsymbol{\sigma}^b(\boldsymbol{u}) \cdot \boldsymbol{n}_K\big) \cdot \boldsymbol{v} \,\mathrm{d}S = \tag{2.22}$$

$$= \sum_{\Gamma\in\mathcal{F}_h^D} \int_\Gamma \big(\boldsymbol{\sigma}^b(\boldsymbol{u}) \cdot \boldsymbol{n}\big) \cdot \boldsymbol{v} \,\mathrm{d}S + \sum_{\Gamma\in\mathcal{F}_h^N} \int_\Gamma \big(\boldsymbol{\sigma}^b(\boldsymbol{u}) \cdot \boldsymbol{n}\big) \cdot \boldsymbol{v} \,\mathrm{d}S$$

$$+ \sum_{\Gamma\in\mathcal{F}_h^I} \int_\Gamma \Big(\big(\boldsymbol{\sigma}^b(\boldsymbol{u}^{(L)}) \cdot \boldsymbol{n}\big) \cdot \boldsymbol{v}_\Gamma^{(L)} - \big(\boldsymbol{\sigma}^b(\boldsymbol{u}^{(R)}) \cdot \boldsymbol{n}\big) \cdot \boldsymbol{v}_\Gamma^{(R)} \Big) \,\mathrm{d}S.$$

Due to the assumption that $\boldsymbol{u} \in H^2(\Omega^b)$, we have

$$[\boldsymbol{u}]_\Gamma = [\nabla \boldsymbol{u}]_\Gamma = \boldsymbol{0} \quad \forall \Gamma \in \mathcal{F}_h^I, \tag{2.23}$$

and

$$\boldsymbol{\sigma}^b(\boldsymbol{u}^{(L)}) = \boldsymbol{\sigma}^b(\boldsymbol{u}^{(R)}) = \big\langle \boldsymbol{\sigma}^b(\boldsymbol{u}) \big\rangle_\Gamma \quad \forall \Gamma \in \mathcal{F}_h^I. \tag{2.24}$$

Thus, the integrand of the last integral in (2.22) can be written in the form

$$\big(\boldsymbol{\sigma}^b(\boldsymbol{u}^{(L)}) \cdot \boldsymbol{n}\big) \cdot \boldsymbol{v}_\Gamma^{(L)} - \big(\boldsymbol{\sigma}^b(\boldsymbol{u}^{(R)}) \cdot \boldsymbol{n}\big) \cdot \boldsymbol{v}_\Gamma^{(R)} = \big(\big\langle \boldsymbol{\sigma}^b(\boldsymbol{u}) \big\rangle_\Gamma \cdot \boldsymbol{n}\big) \cdot [\boldsymbol{v}]_\Gamma \,. \tag{2.25}$$

Further, we can employ the Neumann boundary condition (1.78) so that

$$\sum_{\Gamma\in\mathcal{F}_h^N} \int_\Gamma \big(\boldsymbol{\sigma}^b(\boldsymbol{u}) \cdot \boldsymbol{n}\big) \cdot \boldsymbol{v} \,\mathrm{d}S = \sum_{\Gamma\in\mathcal{F}_h^N} \int_\Gamma \boldsymbol{g}_N \boldsymbol{v} \,\mathrm{d}S. \tag{2.26}$$

As a consequence of the symmetry of the stress tensor $\boldsymbol{\sigma}^b$ we can write

$$\boldsymbol{\sigma}^b(\boldsymbol{u}) : \nabla \boldsymbol{v} = \boldsymbol{\sigma}^b(\boldsymbol{u}) : \boldsymbol{e}(\boldsymbol{v}), \tag{2.27}$$

where $\boldsymbol{e}(\boldsymbol{v})$ is defined as in (1.67), seeing that

$$\begin{aligned}
\boldsymbol{\sigma}^b(\boldsymbol{u}) : \nabla \boldsymbol{v} &= \sum_{i,j=1}^{2} \sigma_{ij}^b(\boldsymbol{u}) \frac{\partial v_i}{\partial x_j} = \\
&= \frac{1}{2} \sum_{i,j=1}^{2} \sigma_{ij}^b(\boldsymbol{u}) \frac{\partial v_i}{\partial x_j} + \frac{1}{2} \sum_{i,j=1}^{2} \sigma_{ij}^b(\boldsymbol{u}) \frac{\partial v_i}{\partial x_j} = \\
&= \frac{1}{2} \sum_{i,j=1}^{2} \sigma_{ij}^b(\boldsymbol{u}) \frac{\partial v_i}{\partial x_j} + \frac{1}{2} \sum_{j,i=1}^{2} \sigma_{ij}^b(\boldsymbol{u}) \frac{\partial v_j}{\partial x_i} = \\
&= \frac{1}{2} \sum_{i,j=1}^{2} \sigma_{ij}^b(\boldsymbol{u}) \frac{\partial v_i}{\partial x_j} + \frac{1}{2} \sum_{i,j=1}^{2} \sigma_{ij}^b(\boldsymbol{u}) \frac{\partial v_j}{\partial x_i} = \\
&= \sum_{i,j=1}^{2} \sigma_{ij}^b(\boldsymbol{u}) e_{ij}(\boldsymbol{v}).
\end{aligned}$$

Now, (2.21), (2.22), (2.25), (2.26), and (2.27) imply that

$$\sum_{K\in\mathcal{T}_h^b} \int_K \boldsymbol{\sigma}^b(\boldsymbol{u}) : \boldsymbol{e}(\boldsymbol{v}) \,\mathrm{d}\boldsymbol{x} - \sum_{\Gamma\in\mathcal{F}_h^D} \int_\Gamma \big(\boldsymbol{\sigma}^b(\boldsymbol{u}) \cdot \boldsymbol{n}\big) \cdot \boldsymbol{v} \,\mathrm{d}S \tag{2.28}$$

$$- \sum_{\Gamma\in\mathcal{F}_h^I} \int_\Gamma \big(\big\langle \boldsymbol{\sigma}^b(\boldsymbol{u}) \big\rangle \cdot \boldsymbol{n}\big) \cdot [\boldsymbol{v}] \,\mathrm{d}S = \sum_{K\in\mathcal{T}_h^b} \int_K \boldsymbol{f} \cdot \boldsymbol{v} \,\mathrm{d}\boldsymbol{x} + \sum_{\Gamma\in\mathcal{F}_h^N} \int_\Gamma \boldsymbol{g}_N \boldsymbol{v} \,\mathrm{d}S,$$

or we can write

$$\sum_{K\in\mathcal{T}_h^b}\int_K \boldsymbol{\sigma}^b(\boldsymbol{u}):\boldsymbol{e}(\boldsymbol{v})\,\mathrm{d}\boldsymbol{x} - \sum_{\Gamma\in\mathcal{F}_h^I D}\int_\Gamma \left(\left\langle\boldsymbol{\sigma}^b(\boldsymbol{u})\right\rangle\cdot\boldsymbol{n}\right)\cdot[\boldsymbol{v}]\,\mathrm{d}S \tag{2.29}$$
$$= \sum_{K\in\mathcal{T}_h^b}\int_K \boldsymbol{f}\cdot\boldsymbol{v}\,\mathrm{d}\boldsymbol{x} + \sum_{\Gamma\in\mathcal{F}_h^N}\int_\Gamma \boldsymbol{g}_N\boldsymbol{v}\,\mathrm{d}S \quad \forall\boldsymbol{v}\in\boldsymbol{H}^1(\Omega_h^b,\mathcal{T}_h^b).$$

Relation (2.29) is the basis for the DGM discretization of problem (1.76)–(1.78). Further, additional terms representing continuity has to be included in the formulation of the DGM. Hence, we define the *interior and boundary penalty bilinear form*

$$J_h^\eta(\boldsymbol{u},\boldsymbol{v}) = \sum_{\Gamma\in\mathcal{F}_h^I}\int_\Gamma \eta[\boldsymbol{u}]\cdot[\boldsymbol{v}]\,\mathrm{d}S + \sum_{\Gamma\in\mathcal{F}_h^D}\int_\Gamma \eta\boldsymbol{u}\boldsymbol{v}\,\mathrm{d}S \tag{2.30}$$
$$= \sum_{\Gamma\in\mathcal{F}_h^{ID}}\int_\Gamma \eta[\boldsymbol{u}]\cdot[\boldsymbol{v}]\,\mathrm{d}S \quad \boldsymbol{u},\boldsymbol{v}\in\boldsymbol{H}^1(\Omega_h^b,\mathcal{T}_h^b),$$

where $\eta > 0$ is a penalty weight. The choice of the penalty weight is generally important for the theoretical analysis of the DGM, but also in practical computations the penalty weight needs to be estimated as we discuss later. We consider the penalty weight $\eta : \bigcup_{\Gamma\in\mathcal{F}_h^{ID}} \to \mathbb{R}$ in the form

$$\eta|_\Gamma = \eta_\Gamma = \frac{C_W^b}{h_\Gamma}, \quad \Gamma\in\mathcal{F}_h^{ID}, \tag{2.31}$$

where $C_W^b > 0$ is the *penalization constant* and h_Γ is the quantity given by one of the possibilities from (2.9)-(2.11). The penalty terms are defined in order to penalize the measure of discontinuities of approximate solution. The boundary penalty is associated with the boundary linear form

$$J_D^\eta(\boldsymbol{v}) = \sum_{\Gamma\in\mathcal{F}_h^D}\int_\Gamma \eta\boldsymbol{u}_D\boldsymbol{v}\,\mathrm{d}S, \quad \boldsymbol{v}\in\boldsymbol{H}^1(\Omega_h^b,\mathcal{T}_h^b). \tag{2.32}$$

In the standard finite element method the continuity of the approximate solution on interior faces is required. In the DGM the continuity is replaced by the interior penalty. Supplementing the boundary penalty to the discrete problem introduces the Dirichlet boundary condition in the discrete problem. In the DGM is not necessary to construct subsets of finite element spaces formed by functions approximating the Dirichlet boundary condition in a suitable way as in the standard conforming finite elements. Both Dirichlet and Neumann boundary conditions are included automatically in the formulation of the discrete problem.

Further, we introduce additional stabilization terms. We define them in such a way, that they vanish for the exact solution. Therefore, let $\boldsymbol{u}\in\boldsymbol{H}^1(\Omega_h^b)\cap\boldsymbol{H}^2(\Omega_h^b,\mathcal{T}_h^b)$ be a vector function which satisfies the Dirichlet boundary condition (1.77). Then we use the identity

$$\sum_{\Gamma\in\mathcal{F}_h^{ID}}\int_\Gamma \left(\left\langle\boldsymbol{\sigma}^b(\boldsymbol{v})\right\rangle\cdot\boldsymbol{n}\right)\cdot[\boldsymbol{u}]\,\mathrm{d}S = \sum_{\Gamma\in\mathcal{F}_h^D}\int_\Gamma \left(\left\langle\boldsymbol{\sigma}^b(\boldsymbol{v})\right\rangle\cdot\boldsymbol{n}\right)\cdot\boldsymbol{u}_D\,\mathrm{d}S \tag{2.33}$$
$$\forall\boldsymbol{v}\in\boldsymbol{H}^2(\Omega_h^b,\mathcal{T}_h^b),$$

which is valid since $[\boldsymbol{u}]_\Gamma = 0$ for $\Gamma \in \mathcal{F}_h^I$, $[\boldsymbol{u}]_\Gamma = \boldsymbol{u}_\Gamma = \boldsymbol{u}_D$ for $\Gamma \in \mathcal{F}_h^D$, and $\langle \boldsymbol{\sigma}^b(\boldsymbol{v}) \rangle_\Gamma = \boldsymbol{\sigma}^b(\boldsymbol{v})$ for $\Gamma \in \mathcal{F}_h^D$ by definition.

Including (2.29), (2.30), (2.31), and (2.33) in one formulation we obtain the *discontinuous Galerkin weak formulation.* In fact we introduce three different variants of the DGM, because we add equality (2.30) to (2.29) and sum it with (2.33) multiplied by a parameter $\theta \in \mathbb{R}$. This way we arrive at the identity

$$a_h(\boldsymbol{u}, \boldsymbol{v}) = b_h(\boldsymbol{v}), \tag{2.34}$$

where the bilinear form $a_h(\boldsymbol{u}, \boldsymbol{v})$ and the right-hand side linear form $b_h(\boldsymbol{v})$ are defined for $\boldsymbol{u}, \boldsymbol{v} \in \boldsymbol{H}^2(\Omega_h^b, \mathcal{T}_h^b)$ as

$$\begin{aligned} a_h(\boldsymbol{u}, \boldsymbol{v}) = & \sum_{K \in \mathcal{T}_h^b} \int_K \boldsymbol{\sigma}^b(\boldsymbol{u}) : \boldsymbol{e}(\boldsymbol{v}) \, \mathrm{d}\boldsymbol{x} \\ & - \sum_{\Gamma \in \mathcal{F}^{ID}} \int_\Gamma \left(\langle \boldsymbol{\sigma}^b(\boldsymbol{u}) \rangle \cdot \boldsymbol{n} \right) \cdot [\boldsymbol{v}] \, \mathrm{d}S \\ & - \theta \sum_{\Gamma \in \mathcal{F}^{ID}} \int_\Gamma \left(\langle \boldsymbol{\sigma}^b(\boldsymbol{v}) \rangle \cdot \boldsymbol{n} \right) \cdot [\boldsymbol{u}] \, \mathrm{d}S + \sum_{\Gamma \in \mathcal{F}^{ID}} \int_\Gamma \frac{C_W^b}{h_\Gamma} [\boldsymbol{u}] \cdot [\boldsymbol{v}] \, \mathrm{d}S, \end{aligned} \tag{2.35}$$

$$\begin{aligned} b_h(\boldsymbol{v}) = & \sum_{K \in \mathcal{T}_h^b} \int_K \boldsymbol{f} \cdot \boldsymbol{v} \, \mathrm{d}\boldsymbol{x} + \sum_{\Gamma \in \mathcal{F}^N} \int_\Gamma \boldsymbol{g}_N \cdot \boldsymbol{v} \, \mathrm{d}S \\ & - \theta \sum_{\Gamma \in \mathcal{F}^D} \int_\Gamma \left(\langle \boldsymbol{\sigma}^b(\boldsymbol{v}) \rangle \cdot \boldsymbol{n} \right) \cdot \boldsymbol{u}_D \, \mathrm{d}S + \sum_{\Gamma \in \mathcal{F}^D} \int_\Gamma \frac{C_W^b}{h_\Gamma} \boldsymbol{u}_D \cdot \boldsymbol{v} \, \mathrm{d}S. \end{aligned} \tag{2.36}$$

Since $\boldsymbol{S}_{hp} \subset \boldsymbol{H}^2(\Omega_h^b, \mathcal{T}_h^b)$, the forms (2.35) and (2.36) make sense for $\boldsymbol{u}_h, \boldsymbol{v}_h \in \boldsymbol{S}_{hp}$. Consequently, we define three numerical schemes.

Definition 5. A function $\boldsymbol{u}_h \in \boldsymbol{S}_{hp}$ is called a *dicontinuous approximate solution* of problem (1.76)–(1.78), if it satisifies the identity

$$a_h(\boldsymbol{u}_h, \boldsymbol{v}_h) = b_h(\boldsymbol{v}_h) \quad \forall \boldsymbol{v}_h \in \boldsymbol{S}_{hp}, \tag{2.37}$$

where the forms a_h and b_h are defined by (2.35) and (2.36), respectively.

By the choice of θ we distinguish between three variants of the DGM. Scheme with $\theta = 1$ is called *symmetric interior penalty Galerkin* (SIPG) method. Scheme with $\theta = -1$ is called *nonsymmetric interior penalty Galerkin* (NIPG) method. Finally, scheme with $\theta = 0$ is called *incomplete interior penalty Galerkin* (IIPG) method.

The discrete problem (2.37) is equivalent to a system of linear algebraic equations, which can be solved by a suitable direct or iterative solver. Namely, the basis of the finite-dimensional space $\boldsymbol{S}_{hp}$ consists of functions $\{\boldsymbol{\xi}_i\}$, $i = 1, \ldots, 2N$, where $N = \dim S_{hp}$ and

$$\boldsymbol{\xi}_i = \begin{cases} (\xi_i, 0), & i = 1, \ldots, N, \\ (0, \xi_i), & i = N+1, \ldots, 2N. \end{cases} \tag{2.38}$$

For details about the basis of the space S_{hp}, see Section 2.1.3.

The approximate solution $\boldsymbol{u}_h(\boldsymbol{x})$ can be expressed as

$$\boldsymbol{u}_h(\boldsymbol{x}) = \sum_{j=1}^{2N} \alpha_j \boldsymbol{\xi}_j(\boldsymbol{x}), \tag{2.39}$$

where $\alpha_i \in \mathbb{R}$, $i = 1, \ldots, 2N$. Plugging this expression into (2.37) and setting $\boldsymbol{v}_h = \boldsymbol{\xi}_i, i = 1, \ldots, 2N$, we arrive at the system of linear algebraic equations

$$\mathbb{K}\boldsymbol{U} = \boldsymbol{b}, \tag{2.40}$$

where

$$\begin{aligned} \mathbb{K} &= \{k_{ij}\}_{i,j=1}^{2N} = \left\{a_h(\boldsymbol{\xi}_j, \boldsymbol{\xi}_i)\right\}_{i,j=1}^{2N}, \\ \boldsymbol{b} &= \{b_j\}_{j=1}^{2N} = b_h(\boldsymbol{\xi}_j), \\ \boldsymbol{U} &= \{\alpha_j\}_{j=1}^{2N}. \end{aligned}$$

Remark. Integrals appearing in the definitions of the forms a_h and b_h are evaluated with the aid of suitable quadrature formulae. The list of the used quadrature formulae is in Section 6.2.

Discretization of the elasticity term

Let us describe in detail the elasticity terms coming from the discretization. The detailed description of the elasticity terms should be helpful for practical use, because it corresponds to their effective implementation. In this section, the approximate solution and the test function is denoted by $\boldsymbol{u}_h$ and $\boldsymbol{v}_h : \Omega_h^b \to \mathbb{R}^2$, respectively, and the unit outer normal to an element boundary is denoted by $\boldsymbol{n} = (n_1, n_2)$.

For $\boldsymbol{u}_h = (p, 0)$, $\boldsymbol{v}_h = (q, 0)$, where $p, q : \Omega_h^b \to \mathbb{R}$, the strain tensors can be expressed as

$$\boldsymbol{e}(\boldsymbol{u}_h) = \begin{pmatrix} \frac{\partial p}{\partial x_1} & \frac{1}{2}\frac{\partial p}{\partial x_2} \\ \frac{1}{2}\frac{\partial p}{\partial x_2} & 0 \end{pmatrix}, \quad \boldsymbol{e}(\boldsymbol{v}_h) = \begin{pmatrix} \frac{\partial q}{\partial x_1} & \frac{1}{2}\frac{\partial q}{\partial x_2} \\ \frac{1}{2}\frac{\partial q}{\partial x_2} & 0 \end{pmatrix}.$$

Thus, the stress tensor for an isotropic homogeneous material is given by

$$\boldsymbol{\sigma}^b(\boldsymbol{u}_h) = \begin{pmatrix} (\lambda + 2\mu)\frac{\partial p}{\partial x_1} & \mu\frac{\partial p}{\partial x_2} \\ \mu\frac{\partial p}{\partial x_2} & \lambda\frac{\partial p}{\partial x_1} \end{pmatrix},$$

which results to the expressions of the elliptic terms

$$\boldsymbol{\sigma}^b(\boldsymbol{u}_h) : \boldsymbol{e}(\boldsymbol{v}_h) = (\lambda + 2\mu)\frac{\partial p}{\partial x_1}\frac{\partial q}{\partial x_1} + \mu\frac{\partial p}{\partial x_2}\frac{\partial q}{\partial x_2}$$

and

$$\left(\boldsymbol{\sigma}^b(\boldsymbol{u}_h) \cdot \boldsymbol{n}\right) \cdot \boldsymbol{v}_h = (\lambda + 2\mu)\frac{\partial p}{\partial x_1} n_1 q + \mu\frac{\partial p}{\partial x_2} n_2 q.$$

For $\boldsymbol{u}_h = (p, 0)$ we receive the following expression of the term appearing in the discretization of the Dirichlet boundary condition:

$$\left(\boldsymbol{\sigma}^b(\boldsymbol{u}_h) \cdot \boldsymbol{n}\right) \cdot \boldsymbol{u}_D = (\lambda + 2\mu)\frac{\partial p}{\partial x_1} n_1 u_{D1} + \mu\frac{\partial p}{\partial x_2} n_2 u_{D1} + \lambda\frac{\partial p}{\partial x_1} n_2 u_{D2} + \mu\frac{\partial p}{\partial x_2} n_1 u_{D2},$$

where $\boldsymbol{u}_D = (u_{D1}, u_{D2}) : \Gamma_D^b \to \mathbb{R}^2$ is the function from condition (1.77).

For $\boldsymbol{u}_h = (0, p)$, and $\boldsymbol{v}_h = (0, q)$, we get the following relations: the strain tensors

$$\boldsymbol{e}(\boldsymbol{u}_h) = \begin{pmatrix} 0 & \frac{1}{2}\frac{\partial p}{\partial x_1} \\ \frac{1}{2}\frac{\partial p}{\partial x_1} & \frac{\partial p}{\partial x_2} \end{pmatrix}, \quad \boldsymbol{e}(\boldsymbol{v}_h) = \begin{pmatrix} 0 & \frac{1}{2}\frac{\partial q}{\partial x_1} \\ \frac{1}{2}\frac{\partial q}{\partial x_1} & \frac{\partial q}{\partial x_2} \end{pmatrix},$$

the stress tensor

$$\boldsymbol{\sigma}^b(\boldsymbol{u}_h) = \begin{pmatrix} \lambda\frac{\partial p}{\partial x_2} & \mu\frac{\partial p}{\partial x_1} \\ \mu\frac{\partial p}{\partial x_1} & (\lambda + 2\mu)\frac{\partial p}{\partial x_2} \end{pmatrix}$$

and the elliptic terms

$$\boldsymbol{\sigma}^b(\boldsymbol{u}_h) : \boldsymbol{e}(\boldsymbol{v}_h) = (\lambda + 2\mu)\frac{\partial p}{\partial x_2}\frac{\partial q}{\partial x_2} + \mu\frac{\partial p}{\partial x_1}\frac{\partial q}{\partial x_1}$$

and

$$\big(\boldsymbol{\sigma}^b(\boldsymbol{u}_h) \cdot \boldsymbol{n}\big) \cdot \boldsymbol{v}_h = (\lambda + 2\mu)\frac{\partial p}{\partial x_2} n_2 q + \mu\frac{\partial p}{\partial x_1} n_1 q.$$

Further, for $\boldsymbol{u}_h = (0, p)$ we have

$$\big(\boldsymbol{\sigma}^b(\boldsymbol{u}_h) \cdot \boldsymbol{n}\big) \cdot \boldsymbol{u}_D = (\lambda + 2\mu)\frac{\partial p}{\partial x_2} n_2 u_{D2} + \mu\frac{\partial p}{\partial x_1} n_1 u_{D2} + \lambda\frac{\partial p}{\partial x_2} n_1 u_{D1} + \mu\frac{\partial p}{\partial x_1} n_2 u_{D1}.$$

For $\boldsymbol{u}_h = (p, 0)$, $\boldsymbol{v}_h = (0, q)$, we express the elliptic terms as

$$\boldsymbol{\sigma}^b(\boldsymbol{u}_h) : \boldsymbol{e}(\boldsymbol{v}_h) = \lambda\frac{\partial p}{\partial x_1}\frac{\partial q}{\partial x_2} + \mu\frac{\partial p}{\partial x_2}\frac{\partial q}{\partial x_1}$$

and

$$\big(\boldsymbol{\sigma}^b(\boldsymbol{u}_h) \cdot \boldsymbol{n}\big) \cdot \boldsymbol{v}_h = \lambda\frac{\partial p}{\partial x_1} n_2 q + \mu\frac{\partial p}{\partial x_2} n_1 q.$$

Finally, for $\boldsymbol{u}_h = (0, p)$ and $\boldsymbol{v}_h = (q, 0)$ we have

$$\boldsymbol{\sigma}^b(\boldsymbol{u}_h) : \boldsymbol{e}(\boldsymbol{v}_h) = \lambda\frac{\partial p}{\partial x_2}\frac{\partial q}{\partial x_1} + \mu\frac{\partial p}{\partial x_1}\frac{\partial q}{\partial x_2}$$

and

$$\big(\boldsymbol{\sigma}^b(\boldsymbol{u}_h) \cdot \boldsymbol{n}\big) \cdot \boldsymbol{v}_h = \lambda\frac{\partial p}{\partial x_2} n_1 q + \mu\frac{\partial p}{\partial x_1} n_2 q.$$

2.2.2 Nonlinear elasticity

In the following, we discretize the static nonlinear elasticity problem by the DGM. However, there are only minor changes in the procedure introduced for the linear elasticity case. Therefore, we go just briefly through the discretizing procedure and concern us mainly with the resulting nonlinear system. The approximate solution will be again sought in the space $\boldsymbol{S}_{hp}$.

Let $\boldsymbol{u} \in \boldsymbol{H}^2(\Omega^b)$ be a sufficiently regular solution of the static nonlinear elasticity problem defined in (1.55) - (1.57). We assume that a triangulation $\mathcal{T}_h^b$ of a domain Ω_h^b is given. We multiply equation (1.55) by a test function $\boldsymbol{v} \in \boldsymbol{S}_{hp}$, integrate the resulting equation over a finite element $K \in \mathcal{T}_h^b$ and use Green's

theorem on the term containing $\boldsymbol{P}$. Finally we sum the resulting equations over all finite elements $K \in \mathcal{T}_h^b$ to obtain the identity

$$\sum_{K\in\mathcal{T}_h^b} \int_K \boldsymbol{P}(\boldsymbol{u}) : \nabla \boldsymbol{v} \,\mathrm{d}\boldsymbol{x} - \sum_{K\in\mathcal{T}_h^b} \int_{\partial K} (\boldsymbol{P}(\boldsymbol{u}) \cdot \boldsymbol{n}_K) \cdot \boldsymbol{v} \,\mathrm{d}S = \sum_{K\in\mathcal{T}_h^b} \int_K \boldsymbol{f} \cdot \boldsymbol{v} \,\mathrm{d}\boldsymbol{x}, \quad (2.41)$$

where $\boldsymbol{n}_K$ denotes the unit outer normal to ∂K. As we can see identity (2.41) is almost identical with (2.21). Further, we reorganize sums over element boundaries ∂K into sums over element edges $\Gamma \in \mathcal{F}_h$ and due to the relation analogous to (2.22), (2.25), and (2.26) we can rewrite (2.41) in the form

$$\begin{aligned} &\sum_{K\in\mathcal{T}_h^b} \int_K \boldsymbol{P}(\boldsymbol{u}) : \nabla \boldsymbol{v} \,\mathrm{d}\boldsymbol{x} - \sum_{\Gamma\in\mathcal{F}_h^{ID}} \int_\Gamma (\langle \boldsymbol{P}(\boldsymbol{u})\rangle \cdot \boldsymbol{n}) \cdot [\boldsymbol{v}] \,\mathrm{d}S \\ &\qquad = \sum_{K\in\mathcal{T}_h^b} \int_K \boldsymbol{f} \cdot \boldsymbol{v} \,\mathrm{d}\boldsymbol{x} + \sum_{\Gamma\in\mathcal{F}_h^N} \int_\Gamma \boldsymbol{g}_N \cdot \boldsymbol{v} \,\mathrm{d}S \quad \forall \boldsymbol{v} \in \boldsymbol{H}^1(\Omega_h^b, \mathcal{T}_h^b). \end{aligned} \quad (2.42)$$

Moreover, to this relation we add the interior and boundary penalty forms $J_h^\eta(\boldsymbol{u}, \boldsymbol{v})$ and the boundary linear form $J_D^\eta(\boldsymbol{v})$ defined in (2.30) and in (2.32), respectively. We consider the penalty weight to be again in the form (2.31). In contrast to the linear elasticity case we do not introduce any symmetry terms and we define only one variant of the DGM denoted by IIPG in the previous section. There is no symmetry as in the linear elasticity case, so it would not make sense to introduce SIPG and NIPG variants of the DGM. The discontinuous Galerkin weak formulation can be written as

$$a_h(\boldsymbol{u}, \boldsymbol{v}) = b_h(\boldsymbol{v}), \quad (2.43)$$

where the semilinear form $a_h(\boldsymbol{u}, \boldsymbol{v})$ and the linear right-hand side functional $b_h(\boldsymbol{v})$ are defined for $\boldsymbol{u}, \boldsymbol{v} \in \boldsymbol{H}^2(\Omega_h^b, \mathcal{T}_h^b)$ by

$$\begin{aligned} a_h(\boldsymbol{u}, \boldsymbol{v}) = &\sum_{K\in\mathcal{T}_h^b} \int_K \boldsymbol{P}(\boldsymbol{u}) : \nabla \boldsymbol{v} \,\mathrm{d}\boldsymbol{x} - \sum_{\Gamma\in\Gamma_{ID}} \int_\Gamma \langle \boldsymbol{P}(\boldsymbol{u})\rangle \boldsymbol{n} \cdot [\boldsymbol{v}] \,\mathrm{d}S + \\ &+ \sum_{\Gamma\in\Gamma_{ID}} \int_\Gamma \frac{C_W^b}{h_\Gamma} [\boldsymbol{u}] \cdot [\boldsymbol{v}] \,\mathrm{d}S, \end{aligned} \quad (2.44)$$

$$b_h(\boldsymbol{v}) = \sum_{K\in\mathcal{T}_h^b} \int_K \boldsymbol{f} \cdot \boldsymbol{v} \,\mathrm{d}\boldsymbol{x} + \sum_{\Gamma\in\Gamma_D} \int_\Gamma \frac{C_W^b}{h_\Gamma} \boldsymbol{u}_D \cdot \boldsymbol{v} \,\mathrm{d}S + \sum_{\Gamma\in\Gamma_N} \int_\Gamma \boldsymbol{g}_N \cdot \boldsymbol{v} \,\mathrm{d}S. \quad (2.45)$$

Consequently, we define the numerical scheme for the solution $\boldsymbol{u}_h \in \boldsymbol{S}_{hp} \subset \boldsymbol{H}^2(\Omega_h^b, \mathcal{T}_h^b)$.

Definition 6. A function $\boldsymbol{u}_h \in \boldsymbol{S}_{hp}$ is called a *dicontinuous approximate solution* of problem (1.76)–(1.78), if it satisifies the identity

$$a_h(\boldsymbol{u}_h, \boldsymbol{v}_h) = b_h(\boldsymbol{v}_h) \quad \forall \boldsymbol{v}_h \in \boldsymbol{S}_{hp}, \quad (2.46)$$

where the forms a_h and b_h are defined by (2.44) and (2.45), respectively.

The form $a_h(\boldsymbol{u}_h, \boldsymbol{v}_h)$ is linear with respect to $\boldsymbol{v}_h$, but nonlinear in $\boldsymbol{u}_h$. For this reason, the problem (2.46) results in a system of nonlinear algebraic equations, which needs to be solved by a suitable nonlinear algebraic solver. Consequently, we apply the Newton method (see [15]). This method was also applied e.g., in the works [33] and [58], where incompressible flow model and conforming finite element discretization were used. Here we put emphasis on the DGM and therefore for the completeness we describe the realization of the method in detail. In the following, we introduce the Newton method in general and we discuss the realization of the discrete nonlinear elasticity problem in detail.

2.2.3 Newton method

Let $\mathcal{F} : \mathbb{R}^N \to \mathbb{R}^N$, $\mathcal{F} \in [C^1(\mathbb{R})]^N$. By $\nabla_{\boldsymbol{\alpha}}\mathcal{F}$ we denote the *Jacobian matrix* of the mapping $\mathcal{F}$:

$$\nabla_{\boldsymbol{\alpha}}\mathcal{F} = \begin{pmatrix} \frac{\partial \mathcal{F}_1}{\partial \alpha_1} & \cdots & \frac{\partial \mathcal{F}_1}{\partial \alpha_N} \\ \vdots & \ddots & \vdots \\ \frac{\partial \mathcal{F}_N}{\partial \alpha_1} & \cdots & \frac{\partial \mathcal{F}_N}{\partial \alpha_N} \end{pmatrix}. \tag{2.47}$$

We seek a solution $\boldsymbol{\alpha} \in \mathbb{R}^N$ such that $\mathcal{F}(\boldsymbol{\alpha}) = 0$. The Newton algorithm to obtain a solution is the following: let $\boldsymbol{\alpha}^{(0)}$ be an initial guess of the sought solution and let $\varepsilon > 0$ be a given tolerance. For $i \geq 0$ iterate:

1. Evaluate the residual
$$\boldsymbol{r}^{(i)} = \mathcal{F}\left(\boldsymbol{\alpha}^{(i)}\right). \tag{2.48}$$
2. Check residual and stop iterations with $\boldsymbol{\alpha} = \boldsymbol{\alpha}^{(i)}$ if
$$\left\|\boldsymbol{r}^{(i)}\right\| \leq \varepsilon. \tag{2.49}$$
3. Compute $\delta\boldsymbol{\alpha}$ from
$$\nabla_{\boldsymbol{\alpha}}\mathcal{F}\left(\boldsymbol{\alpha}^{(i)}\right)\delta\boldsymbol{\alpha} = \boldsymbol{r}^{(i)}. \tag{2.50}$$
4. Update
$$\boldsymbol{\alpha}^{(i+1)} := \boldsymbol{\alpha}^{(i)} - \delta\boldsymbol{\alpha}. \tag{2.51}$$
5. Set $i = i + 1$ and go to 1.

Note that (2.50) represents a system of linear algebraic equations, which needs to be solved by a suitable direct or iterative solver.

2.2.4 Realization of the discrete nonlinear elasticity problem

We shall now briefly discuss the application of the Newton method to our discretization of the nonlinear elasticity problem. We can express the sought approximate solution as a linear combination of basis functions in the space $\boldsymbol{S}_{hp}$. Let $\{\boldsymbol{\xi}_i\}, i = 1, \ldots, 2N$, form the basis of $\boldsymbol{S}_{hp}$ as in (2.38). Then the sought solution $\boldsymbol{u}_h$ can be expressed as

$$\boldsymbol{u}_h = \boldsymbol{u}_h(\boldsymbol{\alpha}) = \sum_{i=1}^{2N} \alpha_i \boldsymbol{\xi}_i, \tag{2.52}$$

where $\boldsymbol{\alpha} = (\alpha_i)_{i=1}^{2N}$ is formed by the finite element coefficients.

In order to apply the Newton method as defined in Section 2.2.3, we must differentiate the form $a_h(\boldsymbol{u}_h(\boldsymbol{\alpha}), \boldsymbol{v}_h)$ (and subsequently the tensor $\boldsymbol{P}$) with respect to the coefficients $\alpha_1, \ldots, \alpha_N$. For clarity, we shall denote the gradient with respect to $\boldsymbol{\alpha}$ by $\nabla_{\boldsymbol{\alpha}}$ and the gradient with respect to $\boldsymbol{x}$ by $\nabla_{\boldsymbol{x}}$. Clearly

$$\begin{aligned} \frac{\partial}{\partial \alpha_k} \boldsymbol{u}_h &= (\xi_i, 0)\,, \quad 1 \le k \le N,\ i = k, \\ \frac{\partial}{\partial \alpha_k} \boldsymbol{u}_h &= (0, \xi_i)\,, \quad N < k \le 2N,\ i = k - N, \end{aligned} \tag{2.53}$$

and

$$\begin{aligned} \nabla_x \boldsymbol{u}_h &= \sum_{i=1}^{N} \alpha_i \nabla_x (\xi_i, 0) + \sum_{i=1}^{N} \alpha_{i+N} \nabla_x (0, \xi_i) = \\ &= \begin{pmatrix} \sum_{i=1}^{N} \alpha_i \frac{\partial \xi_i}{\partial x_1}, & \sum_{i=1}^{N} \alpha_i \frac{\partial \xi_i}{\partial x_2} \\ \sum_{i=1}^{N} \alpha_{i+N} \frac{\partial \xi_i}{\partial x_1}, & \sum_{i=1}^{N} \alpha_{i+N} \frac{\partial \xi_i}{\partial x_2} \end{pmatrix}. \end{aligned} \tag{2.54}$$

The gradient of the form a_h can be expressed as

$$\begin{aligned} \nabla_{\boldsymbol{\alpha}} a_h(\boldsymbol{u}_h(\boldsymbol{\alpha}), \boldsymbol{v}_h) = &\sum_{K \in \mathcal{T}_h^d} \int_K \nabla_{\boldsymbol{\alpha}} \left(\boldsymbol{P}\left(\boldsymbol{u}_h(\boldsymbol{\alpha})\right) : \nabla_x \boldsymbol{v}_h \right) \mathrm{d}\boldsymbol{x} \\ &- \sum_{\Gamma \in \mathcal{F}_h^{bID}} \int_\Gamma \nabla_{\boldsymbol{\alpha}} \left(\langle \boldsymbol{P}\left(\boldsymbol{u}_h(\boldsymbol{\alpha})\right) \rangle \boldsymbol{n} \cdot [\boldsymbol{v}_h] \right) \mathrm{d}S \\ &+ \sum_{\Gamma \in \mathcal{F}_h^{bID}} \int_\Gamma \frac{C_W^b}{h_\Gamma} \nabla_{\boldsymbol{\alpha}} \left([\boldsymbol{u}_h(\boldsymbol{\alpha})] \cdot [\boldsymbol{v}_h] \right) \mathrm{d}S. \end{aligned} \tag{2.55}$$

Let $\boldsymbol{P}\left(\boldsymbol{u}_h(\boldsymbol{\alpha})\right) = (P_{ij})_{i,j=1}^2$ (here for simplicity we do not explicitly write the dependence of P_{ij} on $\boldsymbol{u}_h(\boldsymbol{\alpha})$) and let $\boldsymbol{v}_h = (v_1, v_2)$. From the relation

$$\boldsymbol{P}\left(\boldsymbol{u}_h(\boldsymbol{\alpha})\right) : \nabla_x \boldsymbol{v}_h = P_{11} \frac{\partial v_1}{\partial x_1} + P_{12} \frac{\partial v_1}{\partial x_2} + P_{21} \frac{\partial v_2}{\partial x_1} + P_{22} \frac{\partial v_2}{\partial x_2}, \tag{2.56}$$

it follows that

$$\begin{aligned} \frac{\partial}{\partial \alpha_k} \left(\boldsymbol{P}\left(\boldsymbol{u}_h(\boldsymbol{\alpha})\right) : \nabla_x \boldsymbol{v}_h \right) &= \frac{\partial}{\partial \alpha_k} P_{11} \frac{\partial v_1}{\partial x_1} + \frac{\partial}{\partial \alpha_k} P_{12} \frac{\partial v_1}{\partial x_2} \\ &\quad + \frac{\partial}{\partial \alpha_k} P_{21} \frac{\partial v_2}{\partial x_1} + \frac{\partial}{\partial \alpha_k} P_{22} \frac{\partial v_2}{\partial x_2}, \\ \frac{\partial}{\partial \alpha_k} \left(\langle \boldsymbol{P}\left(\boldsymbol{u}_h(\boldsymbol{\alpha})\right) \rangle \boldsymbol{n} \cdot [\boldsymbol{v}_h] \right) &= \left(\frac{\partial}{\partial \alpha_k} \langle P_{11} \rangle n_1 + \frac{\partial}{\partial \alpha_k} \langle P_{12} \rangle n_2 \right) [v_1] \\ &\quad + \left(\frac{\partial}{\partial \alpha_k} \langle P_{21} \rangle n_1 + \frac{\partial}{\partial \alpha_k} \langle P_{22} \rangle n_2 \right) [v_2]\,. \end{aligned} \tag{2.57}$$

Now for $\boldsymbol{v}_h = (\xi_j, 0)$ we have

$$\boldsymbol{P}\left(\boldsymbol{u}_h(\boldsymbol{\alpha})\right) : \nabla_x \boldsymbol{v}_h = P_{11} \frac{\partial \xi_j}{\partial x_1} + P_{12} \frac{\partial \xi_j}{\partial x_2}, \tag{2.58}$$

$$\frac{\partial}{\partial \alpha_k} \left(\boldsymbol{P}\left(\boldsymbol{u}_h(\boldsymbol{\alpha})\right) : \nabla_x \boldsymbol{v}_h \right) = \frac{\partial}{\partial \alpha_k} P_{11} \frac{\partial \xi_j}{\partial x_1} + \frac{\partial}{\partial \alpha_k} P_{12} \frac{\partial \xi_j}{\partial x_2}, \tag{2.59}$$

$$\frac{\partial}{\partial \alpha_k} \left(\langle \boldsymbol{P}\left(\boldsymbol{u}_h(\boldsymbol{\alpha})\right) \rangle \boldsymbol{n} \cdot [\boldsymbol{v}_h] \right) = \left(\frac{\partial}{\partial \alpha_k} \langle P_{11} \rangle n_1 + \frac{\partial}{\partial \alpha_k} \langle P_{12} \rangle n_2 \right) [\xi_j]\,, \tag{2.60}$$

while for $\boldsymbol{v}_h = (0, \xi_j)$ we have

$$\boldsymbol{P}\left(\boldsymbol{u}_h(\boldsymbol{\alpha})\right) : \nabla_x \boldsymbol{v}_h = P_{21}\frac{\partial \xi_j}{\partial x_1} + P_{22}\frac{\partial \xi_j}{\partial x_2}, \tag{2.61}$$

$$\frac{\partial}{\partial \alpha_k}\left(\boldsymbol{P}\left(\boldsymbol{u}_h(\boldsymbol{\alpha})\right) : \nabla_x \boldsymbol{v}_h\right) = \frac{\partial}{\partial \alpha_k}P_{21}\frac{\partial \xi_j}{\partial x_1} + \frac{\partial}{\partial \alpha_k}P_{22}\frac{\partial \xi_j}{\partial x_2}, \tag{2.62}$$

$$\frac{\partial}{\partial \alpha_k}\left(\left\langle \boldsymbol{P}\left(\boldsymbol{u}_h(\boldsymbol{\alpha})\right)\right\rangle \boldsymbol{n} \cdot [\boldsymbol{v}_h]\right) = \left(\frac{\partial}{\partial \alpha_k}\left\langle P_{21}\right\rangle n_1 + \frac{\partial}{\partial \alpha_k}\left\langle P_{22}\right\rangle n_2\right)[\xi_j]. \tag{2.63}$$

It remains to express the derivatives of the tensor $\boldsymbol{P}$ for our choice of the St. Venant-Kirchhoff and neo-Hookean material, which can be found in Section 2.2.5 and Section 2.2.6 respectively.

Remark. Integrals appearing in the definition of the gradient $\nabla_{\boldsymbol{\alpha}} a_h$ and in the form b_h are evaluated with the aid of suitable quadrature formulae. The list of the used quadrature formulae is in Section 6.2.

2.2.5 St. Venant-Kirchhoff material - derivatives

Let $\boldsymbol{P} = \boldsymbol{P}(\boldsymbol{u}_h(\boldsymbol{\alpha})) = (P_{ij})_{i,j=1}^2$ be the first Piola-Kirchhoff tensor of the St. Venant-Kirchhoff material as defined in (1.70). Let $\boldsymbol{u}_h(\boldsymbol{\alpha}) = (u_1, u_2)$. From (1.17), (1.70) and (1.63) we get

$$\begin{aligned} P_{11} = {} & \mu\frac{\partial u_1}{\partial x_2}\frac{\partial u_2}{\partial x_1}\left(\frac{\partial u_2}{\partial x_2}+1\right) + \frac{\lambda}{2}\left(\frac{\partial u_1}{\partial x_1}+1\right)\left(\left(\frac{\partial u_2}{\partial x_2}+1\right)^2 - 1\right) \\ & + \left(\mu + \frac{\lambda}{2}\right)\left(\frac{\partial u_1}{\partial x_1}+1\right)\left(\frac{\partial u_1}{\partial x_2}^2 + \frac{\partial u_2}{\partial x_1}^2 + \left(\frac{\partial u_1}{\partial x_1}+1\right)^2 - 1\right), \end{aligned} \tag{2.64}$$

$$\begin{aligned} P_{12} = {} & \mu\left(\frac{\partial u_1}{\partial x_1}+1\right)\frac{\partial u_2}{\partial x_1}\left(\frac{\partial u_2}{\partial x_2}+1\right) + \frac{\lambda}{2}\frac{\partial u_1}{\partial x_2}\left(\frac{\partial u_2}{\partial x_1}^2 - 1\right) \\ & + \left(\mu + \frac{\lambda}{2}\right)\frac{\partial u_1}{\partial x_2}\left(\frac{\partial u_1}{\partial x_2}^2 + \left(\frac{\partial u_1}{\partial x_1}+1\right)^2 + \left(\frac{\partial u_2}{\partial x_2}+1\right)^2 - 1\right), \end{aligned} \tag{2.65}$$

$$\begin{aligned} P_{21} = {} & \mu\left(\frac{\partial u_2}{\partial x_2}+1\right)\frac{\partial u_1}{\partial x_2}\left(\frac{\partial u_1}{\partial x_1}+1\right) + \frac{\lambda}{2}\frac{\partial u_2}{\partial x_1}\left(\frac{\partial u_1}{\partial x_2}^2 - 1\right) \\ & + \left(\mu + \frac{\lambda}{2}\right)\frac{\partial u_2}{\partial x_1}\left(\frac{\partial u_2}{\partial x_1}^2 + \left(\frac{\partial u_1}{\partial x_1}+1\right)^2 + \left(\frac{\partial u_2}{\partial x_2}+1\right)^2 - 1\right), \end{aligned} \tag{2.66}$$

$$\begin{aligned} P_{22} = {} & \mu\frac{\partial u_2}{\partial x_1}\frac{\partial u_1}{\partial x_2}\left(\frac{\partial u_1}{\partial x_1}+1\right) + \frac{\lambda}{2}\left(\frac{\partial u_2}{\partial x_2}+1\right)\left(\left(\frac{\partial u_1}{\partial x_1}+1\right)^2 - 1\right) \\ & + \left(\mu + \frac{\lambda}{2}\right)\left(\frac{\partial u_2}{\partial x_2}+1\right)\left(\frac{\partial u_1}{\partial x_2}^2 + \frac{\partial u_2}{\partial x_1}^2 + \left(\frac{\partial u_2}{\partial x_2}+1\right)^2 - 1\right). \end{aligned} \tag{2.67}$$

Now let $\boldsymbol{u}_h(\boldsymbol{\alpha}) = (u_1, u_2) = \sum_{k=1}^{2N} \alpha_k \boldsymbol{\xi}_k$, where $\boldsymbol{\xi}_k = (\xi_k, 0)$ for $1 \leq k \leq N$ and $\boldsymbol{\xi}_k = (0, \xi_{k-N})$ for $N < k \leq 2N$. The derivatives of $\boldsymbol{P}(\boldsymbol{u}_h(\boldsymbol{\alpha}))$ with respect to the coefficient α_k are given as follows: For $1 \leq k \leq N$ we set $i = k$ and we get

$$\begin{aligned}\frac{\partial}{\partial \alpha_k} P_{11} &= \mu \frac{\partial \xi_i}{\partial x_2} \frac{\partial u_2}{\partial x_1} \left(\frac{\partial u_2}{\partial x_2} + 1 \right) + \frac{\lambda}{2} \frac{\partial \xi_i}{\partial x_1} \left(\left(\frac{\partial u_2}{\partial x_2} + 1 \right)^2 - 1 \right) \\ &\quad + \left(\mu + \frac{\lambda}{2} \right) \frac{\partial \xi_i}{\partial x_1} \left(\frac{\partial u_1}{\partial x_2}^2 + \frac{\partial u_2}{\partial x_1}^2 + \left(\frac{\partial u_1}{\partial x_1} + 1 \right)^2 - 1 \right) \\ &\quad + 2 \left(\mu + \frac{\lambda}{2} \right) \left(\frac{\partial u_1}{\partial x_1} + 1 \right) \left(\frac{\partial u_1}{\partial x_2} \frac{\partial \xi_i}{\partial x_2} + \left(\frac{\partial u_1}{\partial x_1} + 1 \right) \frac{\partial \xi_i}{\partial x_1} \right), \end{aligned} \tag{2.68}$$

$$\begin{aligned}\frac{\partial}{\partial \alpha_k} P_{12} &= \mu \frac{\partial \xi_i}{\partial x_1} \frac{\partial u_2}{\partial x_1} \left(\frac{\partial u_2}{\partial x_2} + 1 \right) + \frac{\lambda}{2} \frac{\partial \xi_i}{\partial x_2} \left(\frac{\partial u_2}{\partial x_1}^2 - 1 \right) \\ &\quad + \left(\mu + \frac{\lambda}{2} \right) \frac{\partial \xi_i}{\partial x_2} \left(\frac{\partial u_1}{\partial x_2}^2 + \left(\frac{\partial u_1}{\partial x_1} + 1 \right)^2 + \left(\frac{\partial u_2}{\partial x_2} + 1 \right)^2 - 1 \right) \\ &\quad + 2 \left(\mu + \frac{\lambda}{2} \right) \frac{\partial u_1}{\partial x_2} \left(\frac{\partial u_1}{\partial x_2} \frac{\partial \xi_i}{\partial x_2} + \left(\frac{\partial u_1}{\partial x_1} + 1 \right) \frac{\partial \xi_i}{\partial x_1} \right), \end{aligned} \tag{2.69}$$

$$\begin{aligned}\frac{\partial}{\partial \alpha_k} P_{21} &= \mu \left(\frac{\partial u_2}{\partial x_2} + 1 \right) \frac{\partial \xi_i}{\partial x_2} \left(\frac{\partial u_1}{\partial x_1} + 1 \right) + \mu \left(\frac{\partial u_2}{\partial x_2} + 1 \right) \frac{\partial u_1}{\partial x_2} \frac{\partial \xi_i}{\partial x_1} \\ &\quad + \lambda \frac{\partial u_2}{\partial x_1} \frac{\partial u_1}{\partial x_2} \frac{\partial \xi_i}{\partial x_2} + 2 \left(\mu + \frac{\lambda}{2} \right) \frac{\partial u_2}{\partial x_1} \left(\frac{\partial u_1}{\partial x_1} + 1 \right) \frac{\partial \xi_i}{\partial x_1}, \end{aligned} \tag{2.70}$$

$$\begin{aligned}\frac{\partial}{\partial \alpha_k} P_{22} &= \mu \frac{\partial u_2}{\partial x_1} \frac{\partial \xi_i}{\partial x_2} \left(\frac{\partial u_1}{\partial x_1} + 1 \right) + \mu \frac{\partial u_2}{\partial x_1} \frac{\partial u_1}{\partial x_2} \frac{\partial \xi_i}{\partial x_1} \\ &\quad + \lambda \left(\frac{\partial u_2}{\partial x_2} + 1 \right) \left(\frac{\partial u_1}{\partial x_1} + 1 \right) \frac{\partial \xi_i}{\partial x_1} + 2 \left(\mu + \frac{\lambda}{2} \right) \left(\frac{\partial u_2}{\partial x_2} + 1 \right) \frac{\partial u_1}{\partial x_2} \frac{\partial \xi_i}{\partial x_2}. \end{aligned} \tag{2.71}$$

For $N < k \leq 2N$ we set $i := k - N$ and get

$$\begin{aligned}\frac{\partial}{\partial \alpha_k} P_{11} &= \mu \frac{\partial u_1}{\partial x_2} \frac{\partial \xi_i}{\partial x_1} \left(\frac{\partial u_2}{\partial x_2} + 1 \right) + \mu \frac{\partial u_1}{\partial x_2} \frac{\partial u_2}{\partial x_1} \frac{\partial \xi_i}{\partial x_2} \\ &\quad + \lambda \left(\frac{\partial u_1}{\partial x_1} + 1 \right) \left(\frac{\partial u_2}{\partial x_2} + 1 \right) \frac{\partial \xi_i}{\partial x_2} + 2 \left(\mu + \frac{\lambda}{2} \right) \left(\frac{\partial u_1}{\partial x_1} + 1 \right) \frac{\partial u_2}{\partial x_1} \frac{\partial \xi_i}{\partial x_1}, \end{aligned} \tag{2.72}$$

$$\begin{aligned}\frac{\partial}{\partial \alpha_k} P_{12} &= \mu \left(\frac{\partial u_1}{\partial x_1} + 1 \right) \frac{\partial \xi_i}{\partial x_1} \left(\frac{\partial u_2}{\partial x_2} + 1 \right) + \mu \left(\frac{\partial u_1}{\partial x_1} + 1 \right) \frac{\partial u_2}{\partial x_1} \frac{\partial \xi_i}{\partial x_2} \\ &\quad + \lambda \frac{\partial u_1}{\partial x_2} \frac{\partial u_2}{\partial x_1} \frac{\partial \xi_i}{\partial x_1} + 2 \left(\mu + \frac{\lambda}{2} \right) \frac{\partial u_1}{\partial x_2} \left(\frac{\partial u_2}{\partial x_2} + 1 \right) \frac{\partial \xi_i}{\partial x_2}, \end{aligned} \tag{2.73}$$

$$\begin{aligned}\frac{\partial}{\partial \alpha_k} P_{21} &= \mu \frac{\partial \xi_i}{\partial x_2} \frac{\partial u_1}{\partial x_2} \left(\frac{\partial u_1}{\partial x_1} + 1 \right) + \frac{\lambda}{2} \frac{\partial \xi_i}{\partial x_1} \left(\frac{\partial u_1}{\partial x_2}^2 - 1 \right) \\ &\quad + \left(\mu + \frac{\lambda}{2} \right) \frac{\partial \xi_i}{\partial x_1} \left(\frac{\partial u_2}{\partial x_1}^2 + \left(\frac{\partial u_1}{\partial x_1} + 1 \right)^2 + \left(\frac{\partial u_2}{\partial x_2} + 1 \right)^2 - 1 \right) \\ &\quad + 2 \left(\mu + \frac{\lambda}{2} \right) \frac{\partial u_2}{\partial x_1} \left(\frac{\partial u_2}{\partial x_1} \frac{\partial \xi_i}{\partial x_1} + \left(\frac{\partial u_2}{\partial x_2} + 1 \right) \frac{\partial \xi_i}{\partial x_2} \right), \end{aligned} \tag{2.74}$$

$$\frac{\partial}{\partial \alpha_k} P_{22} = \mu \frac{\partial \xi_i}{\partial x_1} \frac{\partial u_1}{\partial x_2} \left(\frac{\partial u_1}{\partial x_1} + 1 \right) + \frac{\lambda}{2} \frac{\partial \xi_i}{\partial x_2} \left(\left(\frac{\partial u_1}{\partial x_1} + 1 \right)^2 - 1 \right)$$
$$+ \left(\mu + \frac{\lambda}{2} \right) \frac{\partial \xi_i}{\partial x_2} \left(\frac{\partial u_1}{\partial x_2}^2 + \frac{\partial u_2}{\partial x_1}^2 + \left(\frac{\partial u_2}{\partial x_2} + 1 \right)^2 - 1 \right)$$
$$+ 2 \left(\mu + \frac{\lambda}{2} \right) \left(\frac{\partial u_2}{\partial x_2} + 1 \right) \left(\frac{\partial u_2}{\partial x_1} \frac{\partial \xi_i}{\partial x_1} + \left(\frac{\partial u_2}{\partial x_2} + 1 \right) \frac{\partial \xi_i}{\partial x_2} \right). \tag{2.75}$$

2.2.6 Neo-Hookean material - derivatives

Analogously to the case of St. Venant-Kirchhoff material let $\boldsymbol{P} = \boldsymbol{P}(\boldsymbol{u}_h(\boldsymbol{\alpha})) = (P_{ij})_{i,j=1}^2$ be the first Piola-Kirchhoff tensor of the neo-Hookean material as defined in (1.65). Let $\boldsymbol{u}_h(\boldsymbol{\alpha}) = (u_1, u_2)$. From (1.17), (1.8) and (1.65) we get

$$P_{11} = \mu \left(1 + \frac{\partial u_1}{\partial x_1} \right) + c_1 \left(1 + \frac{\partial u_2}{\partial x_2} \right), \tag{2.76}$$
$$P_{12} = \mu \frac{\partial u_1}{\partial x_2} - c_1 \frac{\partial u_2}{\partial x_1}, \tag{2.77}$$
$$P_{21} = \mu \frac{\partial u_2}{\partial x_1} - c_1 \frac{\partial u_1}{\partial x_2}, \tag{2.78}$$
$$P_{22} = \mu \left(1 + \frac{\partial u_2}{\partial x_2} \right) + c_1 \left(1 + \frac{\partial u_1}{\partial x_1} \right), \tag{2.79}$$

where

$$c_1 = \frac{\lambda \log(\det \boldsymbol{F}) - \mu}{\det \boldsymbol{F}}. \tag{2.80}$$

Now let $\boldsymbol{u}_h(\boldsymbol{\alpha}) = (u_1, u_2) = \sum_{k=1}^{2N} \alpha_k \boldsymbol{\xi}_k$, where $\boldsymbol{\xi}_k = (\xi_k, 0)$ for $1 \leq k \leq N$ and $\boldsymbol{\xi}_k = (0, \xi_{k-N})$ for $N < k \leq 2N$.

Let us express at first the derivative of the determinant of $\boldsymbol{F}$ with respect to the coefficient α_k. If $1 \leq k \leq N$ and $i := k$, then

$$\frac{\partial}{\partial \alpha_k} (\det \boldsymbol{F}) = \frac{\partial \xi_i}{\partial x_1} \left(\frac{\partial u_2}{\partial x_2} + 1 \right) - \frac{\partial \xi_i}{\partial x_2} \frac{\partial u_2}{\partial x_1}, \tag{2.81}$$

and for $N < k \leq 2N$, $i := k - N$:

$$\frac{\partial}{\partial \alpha_k} (\det \boldsymbol{F}) = \frac{\partial \xi_i}{\partial x_2} \left(\frac{\partial u_1}{\partial x_1} + 1 \right) - \frac{\partial \xi_i}{\partial x_1} \frac{\partial u_1}{\partial x_2}. \tag{2.82}$$

The derivatives of $\boldsymbol{P}(\boldsymbol{u}_h(\boldsymbol{\alpha}))$ with respect to the coefficient α_k are given as follows: If $1 \leq k \leq N$ and $i := k$, then

$$\frac{\partial}{\partial \alpha_k} P_{11} = \mu \frac{\partial \xi_i}{\partial x_1} + c_2 \frac{\partial}{\partial \alpha_k} (\det \boldsymbol{F}) \left(1 + \frac{\partial u_2}{\partial x_2} \right), \tag{2.83}$$
$$\frac{\partial}{\partial \alpha_k} P_{12} = \mu \frac{\partial \xi_i}{\partial x_2} - c_2 \frac{\partial}{\partial \alpha_k} (\det \boldsymbol{F}) \frac{\partial u_2}{\partial x_1}, \tag{2.84}$$
$$\frac{\partial}{\partial \alpha_k} P_{21} = -c_1 \frac{\partial \xi_i}{\partial x_2} - c_2 \frac{\partial}{\partial \alpha_k} (\det \boldsymbol{F}) \frac{\partial u_1}{\partial x_2}, \tag{2.85}$$
$$\frac{\partial}{\partial \alpha_k} P_{22} = c_1 \frac{\partial \xi_i}{\partial x_1} + c_2 \frac{\partial}{\partial \alpha_k} (\det \boldsymbol{F}) \left(1 + \frac{\partial u_1}{\partial x_1} \right), \tag{2.86}$$

where c_1 is as in (2.80),

$$c_2 = \frac{\lambda - \lambda \log(\det \boldsymbol{F}) + \mu}{\det \boldsymbol{F}}, \tag{2.87}$$

and $\frac{\partial}{\partial \alpha_k}(\det \boldsymbol{F})$ is expressed in (2.81).

Finally for $N < k \leq 2N$ we set $i = k - N$ and get

$$\frac{\partial}{\partial \alpha_k} P_{11} = c_1 \frac{\partial \xi_i}{\partial x_2} + c_2 \frac{\partial}{\partial \alpha_k}(\det \boldsymbol{F}) \left(1 + \frac{\partial u_2}{\partial x_2}\right), \tag{2.88}$$

$$\frac{\partial}{\partial \alpha_k} P_{12} = -c_1 \frac{\partial \xi_i}{\partial x_1} - c_2 \frac{\partial}{\partial \alpha_k}(\det \boldsymbol{F}) \frac{\partial u_2}{\partial x_1}, \tag{2.89}$$

$$\frac{\partial}{\partial \alpha_k} P_{21} = \mu \frac{\partial \xi_i}{\partial x_1} - c_2 \frac{\partial}{\partial \alpha_k}(\det \boldsymbol{F}) \frac{\partial u_1}{\partial x_2}, \tag{2.90}$$

$$\frac{\partial}{\partial \alpha_k} P_{22} = \mu \frac{\partial \xi_i}{\partial x_2} + c_2 \frac{\partial}{\partial \alpha_k}(\det \boldsymbol{F}) \left(1 + \frac{\partial u_1}{\partial x_1}\right) \tag{2.91}$$

where c_1 is as in (2.80), c_2 as in (2.87) and $\frac{\partial}{\partial \alpha_k}(\det \boldsymbol{F})$ is expressed in (2.82).

2.3 Discretization of the dynamic elasticity problem

In this section we introduce the discretization of both the dynamic linear elasticity problem (1.72)-(1.75) and the dynamic nonlinear elasticity problem (1.51)-(1.54). For simplicity, we shall only describe the discretization of the dynamic nonlinear elasticity equation. The discretization of the dynamic linear elasticity equation can be carried out analogously, because the main differences are already described in the previous section.

Because of the time discretization of problem (1.51)-(1.54), we rewrite it as the following problem of first-order in time for the displacement $\boldsymbol{u} : \Omega^b \times [0,T] \to \mathbb{R}^2$ and the deformation velocity $\boldsymbol{z} : \Omega^b \times [0,T] \to \mathbb{R}^2$:

$$\rho^b \frac{\partial \boldsymbol{z}}{\partial t} + C_M \rho^b \boldsymbol{z} - \operatorname{div} \boldsymbol{P} = \boldsymbol{f} \qquad \text{in } \Omega^b \times [0,T], \tag{2.92}$$

$$\frac{\partial \boldsymbol{u}}{\partial t} - \boldsymbol{z} = 0 \qquad \text{in } \Omega^b \times [0,T], \tag{2.93}$$

$$\boldsymbol{u} = \boldsymbol{u}_D \qquad \text{in } \Gamma_D^b \times [0,T], \tag{2.94}$$

$$\boldsymbol{P} \cdot \boldsymbol{n} = \boldsymbol{g}_N \qquad \text{in } \Gamma_N^b \times [0,T], \tag{2.95}$$

$$\boldsymbol{u}(\cdot,0) = \boldsymbol{u}_0, \quad \boldsymbol{z}(\cdot,0) = \boldsymbol{v}_0^b \qquad \text{in } \Omega^b. \tag{2.96}$$

Let us note that the deformation velocity $\boldsymbol{z}$ is equal to the velocity $\boldsymbol{v}^b$ defined in (1.23). The reason for the use of another notation is the better distinction to the test functions denoted by $\boldsymbol{v}$.

First, we introduce the discretization in space of the dynamic nonlinear elasticity equation, which is carried out analogously to the static elasticity problem. The time variable is left continuous. This means that we deal with the *space semidiscretization*. The elasticity terms are discretized in space by interior

penalty Galerkin technique (IIPG and for linear elasticity also NIPG and SIPG) introduced in the previous section.

In the derivation of the space discretization by the DGM the following process is essential. We multiply equations (2.92) and (2.93) by a test function $\boldsymbol{v} \in \boldsymbol{H}^2(\Omega_h^b, \mathcal{T}_h^b)$, integrate the resulting relations over elements $K \in \mathcal{T}_h^b$, apply Green's theorem to the term containing $\boldsymbol{P}$, add the interior and boundary penalty and in case of linear elasticity also the stabilization terms, use boundary conditions and sum over all elements. Moreover, we introduce the scalar product in $\boldsymbol{L}^2(\Omega_h^b) = L^2(\Omega_h^b) \times L^2(\Omega_h^b)$:

$$(\boldsymbol{u}, \boldsymbol{v})_{\Omega_h^b} = \int_{\Omega_h^b} \boldsymbol{u} \cdot \boldsymbol{v} \, \mathrm{d}\boldsymbol{x} = \sum_{K \in \mathcal{T}_h^b} \int_K \boldsymbol{u} \cdot \boldsymbol{v} \, \mathrm{d}\boldsymbol{x}, \quad \boldsymbol{u}, \boldsymbol{v} \in \boldsymbol{L}^2(\Omega_h^b). \tag{2.97}$$

We obtain the identities

$$\left(\rho^b \frac{\partial \boldsymbol{z}(t)}{\partial t}, \boldsymbol{v}\right)_{\Omega_h^b} + \left(C_M \rho^b \boldsymbol{z}(t), \boldsymbol{v}\right)_{\Omega_h^b} + a_h(\boldsymbol{u}(t), \boldsymbol{v}) = b(\boldsymbol{v})(t) \tag{2.98}$$

$$\forall \boldsymbol{v} \in \boldsymbol{H}^2(\Omega_h^b, \mathcal{T}_h^b), \forall t \in [0, T],$$

$$\left(\frac{\partial \boldsymbol{u}(t)}{\partial t}, \boldsymbol{v}\right)_{\Omega_h^b} - (\boldsymbol{z}, \boldsymbol{v})_{\Omega_h^b} = 0 \tag{2.99}$$

$$\forall \boldsymbol{v} \in \boldsymbol{H}^2(\Omega_h^b, \mathcal{T}_h^b), \forall t \in [0, T],$$

$$(\boldsymbol{u}(0), \boldsymbol{v})_{\Omega_h^b} = (\boldsymbol{u}_0, \boldsymbol{v})_{\Omega_h^b}, \quad (\boldsymbol{z}(0), \boldsymbol{v})_{\Omega_h^b} = \left(\boldsymbol{v}_0^b, \boldsymbol{v}\right)_{\Omega_h^b} \tag{2.100}$$

$$\forall \boldsymbol{v} \in \boldsymbol{H}^2(\Omega_h^b, \mathcal{T}_h^b).$$

By $\boldsymbol{u}(t)$, $\boldsymbol{z}(t)$ we denote the functions in Ω_h^b such that $(\boldsymbol{u}(t))(\boldsymbol{x}) = \boldsymbol{u}(\boldsymbol{x}, t)$, $(\boldsymbol{z}(t))(\boldsymbol{x}) = \boldsymbol{z}(\boldsymbol{x}, t)$, $\boldsymbol{x} \in \Omega_h^b$, respectively. The forms $\boldsymbol{a}_h$, $\boldsymbol{b}_h$ are defined as in (2.44) and (2.45), respectively and for the linear elasticity they are defined as in (2.35) and (2.36), respectively.

Let $\boldsymbol{S}_{hp}$ be the space of discontinuous piecewise polynomial functions defined in (2.18). Since $\boldsymbol{S}_{hp} \subset \boldsymbol{H}^2(\Omega_h^b, \mathcal{T}_h^b) \cap \boldsymbol{L}^\infty(\Omega_h^b)$, the forms $\boldsymbol{a}_h$, $\boldsymbol{b}_h$ make sense for $\boldsymbol{u} := \boldsymbol{u}_h$, $\boldsymbol{v} := \boldsymbol{v}_h \in \boldsymbol{S}_{hp}$. Then we introduce the discontinuous Galerkin space semidiscretization of (2.92)-(2.96).

Definition 7. We define the *semidiscrete approximate solution* of (2.92)-(2.96) as a displacement function $\boldsymbol{u}_h : \Omega_h^b \times [0, T] \to \mathbb{R}^2$ and a deformation velocity function $\boldsymbol{z}_h : \Omega_h^b \times [0, T] \to \mathbb{R}^2$ satisfying the conditions

$$\boldsymbol{u}_h \in \boldsymbol{C}^1([0, T]; \boldsymbol{S}_{hp}), \boldsymbol{z}_h \in \boldsymbol{C}^1([0, T]; \boldsymbol{S}_{hp}), \tag{2.101}$$

$$\left(\rho^b \frac{\partial \boldsymbol{z}_h(t)}{\partial t}, \boldsymbol{v}_h\right)_{\Omega_h^b} + \left(C_M \rho^b \boldsymbol{z}_h(t), \boldsymbol{v}_h\right)_{\Omega_h^b} + a_h(\boldsymbol{u}_h(t), \boldsymbol{v}_h) = b(\boldsymbol{v}_h)(t) \tag{2.102}$$

$$\forall \boldsymbol{v}_h \in \boldsymbol{S}_{hp}, \forall t \in [0, T],$$

$$\left(\frac{\partial \boldsymbol{u}_h(t)}{\partial t}, \boldsymbol{v}_h\right)_{\Omega_h^b} - (\boldsymbol{z}_h(t), \boldsymbol{v}_h)_{\Omega_h^b} = 0 \tag{2.103}$$

$$\forall \boldsymbol{v}_h \in \boldsymbol{S}_{hp}, \forall t \in [0, T],$$

$$(\boldsymbol{u}_h(0), \boldsymbol{v}_h)_{\Omega_h^b} = (\boldsymbol{u}_0, \boldsymbol{v}_h)_{\Omega_h^b}, \quad (\boldsymbol{z}_h(0), \boldsymbol{v}_h)_{\Omega_h^b} = \left(\boldsymbol{v}_0^b, \boldsymbol{v}_h\right)_{\Omega_h^b} \tag{2.104}$$

$$\forall \boldsymbol{v}_h \in \boldsymbol{S}_{hp}.$$

Order of the method q	Coefficients $c_0, \dots, c_q$
1	$\frac{1}{\tau_m}, -\frac{1}{\tau_m}$
2	$\frac{2\tau_m+\tau_{m-1}}{\tau_m(\tau_m+\tau_{m-1})}, -\frac{\tau_m+\tau_{m-1}}{\tau_m\tau_{m-1}}, \frac{\tau_m}{\tau_{m-1}(\tau_m+\tau_{m-1})}$
3	$\frac{(2\tau_m+\tau_{m-1})(2\tau_m+\tau_{m-1}+\tau_{m-2})-\tau_m^2}{\tau_m(\tau_m+\tau_{m-1})(\tau_m+\tau_{m-1}+\tau_{m-2})}, -\frac{(\tau_m+\tau_{m-1})(\tau_m+\tau_{m-1}+\tau_{m-2})}{\tau_m\tau_{m-1}(\tau_{m-1}+\tau_{m-2})}, \frac{\tau_m(\tau_m+\tau_{m-1}+\tau_{m-2})}{\tau_{m-1}\tau_{m-2}(\tau_m+\tau_{m-1})}, -\frac{\tau_m(\tau_m+\tau_{m-1})}{\tau_{m-2}(\tau_m+\tau_{m-1}+\tau_{m-2})(\tau_{m-1}+\tau_{m-2})}$

Table 2.1: Coefficients of the backward difference formula of order 1, 2, and 3.

We see that the initial conditions (2.104) can be written as $\boldsymbol{u}_h(0) = \Pi_{hp}\boldsymbol{u}_0$, $\boldsymbol{z}_h(0) = \Pi_{hp}\boldsymbol{v}_0^b$, where Π_{hp} is the operator of the $L^2(\Omega_h^b)$–projection onto the space $\boldsymbol{S}_{hp}$.

In order to obtain a fully discrete problem, we apply the backward difference formula method to the semidiscrete problem (2.102)–(2.104).

2.3.1 Backward-difference formula method

Let us consider a partition of the time interval $[0, T]$ formed by time instants

$$t_m, m = 0, \dots, M, \quad 0 = t_0 < t_1 < \dots < t_M = T, \tag{2.105}$$

where M is a sufficiently large positive integer and define the time step

$$\tau_m = t_m - t_{m-1}, \quad m = 1, \dots, M. \tag{2.106}$$

By $\boldsymbol{u}^m$ and $\boldsymbol{z}^m$ we denote the approximate solution at time t_m, $m = 0, \dots, M$, i.e.

$$\boldsymbol{u}^m \approx \boldsymbol{u}(t_m), \quad \boldsymbol{z}^m \approx \boldsymbol{z}(t_m). \tag{2.107}$$

A general backward difference formula approximating the time derivative reads

$$\frac{\partial \boldsymbol{u}}{\partial t}(t_{m+1}) \approx \sum_{l=0}^{q} c_l \boldsymbol{u}^{m+1-l}, \tag{2.108}$$

where q is the order of the method and c_l, $l = 0, \dots, q$, are the coefficients depending on τ_{m-l}, $l = 0, \dots, q-1$.

In the beginning of the computation, when $m < q - 1$, we use the backward difference formula of order $m + 1$. The coefficients of the BDF methods of the order 1, 2, and 3, are in Table 2.1. BDF methods of higher order degree are rarely used in practical computations. In numerical experiments we use second order BDF.

For simplicity we can also consider a constant time step and, hence, a uniform partition of the interval $[0, T]$. Then $t_m = m\tau, m = 0, \dots, M$, where τ is the uniform time step. The coefficients of the BDF methods up to the order 6 considering uniform partition can be found in Table 2.2.

Order of the method q	Coefficients $c_0, \dots, c_q$ multiplied by τ
1	$1, -1$
2	$3/2, -2, 1/2$
3	$11/6, -3, 3/2, -1/3$
4	$25/12, -4, 3, -4/3, 1/4$
5	$137/60, -5, 5, -10/3, 5/4, -1/5$
6	$49/20, -6, 15/2, -20/3, 15/4, -6/5, 1/6$

Table 2.2: Coefficients of the backward difference formula of order 1,...,6, considering uniform partition with time step τ.

The BDF time discretization of system (2.102)–(2.104) implies the definition of the fully discrete solution discretized by the BDF in time and DGM in space.

Definition 8. *The BDF-DG approximate solution* of problem (2.92)–(2.96) is defined as a couple of sequences $\{\boldsymbol{u}_h^m\}_{m=0}^M$, $\{\boldsymbol{z}_h^m\}_{m=0}^M$ such that

$$\boldsymbol{u}_h^m, \boldsymbol{z}_h^m \in \boldsymbol{S}_{hp}, \quad m = 0, \dots, M, \tag{2.109}$$

$$\left(\rho^b \sum_{l=0}^{q} c_l \boldsymbol{z}_h^{m+1-l}, \boldsymbol{v}_h\right)_{\Omega_h^b} + \left(C_M \rho^b \boldsymbol{z}_h^{m+1}, \boldsymbol{v}_h\right)_{\Omega_h^b} + a_h(\boldsymbol{u}_h^{m+1}, \boldsymbol{v}_h) = b_h(\boldsymbol{v}_h)(t_{m+1}) \tag{2.110}$$

$$\forall \boldsymbol{v}_h \in \boldsymbol{S}_{hp},$$

$$\left(\sum_{l=0}^{q} c_l \boldsymbol{u}_h^{m+1-l}, \boldsymbol{v}_h\right)_{\Omega_h^b} - \left(\boldsymbol{z}_h^{m+1}, \boldsymbol{v}_h\right)_{\Omega_h^b} = 0 \tag{2.111}$$

$$\forall \boldsymbol{v}_h \in \boldsymbol{S}_{hp},$$

$$\left(\boldsymbol{u}_h^0 - \boldsymbol{u}_0, \boldsymbol{v}_h\right)_{\Omega_h^b} = 0, \quad \left(\boldsymbol{z}_h^0 - \boldsymbol{v}_0^b, \boldsymbol{v}_h\right)_{\Omega_h^b} = 0 \tag{2.112}$$

$$\forall \boldsymbol{v}_h \in \boldsymbol{S}_{hp}. \tag{2.113}$$

The initial values $\boldsymbol{u}_h^m$, $\boldsymbol{z}_h^m$, $m = 1, \dots, q$, are obtained by m-step BDF schemes.

In the case of nonlinear elasticity the BDF-DG discretization of problem (2.92)–(2.96) leads to the solution of the nonlinear algebraic system at each time step. Therefore the Newton method defined in Section 2.2.3 is applied at each time step for the solution of the nonlinear discrete problem. In the case of linear elasticity problem we obtain a linear algebraic system at each time step. Let us describe the realization of the discrete dynamic elasticity problem in detail.

2.3.2 Realization of the discrete dynamic elasticity problem

We transform equations (2.110) and (2.111) so that there are just the terms with unknowns on the left hand side at each time step. Hence,

$$\left(c_0\rho^b \boldsymbol{z}_h^{m+1}, \boldsymbol{v}_h\right)_{\Omega_h^b} + \left(C_M\rho^b \boldsymbol{z}_h^{m+1}, \boldsymbol{v}_h\right)_{\Omega_h^b} + a_h(\boldsymbol{u}_h^{m+1}, \boldsymbol{v}_h) = \tag{2.114}$$

$$= b_h(\boldsymbol{v}_h)(t_{m+1}) - \left(\rho^b \sum_{l=1}^{q} c_l \boldsymbol{z}_h^{m+1-l}, \boldsymbol{v}_h\right)_{\Omega_h^b} \qquad \forall \boldsymbol{v}_h \in \boldsymbol{S}_{hp},$$

$$\left(c_0\boldsymbol{u}_h^{m+1}, \boldsymbol{v}_h\right)_{\Omega_h^b} - \left(\boldsymbol{z}_h^{m+1}, \boldsymbol{v}_h\right)_{\Omega_h^b} = \tag{2.115}$$

$$= \left(\sum_{l=1}^{q} c_l \boldsymbol{u}_h^{m+1-q}, \boldsymbol{v}_h\right)_{\Omega_h^b} \qquad \forall \boldsymbol{v}_h \in \boldsymbol{S}_{hp}.$$

We can express the sought approximate solution at each time step as a linear combination of basis functions in the space $\boldsymbol{S}_{hp}$. Let $\{\boldsymbol{\xi}_i\}, i = 1, \ldots, 2N$, form the basis of $\boldsymbol{S}_{hp}$ as in (2.38). Then the sought solution couple $(\boldsymbol{u}_h^m, \boldsymbol{z}_h^m)$, $m = 0, \ldots, M$, can be expressed as

$$\boldsymbol{u}_h^m = \boldsymbol{u}_h(\boldsymbol{\alpha}^{1,m}) = \sum_{i=1}^{2N} \alpha_i^m \boldsymbol{\xi}_i, \tag{2.116}$$

$$\boldsymbol{z}_h^m = \boldsymbol{z}_h(\boldsymbol{\alpha}^{2,m}) = \sum_{i=1}^{2N} \alpha_{2N+i}^m \boldsymbol{\xi}_i, \tag{2.117}$$

where $\boldsymbol{\alpha}^m = \left(\boldsymbol{\alpha}^{1,m^T}, \boldsymbol{\alpha}^{2,m^T}\right)^T = (\alpha_i^m)_{i=1}^{4N}$ are the finite element coefficients. Plugging these expressions into (2.114) and (2.115) and setting $\boldsymbol{v}_h = \boldsymbol{\xi}_i, i = 1, \ldots, 2N$, we arrive at the system of nonlinear algebraic equations

$$\begin{pmatrix} \boldsymbol{k}(\boldsymbol{\alpha}^{1,m+1}) + (c_0 + C_M)\rho^b \mathbb{M}\boldsymbol{\alpha}^{2,m+1} \\ c_0\mathbb{M}\boldsymbol{\alpha}^{1,m+1} - \mathbb{M}\boldsymbol{\alpha}^{2,m+1} \end{pmatrix} - \boldsymbol{b}^{m+1} = \boldsymbol{0}, \tag{2.118}$$

where

$$\mathbb{M} = \{m_{ij}\}_{i,j=1}^{2N} = \left\{\left(\boldsymbol{\xi}_j, \boldsymbol{\xi}_i\right)_{\Omega_h^b}\right\}_{i,j=1}^{2N},$$

$$\boldsymbol{k}(\boldsymbol{\alpha}^{1,m+1}) = \left\{a_h\left(\boldsymbol{u}_h^{m+1}(\boldsymbol{\alpha}^{1,m+1}), \boldsymbol{\xi}_j\right)\right\}_{j=1}^{2N},$$

$$\boldsymbol{b}^{m+1} = \left\{b_j^{m+1}\right\}_{j=1}^{4N} = \begin{cases} b_h(\boldsymbol{\xi}_j)(t_{m+1}) - \rho^b \left(\sum_{l=1}^{q} c_l \boldsymbol{z}_h^{m+1-l}, \boldsymbol{\xi}_j\right)_{\Omega_h^b}, & j = 1, \ldots, 2N, \\ \left(\sum_{l=1}^{q} c_l \boldsymbol{u}_h^{m+1-l}, \boldsymbol{\xi}_j\right)_{\Omega_h^b}, & j = 2N+1, \ldots, 4N. \end{cases}$$

This nonlinear algebraic system is solved by the Newton method at each time step. Let us note that the convergence of the Newton method is improved, if we use the solution from the previous time step as an initial guess. In order to apply the Newton method we must differentiate the form $a_h\left(\boldsymbol{u}_h^m(\boldsymbol{\alpha}^{1,m}), \boldsymbol{v}_h\right)$ with respect to the coefficients $\boldsymbol{\alpha}$. However, we proceed analogously as in Sections 2.2.4, 2.2.5, and 2.2.6. In practical computations, integrals appearing in the definitions of the forms a_h, b_h and the scalar products are evaluated with the aid of suitable quadrature formulae. The list of the used quadrature formulae is in Section 6.2.

In the case of linear elasticity the discretization leads to the solution of the linear algebraic system

$$\begin{pmatrix} \mathbb{K} & (c_0 + C_M)\rho^b \mathbb{M} \\ c_0 \mathbb{M} & -\mathbb{M} \end{pmatrix} \boldsymbol{\alpha}^{m+1} = \boldsymbol{b}^{m+1}, \tag{2.119}$$

at each time step, where

$$\mathbb{K} = \{k_{ij}\}_{i,j=1}^{2N} = \left\{a_h(\boldsymbol{\xi}_j, \boldsymbol{\xi}_i)\right\}_{i,j=1}^{2N}, \tag{2.120}$$

and $\mathbb{M}$, $\boldsymbol{b}^{m+1}$, and $\boldsymbol{\alpha}^{m+1}$ are defined in the same way as in the nonlinear elasticity case. Clearly, the system of linear equations needs to be solved by suitable iterative or direct solver.

3. Realization of the discontinuous Galerkin method applied to the elasticity problem

In the previous chapter we described in detail the discretization of the elasticity problem, which allows us to work out a robust numerical solver. For this purpose we developed a .NET library written in C# for the numerical solution of 2D static and dynamic linear and nonlinear elasticity problem with mixed boundary conditions. We briefly present this library or better the part of the library dealing with the elasticity problem, because the whole library includes also the solvers of other partial differential equations, namely the Laplace equation, parabolic equations, and linear or nonlinear convection-diffusion equations. This library was used, for example, for the realization of numerical experiments [2] concerned with the numerical analysis of the space-time discontinuous Galerkin method for the solution of nonstationary, nonlinear, convection-diffusion problems.

These results of numerical experiments encouraged us for the use of the same schemes for the solution of the elasticity problems, where the proper numerical analysis is not so complete as by these simpler but still difficult problems. For the sake of completeness of this paragraph let us mention, that the library also includes the wrapper for the solver of compressible viscous flow in time-dependent domains and a program unit, which operates the fluid-structure interaction problem. The fluid and FSI solver is the subject of further chapters of this thesis.

In this chapter we deal with numerical experiments for the elasticity problems. To verify that our computational tool is enough efficient, we compare our results with a benchmark problem. Therefore in this chapter we present results of the solution of a benchmark introduced by Turek and Hron in [64], in order to demonstrate that the developed method produces comparable results. This benchmark defines both static elasticity test problem and dynamic elasticity test problem.

There are basically several possibilities of interests of our numerical experiments. The implementation offers us the linear and nonlinear elasticity solver. Therefore, we will present the difference between the results obtained using different material properties. Other results are presented for the St. Venant-Kirchhoff, neo-Hookean, and linearized material separately. For them we will check the quality of the discretization by the DGM in space and by the finite difference method in time. In principal, the implementation allows us to use arbitrary order of the space and time discretization. We set by our computations up to the cubic polynomial approximation in space and we employ the backward-difference formula of first and second order for the time discretization. The DGM has some other specific characteristics as described in the previous chapter. For the linear elasticity problem we compare the symmetric, nonsymmetric and incomplete version of the DGM. Further, we discuss the use of different parameters for the settings of the initial and boundary penalty.

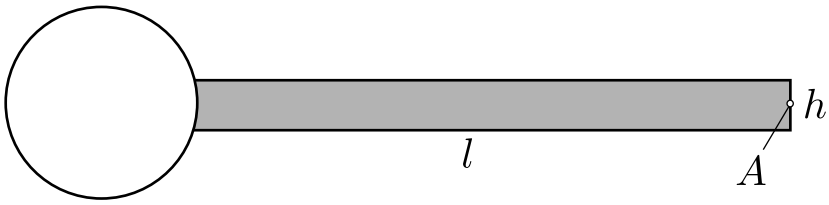

Figure 3.1: Rigid cylinder with an elastic beam for the nonlinear elasticity benchmark problem.

3.1 Static elasticity test problem

First, let us describe the setup of the benchmark. We consider a 2D domain of a cylinder with an attached elastic beam behind, see Figure 3.1. The circle has radius $r = 0.05$ m and the beam has length $l = 0.35$ m and height $h = 0.02$ m. Further we define a control point A in the middle of the end of the beam as shown in Figure 3.1. The evolution of the displacement of the point $A = A(t)$ is the quantity of our interest. The structural tests for the elastic beam in [64] are denoted as CSM tests. There are two steady state problems CSM1 and CSM2 and a time dependent benchmark CSM3. The cylinder is considered as a rigid body and the elastic beam is modelled as the St. Venant-Kirchhoff material. In addition to [64] we consider also neo-Hookean material and the linear elasticity model.

In the case of the static nonlinear elasticity we solve the problem defined in Definition 2 and in the case of the static linear elasticity the problem defined in Definition 4. The domain Ω^b, defined in the previous paragraph, represents the elastic beam. For both CSM1 and CSM2 we prescribe the acting body force density $\boldsymbol{f}$ by the density

$$\boldsymbol{b} = (0, -2)^T \ \ [\mathrm{m.s}^{-2}] \tag{3.1}$$

and the mass density

$$\rho^b = 10^3 \ [\mathrm{kg.m}^{-3}]. \tag{3.2}$$

On the left part of the boundary connected to the rigid body we prescribe homogeneous Dirichlet boundary condition

$$\boldsymbol{u}_D = \boldsymbol{0} \quad \text{on } \Gamma_D^b, \tag{3.3}$$

and on the rest of the boundary we prescribe the Neumann boundary condition with no surface traction

$$\boldsymbol{g}_N = \boldsymbol{0} \quad \text{on } \Gamma_N^b. \tag{3.4}$$

Finally, the material is characterized by Young's modulus E^b and Poisson's ratio ν^b. For case CSM1 we set

$$E^b = 1.4 \cdot 10^6, \quad \nu^b = 0.4, \tag{3.5}$$

and for case CSM2

$$E^b = 5.6 \cdot 10^6, \quad \nu^b = 0.4. \tag{3.6}$$

The Lamé parameters are determined by relations (1.69). These parameters characterize the considered nonlinear elasticity materials and the linear elasticity

material as well. Hereby we defined actually six different static elasticity problems given by the choice of CSM case and given material.

The static test problems were computed on 4 different triangular computational meshes. The computational meshes are visualized in Figure 3.2 and their characteristics are assigned in Table 3.1. For the generation of the triangular meshes we used the finite element grid generator Gmsh [34].

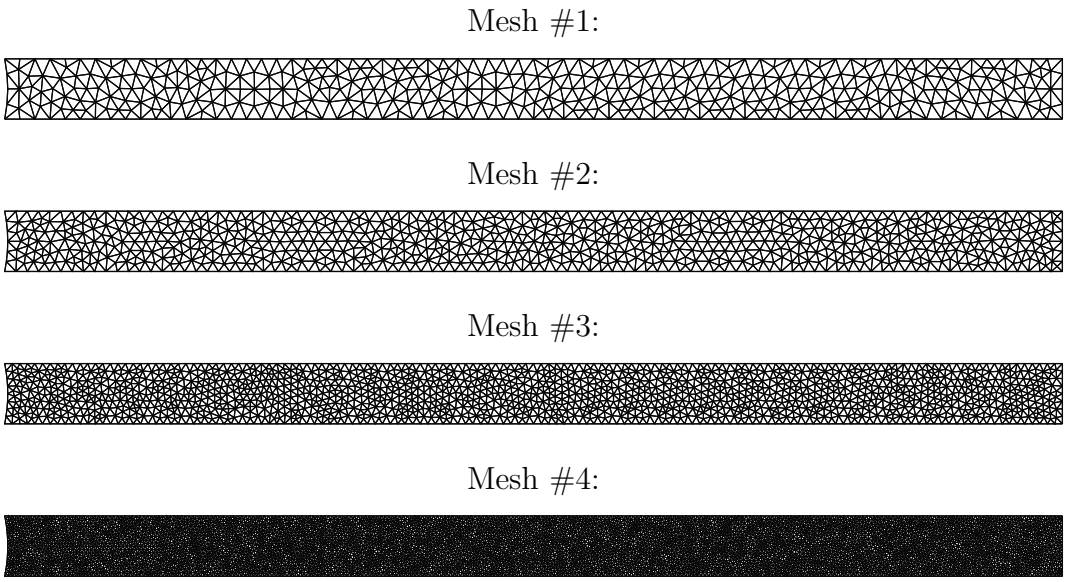

Figure 3.2: Computational meshes for elasticity benchmark problems.

	number of elements	$\sim h[10^{-3}]$
Mesh #1	722	7.31
Mesh #2	1348	5.17
Mesh #3	2822	3.40
Mesh #4	11787	1.75

Table 3.1: Size of the meshes for elasticity benchmark problems.

3.1.1 Linear elasticity

First we introduce results for the simplest linear elasticity problem. The visualization of the solution obtained for the CSM1 case considering the linear elasticity is illustrated in Figure 3.3 and accordingly the CSM2 case in Figure 3.4. The colour scale represents the magnitude of the displacement. We tested all three variants of the DGM for the linear elasticity model. That is the IIPG, SIPG, and NIPG, which were introduced in Section 2.2.1. We considered different degrees of the polynomial approximation and for the computation we used all the computational meshes mentioned above.

In Tables 3.2, 3.3, and 3.4, respectively, we present the comparison of the displacement of the point A for different meshes and space polynomial degree p using the IIPG, SIPG, and NIPG methods, respectively. Let us denote that the displacement in the x_1 direction is practically zero. It is negligible with respect to the size of the whole body.

According to the Section 3.3, where we discuss the choice of the penalty coefficient, we set the parameter $C_W^b = 4 \cdot 10^6$ for the CSM1 case and $C_W^b = 1.6 \cdot 10^7$ for the CSM2 case. The results show that the displacement of the point A is approximately converging to the value $(0.0, -68.00 \cdot 10^{-3})$ in case CSM1 and $(0.0, -17.00 \cdot 10^{-3})$ in case CSM2, respectively, considering the linear elasticity model. Further we can observe that all variants of the DGM give similar results. For the third polynomial degree of the approximation the displacement is varying more than expected. This can be improved by the choice of the penalty parameter. On the other hand in view of our experience with practical use of the DGM for elasticity problems, there is no need to use higher degree of polynomial approximation.

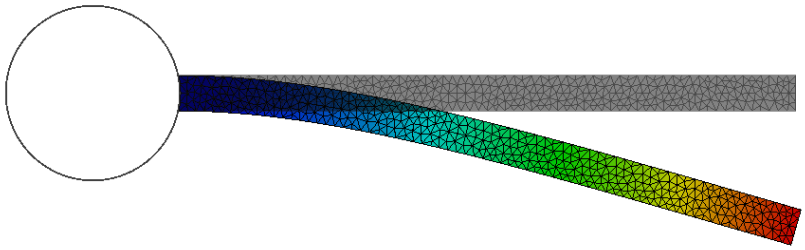

Figure 3.3: Linear elasticity: Deformation of the beam in case CSM1.

		CSM1		CSM2	
# elem.	p	$u_1\,[\times 10^{-6}]$	$u_2\,[\times 10^{-3}]$	$u_1\,[\times 10^{-7}]$	$u_2\,[\times 10^{-3}]$
722	1	1.2375	-69.6795	3.0939	-17.4199
1348	1	0.0117	-68.3748	0.0293	-17.0937
2822	1	-0.0893	-68.1856	-0.2243	-17.0461
11787	1	-0.0203	-68.0673	-0.0508	-17.0168
722	2	-0.0697	-68.1057	-0.1744	-17.0264
1348	2	-0.0437	-68.0419	-0.1092	-17.0105
2822	2	0.0074	-68.0308	0.0186	-17.0077
11787	2	-0.0006	-68.0229	-0.0014	-17.0057
722	3	-0.0019	-68.0840	-0.0048	-17.0210
1348	3	0.0029	-68.0354	0.0098	-17.0123
2822	3	0.0004	-68.0492	0.0073	-17.0089
11787	3	0.0033	-68.0242	0.0032	-17.0061

Table 3.2: Linear Elasticity, IIPG method: Comparison of the displacement of the point A for different meshes and space polynomial degree p. CSM1 (left) and CSM2 (right).

		CSM1		CSM2	
# elem.	p	$u_1\,[\times 10^{-6}]$	$u_2\,[\times 10^{-3}]$	$u_1\,[\times 10^{-7}]$	$u_2\,[\times 10^{-3}]$
722	1	1.3593	-67.4657	3.3984	-16.8664
1348	1	-1.5105	-67.2251	-3.7763	-16.8063
2822	1	0.0331	-67.6397	0.0827	-16.9099
11787	1	-0.1014	-67.9179	-0.2536	-16.9795
722	2	0.0126	-68.0612	0.0316	-17.0153
1348	2	0.0228	-68.0294	0.0571	-17.0073
2822	2	0.0230	-68.0393	0.0576	-17.0098
11787	2	-0.0044	-68.0244	-0.0111	-17.0061
722	3	-0.0772	-68.0680	-0.1931	-17.0170
1348	3	-0.1811	-68.0804	-0.4527	-17.0201
2822	3	0.5117	-68.0970	1.2792	-17.0242
11787	3	-10.024	-68.0647	-25.061	-17.0162

Table 3.3: Linear Elasticity, SIPG method: Comparison of the displacement of the point A for different meshes and space polynomial degree p. CSM1 (left) and CSM2 (right).

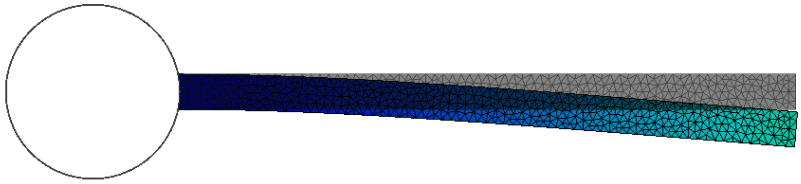

Figure 3.4: Linear elasticity: Deformation of the beam in case CSM2.

		CSM1		CSM2	
# elem.	p	$u_1\,[\times 10^{-6}]$	$u_2\,[\times 10^{-3}]$	$u_1\,[\times 10^{-7}]$	$u_2\,[\times 10^{-3}]$
722	1	0.7784	-69.1857	1.9461	-17.2964
1348	1	-0.0692	-68.2617	-0.1730	-17.0654
2822	1	-0.0842	-68.1317	-0.2106	-17.0329
11787	1	-0.0307	-68.0549	-0.0767	-17.0137
722	2	-0.0393	-68.1159	-0.0982	-17.0290
1348	2	-0.0452	-68.0530	-0.1130	-17.0132
2822	2	-0.0001	-68.0370	-0.0003	-17.0092
11787	2	0.0001	-68.0264	0.0003	-17.0066
722	3	-0.0013	-68.0549	-0.0033	-17.0137
1348	3	0.0014	-68.0260	0.0036	-17.0065
2822	3	0.0019	-68.0223	0.0048	-17.0056
11787	3	0.0595	-68.0122	0.1488	-17.0031

Table 3.4: Linear Elasticity, NIPG method: Comparison of the displacement of the point A for different meshes and space polynomial degree p. CSM1 (left) and CSM2 (right).

3.1.2 Nonlinear elasticity

In this section we consider the static nonlinear elasticity problem. As we explained in Section 2.2, only the IIPG variant of the DGM makes sense for the discretization of the nonlinear elasticity problem. We need to choose a penalty coefficient similarly as for the linear elasticity problem. This parameter was chosen using the same strategy as described in Section 3.3. This time we set the parameter $C_W^b = 6 \cdot 10^6$ for the CSM1 case and $C_W^b = 2.0 \cdot 10^7$ for the CSM2 case. Again we consider different degrees of the polynomial approximation and for the computation we use meshes described in Table 3.1 and visualized in Figure 3.2. The nonlinear algebraic problem was solved with the Newton method with given tolerance $\varepsilon = 10^{-8}$.

In Table 3.5 we present the results for the St. Venant-Kirchhoff model and in Table 3.6 the results for the neo-Hookean model. Similarly as in the case of linear elasticity we compare the displacement of the point A for different meshes and space polynomial degree p. The visualization of the solution obtained for the CSM1 case and CSM2 case considering the St. Venant-Kirchoff model and neo-Hookean model is illustrated in Figures 3.5 and 3.8 and in Figures 3.6 and 3.9, respectively. In all figures the colour scale represents the magnitude of the displacement mapping. We can see, that the results are almost identical. On the other hand they are different to the linear elasticity model. We show the difference between the linear elasticity model and St. Venant-Kirchoff model also in the visualization of the deformation in Figure 3.7 and in Figure 3.10 for the case CSM1 and CSM2, respectively. The linear elasticity model is suitable for small deformations, where it should be roughly equal to the nonlinear elasticity model. As we can see in case CSM2, the results are corresponding to this assumption, whereas in case CSM1 by larger deformation the results are different. We use the results obtained by the use of the IIPG variant of the DGM for linear elasticity.

For the St. Venant-Kirchhoff model we can compare our results with results obtained in [64]. The reference displacement of the point A in [64] is given as $(-7.187 \cdot 10^{-3}, -66.10 \cdot 10^{-3})$ in case CSM1 and $(-0.469 \cdot 10^{-3}, -16.97 \cdot 10^{-3})$ in case CSM2, respectively. Our results show a good agreement with computations in [64].

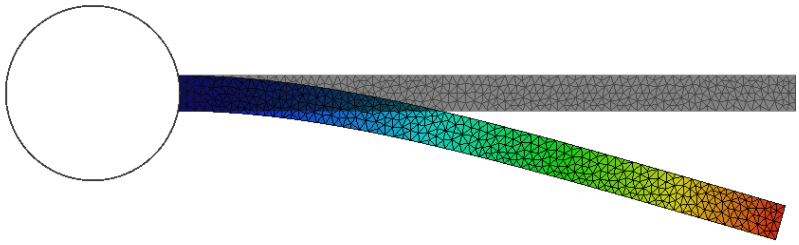

Figure 3.5: St. Venant-Kirchhoff material: Deformation of the beam in case CSM1.

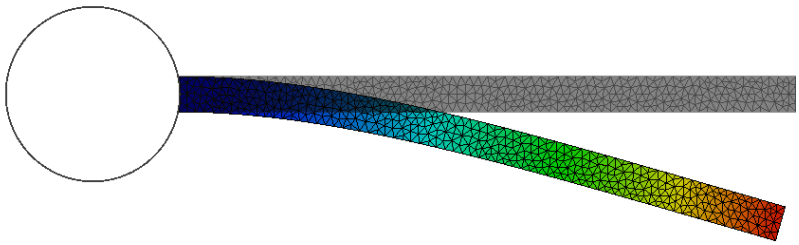

Figure 3.6: Neo-Hookean material : Deformation of the beam in case CSM1.

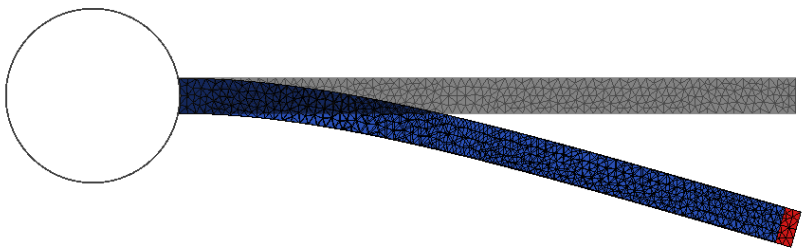

Figure 3.7: Comparison of linear elastic material (red) and nonlinear St. Venant-Kirchhoff material (blue): Deformation of the beam in case CSM1.

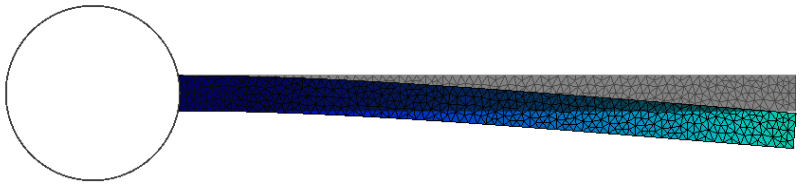

Figure 3.8: St. Venant-Kirchhoff material: Deformation of the beam in case CSM2.

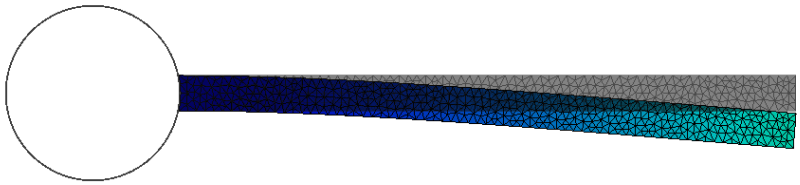

Figure 3.9: Neo-Hookean material : Deformation of the beam in case CSM2.

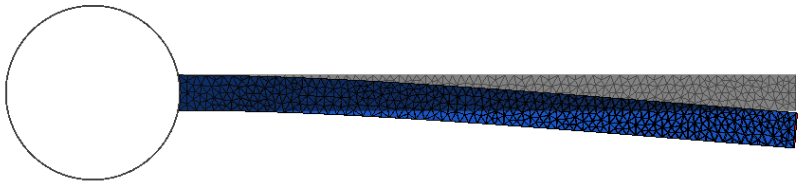

Figure 3.10: Comparison of linear elastic material (red, but in fact not visible, because the difference is minimal) and nonlinear St. Venant-Kirchhoff material (blue): Deformation of the beam in case CSM2.

		CSM1		CSM2	
# elem.	p	$u_1\,[\times 10^{-3}]$	$u_2\,[\times 10^{-3}]$	$u_1\,[\times 10^{-3}]$	$u_2\,[\times 10^{-3}]$
ref		-7.187	-66.10	-0.469	-16.97
722	1	-7.20401	-66.2164	-0.47908	-17.1700
1348	1	-7.11515	-65.7639	-0.46835	-16.9609
2822	1	-7.14785	-65.9148	-0.46850	-16.9634
11787	1	-7.17825	-66.0579	-0.46892	-16.9721
722	2	-7.19961	-66.1617	-0.46995	-16.9922
1348	2	-7.18807	-66.1028	-0.46914	-16.9761
2822	2	-7.18782	-66.1024	-0.46906	-16.9749
11787	2	-7.18749	-66.1012	-0.46900	-16.9739
722	3	-7.19784	-66.1558	-0.46972	-16.9888
1348	3	-7.19137	-66.1217	-0.46929	-16.9798
2822	3	-7.18955	-66.1122	-0.46915	-16.9769
11787	3	-7.18774	-66.1032	-0.46901	-16.9743

Table 3.5: St. Venant-Kirchhoff material: Comparison of the displacement of the point A for different meshes and space polynomial degree p. CSM1 (left) and CSM2 (right).

		CSM1		CSM2	
# elem.	p	$u_1\,[\times 10^{-3}]$	$u_2\,[\times 10^{-3}]$	$u_1\,[\times 10^{-3}]$	$u_2\,[\times 10^{-3}]$
722	1	-7.17686	-66.2116	-0.47734	-17.1692
1348	1	-7.08933	-65.7710	-0.46660	-16.9610
2822	1	-7.12204	-65.9243	-0.46672	-16.9638
11787	1	-7.15143	-66.0644	-0.46711	-16.9722
722	2	-7.17255	-66.1696	-0.46810	-16.9924
1348	2	-7.16094	-66.1093	-0.46731	-16.9762
2822	2	-7.16077	-66.1090	-0.46723	-16.9750
11787	2	-7.16050	-66.1077	-0.46732	-16.9770
722	3	-7.17083	-66.1623	-0.46790	-16.9889
1348	3	-7.16435	-66.1281	-0.46746	-16.9799
2822	3	-7.16255	-66.1186	-0.46718	-16.9740
11787	3	-7.16075	-66.1097	-0.46719	-16.9744

Table 3.6: Neo-Hookean material: Comparison of the displacement of the point A for different meshes and space polynomial degree p. CSM1 (left) and CSM2 (right).

3.2 Dynamic elasticity test problem

The dynamic elasticity case CSM3 is set similarly to the static elasticity case CSM1. We prescribe the homogeneous Dirichlet boundary condition on the part of the boundary where the beam is attached to the cylinder. The volume force acting on the body mimics the gravity. No surface forces are considered and the damping coefficient is set to zero. The initial condition for the time-dependent problem CSM3 is given by the reference configuration and zero initial deformation velocity. More precisely, we set boundary conditions

$$\boldsymbol{u}_D = \mathbf{0} \quad \text{on } \Gamma_D^b \times [0,T], \qquad \boldsymbol{g}_N = \mathbf{0} \quad \text{on } \Gamma_N^b \times [0,T], \tag{3.7}$$

initial condition

$$\boldsymbol{u}_0 = 0, \ \boldsymbol{v}_0^b = \mathbf{0} \quad \text{in } \Omega^b, \tag{3.8}$$

acting body force

$$\boldsymbol{f} = \rho^b \boldsymbol{b}, \ \boldsymbol{b} = (0,-2)^T, \quad \rho^b = 10^3 \text{ in } \Omega^b \times [0,T], \tag{3.9}$$

and damping coefficient $C_M = 0$. Further, for CSM3 we set

$$E^b = 1.4 \cdot 10^6, \quad \nu^b = 0.4 \tag{3.10}$$

as for CSM1.

The CSM3 is solved only on two different unstructured triangulations Mesh #1 and Mesh #3 with 722 and 2822 elements , see Figure 3.2. The time discretization is carried out by the first and second order BDF method with constant time step. For all computations the constant C_W^b is set in correspondence with given Lamé parameters as it was described in Section 3.3. According to our numerical tests, we choose $C_W^b = 6 \cdot 10^6$. Except of the results in Tables 3.9 and 3.10 we consider piecewise linear approximation in space and triangulation Mesh #1.

Figures 3.11, 3.12, and 3.13, demonstrate the deformation of the beam for the test case CSM3 for the linear elasticity, St. Venant-Kirchhoff, and neo-Hookean material, respectively. There is no significant difference between the two nonlinear materials. Comparison of the displacement of the point A for different materials for BDF2 and time step 0.01 is shown in Figure 3.14. For the case of linear elasticity material we compare the different variants of the DG discretization, see Figure 3.15. We can see that the results are almost the same for NIPG and IIPG. For SIPG we see slightly different solution as in static case. In all other experiments the IIPG method is used. Further, we show the evolution of the displacement of the point A for BDF1 and BDF2 and different time steps. The results for linear elastic material are shown in Figures 3.16 and 3.17, the results for St. Venant-Kirchhoff material are shown in Figures 3.18 and 3.19, and the results for neo-Hookean material are shown in Figures 3.20 and 3.21.

According to [64] for the St. Venant-Kirchhoff material we compare the time dependent values of the displacement of the point A, which are represented by the mean value, amplitude and frequency. The mean value and amplitude are computed from the last period of the oscillations by taking the maximum (max) and minimum (min) values. Then mean $= 1/2(\max + \min)$, and amplitude $= 1/2(\max - \min)$. The frequency of the oscillations is computed by the fast Fourier transform (FFT) and taking the lowest significant frequency present in the

spectrum. The data denoted by "ref" represent results from [64]. In Tables 3.7 and 3.8, respectively, are the data obtained for different time steps for the method BDF1 and BDF2, respectively. We can see that for BDF1 we need even smaller time step to obtain satisfactory results. The space polynomial degree was set to $p = 1$ and we used the triangulation Mesh #1. In Table 3.9 we compare the results obtained by the use of different polynomial approximations in space. Finally, in Table 3.10 we compare the results obtained for different triangulations. Our results show a very good agreement with computations from [64].

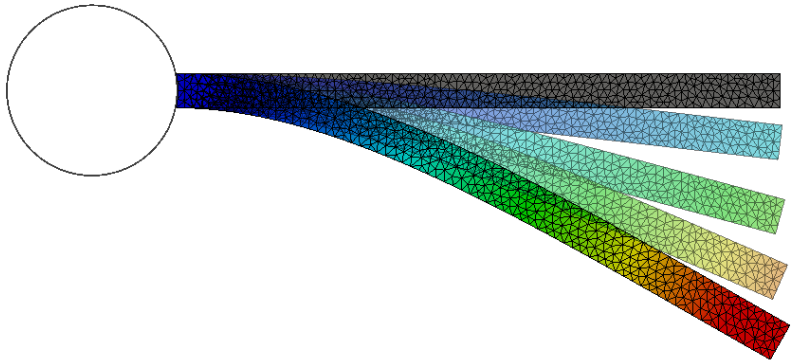

Figure 3.11: Linear elasticity: Deformation of the beam in case CSM3.

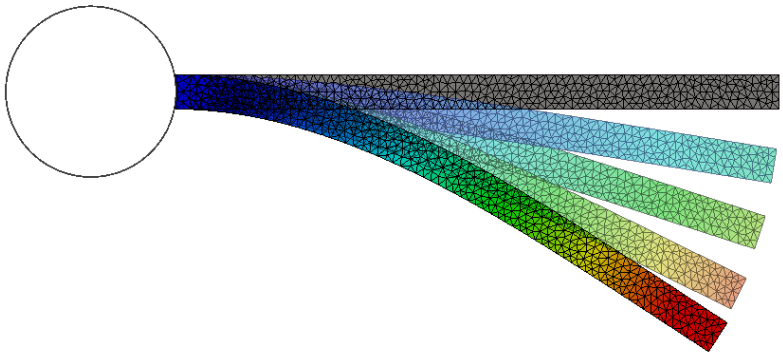

Figure 3.12: St. Venant-Kirchhoff: Deformation of the beam in case CSM3.

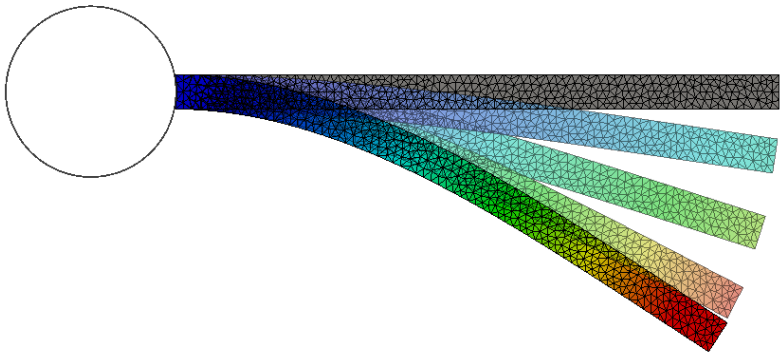

Figure 3.13: Neo-Hookean: Deformation of the beam in case CSM3.

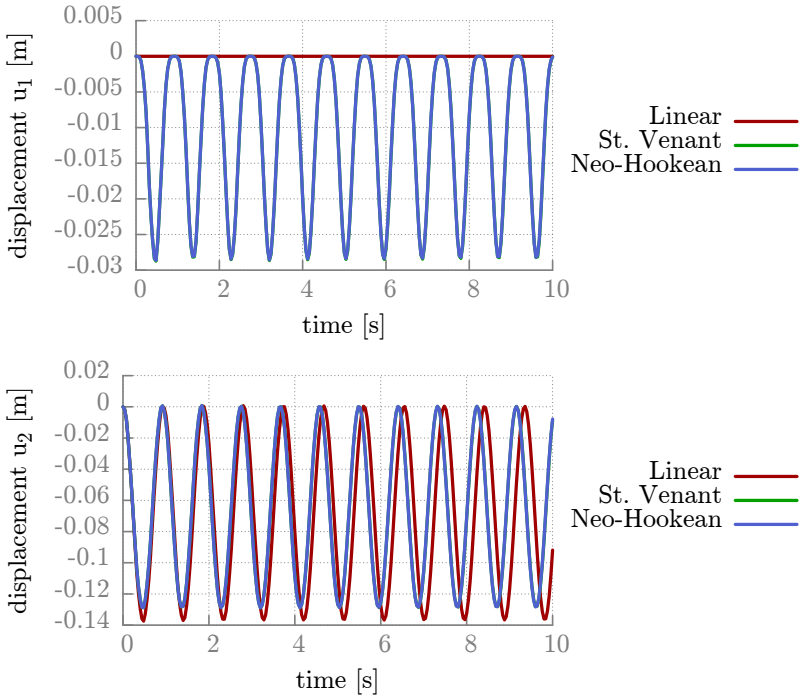

Figure 3.14: Comparison of the displacement of the point A for BDF2 and different materials, IIPG variant, time step 0.01.

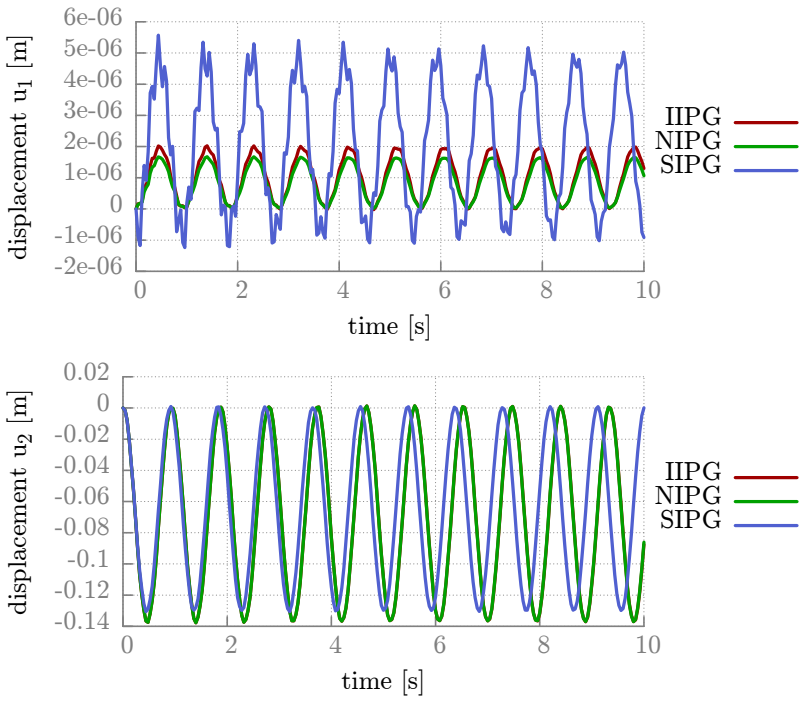

Figure 3.15: Linear elasticity: Comparison of the displacement of the point A for BDF2 and different variants of the DGM, time step 0.01.

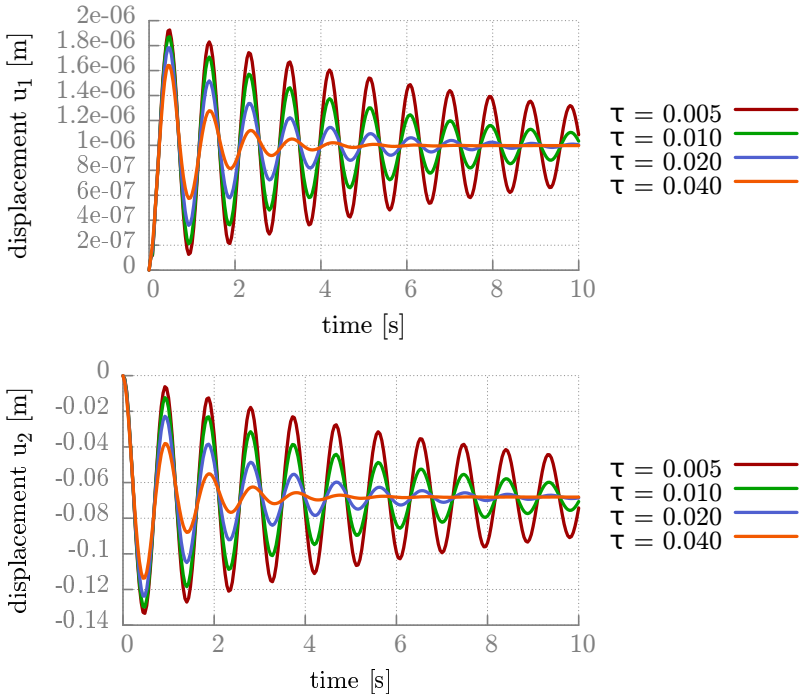

Figure 3.16: Linear elasticity, IIPG variant: Displacement of the point A for BDF1 and different time steps.

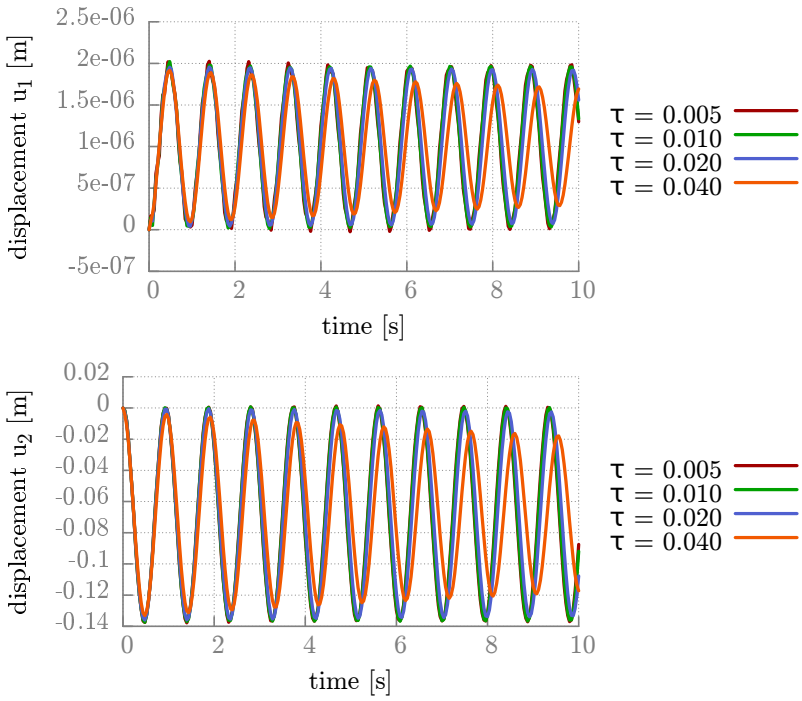

Figure 3.17: Linear elasticity, IIPG variant: Displacement of the point A for BDF2 and different time steps.

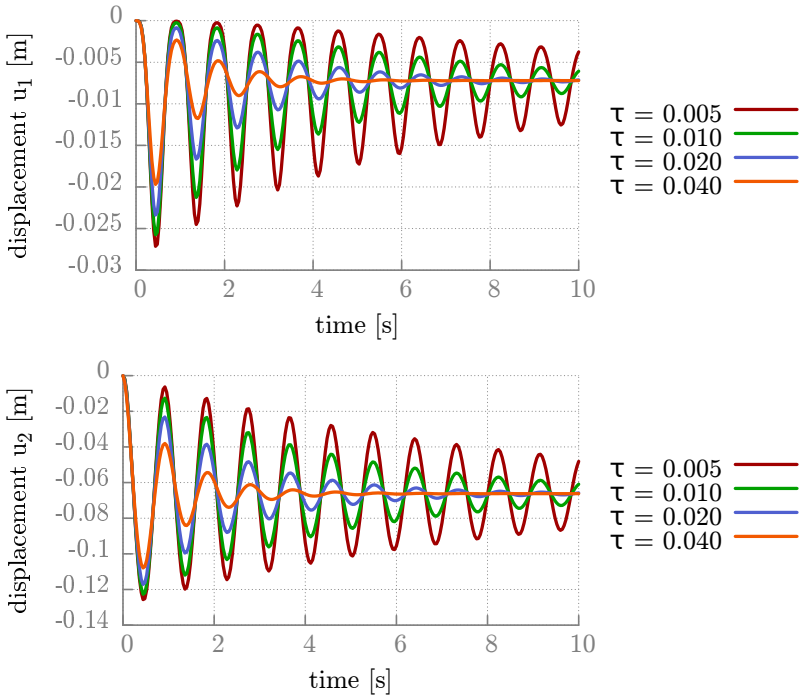

Figure 3.18: St. Venant-Kirchhoff: Displacement of the point A for BDF1 and different time steps.

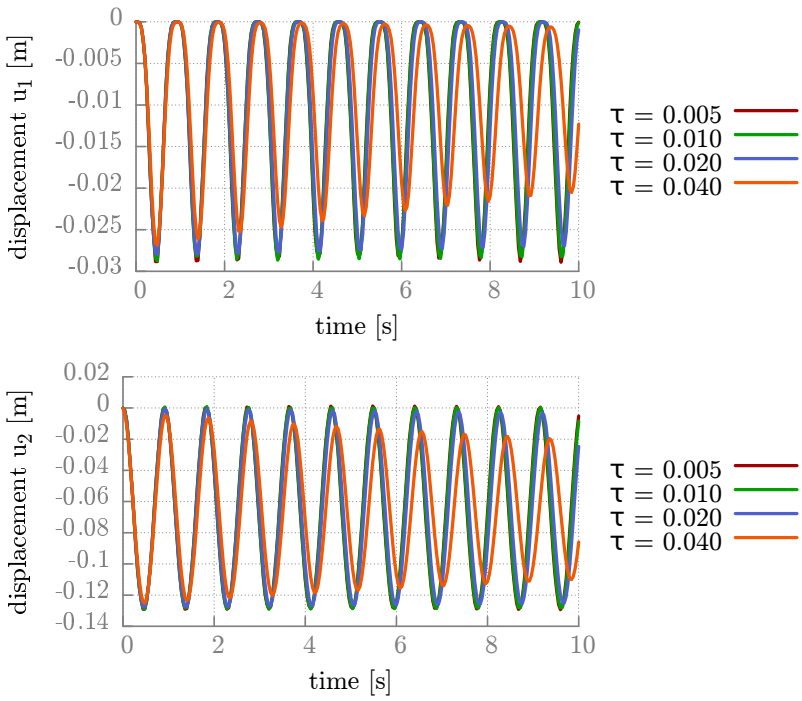

Figure 3.19: St. Venant-Kirchhoff: Displacement of the point A for BDF2 and different time steps.

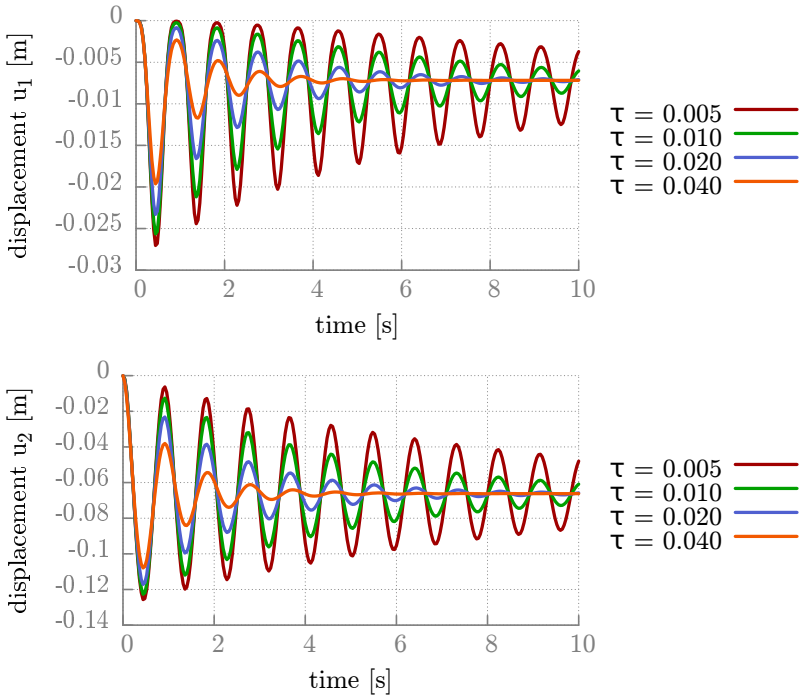

Figure 3.20: Neo-Hookean: Displacement of the point A for BDF1 and different time steps.

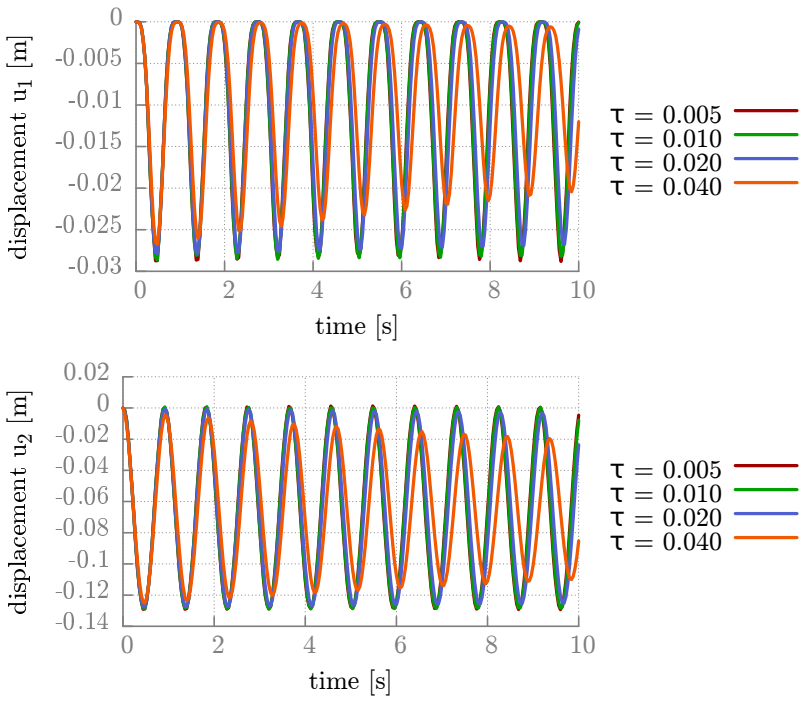

Figure 3.21: Neo-Hookean: Displacement of the point A for BDF2 and different time steps.

method	τ	$u_1\,[\times 10^{-3}]$		$u_2\,[\times 10^{-3}]$	
ref		-14.305 ± 14.305	[1.0995]	-63.607 ± 65.160	[1.0995]
BDF1	0.04	-7.205 ± 0.003	[1.0720]	-66.220 ± 0.016	[1.0720]
BDF1	0.02	-7.186 ± 0.175	[1.0805]	-66.130 ± 0.789	[1.0805]
BDF1	0.01	-7.200 ± 1.564	[1.0875]	-65.795 ± 7.079	[1.0875]
BDF1	0.005	-7.846 ± 4.702	[1.0925]	-65.449 ± 21.353	[1.0925]

Table 3.7: CSM3: Comparison of the displacement of the point A for BDF1, St. Venant-Kirchhoff material and different time steps τ. The values are written in the format "*mean value* $\pm$ *amplitude [frequency]*".

method	τ	$u_1\,[\times 10^{-3}]$		$u_2\,[\times 10^{-3}]$	
ref		-14.305 ± 14.305	[1.0995]	-63.607 ± 65.160	[1.0995]
BDF2	0.04	-10.566 ± 9.963	[1.0675]	-64.866 ± 45.218	[1.0675]
BDF2	0.02	-13.477 ± 13.462	[1.0850]	-64.133 ± 61.177	[1.0850]
BDF2	0.01	-14.119 ± 14.111	[1.0900]	-63.905 ± 64.212	[1.0900]
BDF2	0.005	-14.454 ± 14.453	[1.0925]	-64.384 ± 64.939	[1.0925]

Table 3.8: CSM3: Comparison of the displacement of the point A for BDF2, St. Venant-Kirchhoff material and different time steps τ. The values are written in the format "*mean value* $\pm$ *amplitude [frequency]*".

p. degree	τ	$u_1\,[\times 10^{-3}]$		$u_2\,[\times 10^{-3}]$	
ref		-14.305 ± 14.305	[1.0995]	-63.607 ± 65.160	[1.0995]
1	0.01	-14.119 ± 14.111	[1.0900]	-63.905 ± 64.212	[1.0900]
2	0.01	-14.159 ± 14.150	[1.0900]	-63.928 ± 64.290	[1.0900]
3	0.01	-14.061 ± 14.054	[1.0925]	-63.969 ± 64.246	[1.0925]

Table 3.9: CSM3: Comparison of the displacement of the point A for BDF2, St. Venant-Kirchhoff material and different polynomial degrees of approximation in space. The values are written in the format "*mean value* $\pm$ *amplitude [frequency]*".

# elements	τ	$u_1\,[\times 10^{-3}]$		$u_2\,[\times 10^{-3}]$	
ref		-14.305 ± 14.305	[1.0995]	-63.607 ± 65.160	[1.0995]
722	0.01	-14.119 ± 14.111	[1.0900]	-63.905 ± 64.212	[1.0900]
2822	0.01	-14.115 ± 14.108	[1.0900]	-63.869 ± 64.139	[1.0900]

Table 3.10: CSM3: Comparison of the displacement of the point A for BDF2, St. Venant-Kirchhoff material and different meshes. The values are written in the format "*mean value* $\pm$ *amplitude [frequency]*".

3.3 Choice of the penalty coefficient

The discretization by the DGM includes one optional parameter, which estimates the penalty weight in the interior and boundary penalty term. In Chapter 2 we introduced the penalty weight in the form $\frac{C_W^b}{h_\Gamma}$, where $C_W^b > 0$ is the penalization constant and h_Γ is in some way proportional to the length of the edge Γ. The following three possibilities are implemented: mean average of diameters of the neighbouring elements, their maximum, or the length of the edge, see (2.9)–(2.11). Our experiments were computed on meshes, where the value of h_Γ does not differ a lot for these three possibilities. Therefore in our computations we consider just the last one and concern more about the choice of the parameter C_W^b. From the error analysis of the DGM for simpler problems we know that the penalty coefficient should be large enough. On the other hand, stronger penalty causes worse computational properties of the corresponding algebraic system.

Let us describe the following simple static linear elasticity problem with given exact solution

$$\boldsymbol{u} = \left(\sin(2(x_1+1))\cos(x_2+1)^2, \cos(\pi(x_1+1))\sin(x_2+1)^2\right)^T, \tag{3.11}$$

see the visualization of the deformation given by this exact solution in Figure 3.23. We consider a unit square as a computational domain, see Fig. 3.22. The material is characterized by Young's modulus E^b and Poisson's ratio ν^b:

$$E^b = 1.0 \cdot 10^5, \quad \nu^b = 0.3. \tag{3.12}$$

According to the exact solution we define the acting body force density $\boldsymbol{f}$ and on the boundary we prescribe the Dirichlet boundary condition

$$\boldsymbol{u}_D = \boldsymbol{u} \quad \text{on } \partial\Omega^b. \tag{3.13}$$

We solve the problem on different meshes, with different polynomial order of approximation and with different C_W^b. For every computation we estimate the error in L^2-norm and we show the dependence of the error on the choice of C_W^b. The comparisons for the IIPG, NIPG, and SIPG, respectively, are in Figures 3.24, 3.25, and 3.26, respectively. We can see, that we can approximately estimate the optimal choice $C_W^b = 30000$ for linear approximation. With higher polynomial degree the approximate optimal choice can slightly vary, see Figures 3.27, and 3.28. When we modify the case and increase E^b, we can see that the approximate optimal choice is also increasing. Let us take $E^b = 1 \cdot 10^5$, $2 \cdot 10^5$, and $4 \cdot 10^5$, respectively. In these cases the optimal choices are approximately $C_W^b = 3 \cdot 10^5$, $C_W^b = 6 \cdot 10^5$, and $C_W^b = 1 \cdot 10^6$, respectively, see Figure 3.29. The same thing happens, when we vary the Poisson's ratio taking $\nu^b = 0.3$, $\nu^b = 0.49$, and $\nu^b = 0.499$, respectively. Then we obtain as the optimal choice approximately $C_W^b = 3 \cdot 10^5$, $C_W^b = 6 \cdot 10^6$, and $C_W^b = 3 \cdot 10^7$, respectively, see Figure 3.30. By this observation we can say that the approximate optimal choice of the parameter C_W^b depends on the given Lamé parameters λ and μ, see Table 3.11.

According to our results we recommend to set the parameter C_W^b as a multiple of the Lamé parameter λ. As approximately optimal value seems to be the double of parameter λ. We should not set C_W^b less than 2λ. We use the strategy to set C_W^b at first as 2λ and if we are not satisfied with our solution, we increase the

value. The choice of the penalty parameter is a drawback of DGM, but from our experiments we can see, that the interval, which leads to sufficiently good approximation, is large enough.

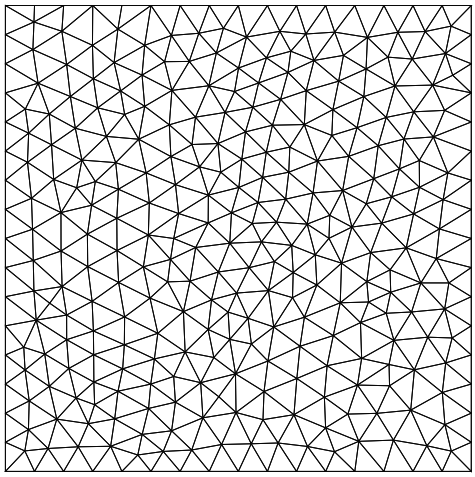

Figure 3.22: Unit square mesh.

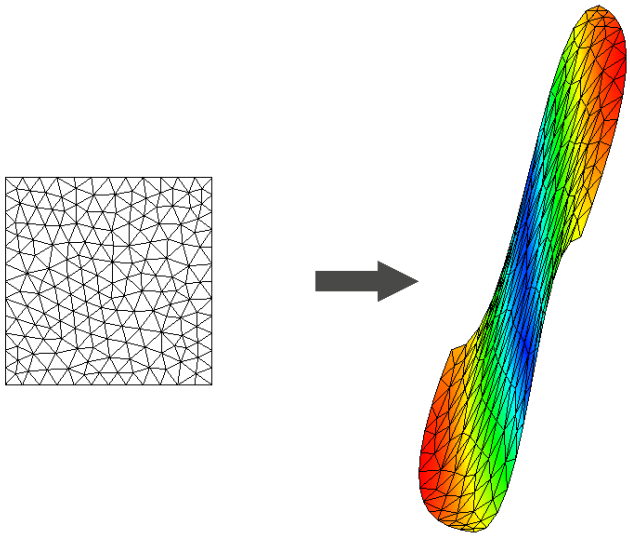

Figure 3.23: Solution on the unit square, visualization of the deformation, displacement magnitude (blue to red).

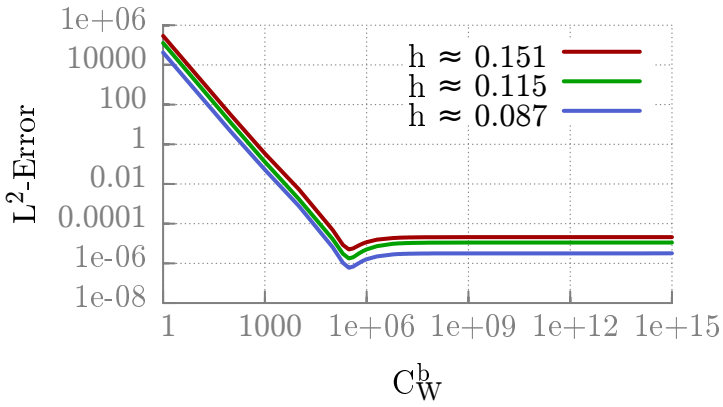

Figure 3.24: IIPG: L^2-norm error, P1 approximation.

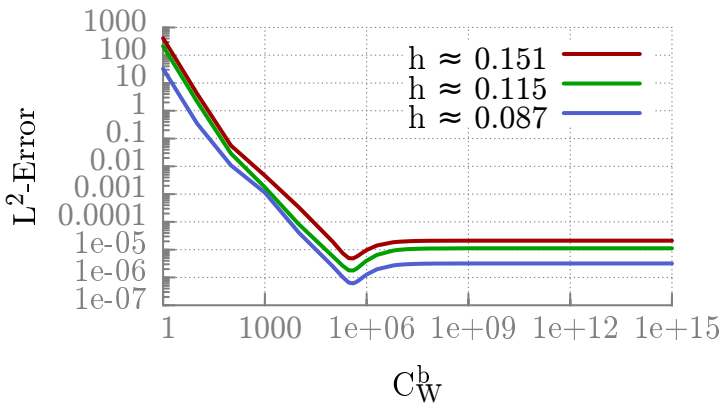

Figure 3.25: NIPG: L^2-norm error, P1 approximation.

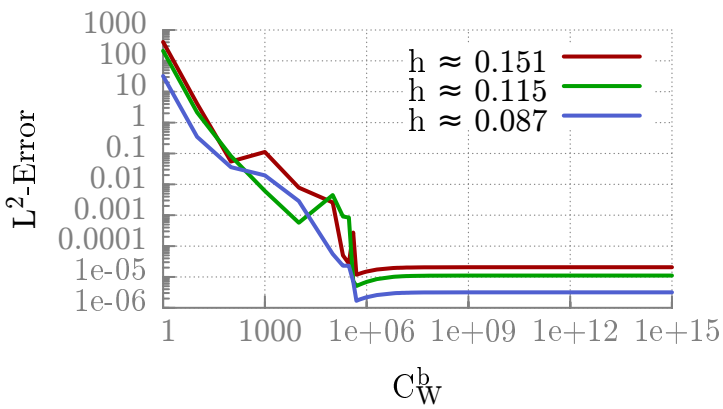

Figure 3.26: SIPG: L^2-norm error, P1 approximation.

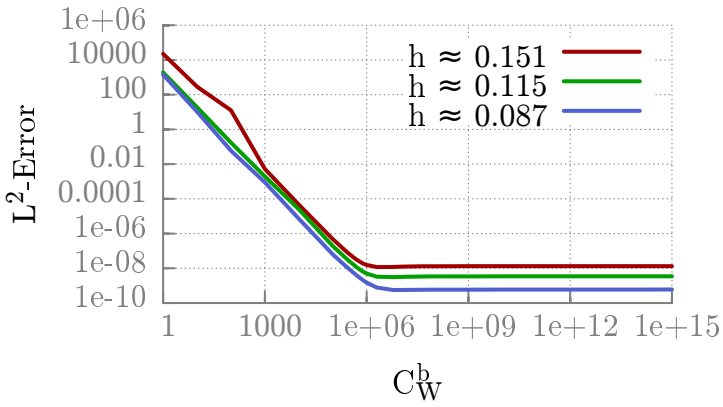

Figure 3.27: IIPG: L^2-norm error, P2 approximation.

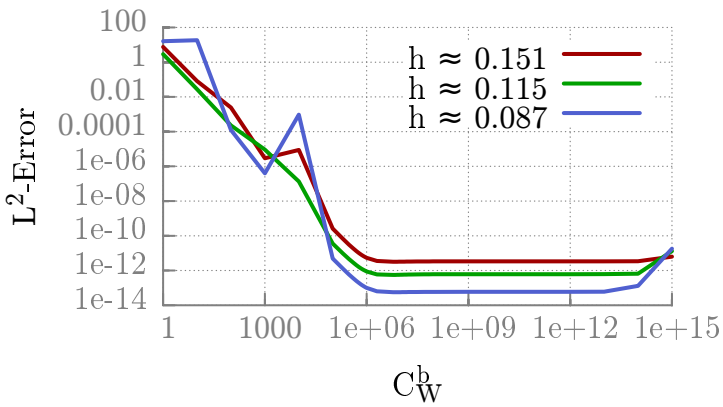

Figure 3.28: IIPG: L^2-norm error, P3 approximation.

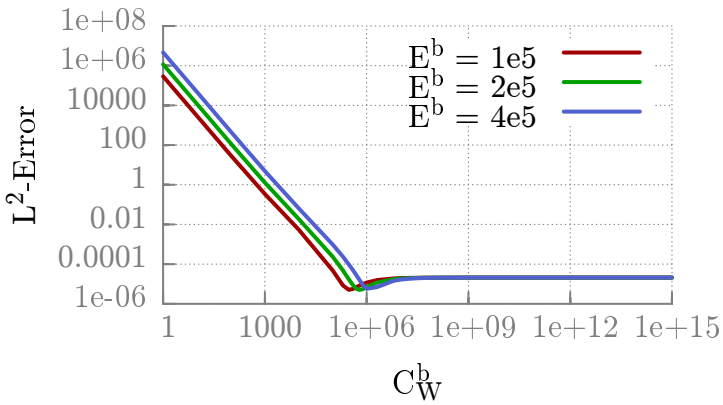

Figure 3.29: IIPG: L^2-norm error, P1 approximation, various Young's modulus.

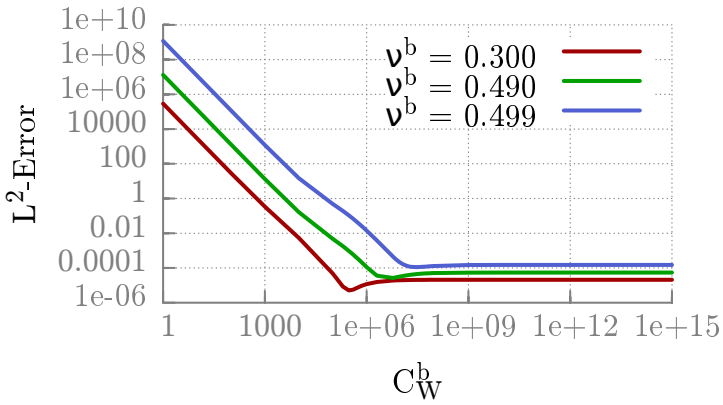

Figure 3.30: IIPG: L^2-norm error, P1 approximation, various Poisson's ratio.

E^b	ν^b	λ	μ	$\approx C^b_{W,\text{opt}}$
$1 \cdot 10^5$	0.3	57692	38462	$3 \cdot 10^5$
$2 \cdot 10^5$	0.3	115384	76923	$6 \cdot 10^5$
$4 \cdot 10^5$	0.3	230769	153846	$1 \cdot 10^6$
$1 \cdot 10^5$	0.49	1644295	33557	$6 \cdot 10^6$
$1 \cdot 10^5$	0.499	16644429	33356	$3 \cdot 10^7$

Table 3.11: Approximation of the optimal value of the penalty parameter for different material characteristics, IIPG variant.

3.4 Comparison of the DGM and FEM

The standard conforming finite element method (FEM) is more popular for the solution of elasticity problems. In this section we compare the DGM and the FEM for the dynamic elasticity problem. We use our own FEM implementation, which is described in [31, 40, 48]. It is based on continuous piecewise linear semidiscretization in space. The approximate solution of the structural problem is sought in the finite-dimensional space of the continuous functions, which are piecewise linear on every element of the triangulation $\mathcal{T}_h^b$. The triangulation is constructed similarly as for the DGM, but the standard conforming properties from the finite element method are required, see e.g. [10]. Nevertheless in all our numerical experiments in this work we use just the triangulations fulfilling these properties. The space semidiscretization of the problem leads to the system of ordinary differential equations, which is equipped with the initial conditions. By that is obtained the discrete initial value problem, which is solved by the Newmark method [9]. For more detailed description of the discretization see [31, 48].

For the numerical comparison of the introduced FEM method with the DGM method we use the case CSM3, described in Section 3.2, considering the linear elasticity model. The CSM3 is solved similarly on different unstructured triangulations. We compare the obtained results with the solution obtained by the IIPG variant of the DGM, where the time discretization was carried out by the second order BDF method with constant time step. Further for the DGM we set the constant $C_W^b = 6 \cdot 10^6$ and consider the piecewise linear approximation in space. In all experiments we use constant time step $\tau = 0.005$.

As in Section 3.2, we compare the time dependent values of the position of the point A, which are represented by the mean value, amplitude and frequency. In Table 3.12 are the obtained data for different methods and triangulations. Furthermore in Figure 3.31 we show the evolution at the point A. For the FEM we use finer mesh, in order to compute the problem with similar number of degrees of freedom. The results obtained by the FEM and the DGM for the particular test case are approximately the same for similar number of degrees of freedom.

The goal of this comparison is to show, that by the DGM we get comparable results with the FEM. Our main motivation for the choice of the DGM was that we are using the DGM for the fluid flow problem and therefore we use the same implementation technique also for the elasticity problem. Although we do not compare the DGM and the FEM for wide range of test cases, we can say that the DGM is suitable for the numerical solution of the particular case and at least as good as the FEM. However, in the future, it will be interesting to compare our implementation with other FEM based solvers and for different test cases.

method	# elem.	# DOF	u_2 [$\times 10^{-3}$]	
DGM (IIPG)	722	8664	-66.298 ± 70.739	[1.070]
FEM	2822	3102	-65.642 ± 67.066	[1.090]
FEM	8472	8940	-66.771 ± 68.313	[1.080]

Table 3.12: CSM3: Comparison of the displacement of the point A for BDF2, IIPG variant of the DGM and FEM with Newmark method for the linear elasticity material. The values are written in the format "*mean value* $\pm$ *amplitude [frequency]*".

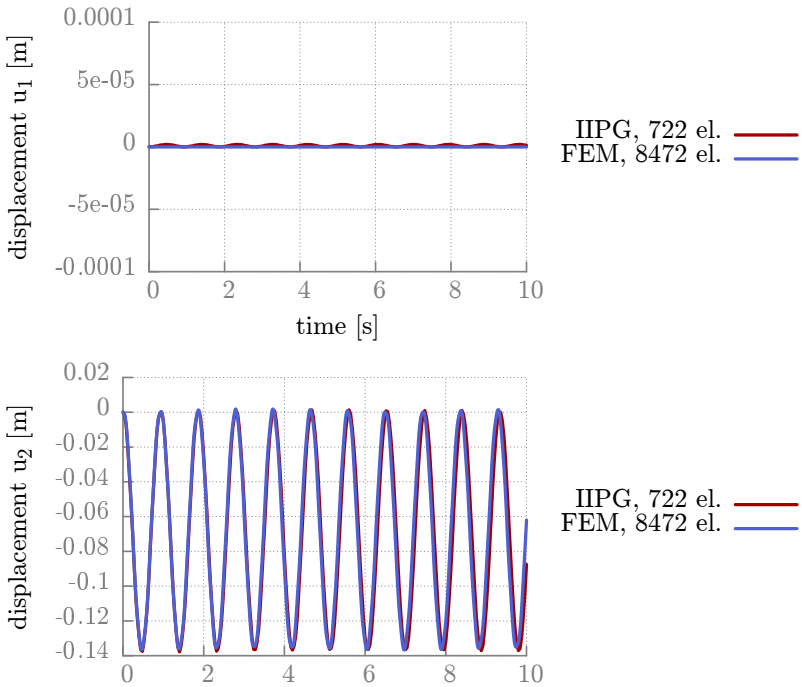

Figure 3.31: CSM3: Comparison of the displacement of the point A for BDF2, IIPG variant of the DGM and FEM with Newmark method for the linear elasticity material.

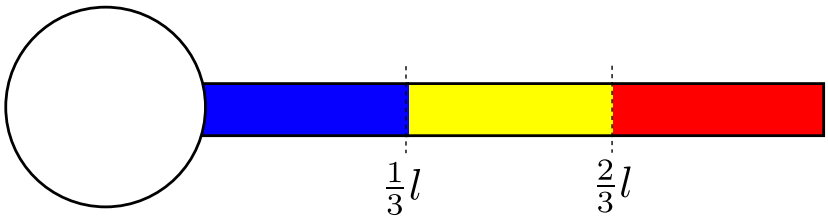

Figure 3.32: Nonhomogeneous elastic beam.

3.5 Nonhomogeneous material

In previous sections we presented numerical experiments, where the material was considered to be homogeneous. The current implementation allows us to formulate the problem also for the nonhomogeneous elasticity material. We still assume, that the material is given to be linear or nonlinear in the whole domain. In the case of nonlinear elasticity we also require the same nonlinear elasticity model for the whole domain. This means that the material parameters are given as functions over the domain Ω^b.

Our goal in this section is to present numerical results obtained for the nonhomogeneous elasticity model without further numerical analysis. In Chapter 5 the nonhomogeneous elasticity model is used for the simulation of the simplified model of the vocal folds. Here, we follow the problem solved in previous section, which can be compared with results obtained for the homogeneous material. Further, we introduce problem, which is motivated by the simulation of the vocal folds motion.

3.5.1 Nonhomogeneous elastic beam

Let us introduce the static elasticity problem similar to CSM1 or CSM2. Contrary to them we assume, that the Lamé parameters are given not as constants, but as functions defined on the reference domain Ω^b, so that

$$\lambda(\boldsymbol{x}) = \begin{cases} 1.0 \cdot 10^6 & \text{for } x_1 \leq \frac{1}{3}l, \\ 2.0 \cdot 10^6 & \text{for } \frac{1}{3}l < x_1 \leq \frac{2}{3}l, \\ 8.0 \cdot 10^6 & \text{for } \frac{2}{3}l < x_1, \end{cases} \tag{3.14}$$

$$\mu(\boldsymbol{x}) = \begin{cases} 0.25 \cdot 10^6 & \text{for } x_1 \leq \frac{1}{3}l, \\ 0.5 \cdot 10^6 & \text{for } \frac{1}{3}l < x_1 \leq \frac{2}{3}l, \\ 2.0 \cdot 10^6 & \text{for } \frac{2}{3}l < x_1, \end{cases} \tag{3.15}$$

where l is the length of the beam. The division of the domain into three parts is visualized in Figure 3.32. In practical computations the Lamé parameters are evaluated as functions in quadrature points.

The boundary conditions and the applied forces are set as in Section 3.1, i.e. the acting body force density $\boldsymbol{f}$ is prescribed by the density

$$\boldsymbol{b} = (0, -2)^T \ \ [\text{m.s}^{-2}] \tag{3.16}$$

and the mass density

$$\rho^b = 10^3 \ [\text{kg.m}^{-3}]. \tag{3.17}$$

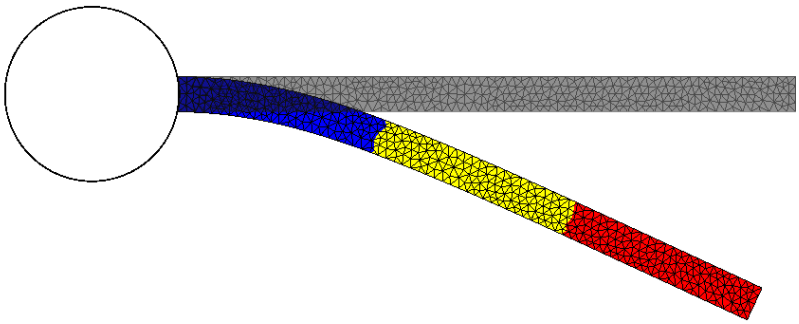

Figure 3.33: Static deformation of the nonhomogeneous elastic beam, neo-Hookean material.

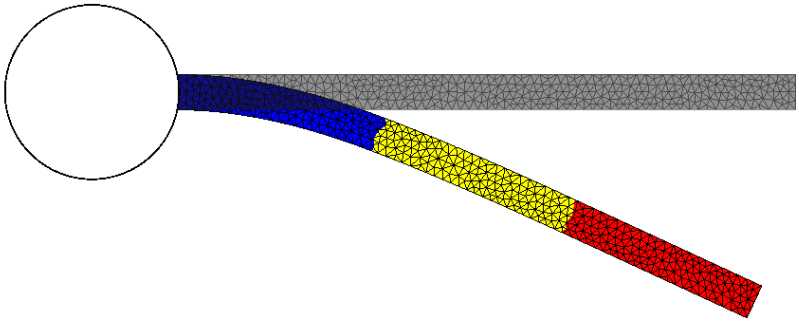

Figure 3.34: Static deformation of the nonhomogeneous elastic beam, St. Venant-Kirchhoff material.

On the left part of the boundary connected with the rigid body we prescribe homogeneous Dirichlet boundary condition

$$\boldsymbol{u}_D = \mathbf{0} \quad \text{on } \Gamma_D^b, \tag{3.18}$$

and on the rest of the boundary we prescribe the Neumann boundary condition with no surface traction

$$\boldsymbol{g}_N = \mathbf{0} \quad \text{on } \Gamma_N^b. \tag{3.19}$$

The test problem was computed on Mesh #1, see Figure 3.2 and Table 3.1, for both introduced nonlinear materials. The visualization of the solution using the neo-Hookean material is in Figure 3.33 and using the St. Venant-Kirchhoff material in Figure 3.34. We can see in Table 3.13, that there is a small difference between the displacements of the point A.

material	$u_1\,[\times 10^{-3}]$	$u_2\,[\times 10^{-3}]$
St. Venant-Kirchhoff	-23.378	-119.191
neo-Hookean	-23.277	-119.168

Table 3.13: CSM3: Comparison of the displacement of the point A for St. Venant-Kirchhoff and neo-Hookean material.

3.5.2 Nonhomogeneous model of vocal folds

Finally, let us define the dynamic elasticity problem, where the elastic body is motivated by the cut of a vocal fold. The body is divided into a few regions with different material properties. We prescribe the surface force acting on the body for short time and let the body vibrate further without any other influence.

The division of the domain into 4 regions with different material characteristics is illustrated in Figure 3.35 by the Lamé parameters. The boundaries of the subdomains are given by spline interpolations, see the .NET implementation of the model of vocal folds in Attachment A.1. Additionally, the settings of the material characteristics are described in Table 3.14. Further, we consider, that material density is the same for all subdomains and we set the acting body force density $\boldsymbol{f}$ to zero

$$\rho^b = 1040 \ [\mathrm{kg.m}^{-3}], \quad \boldsymbol{f} = \boldsymbol{0} \quad \text{in } \Omega^b \times [0, T]. \tag{3.20}$$

We prescribe the initial displacement and initial velocity to be zero

$$\boldsymbol{u}_0 = \boldsymbol{0}, \quad \boldsymbol{v}_0^b = \boldsymbol{0} \quad \text{in } \Omega^b. \tag{3.21}$$

On the bottom, right and left straight part of the boundary we prescribe homogeneous Dirichlet boundary condition

$$\boldsymbol{u}_D = \boldsymbol{0} \quad \text{in } \Gamma_D^b \times [0, T], \tag{3.22}$$

and on the curved part of the boundary we prescribe the Neumann boundary condition in the following way

$$\boldsymbol{g}_N = -p_N \boldsymbol{n} \quad \text{in } \Gamma_N^b \times [0, T], \tag{3.23}$$

where p_N is a pressure defined as

$$p_N = \begin{cases} 800 & \text{for } x_1 \in [0, 0.00875), \quad t \in [0, 0.02), \\ -1000 & \text{for } x_1 \in [0.00875, 0.015), \quad t \in [0, 0.02), \\ 200 & \text{for } x_1 \in [0.015, 0.0175], \quad t \in [0, 0.02), \\ 0 & \text{else.} \end{cases} \tag{3.24}$$

The visualization of the solution at time instants 0.0, 0.002, ..., 0.018 s using the neo-Hookean material is in Figure 3.37. (The figures are ordered in such a way that in the first line are the patterns corresponding to the time instants $t = 0.0$, 0.002 s, the second line corresponds to $t = 0.004$, 0.006 s, etc.) We used the same colours to distinguish the regions with different material characteristics as in Figure 3.35. Further we show the displacement $\boldsymbol{u}$ of the point $[0.01, -0.001]$ in Figure 3.38 and the Fourier analysis of the displacement in the x_1 and x_2 directions in Figures 3.39 and 3.40, respectively. The value of the first main frequencies is approximately 90 and 144 Hz.

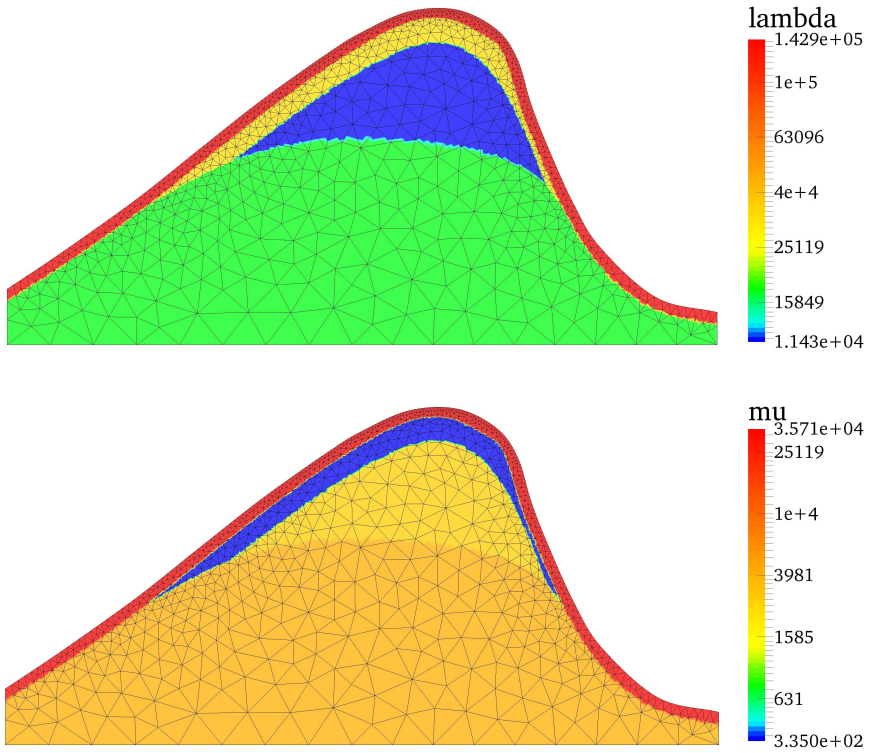

Figure 3.35: Nonhomogeneous model of vocal folds - Lamé parameters.

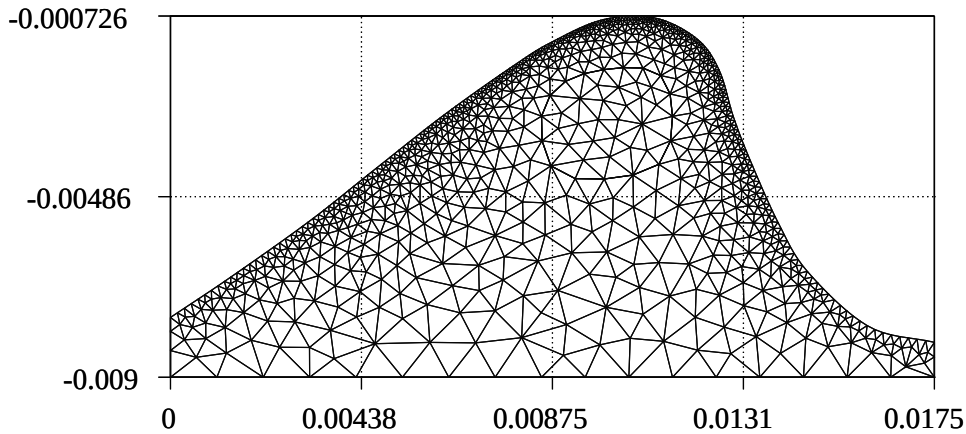

Figure 3.36: Model of vocal folds - computational mesh.

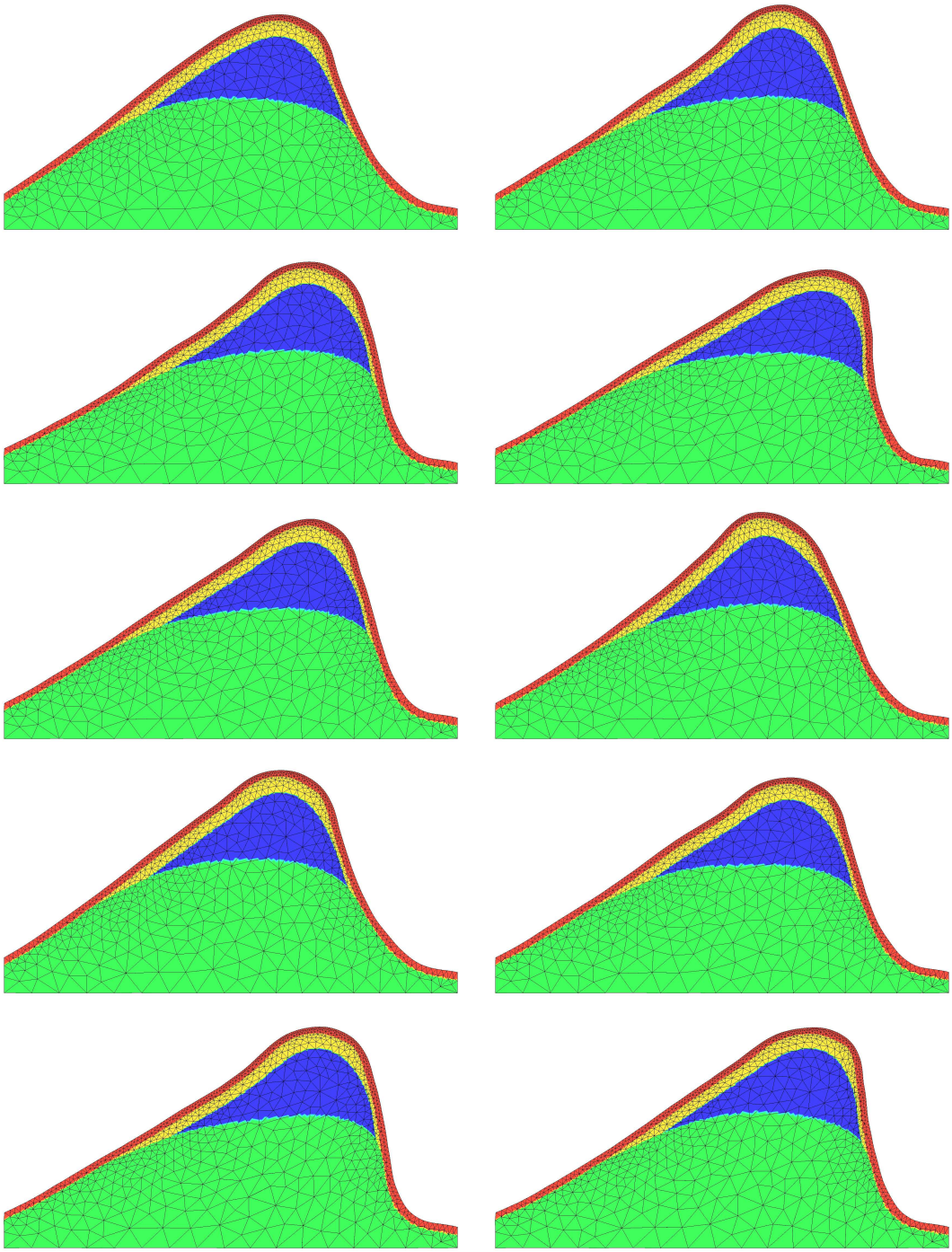

Figure 3.37: Nonhomogeneous model of vocal folds, visualization of the deformation at time instants 0.0, 0.002, . . . , 0.018 s.

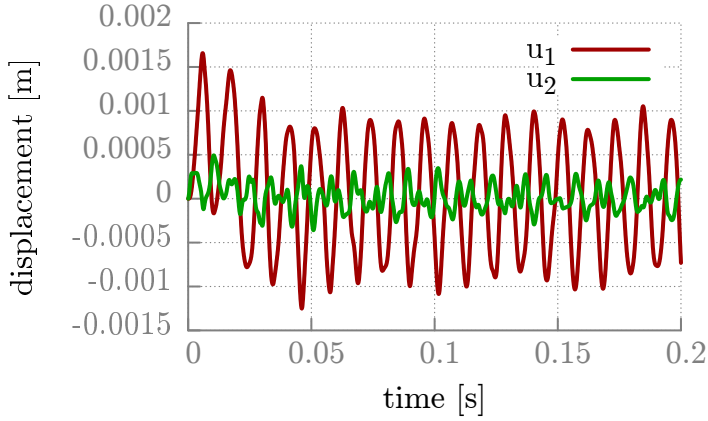

Figure 3.38: Nonhomogeneous model of vocal folds, displacement of the point [0.01, -0.001].

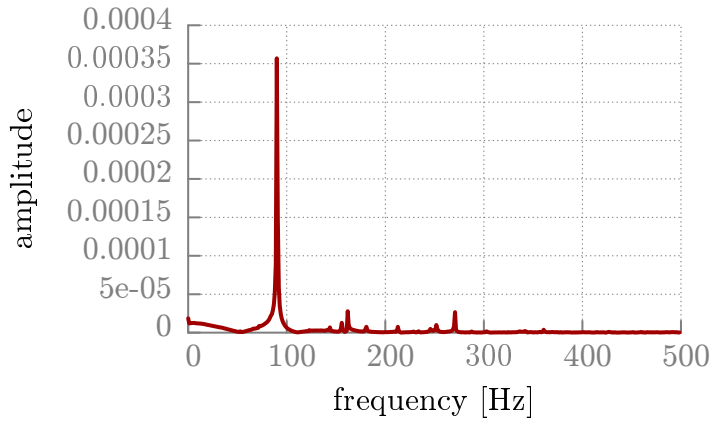

Figure 3.39: Nonhomogeneous model of vocal folds, Fourier analysis of the displacement of the point [0.01, -0.001] in the direction x_1.

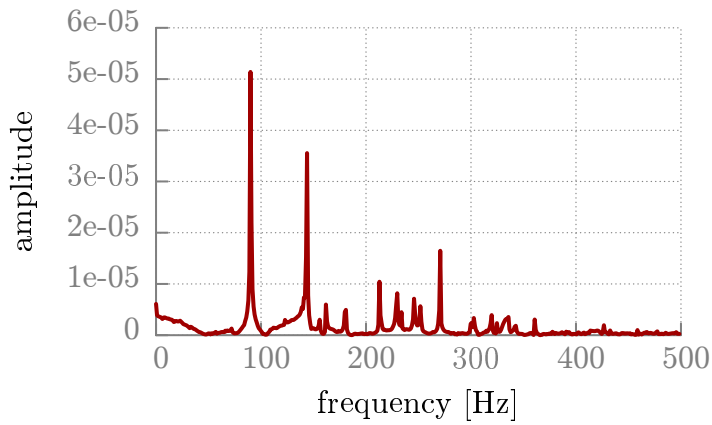

Figure 3.40: Nonhomogeneous model of vocal folds, Fourier analysis of the displacement of the point [0.01, -0.001] in the direction x_2.

E^b	ν^b	λ	μ
$12 \cdot 10^3$	0.4	17143	4285
$8 \cdot 10^3$	0.4	11430	2857
$1 \cdot 10^3$	0.495	33110	335
$100 \cdot 10^3$	0.4	142857	35714

Table 3.14: Nonhomogeneous model of vocal folds - Lamé parameters.
See Figure 3.35 for the visualization of the corresponding subdomains, ordered from the lower layer to the upper layer.

4. Compressible Navier-Stokes equations

In this chapter we shall deal with the problem of compressible viscous flow in a bounded two-dimensional domain depending on time. This problem is described by the system of compressible Navier-Stokes equations. The derivation of this system can be found e.g. in [27]. We consider Newtonian fluid flow, which means that the viscous part of the stress tensor depends linearly on the velocity deformation tensor. Examples of Newtonian fluids are air or water, but also other gases and many common liquids.

Contrary to the elasticity problem, the fluid flow problem is formulated in *Eulerian coordinates*. However, because of the time-dependence of the computational domain, we rewrite this system with the aid of the *arbitrary Lagrangian-Eulerian* (ALE) method. We use the same notation $\boldsymbol{x}$ as for the *Lagrangian coordinates*. In Chapter 5, which deals with FSI problems, we pay attention to the use of different coordinates. For the numerical solution, we apply the discontinuous Galerkin finite element method to the governing problem and finish the chapter with implementation notes.

4.1 Problem formulation

Let $\Omega_t^f = \Omega^f(t) \subset \mathbb{R}^2$, $t \in [0,T]$, $T > 0$ be a bounded domain depending on time.

The system describing compressible flow consists of the continuity equation, the Navier-Stokes equations and the energy equation:

$$\begin{aligned}
\frac{\partial \rho}{\partial t} + \operatorname{div}(\rho \boldsymbol{v}) &= 0, \qquad (4.1)\\
\frac{\partial \rho v_i}{\partial t} + \operatorname{div}(\rho v_i \boldsymbol{v}) &= \sum_{j=1}^{2} \frac{\partial \sigma_{ij}^f}{\partial x_j}, \quad \text{for } i = 1,2\ ,\\
\frac{\partial E}{\partial t} + \operatorname{div}(E \boldsymbol{v}) &= \sum_{i=1}^{2} \frac{\partial}{\partial x_i} \left(\sum_{j=1}^{2} \sigma_{ij}^f v_j + \kappa \frac{\partial \theta}{\partial x_i} \right),
\end{aligned}$$

where

$$\sigma_{ij}^f = -p\delta_{ij} + \sigma_{ij}^V, \quad i,j = 1,2\ , \qquad (4.2)$$

$$\sigma_{ij}^V = \lambda \operatorname{div}\boldsymbol{v}\, \delta_{ij} + 2\mu\, d_{ij}(\boldsymbol{v}),\ d_{ij}(\boldsymbol{v}) = \frac{1}{2}\left(\frac{\partial v_i}{\partial x_j} + \frac{\partial v_j}{\partial x_i} \right). \qquad (4.3)$$

The above system is completed by the thermodynamical relations for the perfect gas:

$$p = (\gamma - 1)\left(E - \frac{1}{2}\rho |\boldsymbol{v}|^2 \right), \quad \theta = \frac{1}{c_v}\left(\frac{E}{\rho} - \frac{1}{2}|\boldsymbol{v}|^2 \right). \qquad (4.4)$$

We use the following notation:

$$
\begin{aligned}
\rho &\ - \ \text{fluid density,}\\
p &\ - \ \text{pressure,}\\
E &\ - \ \text{total energy,}\\
\boldsymbol{v} = (v_1, v_2) &\ - \ \text{velocity vector,}\\
\theta &\ - \ \text{absolute temperature,}\\
c_v > 0 &\ - \ \text{specific heat at constant volume,}\\
c_p > 0 &\ - \ \text{specific heat at constant pressure,}\\
\gamma = \tfrac{c_p}{c_v} > 1 &\ - \ \text{Poisson adiabatic constant,}\\
\mu > 0, \lambda = -2\mu/3 &\ - \ \text{viscosity coefficients,}\\
\kappa > 0 &\ - \ \text{heat conduction coefficient,}\\
\sigma^V_{ij} &\ - \ \text{components of the viscous part of the stress tensor,}\\
\sigma^f_{ij} &\ - \ \text{components of the stress tensor } \sigma^f,\\
\boldsymbol{z}_D &\ - \ \text{velocity of a moving wall.}
\end{aligned}
$$

Finally the resulting system (4.1) needs to be equipped with initial and boundary conditions characterizing the behaviour of the fluid flow at initial time $t = 0$ and on the boundary $\partial\Omega^f_t$ of the domain Ω^f_t. The initial conditions are simply given by initial data $\boldsymbol{v}^0$, ρ^0 and p^0:

$$
\begin{aligned}
\boldsymbol{v}(\boldsymbol{x}, 0) &= \boldsymbol{v}^0(\boldsymbol{x}),\\
\rho(\boldsymbol{x}, 0) &= \rho^0(\boldsymbol{x}),\\
p(\boldsymbol{x}, 0) &= p^0(\boldsymbol{x}).
\end{aligned}
\tag{4.5}
$$

For the choice of the boundary conditions let us assume that the boundary of Ω^f_t consists of three disjoint parts: $\partial\Omega^f_t = \Gamma_I \cup \Gamma_O \cup \Gamma_{Wt}$, where Γ_I is the inlet, Γ_O is the outlet and $\Gamma_{Wt} = \Gamma_W(t)$ denotes impermeable walls that may move in dependence on time. On the individual parts of the boundary we prescribe the following conditions:

$$
\text{a)}\ \ \rho|_{\Gamma_I} = \rho_D, \quad \text{b)}\ \ \boldsymbol{v}|_{\Gamma_I} = \boldsymbol{v}_D = (v_{D1}, v_{D2})^{\mathrm{T}}, \tag{4.6}
$$

$$
\text{c)}\ \ \sum_{i,j=1}^{2} \sigma^V_{ij} n_i v_j + \kappa \frac{\partial \theta}{\partial n} = 0 \quad \text{on } \Gamma_I,
$$

$$
\text{a)}\ \ \sum_{i=1}^{2} \sigma^V_{ij} n_i = 0, \quad j = 1,\, 2, \quad \text{b)}\ \ \frac{\partial \theta}{\partial n} = 0 \text{ on } \Gamma_O, \tag{4.7}
$$

$$
\text{a)}\ \ \boldsymbol{v} = \boldsymbol{z}_D, \quad \text{b)}\ \ \frac{\partial \theta}{\partial n} = 0 \text{ on } \Gamma_{Wt}, \tag{4.8}
$$

where ρ_D and $\boldsymbol{v}_D$ are given functions.

4.2 Dimensionless form

For the numerical solution of the compressible viscous flow it is suitable to use the dimensionless form of the Navier-Stokes equations. According to [27] let us introduce positive reference quantities:

L^*	-	reference length,
U^*	-	reference magnitude of velocity,
ρ^*	-	reference density,
μ^*	-	reference viscosity.

All other reference quantities can be derived from these basic ones:

L^*/U^*	-	reference quantity for time,
$\rho^* U^{*2}$	-	reference quantity for both pressure and total energy,
U^{*2}/c_v	-	reference quantity for temperature.

With primes we denote the dimensionless quantities

$$
\begin{aligned}
&x_i^{'} = \frac{x_i}{L^*}, \quad v_i^{'} = \frac{v_i}{U^*}, \quad \boldsymbol{v}^{'} = \frac{\boldsymbol{v}}{U^*}, \quad \rho^{'} = \frac{\rho}{\rho^*}, \\
&p^{'} = \frac{p}{\rho^* U^{*2}}, \quad E^{'} = \frac{E}{\rho^* U^{*2}}, \quad \theta^{'} = \frac{c_v \theta}{U^{*2}}, \quad t^{'} = \frac{t U^*}{L^*}, \\
&\mu^{'} = \frac{\mu}{\mu^*}, \quad \lambda^{'} = \frac{\lambda}{\mu^*}.
\end{aligned} \tag{4.9}
$$

Then system (4.1) can be written in the dimensionless form

$$
\begin{aligned}
&\frac{\partial \rho^{'}}{\partial t^{'}} + \mathrm{div}(\rho^{'} \boldsymbol{v}^{'}) = 0, \\
&\frac{\partial \rho^{'} v_i^{'}}{\partial t^{'}} + \mathrm{div}(\rho^{'} v_i^{'} \boldsymbol{v}^{'}) = -\frac{\partial p^{'}}{\partial x_i^{'}} + \frac{1}{Re} \sum_{j=1}^{2} \frac{\partial \sigma_{ij}^{'V}}{\partial x_j^{'}}, \quad \text{for } i = 1, 2\ , \\
&\frac{\partial E^{'}}{\partial t^{'}} + \mathrm{div}(E^{'} \boldsymbol{v}^{'}) = -\mathrm{div}(p^{'} \boldsymbol{v}^{'}) + \frac{1}{Re} \left(\sum_{i=1}^{2} \frac{\partial}{\partial x_i^{'}} \left(\sum_{j=1}^{2} \sigma_{ij}^{'V} v_j^{'} \right) \right) + \frac{\gamma}{Re\ Pr} \Delta \theta^{'},
\end{aligned} \tag{4.10}
$$

where

$$
\sigma_{ij}^{'V} = \lambda^{'}\ \mathrm{div} \boldsymbol{v}^{'}\ \delta_{ij} + 2\mu^{'}\ d_{ij}^{'}(\boldsymbol{v}^{'}), \tag{4.11}
$$

$$
d_{ij}^{'}(\boldsymbol{v}^{'}) = \frac{1}{2} \left(\frac{\partial v_i^{'}}{\partial x_j^{'}} + \frac{\partial v_j^{'}}{\partial x_i^{'}} \right), \tag{4.12}
$$

is the viscous part of the stress tensor in dimensionless form. Further,

$$
Re = \frac{\rho^* U^* L^*}{\mu^*}, \tag{4.13}
$$

$$
Pr = \frac{c_p \mu^*}{\kappa} \tag{4.14}
$$

are the so-called Reynolds and Prandtl numbers. Finally we have to complete system (4.10) with equations (4.4) in the dimensionless form

$$p' = (\gamma - 1)(E' - \frac{1}{2}\rho'|\boldsymbol{v}'|^2), \tag{4.15}$$

$$\theta' = \left(\frac{E'}{\rho'} - \frac{1}{2}|\boldsymbol{v}'|^2\right). \tag{4.16}$$

Furthermore the primes will be omitted, because system (4.10) has formally the same form and properties as system (4.1). Then the system of governing equations can be written in the dimensionless conservative form

$$\frac{\partial \boldsymbol{w}}{\partial t} + \sum_{s=1}^{2} \frac{\partial \boldsymbol{f}_s(\boldsymbol{w})}{\partial x_s} = \sum_{s=1}^{2} \frac{\partial \boldsymbol{R}_s(\boldsymbol{w}, \nabla \boldsymbol{w})}{\partial x_s}, \tag{4.17}$$

where

$$\begin{aligned}
\boldsymbol{w} &= (w_1, \ldots, w_4)^T = (\rho, \rho v_1, \rho v_2, E)^T \in \mathbb{R}^4, \qquad (4.18)\\
\boldsymbol{w} &= \boldsymbol{w}(\boldsymbol{x}, t),\ \ \boldsymbol{x} \in \Omega_t^f,\ \ t \in (0, T),\\
\boldsymbol{f}_s(\boldsymbol{w}) &= (f_{s1}, \cdots, f_{s4})^T = (\rho v_s, \rho v_1 v_s + \delta_{1s}\, p, \rho v_2 v_s + \delta_{2s}\, p, (E + p) v_s)^T,\\
\boldsymbol{R}_s(\boldsymbol{w}, \nabla \boldsymbol{w}) &= (R_{s1}, \ldots, R_{s4})^T = \frac{1}{Re}\left(0, \sigma_{s1}^V, \sigma_{s2}^V, \sigma_{s1}^V\, v_1 + \sigma_{s2}^V\, v_2 + \frac{\gamma}{Pr}\frac{\partial \theta}{\partial x_s}\right)^T,\\
\sigma_{ij}^V &= \lambda\, \mathrm{div}\boldsymbol{v}\, \delta_{ij} + 2\mu\, d_{ij}(\boldsymbol{v}),\ \ d_{ij}(\boldsymbol{v}) = \frac{1}{2}\left(\frac{\partial v_i}{\partial x_j} + \frac{\partial v_j}{\partial x_i}\right).
\end{aligned}$$

The vector-valued function $\boldsymbol{w}$ is called the state vector, functions $\boldsymbol{f}_s$ are the so-called inviscid fluxes and $\boldsymbol{R}_s$ represent viscous terms.

Let us present some properties of the inviscid and viscous fluxes $\boldsymbol{f}_s$ and $\boldsymbol{R}_s$, which are important for introducing the linearization of the nonlinear fluxes, which is fundamental for semi-implicit time discretization schemes. It is easy to see that $\boldsymbol{f}_s(\alpha \boldsymbol{w}) = \alpha\ \boldsymbol{f}_s(\boldsymbol{w})$ for $\alpha > 0$. This property implies that

$$\boldsymbol{f}_s(\boldsymbol{w}) = \boldsymbol{A}_s(\boldsymbol{w})\boldsymbol{w}, \quad s = 1, 2, \tag{4.19}$$

where

$$\boldsymbol{A}_s(\boldsymbol{w}) = \frac{D\boldsymbol{f}_s(\boldsymbol{w})}{D\boldsymbol{w}}, \quad s = 1, 2, \tag{4.20}$$

are the Jacobi matrices of the mappings $\boldsymbol{f}_s$. The viscous terms $\boldsymbol{R}_s(\boldsymbol{w}, \nabla \boldsymbol{w})$ can be written in the form

$$\boldsymbol{R}_s(\boldsymbol{w}, \nabla \boldsymbol{w}) = \sum_{k=1}^{2} \boldsymbol{K}_{s,k}(\boldsymbol{w}) \frac{\partial \boldsymbol{w}}{\partial x_k}, \quad s = 1, 2, \tag{4.21}$$

where $\boldsymbol{K}_{s,k}(\boldsymbol{w}) \in \mathbb{R}^{4\times 4}$ are matrices depending on $\boldsymbol{w}$ in a nonlinear way (cf. [22]). They can be expressed in the following form:

$$\boldsymbol{K}_{1,1}(\boldsymbol{w}) = \frac{1}{Re}\begin{pmatrix} 0, & 0, & 0, & 0 \\ -(2\mu+\lambda)\frac{w_2}{w_1^2}, & (2\mu+\lambda)\frac{1}{w_1}, & 0, & 0 \\ -\mu\frac{w_3}{w_1^2}, & 0, & \frac{\mu}{w_1}, & 0 \\ \{\boldsymbol{K}_{1,1}\}_{4,1}, & \left(2\mu+\lambda-\frac{\gamma}{Pr}\right)\frac{w_2}{w_1^2}, & \left(\mu-\frac{\gamma}{Pr}\right)\frac{w_3}{w_1^2}, & \frac{\gamma}{Pr\ w_1} \end{pmatrix},$$

$$\boldsymbol{K}_{1,2}(\boldsymbol{w}) = \frac{1}{Re}\begin{pmatrix} 0, & 0, & 0, & 0 \\ -\lambda\frac{w_3}{w_1^2}, & 0, & \frac{\lambda}{w_1}, & 0 \\ -\mu\frac{w_2}{w_1^2}, & \frac{\mu}{w_1}, & 0, & 0 \\ -(\lambda+\mu)\frac{w_2w_3}{w_1^3}, & \mu\frac{w_3}{w_1^2}, & \lambda\frac{w_2}{w_1^2}, & 0 \end{pmatrix},$$

$$\boldsymbol{K}_{2,1}(\boldsymbol{w}) = \frac{1}{Re}\begin{pmatrix} 0, & 0, & 0, & 0 \\ -\mu\frac{w_3}{w_1^2}, & 0, & \frac{\mu}{w_1}, & 0 \\ -\lambda\frac{w_2}{w_1^2}, & \frac{\lambda}{w_1}, & 0, & 0 \\ -(\lambda+\mu)\frac{w_2w_3}{w_1^3}, & \lambda\frac{w_3}{w_1^2}, & \mu\frac{w_2}{w_1^2}, & 0 \end{pmatrix},$$

$$\boldsymbol{K}_{2,2}(\boldsymbol{w}) = \frac{1}{Re}\begin{pmatrix} 0, & 0, & 0, & 0 \\ -\mu\frac{w_2}{w_1^2}, & \frac{\mu}{w_1}, & 0, & 0 \\ -(2\mu+\lambda)\frac{w_3}{w_1^2}, & 0, & (2\mu+\lambda)\frac{1}{w_1}, & 0 \\ \{\boldsymbol{K}_{2,2}\}_{4,1}, & \left(\mu-\frac{\gamma}{Pr}\right)\frac{w_2}{w_1^2}, & \left(2\mu+\lambda-\frac{\gamma}{Pr}\right)\frac{w_3}{w_1^2}, & \frac{\gamma}{Pr\ w_1} \end{pmatrix},$$

where

$$\{\boldsymbol{K}_{1,1}\}_{4,1} = -(2\mu+\lambda)\frac{w_2^2}{w_1^3} - \mu\frac{w_3^2}{w_1^3} + \frac{\gamma}{Pr}\left(-\frac{w_4}{w_1^2} + \frac{w_2^2+w_3^2}{w_1^3}\right),$$
$$\{\boldsymbol{K}_{2,2}\}_{4,1} = -\mu\frac{w_2^2}{w_1^3} - (2\mu+\lambda)\frac{w_3^2}{w_1^3} + \frac{\gamma}{Pr}\left(-\frac{w_4}{w_1^2} + \frac{w_2^2+w_3^2}{w_1^3}\right).$$

4.3 The Arbitrary Lagrangian-Eulerian form

Because of the dependence of the computational domain on time, we employ the *arbitrary Lagrangian-Eulerian* (ALE) method, see e.g. [52]. It is based on a regular one-to-one ALE mapping of the reference configuration Ω_0^f onto the current configuration Ω_t^f. Let us denote by $\boldsymbol{X}$ the points of the reference domain Ω_0^f and by $\boldsymbol{x}$ the points of the domain Ω_t^f. Then

$$\mathcal{A}_t : \overline{\Omega}_0^f \longrightarrow \overline{\Omega}_t^f, \text{ i.e. } \boldsymbol{X} \in \overline{\Omega}_0^f \longmapsto \boldsymbol{x} = \boldsymbol{x}(\boldsymbol{X}, t) = \mathcal{A}_t(\boldsymbol{X}) \in \overline{\Omega}_t^f.$$

We define the domain velocity $\boldsymbol{z} = (z_1, z_2)$ by the relations

$$\tilde{\boldsymbol{z}}(\boldsymbol{X}, t) = \frac{\partial}{\partial t}\mathcal{A}_t(\boldsymbol{X}), \quad t \in [0,T],\ \boldsymbol{X} \in \Omega_0^f, \tag{4.22}$$
$$\boldsymbol{z}(\boldsymbol{x}, t) = \tilde{\boldsymbol{z}}(\mathcal{A}_t^{-1}(\boldsymbol{x}), t), \quad t \in [0,T],\ \boldsymbol{x} \in \Omega_t^f,$$

and the ALE derivative of a vector function $\boldsymbol{w} = \boldsymbol{w}(\boldsymbol{x}, t)$ defined for $\boldsymbol{x} \in \Omega_t^f$ and $t \in [0,T]$:

$$\frac{D^A}{Dt}\boldsymbol{w}(\boldsymbol{x}, t) = \frac{\partial \tilde{\boldsymbol{w}}}{\partial t}(\boldsymbol{X}, t), \tag{4.23}$$

where

$$\tilde{\boldsymbol{w}}(\boldsymbol{X},t) = \boldsymbol{w}(\mathcal{A}_t(\boldsymbol{X}),t),\ \boldsymbol{X} \in \Omega_0^f,\ \boldsymbol{x} = \mathcal{A}_t(\boldsymbol{X}).$$

Then by the chain rule and simple manipulation we have

$$\frac{D^A\boldsymbol{w}}{Dt} = \frac{\partial \boldsymbol{w}}{\partial t} + \sum_{s=1}^{2} \frac{\partial\,(z_s\boldsymbol{w})}{\partial x_s} - \boldsymbol{w}\,\mathrm{div}\boldsymbol{z}, \tag{4.24}$$

and system (4.17), describing the compressible flow, can be written in the ALE form (see, e.g. [30]) as

$$\frac{D^A\boldsymbol{w}}{Dt} + \sum_{s=1}^{2} \frac{\partial \boldsymbol{g}_s(\boldsymbol{w})}{\partial x_s} + \boldsymbol{w}\,\mathrm{div}\boldsymbol{z} = \sum_{s=1}^{2} \frac{\partial \boldsymbol{R}_s(\boldsymbol{w},\nabla\boldsymbol{w})}{\partial x_s}, \tag{4.25}$$

where

$$\boldsymbol{g}_s(\boldsymbol{w}) = \boldsymbol{f}_s(\boldsymbol{w}) - z_s\boldsymbol{w}, \quad s = 1,2. \tag{4.26}$$

Now we can summarize the formulation of the flow problem in the following definition.

Definition 9. *(ALE formulation of the compressible Navier-Stokes equations)* Let us consider a time interval $[0,T]$ with $T > 0$ and a bounded domain $\Omega_t^f = \Omega^f(t) \subset \mathbb{R}^2$, $t \in [0,T]$, depending on time, with Lipschitz boundary $\partial\Omega_t^f$. We assume that the boundary of the domain Ω_t^f consists of three disjoint parts: the inlet Γ_I, the outlet Γ_O and the impermeable walls Γ_{Wt} that may move in dependence on time. It holds that $\partial\Omega_t^f = \Gamma_I \cup \Gamma_O \cup \Gamma_{Wt}$. We define the solution of the compressible Navier-Stokes system as a state vector $\boldsymbol{w} : \Omega_t^f \times [0,T] \to \mathbb{R}^4$ defined in (4.18) such that

$$\frac{D^A\boldsymbol{w}}{Dt} + \sum_{s=1}^{2} \frac{\partial \boldsymbol{g}_s(\boldsymbol{w})}{\partial x_s} + \boldsymbol{w}\,\mathrm{div}\boldsymbol{z} = \sum_{s=1}^{2} \frac{\partial \boldsymbol{R}_s(\boldsymbol{w},\nabla\boldsymbol{w})}{\partial x_s}, \tag{4.27}$$

where $\frac{D^A\boldsymbol{w}}{Dt}$ is the ALE derivative of the function $\boldsymbol{w}$, defined in (4.23), $\boldsymbol{g}_s$ are the inviscid fluxes defined in (4.26), $\boldsymbol{z}$ is the domain velocity defined in (4.22) and $\boldsymbol{R}_s$ represents the viscous terms defined in (4.18). The definition of this problem is completed by initial conditions defined in (4.5) and by boundary conditions defined in (4.6)–(4.8).

4.4 Space semidiscretization of the flow problem

For the space semidiscretization we use the discontinuous Galerkin method (DGM) leading to a system of ordinary differential equations. We construct a polygonal approximation Ω_{ht}^f of the domain Ω_t^f. By $\mathcal{T}_{ht}$ we denote a partition of the closure $\overline{\Omega}_{ht}^f$ of the domain Ω_{ht}^f into a finite number of closed triangles K with mutually disjoint interiors such that

$$\overline{\Omega}_{ht}^f = \bigcup_{K\in\mathcal{T}_{ht}} K. \tag{4.28}$$

By $\mathcal{F}_{ht}$ we denote the system of all faces of all elements $K \in \mathcal{T}_{ht}$. Further, we introduce the set of all boundary faces

$$\mathcal{F}_{ht}^B = \left\{ \Gamma \in \mathcal{F}_{ht};\ \Gamma \subset \partial\Omega_{ht}^f \right\}, \tag{4.29}$$

the set of all "Dirichlet" boundary faces

$$\mathcal{F}_{ht}^D = \left\{ \Gamma \in \mathcal{F}_{ht}^B;\ \text{a Dirichlet condition is given on } \Gamma \right\} \tag{4.30}$$

and the set of all inner faces $\mathcal{F}_{ht}^I = \mathcal{F}_{ht} \setminus \mathcal{F}_{ht}^B$. Each $\Gamma \in \mathcal{F}_{ht}$ is associated with a unit normal vector $\boldsymbol{n}_\Gamma$. For $\Gamma \in \mathcal{F}_{ht}^B$ the normal $\boldsymbol{n}_\Gamma$ has the same orientation as the outer normal to $\partial\Omega_{ht}^f$.

For each $\Gamma \in \mathcal{F}_{ht}^I$ there exist two neighbouring elements $K_\Gamma^{(L)}, K_\Gamma^{(R)} \in \mathcal{T}_{ht}$ such that $\Gamma \subset \partial K_\Gamma^{(R)} \cap \partial K_\Gamma^{(L)}$. We use the convention that $K_\Gamma^{(R)}$ lies in the direction of $\boldsymbol{n}_\Gamma$ and $K_\Gamma^{(L)}$ lies in the opposite direction to $\boldsymbol{n}_\Gamma$. If $\Gamma \in \mathcal{F}_{ht}^B$, then the element adjacent to Γ will be denoted by $K_\Gamma^{(L)}$.

The approximate solution will be sought in the space of piecewise polynomial functions

$$\boldsymbol{S}_{ht} = [S_{ht}]^4, \quad \text{with} \quad S_{ht} = \{\psi; \psi|_K \in P_r(K)\ \forall\, K \in \mathcal{T}_{ht}\}, \tag{4.31}$$

where $r > 0$ is an integer and $P_r(K)$ denotes the space of all polynomials on K of degree $\leq r$. A function $\boldsymbol{\psi} \in \boldsymbol{S}_{ht}$ is, in general, discontinuous on interfaces $\Gamma \in \mathcal{F}_{ht}^I$. By $\boldsymbol{\psi}_\Gamma^{(L)}$ and $\boldsymbol{\psi}_\Gamma^{(R)}$ we denote the values of $\boldsymbol{\psi} \in \boldsymbol{S}_{ht}$ on Γ considered from the side of the element $K_\Gamma^{(L)}$ and $K_\Gamma^{(R)}$ adjacent to Γ lying in the opposite direction to $\boldsymbol{n}_\Gamma$ and in the direction of $\boldsymbol{n}_\Gamma$, respectively. Then we set

$$\langle \boldsymbol{\psi} \rangle_\Gamma = (\boldsymbol{\psi}_\Gamma^{(L)} + \boldsymbol{\psi}_\Gamma^{(R)})/2, \quad [\boldsymbol{\psi}]_\Gamma = \boldsymbol{\psi}_\Gamma^{(L)} - \boldsymbol{\psi}_\Gamma^{(R)}. \tag{4.32}$$

The discrete problem is derived in the following way: We multiply system (4.25) by a test function $\boldsymbol{\psi}_h \in \boldsymbol{S}_{ht}$, integrate over $K \in \mathcal{T}_{ht}$, apply Green's theorem, sum over all elements $K \in \mathcal{T}_{ht}$, use the concept of the numerical flux and introduce suitable terms mutually vanishing for a regular exact solution. Moreover, we carry out a suitable partial linearization of nonlinear terms. Similarly as in [30] we define the following forms.

Convection form:

Taking into account the definition of $\boldsymbol{g}_s$ in (4.26) and notation (4.20), we have

$$\frac{D\boldsymbol{g}_s(\boldsymbol{w})}{D\boldsymbol{w}} = \frac{D\boldsymbol{f}_s(\boldsymbol{w})}{D\boldsymbol{w}} - z_s\boldsymbol{I} = \boldsymbol{A}_s(\boldsymbol{w}) - z_s\boldsymbol{I}, \tag{4.33}$$

and we can write

$$\boldsymbol{P}_g(\boldsymbol{w}, \boldsymbol{n}) = \sum_{s=1}^{2} \frac{D\boldsymbol{g}_s(\boldsymbol{w})}{D\boldsymbol{w}} n_s = \sum_{s=1}^{2} \left(\boldsymbol{A}_s(\boldsymbol{w}) n_s - z_s n_s \boldsymbol{I} \right). \tag{4.34}$$

By [27], this matrix is diagonalizable. It means that there exists a nonsingular matrix $\boldsymbol{T} = \boldsymbol{T}(\boldsymbol{w}, \boldsymbol{n})$ such that

$$\boldsymbol{P}_g = \boldsymbol{T}\boldsymbol{\Lambda}\boldsymbol{T}^{-1}, \quad \boldsymbol{\Lambda} = \operatorname{diag}(\lambda_1, \ldots, \lambda_4), \tag{4.35}$$

where $\lambda_i = \lambda_i(\boldsymbol{w}, \boldsymbol{n})$, $i = 1, \dots, 4$, are eigenvalues of the matrix $\boldsymbol{P}_g$. Now we define the "positive" and "negative" parts of the matrix $\boldsymbol{P}_g$ by

$$\boldsymbol{P}_g^{\pm} = \boldsymbol{T}\boldsymbol{\Lambda}^{\pm}\boldsymbol{T}^{-1}, \quad \boldsymbol{\Lambda}^{\pm} = \mathrm{diag}(\lambda_1^{\pm}, \dots, \lambda_4^{\pm}), \tag{4.36}$$

where $\lambda^+ = \max(\lambda, 0)$, $\lambda^- = \min(\lambda, 0)$. Using the above concepts for arbitrary states $\boldsymbol{w}^L, \boldsymbol{w}^R$ and a unit 2D vector $\boldsymbol{n}$, we introduce the modified Vijayasundaram numerical flux (cf. [27] or [65]) as

$$\boldsymbol{H}_g(\boldsymbol{w}_L, \boldsymbol{w}_R, \boldsymbol{n}) = \boldsymbol{P}_g^+\Big(\frac{\boldsymbol{w}_L + \boldsymbol{w}_R}{2}, \boldsymbol{n}\Big)\boldsymbol{w}_L + \boldsymbol{P}_g^-\Big(\frac{\boldsymbol{w}_L + \boldsymbol{w}_R}{2}, \boldsymbol{n}\Big)\boldsymbol{w}_R. \tag{4.37}$$

In this way we get the form defined for $\overline{\boldsymbol{w}}_h, \boldsymbol{w}_h, \boldsymbol{\psi}_h \in \boldsymbol{S}_{ht}$:

$$\begin{aligned}
&\hat{b}_h(\overline{\boldsymbol{w}}_h, \boldsymbol{w}_h, \boldsymbol{\psi}_h, t) \qquad (4.38)\\
&= -\sum_{K\in\mathcal{T}_{ht}} \int_K \sum_{s=1}^{2} (\boldsymbol{A}_s(\overline{\boldsymbol{w}}_h(x)) - z_s(x))\boldsymbol{I})\boldsymbol{w}_h(x)) \cdot \frac{\partial \boldsymbol{\psi}_h(x)}{\partial x_s}\,\mathrm{d}\boldsymbol{x}\\
&+ \sum_{\Gamma\in\mathcal{F}_{ht}^I} \int_\Gamma \Big(\boldsymbol{P}_g^+\big(\langle\overline{\boldsymbol{w}}_h\rangle, \boldsymbol{n}_\Gamma\big)\boldsymbol{w}_h^{(L)} + \boldsymbol{P}_g^-\big(\langle\overline{\boldsymbol{w}}_h\rangle, \boldsymbol{n}_\Gamma\big)\boldsymbol{w}_h^{(R)}\Big)\cdot[\boldsymbol{\psi}_h]\,\mathrm{d}S\\
&+ \sum_{\Gamma\in\mathcal{F}_{ht}^B} \int_\Gamma \Big(\boldsymbol{P}_g^+\big(\overline{\boldsymbol{w}}_h, \boldsymbol{n}_\Gamma\big)\boldsymbol{w}_h^{(L)} + \boldsymbol{P}_g^-\big(\overline{\boldsymbol{w}}_h, \boldsymbol{n}_\Gamma\big)\overline{\boldsymbol{w}}_h^{(R)}\Big)\cdot\boldsymbol{\psi}_h\,\mathrm{d}S,
\end{aligned}$$

which is linear with respect to $\boldsymbol{w}_h$ and nonlinear with respect to $\overline{\boldsymbol{w}}_h$.

If $\Gamma \in \mathcal{F}_{ht}^B$, it is necessary to specify the boundary state $\overline{\boldsymbol{w}}_{h\Gamma}^{(R)}$ appearing in the numerical flux $\boldsymbol{H}_g$ in the definition of the inviscid form $\hat{b}_h$. Here we use the approach applied in the case of inviscid flow simulation, treated in [27]. This means that on Γ we prescribe m components of $\boldsymbol{w}$ and extrapolate $4-m$ components of $\boldsymbol{w}$, where m is the number of negative eigenvalues of the matrix $\boldsymbol{P}_g(\boldsymbol{w}_h^{(L)}, \boldsymbol{n})$. On the impermeable wall (with a moving part) we prescribe the normal component of the velocity

$$\boldsymbol{v}\cdot\boldsymbol{n} = \boldsymbol{z}_D\cdot\boldsymbol{n}, \tag{4.39}$$

where $\boldsymbol{n}$ is the unit outer normal to Γ_{W_t} and $\boldsymbol{z}_D$ is the wall velocity. Then the numerical flux is approximated on $\Gamma \subset \Gamma_{W_t}$ by

$$\boldsymbol{H}_g := p\,(0, n_1, n_2, \boldsymbol{z}_D\cdot\boldsymbol{n})^T. \tag{4.40}$$

Viscous form

The linearized viscous form is defined on the basis of the fact that $\boldsymbol{R}_s(\boldsymbol{w}_h, \nabla\boldsymbol{w}_h)$ can be expressed as in (4.18). We set $\Theta = 1$, $\Theta = 0$ or $\Theta = -1$ and get the so-called symmetric (SIPG), incomplete (IIPG) or nonsymmetric version (NIPG),

respectively, of the discretization of viscous terms. We set

$$\hat{a}_h(\overline{\boldsymbol{w}}_h, \boldsymbol{w}_h, \boldsymbol{\psi}_h, t) = \sum_{K\in\mathcal{T}_{ht}} \int_K \sum_{s=1}^{2}\sum_{k=1}^{2} \boldsymbol{K}_{s,k}(\overline{\boldsymbol{w}}_h)\, \frac{\partial \boldsymbol{w}_h}{\partial x_k} \cdot \frac{\partial \boldsymbol{\psi}_h}{\partial x_s}\, \mathrm{d}\boldsymbol{x} \tag{4.41}$$

$$- \sum_{\Gamma\in\mathcal{F}_{ht}^I} \int_\Gamma \sum_{s=1}^{2} \left\langle \sum_{k=1}^{2} \boldsymbol{K}_{s,k}(\overline{\boldsymbol{w}}_h) \frac{\partial \boldsymbol{w}_h}{\partial x_k} \right\rangle (\boldsymbol{n}_\Gamma)_s \cdot [\boldsymbol{\psi}_h]\, \mathrm{d}S$$

$$- \sum_{\Gamma\in\mathcal{F}_{ht}^D} \int_\Gamma \sum_{s=1}^{2}\sum_{k=1}^{2} \boldsymbol{K}_{s,k}(\overline{\boldsymbol{w}}_h) \frac{\partial \boldsymbol{w}_h}{\partial x_k} (\boldsymbol{n}_\Gamma)_s \cdot \boldsymbol{\psi}_h\, \mathrm{d}S$$

$$- \Theta \sum_{\Gamma\in\mathcal{F}_{ht}^I} \int_\Gamma \sum_{s=1}^{2} \left\langle \sum_{k=1}^{2} \boldsymbol{K}_{s,k}^T(\overline{\boldsymbol{w}}_h) \frac{\partial \boldsymbol{\psi}_h}{\partial x_k} \right\rangle (\boldsymbol{n}_\Gamma)_s \cdot [\boldsymbol{w}_h]\, \mathrm{d}S$$

$$- \Theta \sum_{\Gamma\in\mathcal{F}_{ht}^D} \int_\Gamma \sum_{s=1}^{2}\sum_{k=1}^{2} \boldsymbol{K}_{s,k}^T(\overline{\boldsymbol{w}}_h) \frac{\partial \boldsymbol{\psi}_h}{\partial x_k} (\boldsymbol{n}_\Gamma)_s \cdot \boldsymbol{w}_h\, \mathrm{d}S.$$

Interior and boundary penalization and right-hand side forms
Further, we define the forms

$$J_h(\boldsymbol{w}_h, \boldsymbol{\psi}_h, t) = \sum_{\Gamma\in\mathcal{F}_{ht}^I} \int_\Gamma \eta [\boldsymbol{w}_h] \cdot [\boldsymbol{\psi}_h]\, \mathrm{d}S + \sum_{\Gamma\in\mathcal{F}_{ht}^D} \int_\Gamma \eta \boldsymbol{w}_h \cdot \boldsymbol{\psi}_h\, \mathrm{d}S, \tag{4.42}$$

$$\ell_h(\boldsymbol{w}_h, \boldsymbol{\psi}_h, t) = \sum_{\Gamma\in\mathcal{F}_{ht}^D} \int_\Gamma \sum_{s=1}^{2} \eta \boldsymbol{w}_B \cdot \boldsymbol{\psi}_h\, \mathrm{d}S \tag{4.43}$$

$$- \Theta \sum_{\Gamma\in\mathcal{F}_{ht}^D} \int_\Gamma \sum_{s=1}^{2}\sum_{k=1}^{2} \boldsymbol{K}_{s,k}^T(\overline{\boldsymbol{w}}_h) \frac{\partial \boldsymbol{\psi}_h}{\partial x_k} (\boldsymbol{n}_\Gamma)_s \cdot \boldsymbol{w}_B\, \mathrm{d}S.$$

Here $\eta|_\Gamma = C_W \mu / h_\Gamma$, where h_Γ can be defined as in (2.9)–(2.11), and $C_W > 0$ is a sufficiently large constant. The boundary state $\boldsymbol{w}_B$ is defined on the basis of the Dirichlet boundary conditions (4.6), a), b), (4.8) a) and extrapolation:

$$\boldsymbol{w}_B = (\rho_D, \rho_D v_{D1}, \rho_D v_{D2}, c_v \rho_D \theta_\Gamma^{(L)} + \frac{1}{2}\rho_D |\boldsymbol{v}_D|^2) \quad \text{on } \Gamma_I, \tag{4.44}$$

$$\boldsymbol{w}_B = \boldsymbol{w}_\Gamma^{(L)} \quad \text{on } \Gamma_O, \tag{4.45}$$

$$\boldsymbol{w}_B = (\rho_\Gamma^{(L)}, \rho_\Gamma^{(L)} z_{D1}, \rho_\Gamma^{(L)} z_{D2}, c_v \rho_\Gamma^{(L)} \theta_\Gamma^{(L)} + \frac{1}{2}\rho_\Gamma^{(L)} |\boldsymbol{z}_D|^2) \quad \text{on } \Gamma_{W_t}. \tag{4.46}$$

The quantities $\rho_\Gamma^{(L)}$, $\theta_\Gamma^{(L)}$, etc. are obtained by the extrapolation of ρ, θ, etc. from from $K_\Gamma^{(L)}$ onto Γ.

Reaction form
The reaction form reads

$$d_h(\boldsymbol{w}_h, \boldsymbol{\psi}_h, t) = \sum_{K\in\mathcal{T}_{ht}} \int_K (\boldsymbol{w}_h \cdot \boldsymbol{\psi}_h)\, \mathrm{div}\boldsymbol{z}\, \mathrm{d}x. \tag{4.47}$$

Artificial viscosity

In order to avoid spurious oscillations in the approximate solution in the vicinity of discontinuities or steep gradients, we apply artificial viscosity forms. They are based on the discontinuity indicator

$$g_t(K) = \int_{\partial K \cap \Omega_t^f} [\overline{\rho}_h]^2 \, \mathrm{d}S \big/ (h_K |K|^{3/4}), \quad K \in \mathcal{T}_{ht}, \tag{4.48}$$

introduced in [18]. By $[\overline{\rho}_h]$ we denote the jump of the function $\overline{\rho}_h$ (= the first component of the vector function $\overline{\boldsymbol{w}}_h$) on the boundary ∂K and $|K|$ denotes the area of the element K. Then we define the discrete discontinuity indicator

$$G_t(K) = 0 \quad \text{if } g_t(K) < 1, \quad G_t(K) = 1 \quad \text{if } g_t(K) \geq 1, \quad K \in \mathcal{T}_{ht}, \tag{4.49}$$

and the artificial viscosity forms (see [28])

$$\hat{\beta}_h(\overline{\boldsymbol{w}}_h, \boldsymbol{w}_h, \boldsymbol{\varphi}_h, t) = \nu_1 \sum_{K \in \mathcal{T}_{ht}} h_K G_t(K) \int_K \nabla \boldsymbol{w}_h \cdot p \nabla \boldsymbol{\varphi}_h \, \mathrm{d}\boldsymbol{x}, \tag{4.50}$$

$$\hat{J}_h(\overline{\boldsymbol{w}}_h, \boldsymbol{w}_h, \boldsymbol{\varphi}_h, t) = \nu_2 \sum_{\Gamma \in \mathcal{F}_{ht}^I} \frac{1}{2}\big(G_t(K_\Gamma^{(L)}) + G_t(K_\Gamma^{(R)})\big) \int_\Gamma [\boldsymbol{w}_h] \cdot [\boldsymbol{\varphi}_h] \, \mathrm{d}S,$$

with parameters ν_1, $\nu_2 = O(1)$.

Remark. For high-speed flows with shock waves and contact discontinuities, spurious overshoots and undershoots may appear near the discontinuities. One possibility, motivated by the paper [44], is to introduce an artificial viscosity form. However, this form is nonzero also in regions, where the exact solution is regular, and a small nonphysical entropy production appears in these regions. Our approach based on the discrete discontinuity indicator introduces the artificial viscosity only in a small neighbourhood of discontinuities. Therefore, the scheme does not produce any nonphysical entropy in the regions, where the solution is regular. Since the form $\hat{\beta}_h$ is rather local, its influence is augmented by the form $\hat{J}_h$, which improves the behaviour of the method in the case, when strongly unstructured and/or anisotropic meshes are used.

4.5 Time discretization by the BDF method

In this section the BDF method is applied analogously as in Section 2.3.1 in order to approximate the ALE derivative of the vector function $\boldsymbol{w}_h$. As in (4.23), it holds for $\boldsymbol{x} \in \Omega_{ht}^f$ and $t \in [0, T]$:

$$\frac{D^A \boldsymbol{w}_h}{Dt}(\boldsymbol{x}, t) = \frac{\partial \tilde{\boldsymbol{w}}_h}{\partial t}(\boldsymbol{X}, t), \tag{4.51}$$

where

$$\tilde{\boldsymbol{w}}_h(\boldsymbol{X}, t) = \boldsymbol{w}_h(\mathcal{A}_t(\boldsymbol{X}), t), \ \boldsymbol{X} \in \Omega_0^f, \ \boldsymbol{x} = \mathcal{A}_t(\boldsymbol{X}).$$

Let us construct a partition $0 = t_0 < t_1 < \cdots < t_M = T$, $M \in \mathbb{N}$, of the time interval $[0, T]$ and define the time step $\tau_n = t_n - t_{n-1}$, $n = 1, \ldots, M$. The ALE

	$q=1$	$q=2$	$q=3$
β_1	$1,$	$\frac{\tau_m+\tau_{m-1}}{\tau_{m-1}},$	$\frac{(\tau_m+\tau_{m-1}+\tau_{m-2})(\tau_m+\tau_{m-1})}{\tau_{m-1}(\tau_{m-1}+\tau_{m-2})}$
β_2		$-\frac{\tau_m}{\tau_{m-1}},$	$-\frac{\tau_m(\tau_m+\tau_{m-1}+\tau_{m-2})}{\tau_{m-1}\tau_{m-2}}$
β_3			$\frac{\tau_m(\tau_m+\tau_{m-1})}{\tau_{m-2}(\tau_{m-1}+\tau_{m-2})}$

Table 4.1: The values of the coefficients β_l.

derivative at time t_m is approximated by the backward finite difference formula (BDF) of order q

$$\frac{D^{\mathcal{A}}\boldsymbol{w}_h}{Dt}(\boldsymbol{x},t_m)=\frac{\partial\tilde{\boldsymbol{w}}_h}{\partial t}(\boldsymbol{X},t_m)\approx\sum_{l=0}^{q}c_l\tilde{\boldsymbol{w}}_h(\boldsymbol{X},t_{m-l}), \tag{4.52}$$

with coefficients $c_l,\ l=0,\dots,q$, depending on $\tau_{m-l},\ l=0,\dots,q-1$.

Further we express the BDF approximation on the domain $\Omega^f_{ht_m}$. We use the approximations

$$\boldsymbol{w}_h^n\approx\boldsymbol{w}_h(t_n)\in\boldsymbol{S}_{ht_n},\quad n=0,1,\dots,M. \tag{4.53}$$

Let us assume that $\boldsymbol{w}_h^n,\ n=0,\dots,m-1$, are already known. Then we introduce the functions

$$\hat{\boldsymbol{w}}_h^n=\boldsymbol{w}_h^n\circ\mathcal{A}_{t_n}\circ\mathcal{A}_{t_m}^{-1} \tag{4.54}$$

for $n=m-1,m-2,\dots$, which are defined in the domain $\Omega^f_{ht_m}$. That implies

$$\tilde{\boldsymbol{w}}_h(\boldsymbol{X},t_n)=\boldsymbol{w}_h(\mathcal{A}_{t_n}(\boldsymbol{X}),t_n)=\boldsymbol{w}_h(\mathcal{A}_{t_n}(\mathcal{A}_{t_m}^{-1}(\boldsymbol{x})),t_n)=\hat{\boldsymbol{w}}_h^n(\boldsymbol{x},t_n),\ \boldsymbol{x}\in\Omega^f_{ht_m}. \tag{4.55}$$

Finally we can express the BDF approximation of order q of the ALE derivative at time t_m as

$$\frac{D^{\mathcal{A}}\boldsymbol{w}_h}{Dt}(t_m)\approx\frac{D^{\mathcal{A}}_{appr}\boldsymbol{w}_h}{Dt}(t_m)=c_0\boldsymbol{w}_h^m+\sum_{l=1}^{q}c_l\hat{\boldsymbol{w}}_h^{m-l}. \tag{4.56}$$

In the beginning of the computation, when $m<q$, we use the BDF of order m. (The derivation of the BDF approximation of order 2 of the ALE derivative can be found e.g. in [11].)

In nonlinear terms we use the extrapolation for the computation of the state $\overline{\boldsymbol{w}}_h^m$:

$$\overline{\boldsymbol{w}}_h^m=\sum_{l=1}^{q}\beta_l\hat{\boldsymbol{w}}_h^{m-l}, \tag{4.57}$$

where $\beta_l,\ l=1,\dots,q$, depend on $\tau_{m-l},\ l=0,\dots,q-1$. If $m<q$, then we apply the extrapolation of order m. The values of the coefficients $c_l, l=0,\dots,q$, and $\beta_l, l=1,\dots,q$, for $q=1,2,3$ are given in Tables 2.1 and 4.1, respectively.

By the symbol $(\cdot,\cdot)_{\Omega^f_{ht_m}}$ we shall denote the scalar product in $L^2(\Omega^f_{ht_m})$, i.e.

$$(\boldsymbol{w}_h,\boldsymbol{\psi}_h)_{\Omega^f_{ht_m}}=\int_{\Omega^f_{ht_m}}\boldsymbol{w}_h\cdot\boldsymbol{\psi}_h\,dx. \tag{4.58}$$

The resulting *BDF-DG scheme* gives us the definition of the fully discrete solution discretized by the BDF in time and DGM in space.

Definition 10. *The BDF-DG approximate solution* of problem (4.1)–(4.8) is defined as a sequence $\{\boldsymbol{w}_h^m\}_{m=1}^M$ such that

$$\boldsymbol{w}_h^m \in \boldsymbol{S}_{ht_m}, \quad m = 1, \dots, M, \tag{4.59}$$

$$\left(\frac{D^{\mathcal{A}}_{appr}\boldsymbol{w}_h}{Dt}(t_m), \boldsymbol{\psi}_h\right)_{\Omega^f_{ht_m}} + \hat{b}_h(\overline{\boldsymbol{w}}_h^m, \boldsymbol{w}_h^m, \boldsymbol{\psi}_h, t_m) + \hat{a}_h(\overline{\boldsymbol{w}}_h^m, \boldsymbol{w}_h^m, \boldsymbol{\psi}_h, t_m) \tag{4.60}$$

$$+ J_h(\boldsymbol{w}_h^m, \boldsymbol{\psi}_h, t_m) + d_h(\boldsymbol{w}_h^m, \boldsymbol{\psi}_h, t_m) + \hat{\beta}_h(\overline{\boldsymbol{w}}_h^m, \boldsymbol{w}_h^m, \boldsymbol{\varphi}_h, t_m)$$

$$+ \hat{J}_h(\overline{\boldsymbol{w}}_h^m, \boldsymbol{w}_h^m, \boldsymbol{\varphi}_h, t_m) = \ell_h(\overline{\boldsymbol{w}}_B^m, \boldsymbol{\varphi}_h, t_m), \quad \forall \boldsymbol{\psi}_h \in \boldsymbol{S}_{ht_m}.$$

4.6 Full space-time DG discretization

Another technique how to construct a method of high-order accuracy both in space and time is the space-time discontinuous Galerkin method (STDGM). We again consider a partition $0 = t_0 < t_1 < \dots < t_M = T$ of the time interval $[0, T]$ and denote $I_m = (t_{m-1}, t_m)$, $\overline{I}_m = [t_{m-1}, t_m]$, $\tau_m = t_m - t_{m-1}$, for $m = 1, \dots, M$. We define the space $\boldsymbol{S}^{r,q}_{h,\tau} = (S^{r,q}_{h,\tau})^4$, where

$$S^{r,q}_{h,\tau} = \left\{ \psi \ ; \psi|_{I_m} = \sum_{i=0}^{q} \zeta_i \psi_i, \text{ where } \psi_i \in S_{ht}, \ \zeta_i \in P^q(I_m) \right\}$$

with integers $r, q \geq 1$, $P^q(I_m)$ denotes the space of all polynomials in t on I_m of degree $\leq q$ and the space S_{ht} is defined in (4.31). For $\boldsymbol{\psi} \in \boldsymbol{S}^{r,q}_{h,\tau}$ we introduce the following notation:

$$\boldsymbol{\psi}_m^{\pm} = \boldsymbol{\psi}(t_m^{\pm}) = \lim_{t \to t_{m\pm}} \boldsymbol{\psi}(t), \quad \{\boldsymbol{\psi}\}_m = \boldsymbol{\psi}_m^+ - \boldsymbol{\psi}_m^-. \tag{4.61}$$

The derivation of the discrete problem can be carried out similarly as above. The difference is now that time t is considered continuous, test functions $\boldsymbol{\psi}_{h\tau} \in \boldsymbol{S}^{r,q}_{h,\tau}$ are used and also the integration over I_m is applied. In order to stick together the solutions on intervals I_{m-1} and I_m, we augment the resulting identity by the penalty expression $\left(\{\boldsymbol{w}_{h\tau}\}_{m-1}, \boldsymbol{\psi}_{h\tau}(t_{m-1}^+)\right)_{\Omega^f_{ht_{m-1}}}$. The initial state $\boldsymbol{w}_{h\tau}(0-) \in \boldsymbol{S}^p_{h0}$ is defined as the $L^2(\Omega^f_{h0})$-projection of $\boldsymbol{w}^0$ onto $\boldsymbol{S}^p_{h0}$, i.e.

$$(\boldsymbol{w}_{h\tau}(0-), \boldsymbol{\psi}_h)_{\Omega^f_{ht_0}} = \left(\boldsymbol{w}^0, \boldsymbol{\psi}_h\right)_{\Omega^f_{ht_0}} \quad \forall \boldsymbol{\psi}_h \in \boldsymbol{S}^p_{h0}. \tag{4.62}$$

Similarly as in Section 4.5 we introduce a suitable linearization. We can use two possibilities.
1) We put $\overline{\boldsymbol{w}}_{h\tau}(t) := \boldsymbol{w}_{h\tau}(t_{m-1}^-)$ for $t \in I_m$. (This represents a simple time extrapolation.)
2) Each component of the vector-valued function $\boldsymbol{w}_{h\tau}|_{I_{m-1}}$ is a polynomial in t of degree $\leq q$ and we define the function $\overline{\boldsymbol{w}}_{h\tau}|_{I_m}$ by the prolongation using values of the polynomial vector function $\boldsymbol{w}_{h\tau}|_{I_{m-1}}$ at time instants $t \in I_m$. Thus, we write $\overline{\boldsymbol{w}}_{h\tau}|_{I_m}(t) := \boldsymbol{w}_{h\tau}|_{I_{m-1}}(t)$ for $t \in I_m$.

Definition 11. *The space-time DG (STDG) approximate solution* is defined as a function $\boldsymbol{w}_{h\tau}$ satisfying (4.62) and the following conditions:

$$1)\ \boldsymbol{w}_{h\tau} \in \boldsymbol{S}^{r,q}_{h,\tau}, \tag{4.63}$$

$$\begin{aligned} 2)\ & \int_{I_m} \left(\left(\frac{D^{\mathcal{A}} \boldsymbol{w}_{h\tau}}{Dt}(t), \boldsymbol{\psi}_{h\tau} \right)_{\Omega^f_{ht}} + \hat{a}_h(\overline{\boldsymbol{w}}_{h\tau}, \boldsymbol{w}_{h\tau}, \boldsymbol{\psi}_{h\tau}, t) \right) \mathrm{d}t \\ & + \int_{I_m} \left(\hat{b}_h(\overline{\boldsymbol{w}}_{h\tau}, \boldsymbol{w}_{h\tau}, \boldsymbol{\psi}_{h\tau}, t) + J_h(\boldsymbol{w}_{h\tau}, \boldsymbol{\psi}_{h\tau}, t) + d_h(\boldsymbol{w}_{h\tau}, \boldsymbol{\psi}_{h\tau}, t) \right) \mathrm{d}t \\ & + \int_{I_m} \left(\hat{\beta}_h(\overline{\boldsymbol{w}}_{h\tau}, \boldsymbol{w}_{h\tau}, \boldsymbol{\psi}_{h\tau}, t) + \hat{J}_h(\overline{\boldsymbol{w}}_{h\tau}, \boldsymbol{w}_{h\tau}, \boldsymbol{\psi}_{h\tau}, t) \right) \mathrm{d}t \\ & + (\{\boldsymbol{w}_{h\tau}\}_{m-1}, \boldsymbol{\psi}_{h\tau}(t_{m-1}+)) \\ & = \int_{I_m} \ell_h(\boldsymbol{w}_{hD}, \boldsymbol{\psi}_{h\tau}, t)\, \mathrm{d}t \quad \forall \boldsymbol{\psi}_{h\tau} \in \boldsymbol{S}^{r,q}_{h,\tau}, \quad m = 1, \dots, M. \end{aligned} \tag{4.64}$$

4.7 Algorithmization of the flow problem

In this section we describe the algorithmization of problems formulated in Definition 10 and 11. In order to find the approximate solution $\boldsymbol{w}_h^m$ or $\boldsymbol{w}_{h\tau}^m$, respectively, we need to transform the problems into the system of linear algebraic equations.

4.7.1 BDF-DG scheme

First, we start with the choice of appropriate basis functions of the space S_{ht}. By $\hat{K}$ we denote the reference element with vertices $\hat{A} = (0,0)$, $\hat{B} = (1,0)$, $\hat{C} = (0,1)$. Further, we assume that the space S_{ht} is created by polynomials of degree $r \geq 1$. For this reason we search for basis functions of the space $P_r(\hat{K})$ in the form

$$\hat{\psi}_j(\hat{x}_1, \hat{x}_2) = \sum_{l=0}^{r} \sum_{k=0}^{r-l} q^j_{kl} (\hat{x}_1)^k (\hat{x}_2)^l, \quad j = 1, \dots, d_r, \tag{4.65}$$

where

$$d_r := \frac{(r+1)(r+2)}{2} \tag{4.66}$$

is the dimension of the space $P_r(\hat{K})$ and $q^j_{kl} \in \mathbb{R}$. Further, we need to define set $\hat{D}$ of points of element $\hat{K}$:

$$\hat{D} = \left\{ \left(\frac{k}{r}, \frac{l}{r} \right);\ k, l = 0, \dots, r, k + l \leq r \right\}. \tag{4.67}$$

It is possible to show that $\mathrm{card}(\hat{D}) = d_r$. Using the notation $\hat{\boldsymbol{x}}_n$, $n = 1, \dots, d_r$, for elements of set $\hat{D}$, there exists a basis $\hat{\psi}_1, \dots \hat{\psi}_{d_r}$ of the space $P_r(\hat{K})$ fulfilling the condition $\hat{\psi}_j(\hat{\boldsymbol{x}}_n) = \delta_{jn}$, for $j, n = 1, \dots, d_p$.

For each element $K_t \in \mathcal{T}_{ht}$ let us define the space $P_r(K_t)$. Element K_t has vertices A^{K_t}, B^{K_t} , C^{K_t}, for which it holds

$$\mathcal{A}_t(A^{\hat{K}}) = A^{K_t} = (a_1^{K_t}, a_2^{K_t}), \tag{4.68}$$

$$\mathcal{A}_t(B^{\hat{K}}) = B^{K_t} = (b_1^{K_t}, b_2^{K_t}), \tag{4.69}$$

$$\mathcal{A}_t(C^{\hat{K}}) = C^{K_t} = (c_1^{K_t}, c_2^{K_t}). \tag{4.70}$$

Further, we consider the affine mapping $F^{K_t} : \hat{K} \to K_t$ with the properties

$$F^{K_t}(\hat{A}) = A^{K_t}, \tag{4.71}$$

$$F^{K_t}(\hat{B}) = B^{K_t}, \tag{4.72}$$

$$F^{K_t}(\hat{C}) = C^{K_t}. \tag{4.73}$$

This is a one-to-one mapping and we can write $\boldsymbol{x} = F^{K_t}(\hat{\boldsymbol{x}}) = \mathbb{U}^{K_t}\hat{\boldsymbol{x}} + \boldsymbol{V}^{K_t}$. The matrices $\mathbb{U}^{K_t}$ and $\boldsymbol{V}^{K_t}$ have the form

$$\mathbb{U}^{K_t} = \begin{pmatrix} b_1^{K_t} - a_1^{K_t} & c_1^{K_t} - a_1^{K_t} \\ b_2^{K_t} - a_2^{K_t} & c_2^{K_t} - a_2^{K_t} \end{pmatrix}, \tag{4.74}$$

$$\boldsymbol{V}^{K_t} = \begin{pmatrix} a_1^{K_t} \\ a_2^{K_t} \end{pmatrix}. \tag{4.75}$$

The inverse mapping can be expressed as $\hat{\boldsymbol{x}} = \left(F^{K_t}\right)^{-1}(\boldsymbol{x}) = \left(\mathbb{U}^{K_t}\right)^{-1}\left(\boldsymbol{x} - \boldsymbol{V}^{K_t}\right)$, where the inverse matrix $\left(\mathbb{U}^{K_t}\right)^{-1}$ has the form

$$\left(\mathbb{U}^{K_t}\right)^{-1} = \frac{1}{\det\left(\mathbb{U}^{K_t}\right)} \begin{pmatrix} c_2^{K_t} - a_2^{K_t} & a_1^{K_t} - c_1^{K_t} \\ a_2^{K_t} - b_2^{K_t} & b_1^{K_t} - a_1^{K_t} \end{pmatrix}. \tag{4.76}$$

Here, we denote by $\det\left(\mathbb{U}^{K_t}\right)$ the determinant of the matrix $\mathbb{U}^{K_t}$. We define the points $\boldsymbol{x}_n^{K_t} := F^{K_t}(\hat{\boldsymbol{x}}_n)$, $K_t \in \mathcal{T}_{ht}$ and seek basis functions $\psi_1^{K_t}, \ldots, \psi_{d_r}^{K_t}$ on the element $K_t \in \mathcal{T}_{ht}$ fulfilling the conditions $\psi_j^{K_t}(\boldsymbol{x}_n^{K_t}) = \delta_{jn}$, $j, n = 1, \ldots, d_r$. These basis functions are defined uniquely. Because of the linearity of the function $(F^{K_t})^{-1}$, $\hat{\psi}_j((F^{K_t})^{-1}(\boldsymbol{x}))$ is a polynomial of degree $\leq r$. For $j, n = 1, \ldots, d_r$ it holds

$$\hat{\psi}_j((F^{K_t})^{-1}(\boldsymbol{x}_n^{K_t})) = \hat{\psi}_j(\hat{\boldsymbol{x}}_n) = \delta_{jn} = \psi_j^{K_t}(\boldsymbol{x}_n^{K_t}). \tag{4.77}$$

From the uniqueness it follows that $\psi_j^{K_t}(\boldsymbol{x}) = \hat{\psi}_j((F^{K_t})^{-1}(\boldsymbol{x}))$, $j = 1, \ldots, d_r$. Using the chain rule we can derive the derivatives of the basis functions $\psi_j^{K_t}$, $j = 1, \ldots, d_r$:

$$\begin{aligned} \frac{\partial \psi_j^{K_t}}{\partial x_1}(\boldsymbol{x}) &= \frac{\partial}{\partial x_1}\hat{\psi}_j\left(\left(F^{K_t}\right)^{-1}(\boldsymbol{x})\right) \\ &= \sum_{k=1}^{2} \frac{\partial \hat{\psi}_j}{\partial \hat{x}_k}((F^{K_t})^{-1}(\boldsymbol{x})) \frac{\partial((F^{K_t})^{-1})_k}{\partial x_1}(\boldsymbol{x}) \\ &= (\nabla\hat{\psi}_j)((F^{K_t})^{-1}(\boldsymbol{x})) \cdot \left((\mathbb{U}^{K_t})^{-1}\begin{pmatrix} 1 \\ 0 \end{pmatrix}\right). \end{aligned} \tag{4.78}$$

For $\hat{\boldsymbol{x}}$ fulfilling $\boldsymbol{x} = F^{K_t}(\hat{\boldsymbol{x}})$ it holds

$$\frac{\partial \psi_j^{K_t}}{\partial x_1}(\boldsymbol{x}) = \frac{\partial \psi_j^{K_t}}{\partial x_1}(F^{K_t}(\hat{\boldsymbol{x}})) = (\nabla\hat{\psi}_j)(\hat{\boldsymbol{x}}) \cdot \left((\mathbb{U}^{K_t})^{-1}\begin{pmatrix} 1 \\ 0 \end{pmatrix}\right). \tag{4.79}$$

Similarly we get

$$\frac{\partial \psi_j^{K_t}}{\partial x_2}(\boldsymbol{x}) = (\nabla\hat{\psi}_j)(\hat{\boldsymbol{x}}) \cdot \left((\mathbb{U}^{K_t})^{-1}\begin{pmatrix} 0 \\ 1 \end{pmatrix}\right), \qquad \boldsymbol{x} = F^{K_t}(\hat{\boldsymbol{x}}). \tag{4.80}$$

Since we have defined the space $P^r(K_t)$ for all elements $K_t \in \mathcal{T}_{ht}$, we can define the vector-valued basis functions

$$\boldsymbol{\psi}_{j,d}^{K_t} = (\psi_j^{K_t}\delta_{1d}, \dots, \psi_j^{K_t}\delta_{4d}), \quad d = 1, \dots, 4, \ j = 1, \dots, d_r. \tag{4.81}$$

These functions form a basis of the space S_{ht}. From this it follows that the number of degrees of freedom dof_h of this space is $\mathrm{dof}_h = 4d_r \mathrm{card}(\mathcal{T}_{ht})$.

For the sake of simplicity we introduce set $I = \{0, 1, \dots, c; c \in \mathbb{N}\}$ of the indices of elements of the triangulation $\mathcal{T}_{ht}$, such that $\mathcal{T}_{ht} = \{K_i; i \in I\}$. Then we shall number the basis functions of the space S_{ht} by the unique index l, where $l = 4d_r i + d_r(d-1) + j$ for $i \in I$, $d \in \{1, \dots, 4\}$, $j \in \{1, \dots, d_r\}$. When we denote $\boldsymbol{\psi}_h^{l,m}(\boldsymbol{x}) := \boldsymbol{\psi}_{j,d}^{K_{t_m}}(\boldsymbol{x})$, the sought solution can be written in the form

$$\boldsymbol{w}_h^m = \sum_{l=1}^{\mathrm{dof}_h} \xi_l^m \boldsymbol{\psi}_h^{l,m}. \tag{4.82}$$

Hence, by setting $\boldsymbol{\psi}_h := \boldsymbol{\psi}_h^{z,m}$, $z = 1, \dots, \mathrm{dof}_h$ in (4.60), we can transform the discrete problem defined in Definition 10 into the form

$$\begin{aligned}
&\sum_{l=1}^{\mathrm{dof}_h} \xi_l^m c_0 \left(\boldsymbol{\psi}_h^{l,m}, \boldsymbol{\psi}_h^{z,m}\right)_{\Omega_{ht_m}^f} + \sum_{l=1}^{\mathrm{dof}_h} \xi_l^m \Big(d_h(\boldsymbol{\psi}_h^{l,m}, \boldsymbol{\psi}_h^{z,m}, t_m) + \hat{b}_h(\overline{\boldsymbol{w}}_h^m, \boldsymbol{\psi}_h^{l,m}, \boldsymbol{\psi}_h^{z,m}, t_m) \\
&\quad + \hat{a}_h(\overline{\boldsymbol{w}}_h^m, \boldsymbol{\psi}_h^{l,m}, \boldsymbol{\psi}_h^{z,m}, t_m) + J_h(\boldsymbol{\psi}_h^{l,m}, \boldsymbol{\psi}_h^{z,m}, t_m) \\
&\quad + \hat{\beta}_h(\overline{\boldsymbol{w}}_h^{m-1}, \boldsymbol{\psi}_h^{l,m}, \boldsymbol{\psi}_h^{z,m}, t_m) + \hat{J}_h(\overline{\boldsymbol{w}}_h^{m-1}, \boldsymbol{\psi}_h^{l,m}, \boldsymbol{\psi}_h^{z,m}, t_m) \Big) \\
&\quad = \ell_h(\overline{\boldsymbol{w}}_B^m, \boldsymbol{\psi}_h^{z,m}, t_m) - \left(\sum_{l=1}^{q} c_l \hat{\boldsymbol{w}}_h^{m-l}, \boldsymbol{\psi}_h^{z,m} \right)_{\Omega_{ht_m}^f}.
\end{aligned} \tag{4.83}$$

Finally we rewrite this system into the form

$$\boldsymbol{A}_h^m \, \boldsymbol{\Xi}_h^m = \boldsymbol{L}_h^m, \tag{4.84}$$

where

$$\begin{aligned}
\{\boldsymbol{A}_h^m\}_{z,l} &= c_0 \left(\boldsymbol{\psi}_h^{l,m}, \boldsymbol{\psi}_h^{z,m}\right)_{\Omega_{ht_m}^f} + d_h(\boldsymbol{\psi}_h^{l,m}, \boldsymbol{\psi}_h^{z,m}, t_m) + \hat{b}_h(\overline{\boldsymbol{w}}_h^m, \boldsymbol{\psi}_h^{l,m}, \boldsymbol{\psi}_h^{z,m}, t_m) \\
&\quad + \hat{a}_h(\overline{\boldsymbol{w}}_h^m, \boldsymbol{\psi}_h^{l,m}, \boldsymbol{\psi}_h^{z,m}, t_m) + J_h(\boldsymbol{\psi}_h^{l,m}, \boldsymbol{\psi}_h^{z,m}, t_m) \\
&\quad + \hat{\beta}_h(\overline{\boldsymbol{w}}_h^{m-1}, \boldsymbol{\psi}_h^{l,m}, \boldsymbol{\psi}_h^{z,m}, t_m) + \hat{J}_h(\overline{\boldsymbol{w}}_h^{m-1}, \boldsymbol{\psi}_h^{l,m}, \boldsymbol{\psi}_h^{z,m}, t_m) \\
\{\boldsymbol{L}_h^m\}_z &= \ell_h(\overline{\boldsymbol{w}}_B^m, \boldsymbol{\psi}_h^{z,m}, t_m) - \left(\sum_{l=1}^{q} c_l \hat{\boldsymbol{w}}_h^{m-l}, \boldsymbol{\psi}_h^{z,m} \right)_{\Omega_{ht_m}^f}, \\
\boldsymbol{\Xi}_h^m &= (\xi_1^m, \dots, \xi_{\mathrm{dof}_h}^m)^T.
\end{aligned}$$

4.7.2 Full space-time DG method

The base functions of the space $\boldsymbol{S}_{h,\tau}^{r,q}$ for the full space-time discontinuous Galerkin method shall be constructed separately on every time level I_m for $m = 1, \dots, M$. Let us consider, that space S_{ht} is constructed in the same way as in the previous section. Now we shall construct basis functions $\zeta_u, u = 0, \dots, q$ of the space $P^q(t_{m-1}, t_m)$. The case $q = 0$ is simple. Further, we shall consider, that $q > 0$. By the obtained numerical results the choice $\zeta_u(t) = t^u$ is not suitable. Thus, for the real implementation we again define the space of polynomials on the reference interval $(0, 1)$. We set $\hat{t}_r = \frac{r}{q},\ r = 0, \dots, q$. Then we can choose basis functions $\hat{\zeta}_u(\hat{t})$ of the space $P^q(0, 1)$, which fulfill $\hat{\zeta}_u(\hat{t}_r) = \delta_{ur}$ for $u, r = 0, \dots, q$. If we define function G^m such that $t = G^m(\hat{t}) = t_{m-1} + \hat{t}\tau_m$, then functions $\zeta_u^m(t) := \hat{\zeta}_u((G^m)^{-1}(t)),\ u = 0, \dots, q$ form a basis of the space $P^q(t_{m-1}, t_m)$.

Hence, for arbitrary $i \in I$ functions $\psi_j^{K_t}$ form a basis of the space $P^p(K_i(t))$. Then functions $\psi_{j,u}^{i,m}(\boldsymbol{x}, t) := \zeta_u^m(t)\psi_j^{K_t}(\boldsymbol{x}, t)$ for $u = 0, \dots, q$ form a basis of the space $P^q(I_m, P^p(K_i(t))$. Space $P^q(I_m, P^p(K_i(t))$ is a space of polynomials of degree p in space and degree q in time. Finally we define $\boldsymbol{\psi}_{j,u,d}^{i,m} := (\psi_{j,u}^{i,m}\delta_{1d}, \dots, \psi_{j,u}^{i,m}\delta_{4d})$ for $d = 1, \dots, 4$. It is obvious, that functions $\boldsymbol{\psi}_{j,u,d}^{i,m}$ for $i \in I,\ j = 1, \dots, d_r,\ u = 0, \dots, q$ and $d = 1, \dots, 4$ form a basis of the space $\boldsymbol{S}_{h,\tau}^{p,q}\big|_{I_m}$, where

$$\boldsymbol{S}_{h,\tau}^{r,q}\big|_{I_m} := \left\{ \boldsymbol{\psi}_{h\tau}|_{I_m};\ \boldsymbol{\psi}_{h\tau} \in \boldsymbol{S}_{h,\tau}^{r,q} \right\}. \tag{4.85}$$

The number of degrees of freedom $\mathrm{dof}_{h\tau}$ of the space $\boldsymbol{S}_{h,\tau}^{r,q}\big|\, I_m$ is

$$\mathrm{dof}_{h\tau} = 4(q+1)d_r\ \mathrm{card}(I). \tag{4.86}$$

We shall number the basis functions of the space $\boldsymbol{S}_{h,\tau}^{r,q}\big|\, I_m$ again with unique index l, where $l = 4(q+1)d_r(i-1) + (d-1)(q+1)d_r + ud_r + j$. Further, we set $\boldsymbol{\psi}_{j,u,d}^{i,m} = \boldsymbol{\psi}_{h\tau}^{l,m}$. We proceed by solving the problem defined in Definition 11 in sequence over the particular time levels. Therefore, let the approximate solution on the previous time level I_{m-1} be known and we seek solution $\boldsymbol{w}_{h\tau}^m := \boldsymbol{w}_{h\tau}|_{I_m}$ on m-th time level, which can be written in the form

$$\boldsymbol{w}_{h\tau}^m = \sum_{l=1}^{\mathrm{dof}_{h\tau}} \xi_l^m \boldsymbol{\psi}_{h\tau}^{l,m}. \tag{4.87}$$

Hence, by setting $\boldsymbol{\psi}_{h\tau} := \boldsymbol{\psi}_{h\tau}^{z,m},\ z = 1, \dots, \mathrm{dof}_{h\tau}$, in (4.64), we can transform the discrete problem defined in Definition 11 for $m = 1$ into the form

$$\begin{aligned}
&\sum_{l=1}^{\mathrm{dof}_{h\tau}} \xi_l^1 \int_{I_1} \Bigg(\left(\frac{D^A \boldsymbol{\psi}_{h\tau}^{l,1}}{Dt}, \boldsymbol{\psi}_{h\tau}^{z,1} \right)_{\Omega_{ht_1}^f} + d_h(\boldsymbol{\psi}_{h\tau}^{l,1}, \boldsymbol{\psi}_{h\tau}^{z,1}, t) + \hat{b}_h(\overline{\boldsymbol{w}}_{h\tau}, \boldsymbol{\psi}_{h\tau}^{l,1}, \boldsymbol{\psi}_{h\tau}^{z,1}, t) \\
&+ \hat{a}_h(\overline{\boldsymbol{w}}_{h\tau}, \boldsymbol{\psi}_{h\tau}^{l,1}, \boldsymbol{\psi}_{h\tau}^{z,1}, t) + J_h(\boldsymbol{\psi}_{h\tau}^{l,1}, \boldsymbol{\psi}_{h\tau}^{z,1}, t) \\
&+ \hat{\beta}_h(\overline{\boldsymbol{w}}_{h\tau}, \boldsymbol{\psi}_{h\tau}^{l,1}, \boldsymbol{\psi}_{h\tau}^{z,1}, t) + \hat{J}_h(\overline{\boldsymbol{w}}_{h\tau}, \boldsymbol{\psi}_{h\tau}^{l,1}, \boldsymbol{\psi}_{h\tau}^{z,1}, t) \Bigg)\, \mathrm{d}t \\
&+ \sum_{l=1}^{\mathrm{dof}_{h\tau}} \xi_l^1 \left(\boldsymbol{\psi}_{h\tau}^{l,1}(t_0^+), \boldsymbol{\psi}_{h\tau}^{z,1}(t_0^+) \right)_{\Omega_{ht_1}^f} \\
&= \int_{I_1} \ell_h(\boldsymbol{w}_{hD}, \boldsymbol{\psi}_{h\tau}^{z,1}, t)\, \mathrm{d}t + \left(\boldsymbol{w}^0, \boldsymbol{\psi}_{h\tau}^{z,1}(t_0^+) \right)_{\Omega_{ht_1}^f} \qquad \forall \boldsymbol{\psi}_{h\tau}^{z,1} \in \boldsymbol{S}_{h,\tau}^{r,q}\big|_{I_1}
\end{aligned}$$

and for $m > 1$ into the form

$$
\begin{aligned}
&\sum_{l=1}^{\mathrm{dof}_{h\tau}} \xi_l^m \int_{I_m} \Bigg(\left(\frac{D^A \boldsymbol{\psi}_{h\tau}^{l,m}}{Dt}, \boldsymbol{\psi}_{h\tau}^{z,m} \right)_{\Omega_{ht_m}^f} + d_h(\boldsymbol{\psi}_{h\tau}^{l,m}, \boldsymbol{\psi}_{h\tau}^{z,m}, t) + \hat{b}_h(\overline{\boldsymbol{w}}_{h\tau}, \boldsymbol{\psi}_{h\tau}^{l,m}, \boldsymbol{\psi}_{h\tau}^{z,m}, t) \\
&+ \hat{a}_h(\overline{\boldsymbol{w}}_{h\tau}, \boldsymbol{\psi}_{h\tau}^{l,m}, \boldsymbol{\psi}_{h\tau}^{z,m}, t) + J_h(\boldsymbol{\psi}_{h\tau}^{l,m}, \boldsymbol{\psi}_{h\tau}^{z,m}, t) \\
&+ \hat{\beta}_h(\overline{\boldsymbol{w}}_{h\tau}, \boldsymbol{\psi}_{h\tau}^{l,m}, \boldsymbol{\psi}_{h\tau}^{z,m}, t) + \hat{J}_h(\overline{\boldsymbol{w}}_{h\tau}, \boldsymbol{\psi}_{h\tau}^{l,m}, \boldsymbol{\psi}_{h\tau}^{z,m}, t) \Bigg) \, \mathrm{d}t \\
&+ \sum_{l=1}^{\mathrm{dof}_{h\tau}} \xi_l^m \left(\boldsymbol{\psi}_{h\tau}^{l,m}(t_{m-1}^+), \boldsymbol{\psi}_{h\tau}^{z,m}(t_{m-1}^+) \right)_{\Omega_{ht_m}^f} \\
&= \int_{I_m} \ell_h(\boldsymbol{w}_{hD}, \boldsymbol{\psi}_{h\tau}^{z,m}, t) \, \mathrm{d}t + \left(\boldsymbol{w}_{h\tau}^{m-1}(t_{m-1}^-), \boldsymbol{\psi}_{h\tau}^{z,m}(t_{m-1}^+) \right)_{\Omega_{ht_m}^f} \qquad \forall \boldsymbol{\psi}_{h\tau}^{z,m} \in \boldsymbol{S}_{h\tau}^{r,q}|_{I_m} .
\end{aligned}
$$

We can convert this system into the form

$$
\boldsymbol{A}_{h\tau}^m \, \boldsymbol{\Xi}_{h\tau}^m = \boldsymbol{L}_{h\tau}^m, \tag{4.88}
$$

where for $m = 1$

$$
\begin{aligned}
\left\{ \boldsymbol{A}_{h\tau}^1 \right\}_{z,l} &= \int_{I_1} \Bigg(\left(\frac{D^A \boldsymbol{\psi}_{h\tau}^{l,1}}{Dt}, \boldsymbol{\psi}_{h\tau}^{z,1} \right)_{\Omega_{ht_1}^f} + d_h(\boldsymbol{\psi}_{h\tau}^{l,1}, \boldsymbol{\psi}_{h\tau}^{z,1}, t) + \hat{b}_h(\overline{\boldsymbol{w}}_{h\tau}, \boldsymbol{\psi}_{h\tau}^{l,1}, \boldsymbol{\psi}_{h\tau}^{z,1}, t) \\
&\quad + \hat{a}_h(\overline{\boldsymbol{w}}_{h\tau}, \boldsymbol{\psi}_{h\tau}^{l,1}, \boldsymbol{\psi}_{h\tau}^{z,1}, t) + J_h(\boldsymbol{\psi}_{h\tau}^{l,1}, \boldsymbol{\psi}_{h\tau}^{z,1}, t) \\
&\quad + \hat{\beta}_h(\overline{\boldsymbol{w}}_{h\tau}, \boldsymbol{\psi}_{h\tau}^{l,1}, \boldsymbol{\psi}_{h\tau}^{z,1}, t) + \hat{J}_h(\overline{\boldsymbol{w}}_{h\tau}, \boldsymbol{\psi}_{h\tau}^{l,1}, \boldsymbol{\psi}_{h\tau}^{z,1}, t) \Bigg) \, \mathrm{d}t \\
&\quad + \left(\boldsymbol{\psi}_{h\tau}^{l,1}(t_0^+), \boldsymbol{\psi}_{h\tau}^{z,1}(t_0^+) \right)_{\Omega_{ht_1}^f} , \\
\left\{ \boldsymbol{L}_{h\tau}^1 \right\}_z &= \int_{I_1} \ell_h(\boldsymbol{w}_{hD}, \boldsymbol{\psi}_{h\tau}^{z,1}, t) \, \mathrm{d}t + \left(\boldsymbol{w}^0, \boldsymbol{\psi}_{h\tau}^{z,1}(t_0^+) \right)_{\Omega_{ht_1}^f} , \\
\boldsymbol{\Xi}_{h\tau}^1 &= (\xi_1^1, \ldots, \xi_{\mathrm{dof}_{h\tau}}^1)^T
\end{aligned}
$$

and for $m > 1$

$$
\begin{aligned}
\{ \boldsymbol{A}_{h\tau}^m \}_{z,l} &= \int_{I_m} \Bigg(\left(\frac{D^A \boldsymbol{\psi}_{h\tau}^{l,m}}{Dt}, \boldsymbol{\psi}_{h\tau}^{z,m} \right)_{\Omega_{ht_m}^f} + d_h(\boldsymbol{\psi}_{h\tau}^{l,m}, \boldsymbol{\psi}_{h\tau}^{z,m}, t) + \hat{b}_h(\overline{\boldsymbol{w}}_{h\tau}, \boldsymbol{\psi}_{h\tau}^{l,m}, \boldsymbol{\psi}_{h\tau}^{z,m}, t) \\
&\quad + \hat{a}_h(\overline{\boldsymbol{w}}_{h\tau}, \boldsymbol{\psi}_{h\tau}^{l,m}, \boldsymbol{\psi}_{h\tau}^{z,m}, t) + J_h(\boldsymbol{\psi}_{h\tau}^{l,m}, \boldsymbol{\psi}_{h\tau}^{z,m}, t) \\
&\quad + \hat{\beta}_h(\overline{\boldsymbol{w}}_{h\tau}, \boldsymbol{\psi}_{h\tau}^{l,m}, \boldsymbol{\psi}_{h\tau}^{z,m}, t) + \hat{J}_h(\overline{\boldsymbol{w}}_{h\tau}, \boldsymbol{\psi}_{h\tau}^{l,m}, \boldsymbol{\psi}_{h\tau}^{z,m}, t) \Bigg) \, \mathrm{d}t \\
&\quad + \left(\boldsymbol{\psi}_{h\tau}^{l,m}(t_{m-1}^+), \boldsymbol{\psi}_{h\tau}^{z,m}(t_{m-1}^+) \right)_{\Omega_{ht_m}^f} , \\
\{ \boldsymbol{L}_{h\tau}^m \}_z &= \int_{I_m} \ell_h(\boldsymbol{w}_{hD}, \boldsymbol{\psi}_{h\tau}^{z,m}, t) \, \mathrm{d}t + \left(\boldsymbol{w}_{h\tau}^{m-1}(t_{m-1}^-), \boldsymbol{\psi}_{h\tau}^{z,m}(t_{m-1}^+) \right)_{\Omega_{ht_m}^f} , \\
\boldsymbol{\Xi}_{h\tau}^m &= (\xi_1^m, \ldots, \xi_{\mathrm{dof}_{h\tau}}^m)^T .
\end{aligned}
$$

Remark. In practical computations, integrals appearing in the definitions of the forms $\hat{a}_h$, $\hat{b}_h$, d_h, J_h, $\hat{J}_h$, $\hat{\beta}_h$ and also the time integrals are evaluated with the aid of quadrature formulae, which will be introduced in Section 6.2.

The linear algebraic systems equivalent to (4.59)–(4.60) and (4.63)–(4.64) are solved either by the direct solver UMFPACK [14] or by the GMRES method with block diagonal preconditioning. In the last case individual blocks correspond to all unknowns on individual elements.

Numerical experiments show that both BDF-DG and STDG techniques with the extrapolation in nonlinear terms behave robust and stable. It has also been demonstrated by the theoretical analysis carried out for a simplified model problem in [21] and [66].

5. Fluid-structure interaction

In the previous chapters we introduced the problem of deformation of an elastic body and the problem of compressible viscous fluid flow in a time-dependent domain. Both the fluid and the elasticity problems represent a part of the fluid-structure interaction (FSI) problem, which we introduce in this chapter. We consider the case of a two-way coupled system, where the deformation of the elastic body is induced by the fluid force and the domain, occupied by the fluid, is given by the deformation of the elastic body. The flow is driven by the inlet boundary conditions and the evolving flow acts on the surface of the elastic body. Thus, the deformation of the elastic body is caused by the flow acting force. This deformation changes the domain occupied by the fluid and by that, the fluid flow is also altered. The definition of the problem implies that there exists a common boundary of the fluid domain and the deformed structure domain. In case of the fluid it is the moving part of the boundary Γ_{Wt} and in case of the structure it is the Neumann part Γ_N^b of the boundary.

The FSI problem is defined by the definition of the fluid flow problem, by the definition of the dynamic elasticity problem and by suitable transmission conditions on the common part of the boundary. Therefore our first goal is to define the transmission conditions and accordingly the FSI problem. Further, we need to introduce the solution of the FSI problem. Generally, there are two strategies how to solve the problem. The first one is to solve the complete monolithic system including the fluid and structure problem at once. Another strategy is to stagger the problem into separate subproblems and introduce a suitable coupling procedure. We are concerned with the latter approach, which means that we solve the fluid flow problem and structure problem separately. The basic idea is that the problems are coupled at certain time instants. The time instants are given by the choice of the time interval partition. At these time instants we require the transmission conditions to be approximately fulfilled. Therefore, the coupling between the subsystems is influenced by the choice of the time step. This approach is denoted *loosely* or *weakly coupled scheme*. Moreover, we also introduce the so called *strongly coupled scheme* or simply *strong coupling*. In this case the two subproblems are solved still separately, but in every time step we proceed several subiterations in order to fulfill the transmission conditions more precisely.

The monolithic approach leads usually to a large system, which costs a lot of computational time and requires a large memory. Contrary to that the partitioned approach is separated in two smaller problems and it also gives us a possibility to use different suitable solvers for the subproblems. However, some of the problems, which are strongly coupled, can lead to a large amount of subiterations. In that case, the partitioned approach can be less efficient. We are motivated by the problem of vocal folds, which represents a problem, where the air is accelerated by the contracting channel and the vocal folds are considered as elastic bodies vibrating with high frequency. In this case the densities of the fluid and solid material are unlike. In our numerical experiments we show, that the strongly coupled scheme is in this case sufficient, because just a few coupling subiterations are needed.

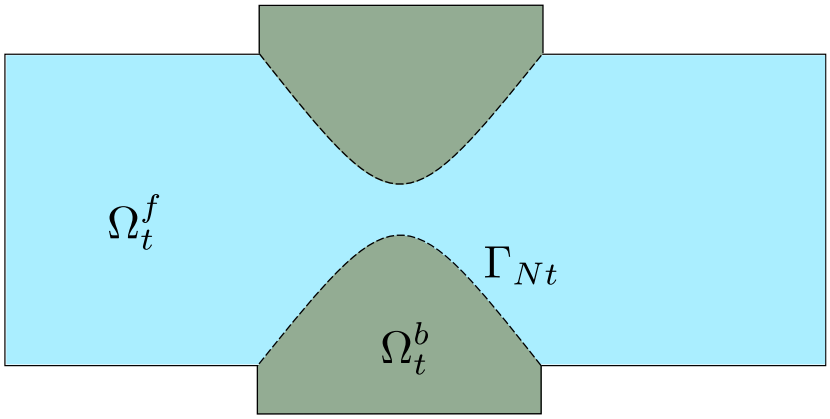

Figure 5.1: Diagram of the computational domain for the FSI problem with the common boundary Γ_{Nt}.

For the solution of the fluid flow problem, the ALE mapping needs to be estimated in every time step. Since the deformation of the computational domain for the fluid flow is given by the deformation of the common part of the boundary, this leads to another nontrivial subproblem. Therefore, we describe a special procedure in order to obtain the deformation of the triangulation for the fluid flow problem. The deformation of the domain is computed as a static linear elasticity problem. We introduce also some ideas, which can improve the quality of the triangulations.

This chapter is concluded by numerical experiments. We consider a simplified 2D initial-boundary value problem. The flow properties are defined according to the characteristics of the airflow in human vocal tract. The material properties are defined in order to model an elastic body constituting a soft tissue. We assume both the linear and nonlinear elasticity model and finally we present several visualizations of the obtained results.

5.1 Fluid-structure interaction problem

Let us define the FSI problem. Let Ω_t^f be a bounded domain depending on time with disjoint parts of the boundary Γ_I, Γ_O and Γ_{Wt} as defined in Definition 9 and Ω^b be a bounded domain with two disjoint parts of the boundary Γ_D^b and Γ_N^b as defined in Definition 1. Let $\Omega \subset \mathbb{R}^2$ be a set such that $\overline{\Omega} = \overline{\Omega}_t^b \cup \overline{\Omega}_t^f$, $t \in [0, T]$, $T > 0$, where $\Omega_t^b = \boldsymbol{\varphi}_t\left(\Omega^b\right)$ is the actual configuration of the elastic body in time t and Ω_t^f is the domain occupied by the fluid in time t. The deformation mapping $\boldsymbol{\varphi}_t$ is defined as in (1.12). The common part of the boundary of the fluid flow domain and the boundary of the elastic body is denoted by $\Gamma_{Nt} = \Gamma_N(t)$, see Figure 5.1. It is given by the deformation of the Neumann part of the boundary Γ_N^b, i.e. $\Gamma_{Nt} = \boldsymbol{\varphi}_t\left(\Gamma_N^b\right)$, and it is a subset of the boundary Γ_{Wt}. We consider the fluid flow problem as defined in Definition 9 and the structure problem as defined in Definition 1. Let us note that for the structure problem we use the Lagrangian coordinates system and for the fluid flow problem the Eulerian coordinates system. We use the notation as in Chapter 1: $\boldsymbol{x}$ will denote

the Lagrangian coordinates and $\boldsymbol{x}^{\boldsymbol{\varphi}}$ the Eulerian coordinates, where $\boldsymbol{\varphi}$ is the deformation of the elastic body. However, for simplicity we try to avoid the use of both notations, if it is not necessary to distinguish between the Lagrangian and the Eulerian coordinate system.

In the FSI problem the coupling of the discrete flow problem and the structural problem is realized, analogously as in [31, 40], via the transmission condition

$$\boldsymbol{\sigma}^b \boldsymbol{n}^{\boldsymbol{\varphi}} = \boldsymbol{\sigma}^f \boldsymbol{n}^{\boldsymbol{\varphi}} \quad \text{on } \Gamma_{Nt},\ t \in [0,T], \tag{5.1}$$

where $\boldsymbol{\sigma}^f$ is the stress tensor of the fluid with components σ_{ij}^f defined in (4.2), $\boldsymbol{\sigma}^b$ is the Cauchy stress tensor of the elastic material defined in Section 1.3.3 and $\boldsymbol{n}^{\boldsymbol{\varphi}}$ is the unit outer normal to the boundary of the deformed body by the deformation $\boldsymbol{\varphi}$. The Cauchy stress tensor $\boldsymbol{\sigma}^b$ can be expressed according to the Section 1.3.4 with the aid of the first Piola-Kirchhoff stress tensor as

$$\boldsymbol{\sigma}^b = J^{-1} \boldsymbol{P} \boldsymbol{F}^T. \tag{5.2}$$

Here $J = \det \boldsymbol{F} > 0$. The normal $\boldsymbol{n}^{\boldsymbol{\varphi}}$ and the unit outer normal $\boldsymbol{n}$ to the reference configuration Ω^b are related by:

$$\boldsymbol{n}^{\boldsymbol{\varphi}} = \frac{\mathrm{Cof}\boldsymbol{F}\ \boldsymbol{n}}{|\mathrm{Cof}\boldsymbol{F}\ \boldsymbol{n}|}, \tag{5.3}$$

where $\mathrm{Cof}\boldsymbol{F} = J\boldsymbol{F}^{-T}$ is the cofactor matrix of $\boldsymbol{F}$. By (5.2) and (5.3) we can rewrite (5.1) as

$$\left(J^{-1}\boldsymbol{P}\boldsymbol{F}^T\right) \mathrm{Cof}\boldsymbol{F}\ \boldsymbol{n} = \boldsymbol{\sigma}^f \mathrm{Cof}\boldsymbol{F}\ \boldsymbol{n}. \tag{5.4}$$

Hence,

$$\boldsymbol{P} \cdot \boldsymbol{n} = \boldsymbol{\sigma}^f \mathrm{Cof}\boldsymbol{F}\boldsymbol{n}. \tag{5.5}$$

In this way we obtain the surface force acting on the Neumann part of the boundary in (1.53).

Further, on the interface between fluid and structure the fluid velocity is defined by the second transmission condition

$$\boldsymbol{v}(\boldsymbol{x}^{\boldsymbol{\varphi}}, t) = \boldsymbol{z}_D(\boldsymbol{x}^{\boldsymbol{\varphi}}, t) = \frac{\partial \boldsymbol{u}(\boldsymbol{x}, t)}{\partial t}, \tag{5.6}$$

where $\boldsymbol{u}$ is the displacement of the elastic structure and $\boldsymbol{x}^{\boldsymbol{\varphi}} = \boldsymbol{\varphi}(\boldsymbol{x})$.

Let us conclude this section with the formulation of the FSI problem.

Definition 12. *(Formulation of the FSI problem)* Let Ω_t^f be a bounded domain depending on time with the disjoint parts of the boundary Γ_I, Γ_O and Γ_{Wt} as defined in Definition 9 and Ω^b be a bounded domain with two disjoint parts of the boundary Γ_D^b and Γ_N^b as defined in Definition 1. Let $\Omega \subset \mathbb{R}^2$ be a set such that $\overline{\Omega} = \overline{\Omega}_t^b \cup \overline{\Omega}_t^f$, $t \in [0,T]$, $T > 0$, where Ω_t^b is the actual configuration of the elastic body in time t and Ω_t^f is the domain occupied by the fluid in time t. Further let Γ_{Nt} be the common part of the boundary of the fluid flow domain and the boundary of the elastic body, such that it is a subset of the part of the boundary Γ_{Wt} and in the same time $\Gamma_{Nt} = \boldsymbol{\varphi}_t\left(\Gamma_N^b\right)$. We define the solution of the FSI problem as a couple $(\boldsymbol{u}, \boldsymbol{w})$, where $\boldsymbol{u} : \Omega^b \times [0,T] \to \mathbb{R}^2$ is the solution of the dynamic elasticity problem defined in Definition 1 with

$$\boldsymbol{g}_N = \boldsymbol{\sigma}^f \mathrm{Cof}\boldsymbol{F}\boldsymbol{n} \quad \text{in } \Gamma_N^b \times [0,T], \tag{5.7}$$

and the state vector $\boldsymbol{w} : \Omega_t^f \times [0,T] \to \mathbb{R}^4$ is the solution of the compressible fluid flow problem defined in Definition 9 with

$$\boldsymbol{z}_D(\boldsymbol{x}^{\boldsymbol{\varphi}}, t) = \boldsymbol{z}_D(\boldsymbol{\varphi}(\boldsymbol{x}), t) = \begin{cases} \frac{\partial \boldsymbol{u}(\boldsymbol{x},t)}{\partial t} & \text{on } \Gamma_{Nt}, \\ \boldsymbol{0} & \text{on } \Gamma_{Wt} \setminus \Gamma_{Nt}, \ t \in [0,T], \end{cases} \tag{5.8}$$

where $\boldsymbol{g}_N$ and $\boldsymbol{n}$ have the same interpretation as in Definition 1, $\boldsymbol{\sigma}^f$ is the stress tensor of the fluid with components σ_{ij}^f defined in (4.2), $\mathrm{Cof}\boldsymbol{F}$ is the cofactor matrix of the deformation gradient $\boldsymbol{F}$ and $\boldsymbol{z}_D$ is the velocity of the moving wall.

Remark. We also consider Definition 12 with the linear elasticity instead of the nonlinear elasticity problem. In that case we simply set that $\boldsymbol{u}$ is the solution of the dynamic elasticity problem defined in Definition 3. Further in condition (5.7) we can assume that the deformation gradient should be approximately a unit matrix, i.e. $\mathrm{Cof}\boldsymbol{F} \approx \boldsymbol{I}$. In the following sections we discuss precisely, how to deal with the transmission conditions in the coupling procedure.

5.2 Coupling procedure

We solve the FSI problem by a partitioned coupling mechanism, where the elasticity problem and the flow problem are solved separately. For the time discretization of both the fluid and the structure problem let us consider same partition of the time interval $[0,T]$ formed by time instants

$$t_m, m = 0, \dots, M, \quad 0 = t_0 < t_1 < \dots < t_M = T, \tag{5.9}$$

where M is a sufficiently large positive integer and define the time step

$$\tau_m = t_m - t_{m-1}, \quad m = 1, \dots, M. \tag{5.10}$$

In the coupling procedure we expect transmission conditions (5.7) and (5.8) to be satisfied in time instants $t_m, m = 0, \dots, M$. The structure and the fluid flow problem are discretized in the same way as we did in the previous chapters. Hence, the boundary conditions of both problems are successively updated during the computational process. Then for the structure problem we obtain the BDF-DG approximate solution as defined in Definition 8, which is a couple of sequences

$$\{\boldsymbol{u}_h^m\}_{m=0}^M, \ \{\boldsymbol{z}_h^m\}_{m=0}^M. \tag{5.11}$$

Let us note that in the definition of the approximate solution we can consider an arbitrary nonlinear elasticity model or the linear elasticity model. In the discretization of the fluid flow we use the full space-time discretization. Hence, we obtain the STDG approximate solution $\boldsymbol{w}_{h\tau}$ as defined in Definition 11. We denote as $\boldsymbol{w}_{h\tau}^m := \boldsymbol{w}_{h\tau}|_{I_m}$ the solution, which we seek in the time interval $I_m = (t_{m-1}, t_m)$. Therefore we can say that we seek the sequence of approximate solutions

$$\{\boldsymbol{w}_{h\tau}^m\}_{m=1}^M. \tag{5.12}$$

Further we denote as

$$\{\mathcal{A}_{t_m}\}_{m=0}^M, \ \{\boldsymbol{z}_\tau^m\}_{m=0}^M, \ \left\{\Omega_{t_m}^f\right\}_{m=0}^M, \tag{5.13}$$

the sequence of the ALE mapping, the sequence of approximations of the domain velocity and the sequence of the domains occupied by the fluid at time instants t_m, $m = 0, \dots, M$.

Using the partitioned coupling mechanism for the numerical solution of the FSI problem, the transmission conditions are satisfied just approximately. This means that we will prescribe a coupling condition and a suitable tolerance for this condition. In order to obtain a well coupled scheme we use a coupling procedure containing a few subiterations. The approximate solutions obtained during the subiterations are denoted with the index l behind the comma, i.e. $\boldsymbol{u}_{h,l}^m$, $\boldsymbol{z}_{h,l}^m$, $\boldsymbol{w}_{h\tau,l}^m$, $\Omega_{t_m,l}^f$, $\mathcal{A}_{t_m,l}$, $\boldsymbol{z}_{\tau,l}^m$, and $\sigma_{ij,l}^f$.

Coupling algorithm

1. Let us assume that the approximate solution $\boldsymbol{w}_{h\tau}^m$ of the flow problem in time interval $I_m = [t_{m-1}, t_m]$ and the displacement of the structure $\boldsymbol{u}_h^m$ at time level t_m are known.

2. We set $\boldsymbol{u}_{h,0}^{m+1} := \boldsymbol{u}_h^m$, $l := 1$ and apply the following iterative process:

   (a) Interpolate $\boldsymbol{u}_{h,l-1}^{m+1}$ on the common part of the boundary of the fluid and the structure domain in order to get a continuous function on this interface. This will be described in detail in Section 5.3.1.

   (b) The approximation $\Omega_{t_{m+1},l}^f$ of the domain $\Omega_{t_{m+1}}^f$ is determined by the interpolated displacement of the moving part of the fluid domain boundary.

   (c) Determine the ALE mapping $\mathcal{A}_{t_{m+1},l}$ and approximate the domain velocity $\boldsymbol{z}_{\tau,l}^{m+1}$. This will be described in detail in Section 5.3.2.

   (d) Solve the flow problem in the domain $\Omega_{t_{m+1},l}^f$ to obtain the approximate solution $\boldsymbol{w}_{h\tau,l}^{m+1}$ in time interval $I_{m+1} = [t_m, t_{m+1}]$.

   (e) Compute components $\sigma_{ij,l}^f$ of the stress tensor and the aerodynamic force acting on the structure and transform it to the interface Γ_N^b. This will be also described in detail in Section 5.3.1.

   (f) Solve the elasticity problem in order to compute the displacement $\boldsymbol{u}_{h,l}^{m+1}$ at time t_{m+1}.

   (g) If the variation
   $$\left|\boldsymbol{u}_{h,l}^{m+1} - \boldsymbol{u}_{h,l-1}^{m+1}\right| \tag{5.14}$$
   of the displacement is larger than a prescribed tolerance, go to (a) and set $l := l + 1$. We prescribe the tolerance for the absolute value and also for the relative value of the variation
   $$\frac{\left|\boldsymbol{u}_{h,l}^{m+1} - \boldsymbol{u}_{h,l-1}^{m+1}\right|}{\max\left\{10^{-5}, \left|\boldsymbol{u}_{h,l}^{m+1}\right|\right\}}. \tag{5.15}$$

   (h) Set $\boldsymbol{u}_h^{m+1} := \boldsymbol{u}_{h,l}^{m+1}$, $\boldsymbol{w}_{h\tau}^{m+1} := \boldsymbol{w}_{h\tau,l}^{m+1}$, $m := m + 1$ and go to 2.

The presented algorithm represents the so-called *strong coupling* scheme. Neglecting step 2(g) yields the so-called *weak coupling* scheme. Figure 5.2 shows the diagram of the algorithm.

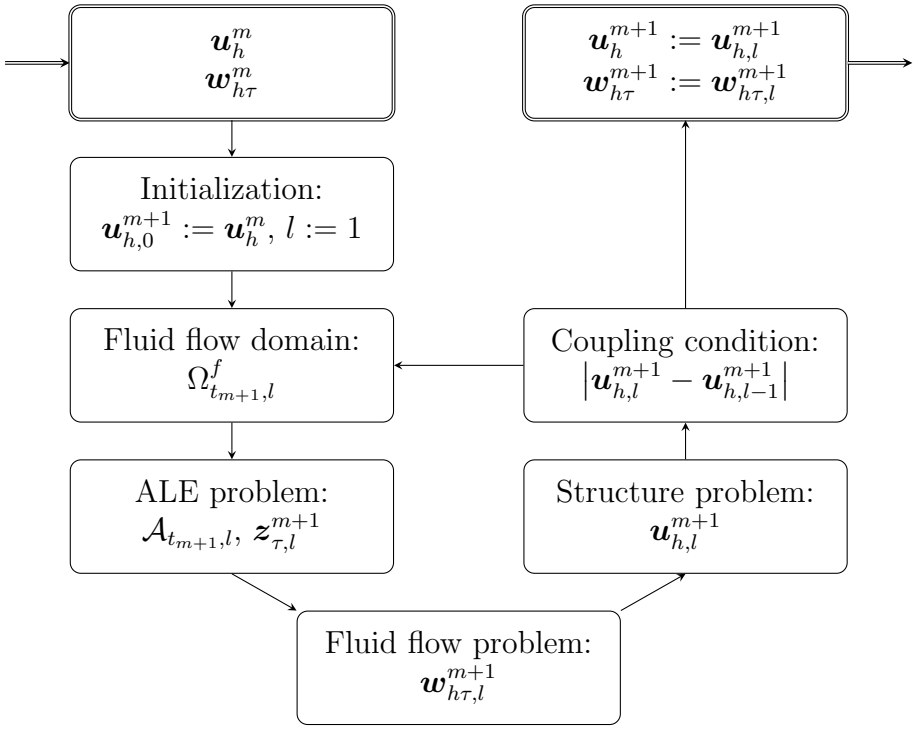

Figure 5.2: Diagram of the coupling algorithm.

Remark. (BDF-DG variant of the algorithm) The coupling algorithm could be also modified for the BDF-DG approximate solution of the flow problem as defined in Definition 10. In that case we consider $\{\boldsymbol{w}_h^m\}_{m=1}^M$, the BDF-DG approximate solution of the flow problem, instead of the sequence of approximate solutions $\{\boldsymbol{w}_{h\tau}^m\}_{m=1}^M$.

5.3 Realization of the discrete FSI problem

In the previous section we described the coupling procedure, but some of the steps of the iterative process need to be discussed in more detail. First of them is the realization of the transmission conditions and the latter one is the derivation of the ALE mapping. The realization of the transmission conditions is more or less just a technical detail, but the derivation of the ALE mapping constitutes a specific subproblem. Actually, we can say that numerical solution of the FSI problem consists of three subproblems: the fluid flow problem, the structure problem, and the derivation of the ALE mapping. In this section we show, that for the construction of the ALE mapping and the domain velocity we can use a solution of the static linear elasticity problem, which is also solved by the DGM.

5.3.1 Transmission conditions

Let us describe in detail, how the transmission conditions (5.7) and (5.8) are fulfilled in the discrete problem. In the introduced discretization we consider, that the initial triangulation $\mathcal{T}_{h0}$ of the reference domain Ω_0^f and the triangulation $\mathcal{T}_h^b$ of the reference domain Ω^b have common edges on the common part of the boundary

$\Gamma_{N0} = \Gamma_N^b$. It means, that every boundary edge $\Gamma \subset \Gamma_{N0}$ lying on the common part of the boundary has its adjacent element in both the fluid and the structure triangulation. Let us denote K_Γ^f the adjacent element in the triangulation $\mathcal{T}_{h0}$ and K_Γ^b the adjacent element in the triangulation $\mathcal{T}_h^b$ for every $\Gamma \subset \Gamma_{N0}$. Both problems are solved with the aid of the DGM in space. Therefore we obtain generally a discontinuous piecewise polynomial solution, but it is continuous on every single element.

First let us consider that we have obtained the approximate solution $\boldsymbol{w}_{h\tau,l}^{m+1}$ of the flow problem as in step 2(d) of the coupling algorithm. Thus, we have obtained the approximations of the pressure p and velocity $\boldsymbol{v}$ on every boundary edge $\Gamma \subset \Gamma_{N,l}^{m+1}$ and the approximation of the common boundary $\Gamma_{Nt_{m+1}}$ given by the deformation approximation $\boldsymbol{\varphi}_{h,l}^{m+1} = \boldsymbol{I} + \boldsymbol{u}_{h,l}^{m+1}$. Using that and (4.2) we compute $\boldsymbol{\sigma}_{h,l}^f$, the approximation of the stress tensor for every boundary edge $\Gamma \subset \Gamma_{N,l}^{m+1}$. The stress tensor is on $\Gamma_{N,l}^{m+1}$ given in Eulerian coordinates, but we express it in Lagrangian coordinates, so it holds

$$\boldsymbol{\sigma}_{h,l}^f(\boldsymbol{x}^{\boldsymbol{\varphi}}) = \boldsymbol{\sigma}_{h,l}^f(\boldsymbol{\varphi}_{h,l}^{m+1}(\boldsymbol{x})), \quad \boldsymbol{x} \in \Gamma,\ \Gamma \subset \Gamma_N^b. \tag{5.16}$$

In order to completely formulate the condition (5.7) we need to estimate $\mathrm{Cof}\boldsymbol{F}$. This can be done again using the deformation approximation $\boldsymbol{\varphi}_{h,l}^{m+1}$. We show that the procedure could also be used for the linear elasticity or we can set $\mathrm{Cof}\boldsymbol{F} \approx \boldsymbol{I}$ respectively, as already mentioned in remark on Definition 12. By that we explained how we proceed in step 2(e) of the coupling algorithm obtaining the Neumann boundary condition from the approximate solution of the flow problem. Obviously, in this case it does not matter, that the solution is discontinuous.

Further we describe in detail the procedure in step 2(a) of the coupling algorithm, in which we get the approximation of the boundary Γ_{Nt} and the boundary condition for the solution of the elasticity problem leading to the derivation of the ALE mapping. For the solution of the fluid flow problem the deformation of the common part of the boundary needs to be linear and continuous on every edge of the common boundary. Therefore, we interpolate the solution of the elasticity problem in the following way. By π we denote the continuous piecewise linear interpolation of the discontinuous displacement of the structure $\boldsymbol{u}_{h,l}^{m+1}$. In every vertex lying on the common boundary of the reference triangulation we set the interpolation π as an average of discontinuous solutions in all adjacent elements. This means that for every vertex with the reference position $\boldsymbol{x}_i$ of the triangulation $\mathcal{T}_h^b$ lying on the boundary Γ_N^b we set

$$\pi(\boldsymbol{u}_{h,l}^{m+1}(\boldsymbol{x}_i)) = \frac{1}{N_i} \sum_{K \in \mathcal{T}_h^b, \boldsymbol{x}_i \in K} \boldsymbol{u}_{h,l}^{m+1}|_K(\boldsymbol{x}_i), \quad i = 1, \dots, N_V, \tag{5.17}$$

where N_i, $i = 1, \dots, N_V$ is the number of the adjacent elements, i.e. $N_i = \sum_{K \in \mathcal{T}_h^b, \boldsymbol{x}_i \in K} 1$. Further we consider the interpolation to be linear on every edge of the common boundary Γ_N^b. Then the continuous piecewise linear function is uniquely determined. The interpolation function π is also used for the definition of the Dirichlet boundary condition in the computation of the ALE mapping as it is described in the following section.

5.3.2 Derivation of the ALE mapping

Let us now describe the derivation of ALE mapping $\mathcal{A}_t$. Obviously, according to the coupling procedure described in Section 5.2, we compute the structure deformation approximations in discrete time instants t_m. Consequently, in every time instant t_m we determine the ALE mapping $\mathcal{A}_{t_m}$ or more precisely the ALE mapping $\mathcal{A}_{t_m,l}$ for every subiteration of the coupling algorithm. We obtain the ALE mapping by solving the static linear elasticity problem, which is defined analogously as in Definition 4. We consider a reference domain $\Omega_0^f \subset \mathbb{R}^2$ occupied by the fluid and generally for every time instant t_m we seek a displacement function $\boldsymbol{u}_{\mathcal{A},l}^m : \Omega_0^f \to \mathbb{R}^2$ such that

$$-\text{div}\, \boldsymbol{\sigma}_{\mathcal{A},l}^m = \boldsymbol{0} \qquad \text{in } \Omega_0^f, \tag{5.18}$$

$$\boldsymbol{u}_{\mathcal{A},l}^m = \boldsymbol{u}_{\mathcal{A}D,l}^m \quad \text{on } \partial\Omega_0^f, \tag{5.19}$$

where $\boldsymbol{\sigma}_{\mathcal{A},l}^m$ is a Cauchy stress tensor of an artificial linear elasticity material. It is given as in (1.71):

$$\boldsymbol{\sigma}_{\mathcal{A},l}^m(\boldsymbol{u}_{\mathcal{A},l}^m) = \lambda_{\mathcal{A}} \text{tr}(\boldsymbol{e}(\boldsymbol{u}_{\mathcal{A},l}^m))\boldsymbol{I} + 2\mu_{\mathcal{A}}\boldsymbol{e}(\boldsymbol{u}_{\mathcal{A},l}^m), \tag{5.20}$$

where $\lambda_{\mathcal{A}}$ and $\mu_{\mathcal{A}}$ are the Lamé parameters. The function $\boldsymbol{u}_{\mathcal{A}D,l}^m$ is given by the displacement of the structure on the common boundary and as zero on the fixed part of the boundary. Hence,

$$\boldsymbol{u}_{\mathcal{A}D,l}^m = \begin{cases} \pi(\boldsymbol{u}_{h,l-1}^m) & \text{on } \Gamma_N^b, \\ \boldsymbol{0} & \text{else}, \end{cases} \tag{5.21}$$

where $\pi(\boldsymbol{u}_{h,l-1}^m)$ is the continuous piecewise linear interpolation of the discontinuous displacement of the structure $\boldsymbol{u}_{h,l-1}^m$ described in (5.17). Then, the ALE mapping $\mathcal{A}_{t_m,l}$ is given by

$$\mathcal{A}_{t_m,l}(\boldsymbol{X}) = \boldsymbol{X} + \pi(\boldsymbol{u}_{\mathcal{A},l}^m(\boldsymbol{X})) \quad \forall \boldsymbol{X} \in \Omega_0^f. \tag{5.22}$$

By π we denote the continuous piecewise linear interpolation of the discontinuous solution $\boldsymbol{u}_{\mathcal{A},l}^m$, which must be applied in order to get a regular one-to-one ALE mapping of the reference configuration Ω_0^f onto the current configuration $\Omega_{t_{m+1},l}^f$. We use the same notation π as for the linear interpolation of the the discontinuous displacement of the structure, because on the boundary of the domain we set $\pi(\boldsymbol{u}_{\mathcal{A},l}^m) = \boldsymbol{u}_{\mathcal{A}D,l}^m$, i.e. $\pi(\boldsymbol{u}_{\mathcal{A},l}^m) = \pi(\boldsymbol{u}_{h,l-1}^m)$ on Γ_N^b. Further we define π in all inner vertices of the reference triangulation as an average of the discontinuous solution in all adjacent elements. Hence,

$$\pi(\boldsymbol{u}_{\mathcal{A},l}^m(\boldsymbol{X}_i)) = \frac{1}{N_i} \sum_{K \in \mathcal{T}_{h0}, \boldsymbol{X}_i \in K} \boldsymbol{u}_{\mathcal{A},l}^m|_K(\boldsymbol{X}_i), \quad i = 1, \ldots, N_V, \tag{5.23}$$

where N_V is the number of vertices of the triangulation, $\boldsymbol{X}_i,\ i = 1, \ldots, N_V$ are the reference positions of the inner vertices and $N_i,\ i = 1, \ldots, N_V$ is the number of the adjacent elements for every vertex, i.e. $N_i = \sum_{K \in \mathcal{T}_{h0}, \boldsymbol{X}_i \in K} 1$. Further, we consider the piecewise linear interpolation, linear on every element $K \in \mathcal{T}_{h0}$. By this assumption and the definition in the vertices is the continuous piecewise linear function uniquely determined.

Moreover, for the STDGM discretization we need to define the ALE mapping on every time interval I_m. We define it using the linear interpolation in time given by

$$\mathcal{A}_{t,l}(\boldsymbol{X}) = \frac{t_m - t}{\tau_m}\mathcal{A}_{t_{m-1}}(\boldsymbol{X}) + \frac{t - t_{m-1}}{\tau_m}\mathcal{A}_{t_m,l}(\boldsymbol{X}), \quad \forall t \in I_m, \boldsymbol{X} \in \Omega_0^f. \tag{5.24}$$

Finally, we need to determine the ALE velocity $\boldsymbol{z}(\boldsymbol{x}, t)$ occurring in the form d_h. In the case of the STDGM discretization ALE velocity $\boldsymbol{z}_{\tau,l}^m(\boldsymbol{x}, t)$ on interval I_m can be expressed as

$$\boldsymbol{z}_{\tau,l}^m(\boldsymbol{x}, t) = \frac{\mathcal{A}_{t_m,l}(\mathcal{A}_{t,l}^{-1}(\boldsymbol{x})) - \mathcal{A}_{t_{m-1}}(\mathcal{A}_{t,l}^{-1}(\boldsymbol{x}))}{\tau_m}, \quad \forall t \in I_m,\ \boldsymbol{x} \in \Omega_t^f. \tag{5.25}$$

In the case of the BDF-DG discretization $\boldsymbol{z}(\boldsymbol{x}, t)$ is approximated as

$$\boldsymbol{z}_l^m(\boldsymbol{x}) = c_0\boldsymbol{x} + \sum_{k=1}^{q} c_l\mathcal{A}_{t_{m-k}}(\mathcal{A}_{t_m,l}^{-1}(\boldsymbol{x})), \quad \forall \boldsymbol{x} \in \Omega_{t_m}^f. \tag{5.26}$$

Examples of the ALE mapping

In the previous section we described the static linear elasticity problem, which we solve to determine the deformation of the computational domain. For the complete definition of this problem we still need to estimate Lamé parameters $\lambda_{\mathcal{A}}$ and $\mu_{\mathcal{A}}$. For this estimation we combine the approaches proposed in [26, 61]. Thus, in our experiments we obtain satisfactory results with the aid of non-physical material constants. We prescribe piecewise constant Lamè parameters by setting

$$\lambda_{\mathcal{A}} = -c_{\mathcal{A}} \cdot \frac{\text{avgsize}(\mathcal{T}_h^b)}{|K|}, \quad \mu_{\mathcal{A}} = -\lambda_{\mathcal{A}}, \tag{5.27}$$

where $c_{\mathcal{A}} > 0$ is a suitable constant, $|K|$ is the area of an element K and $\text{avgsize}(\mathcal{T}_h^b)$ is the average size of elements of the triangulation $\mathcal{T}_h^b$:

$$\text{avgsize}(\mathcal{T}_h^b) = \frac{1}{N_h}\sum_{K \in \mathcal{T}_h^b} |K|, \tag{5.28}$$

where N_h is the number of elements of the triangulation $\mathcal{T}_h^b$. In contrast to a material with physical Lamè parameters, where $\lambda_{\mathcal{A}},\ \mu_{\mathcal{A}} > 0$, we set $\lambda_{\mathcal{A}} + \mu_{\mathcal{A}} = 0$. Moreover, on each element K we divide the Lamè parameters by the relative size of the element. Finally, we choose an appropriate constant $c_{\mathcal{A}} > 0$. Our numerical experiments suggest that smaller values of $c_{\mathcal{A}}$ yield more suitable mesh deformations.

Here, we show the comparison of the mesh deformation obtained using an elastic material (the Lamè parameters are constant and correspond to a real physical material) and a pseudo-elastic material. Our example relates to numerical experiments for the FSI problem in the next section. Let us have a domain, whose geometry is corresponding to the domain described in Figure 5.4. We define the Dirichlet boundary condition by the displacement function, which causes

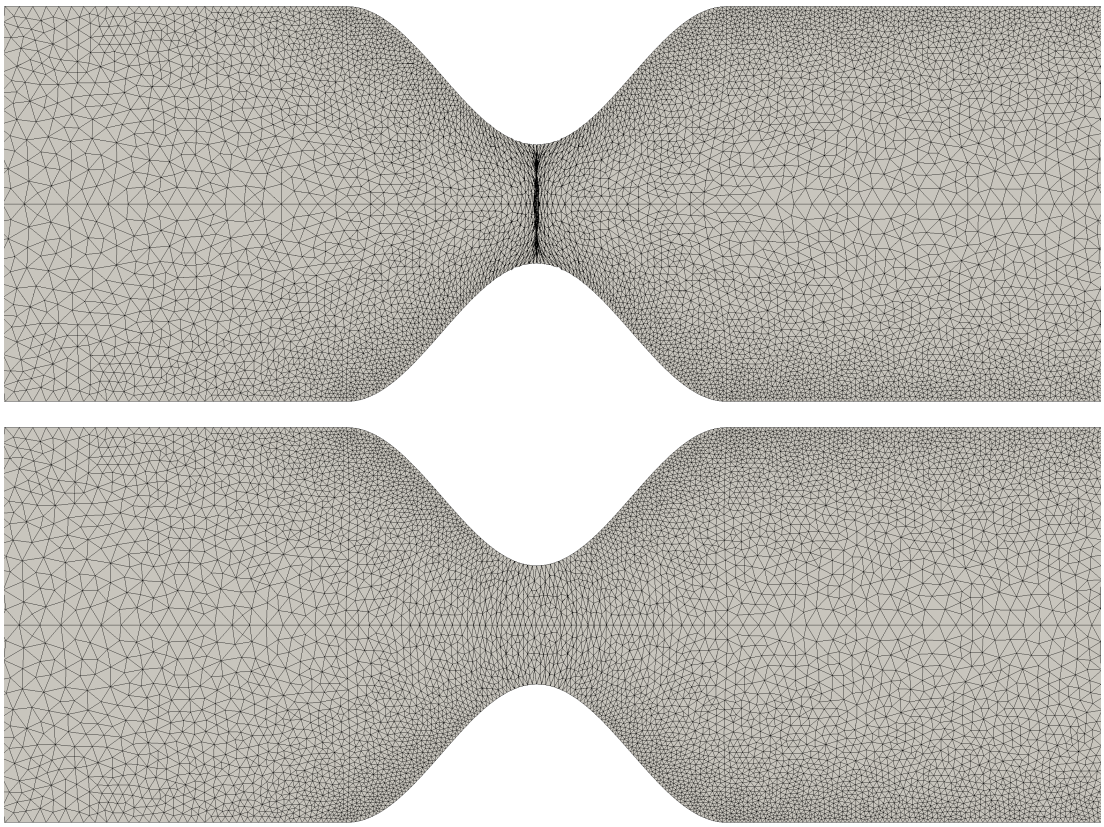

Figure 5.3: Detail of the narrowest part of the computational domain. Comparison of the deformation of the triangulation considering the standard elasticity model (top) and the pseudo-elasticity model (bottom).

an extension of the computational domain in its narrow part. The displacement function is defined on the boundary as

$$\boldsymbol{u}_{\mathcal{A}D} = \begin{cases} \left(0, h_B \operatorname{sgn}(x_2)\left(1 - \cos\left(\frac{2x_1\pi}{L_g}\right)\right)\right)^T & \text{on } \Gamma_N^b, \\ \mathbf{0} & \text{else,} \end{cases} \tag{5.29}$$

where $L_g = 0.0154$ and $h_B = 0.0008$. By that we triple the gap in the narrowest part of the channel. The problem is discretized using the piecewise linear approximation. We use the NIPG variant of the DGM. The penalization constant is set to $C_W^{\mathcal{A}} = 10^3$. For the pseudo-elastic material we set $c_{\mathcal{A}} = 10$ and $\lambda_{\mathcal{A}}$, $\mu_{\mathcal{A}}$ as in (5.27), and for the standard elasticity model we set $\lambda_{\mathcal{A}} = 35714$ and $\mu_{\mathcal{A}} = 8929$. In Figure 5.3 we can see the difference between the mesh deformation obtained by the solution of the static elasticity problem using the standard elasticity model and the described pseudo-elasticity model.

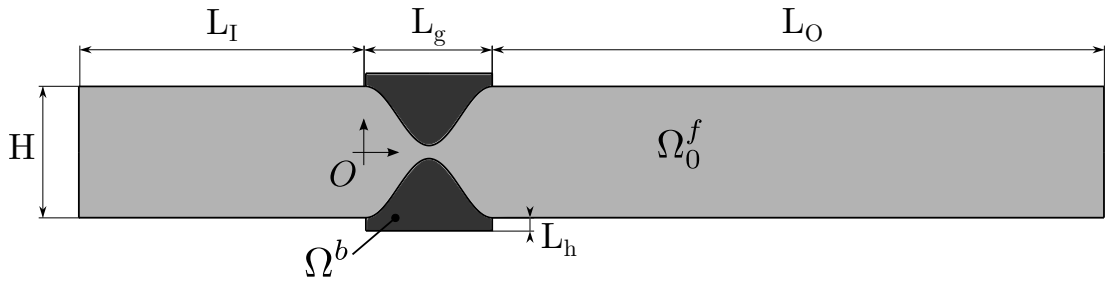

Figure 5.4: Geometry of the computational domain at time $t = 0$ and the description of its size: $L_I = 50.0$ mm, $L_g = 15.4$ mm, $L_h = 1.5$ mm, $L_O = 94.6$ mm, $H = 16.0$ mm. The width of the channel in the narrowest part is 1.6 mm. O is the origin of the coordinate system.

5.4 Numerical experiments for FSI

In this section we present the final results obtained by the introduced method for the numerical solution of the FSI problem. As we have already mentioned, our numerical experiments are motivated by the simulation of vibrations of vocal folds, which are caused by the airflow originated in human lungs. We consider a simplified 2D initial-boundary value problem. The flow properties are defined according to the characteritics of the airflow in trachea and human vocal tract. The material properties are defined in order to model an elastic body constituting a soft tissue. The first solved case is a problem with homogeneuos elasticity model and simplified geometry. Then, in the end of the section we present the obtained results for the model of vocal folds, which is inspired by the experiments described in [43, 60].

5.4.1 Cosine benchmark

We set a problem inspired by the cut of the model of the vocal tract. However the geometry of the channel is simple and the geometry of the elastic bump can be described by the cosine function. Figure 5.4 shows the geometry of the computational domain formed by two subdomains representing the elastic structure and the part occupied by the fluid. The common boundary of the structure and fluid domain is described by the relation

$$x_2 = \pm\frac{H_B}{2}\left(1 + \cos\left(\frac{2\pi x_1}{L_g}\right)\right) \pm h_B, \quad x_1 \in (0.0, L_g), \tag{5.30}$$

where $L_g = 0.0154$, $H_B = 0.0072$ and $h_B = 0.0008$. The other measures of the geometry are stated in Figure 5.4. Further we add to the geometry a semicircle subdomain with a radius 3.0 cm as an outlet. The example of the computational domain with the mesh for the fluid flow and structure problem is in Figure 5.5.

We solve the FSI problem defined in Definition 12, but we start always with a few iterations, in which the structure is considered to be fixed and therefore just the fluid flow problem on a fixed domain is solved. This initial computation leads to the development of the flow field. At first let us describe the settings for the fluid flow problem. We prescribe the inlet boundary conditions on Γ_I (left part

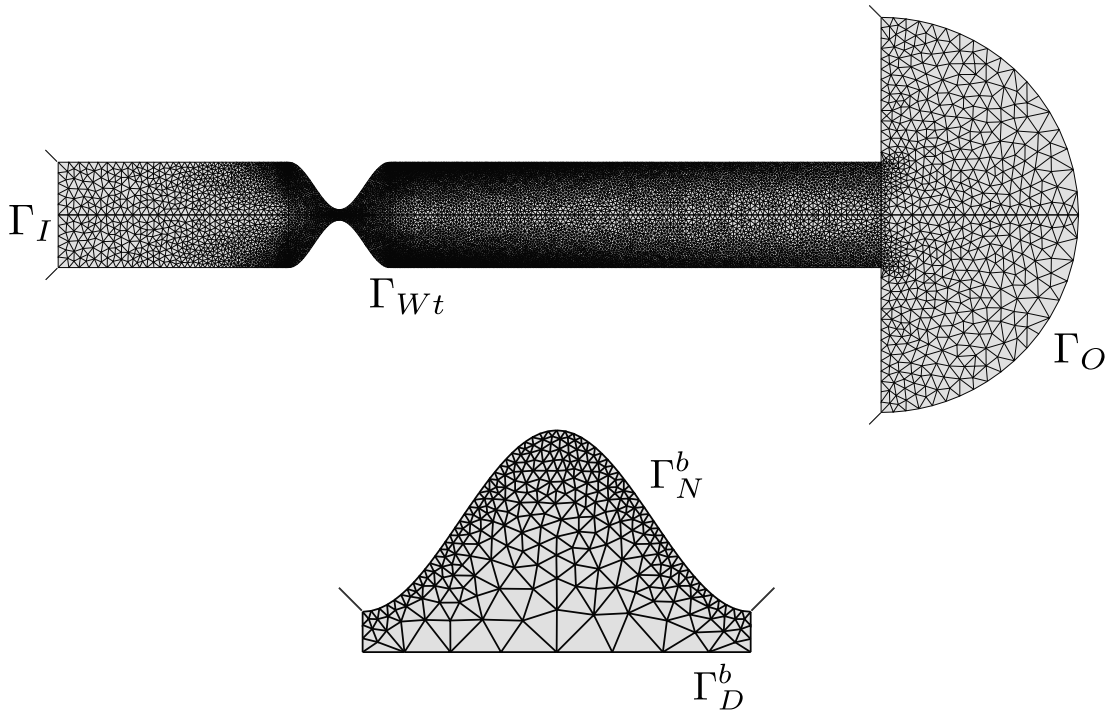

Figure 5.5: Computational domain with the mesh at time $t = 0$.

of the boundary), the outlet boundary conditions on Γ_O (the right part of the boundary, which is a semicircle), and we prescribe the boundary conditions for the impermeable walls that may move in dependence on time on Γ_{Wt} (the rest of the boundary of the domain including the vertical segments of the semicircle). Further, for the definition of the fluid flow problem the following data are used:

the magnitude of the inlet velocity	$v_{in} = 4$ m s^{-1},
the dynamic viscosity	$\mu = 15 \cdot 10^{-6}$ kg m^{-1} s^{-1},
the inlet air density	$\rho_{in} = 1.225$ kg m^{-3},
the outlet pressure	$p_{out} = 97611$ Pa,
the Reynolds number	$Re = \rho_{in} v_{in} H/\mu = 5227$,
where $H = 0.016$ m is the width of the channel,	
the heat conduction coefficient	$\kappa = 2.428 \cdot 10^{-2}$ kg m s^{-2} K^{-1},
the specific heat	$c_v = 721.428$ m^2 s^{-2} K^{-1},
the Poisson adiabatic constant	$\gamma = 1.4$.

The inlet Mach number is $M_{in} = 0.012$. For the fluid solver we use the NIPG variant of the DGM with the choice of the penalization constant $C_W^f = 500$ for inner faces and $C_W^f = 5000$ for boundary edges, respectively (see [12]). The stabilization parameters ν_1 and ν_2 from (4.50) are set to 0.1.

We start with the computation of the flow problem, where the fluid flow domain does not change in time. By that we obtain an initial state vector describing the developed fluid flow in the channel for the solution of the FSI problem. Furthermore we compare the results obtained by the choice of different time steps τ, different meshes and different time discretizations. The computation of the FSI problem is time-consuming and we want to reduce the number of degrees

of freedom and use the largest time step without significant loss of precision of the computation. We employ the STDGM with the polynomial approximation of degree 2 in space and degree 1 in time, or the second order BDF with the DGM with polynomial approximation of degree 2 in space. In order to compare the different numerical solutions of the fluid flow problem we compute the pressure along the x_1-axis at time $4 \cdot 10^{-4}$ s.

At first we compare the numerical simulations obtained with different time discretization schemes applied on the same mesh with 26002 elements. In Figure 5.6 we present the comparison of the pressure along the x_1-axis at time $4 \cdot 10^{-4}$ s for different choices of the time step using the BDF-DGM. Then, in Figure 5.7 is the comparison of the pressure along the x_1-axis at time $4 \cdot 10^{-4}$ s for different choices of the time step using the STDGM. We can see, that we obtain approximately same results for the time step smaller than $4.0 \cdot 10^{-6}$ for the BDF and for the time step smaller than $2.0 \cdot 10^{-5}$ for the STDGM.

Further, in Figure 5.8 we compare the pressure along the x_1-axis at time $4 \cdot 10^{-4}$ s using the BDF-DGM and STDGM for different choices of the time step. We can see, that the numerical solution for the time step $2.0 \cdot 10^{-7}$ using the BDF-DGM and the solution for the time step $4.0 \cdot 10^{-6}$ using the STDGM approximately correspond to each other.

Finally, we compare the results of the computations realized on 4 different triangular computational meshes using the BDF-DGM with the same time step $4 \cdot 10^{-7}$ s. In Figure 5.9 is the comparison of the pressure along the x_1-axis at time $4 \cdot 10^{-4}$ s for computational meshes with 13804, 26002, 55412 and 171774 elements. We obtain approximately same results for all meshes. Only for the case of the coarsest mesh we can see some discrepancy.

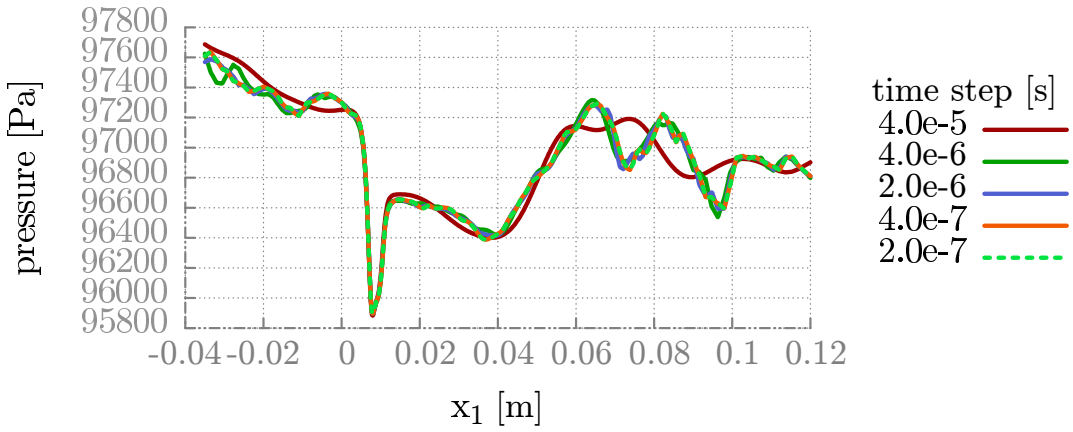

Figure 5.6: Cosine benchmark: Comparison of the pressure along the x_1-axis at time $4 \cdot 10^{-4}$ s for different choices of the time step using the BDF-DGM.

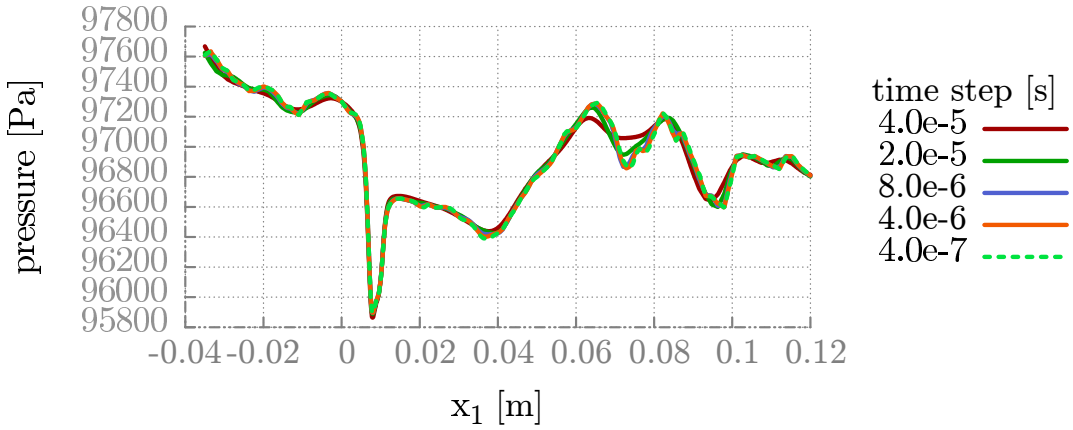

Figure 5.7: Cosine benchmark: Comparison of the pressure along the x_1-axis at time $4 \cdot 10^{-4}$ s for different choices of the time step using the STDGM.

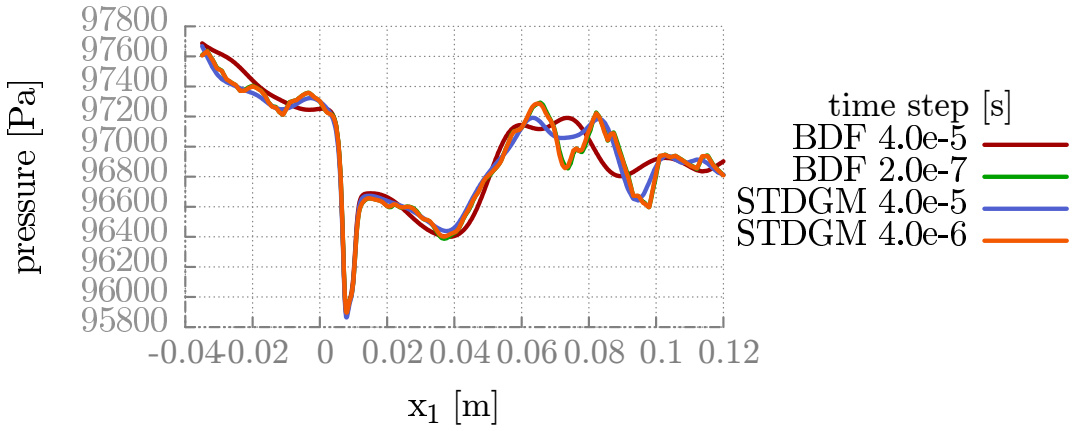

Figure 5.8: Cosine benchmark: Comparison of the pressure along the x_1-axis at time $4 \cdot 10^{-4}$ s for different choices of the time step using the BDF-DGM and STDGM.

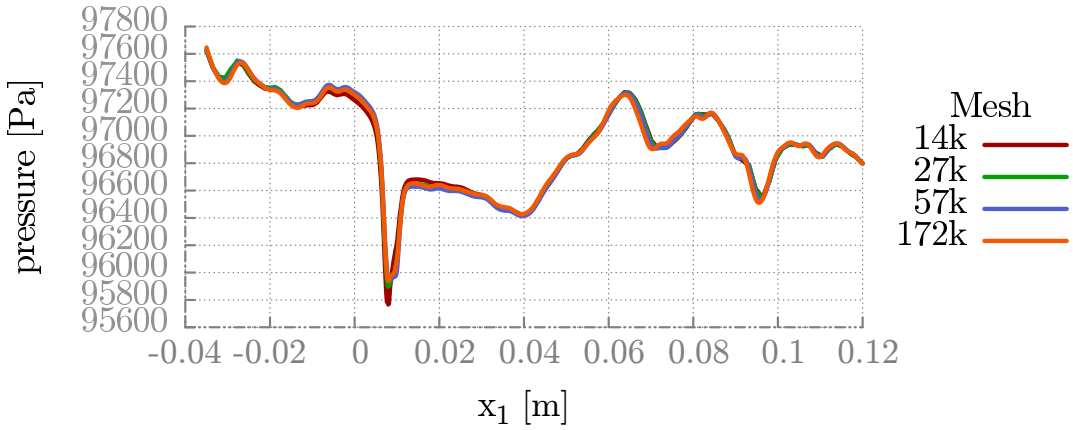

Figure 5.9: Cosine benchmark: Comparison of the pressure along the x_1-axis at time $4 \cdot 10^{-4}$ s for different choices of the computational mesh using the BDF-DGM.

FSI problem

We continue with an example of the complete FSI problem. For the fluid solver we use the same setting as for the previous fluid flow problem with the following adjustment. We employ the STDGM with a polynomial approximation of degree 2 in space and degree 1 in time and we use a computational mesh for the fluid flow problem, which has 26002 elements. The time step τ is set to $2 \cdot 10^{-6}$ s. Before the FSI problem is solved, we compute first 500 time steps with the fixed structure.

The elastic bodies are defined as a simplified model of a vocal tract. The more complicated geometry, motivated by a cut of vocal folds, is defined in the next section. Here, the elastic bodies are considered as homogeneous and isotropic with constant material density $\rho^b = 1040$ kg m^{-3}. Material characteristics are given by the Young modulus and the Poisson ratio with $E^b = 25000$ Pa and $\sigma^b = 0.4$ and the structural damping coefficient $C_M = 0.1$ s^{-1}. We consider the St. Venant-Kirchhoff material. Further, the initial displacement and initial velocity is set to be zero. On the bottom, right and left straight part of the boundary we prescribe homogeneous Dirichlet boundary condition and on the curved part of the boundary we prescribe the Neumann boundary condition. For the solution of the dynamic elasticity problem we employ the NIPG variant of the DGM with the penalization constant set to $C_W^b = 4 \cdot 10^6$. The polynomial degree of the DGM is set to 1. For the time discretization we use the BDF method of the order 2. The computational mesh of the structure problem has 1032 elements.

The ALE mapping is computed with the aid of the artificial static linear elasticity system with Lamé parameters $\lambda_{\mathcal{A}}$, $\mu_{\mathcal{A}}$ defined in (5.27) with $c_{\mathcal{A}} = 100$. For the solution of the static elasticity problem we employ the NIPG variant of the DGM, where the penalization constant is set to $C_W^{\mathcal{A}} = 3 \cdot 10^3$.

We use the strong coupling algorithm described in Section 5.2. The prescribed tolerance for the absolute variation is 10^{-5} and for the relative variation it is 10^{-6}. We consider 5 coupling subiterations as the maximum, but the prescribed tolerance was usually reached after 2 or 3 coupling subiterations.

We present various visualizations of the numerical solution. In Figure 5.10 is the visualization of the distribution of density and the displacement of the elastic body at time instants 0.0834, 0.0842, ..., 0.089 s. Figure 5.11 shows the magnitude of the velocity and Figure 5.12 shows the distribution of the pressure at time instants 0.0834, 0.0842, ..., 0.089 s. Figure 5.13 shows the magnitude of the displacement of the elastic body at time instants 0.0866, 0.0874, 0.0882 and 0.089 s.

Figure 5.14 shows the evolution of the displacement at reference point $[0.0077, -0.0008]$, which is placed close to the narrowest part of the channel, and Figure 5.15 shows the fluid average pressure fluctuation on the inlet and on the outlet. The fluid average pressure on the inlet and on the outlet are computed as

$$p_I(t) = \frac{1}{|\Gamma_I|} \int_{\Gamma_I} p(\boldsymbol{x}, t) \, \mathrm{d}\boldsymbol{x}, \quad p_O(t) = \frac{1}{|\Gamma_O|} \int_{\Gamma_O} p(\boldsymbol{x}, t) \, \mathrm{d}\boldsymbol{x}. \tag{5.31}$$

Further, in Figure 5.16 we present the Fourier analysis of the displacement u_1 and u_2 at reference point $[0.0077, -0.0008]$ and in Figure 5.17 the Fourier analysis of the fluid average pressure fluctuation on the inlet and on the outlet. These diagrams of the Fourier analysis are compared in Figure 5.18. We can see that

the second eigenfrequency of the displacement matches the eigenfrequency of the fluid average pressure fluctuation. This is a good result for the verification of the coupling process. Let us note that in Figure 5.18 we can see that the pressure fluctuation is not affected by the first eigenfrequency. The first eigenfrequency corresponds mainly to the oscillations of the structure in the direction x_1, which does not lead to the closing of the channel and accordingly to it to any significant influence on the fluid flow.

Finally, we wanted to compare the numerical simulation of the defined FSI problem using the St. Venant-Kirchhoff material model with the use of the linear elasticity model. In Figure 5.19 is the comparison of the evolution of the displacement u_1 and u_2 at point $[0.0077, -0.0008]$ using the linear elasticity model and the nonlinear St. Venant-Kirchhoff elasticity model. In Figure 5.20 is the comparison of the fluid average pressure fluctuation on the inlet and on the outlet using the linear elasticity model and the nonlinear St. Venant-Kirchhoff elasticity model. We can see, that the quantities approximately match just in the beginning of the computation. This is expected, because in this case we deal with already large deformations.

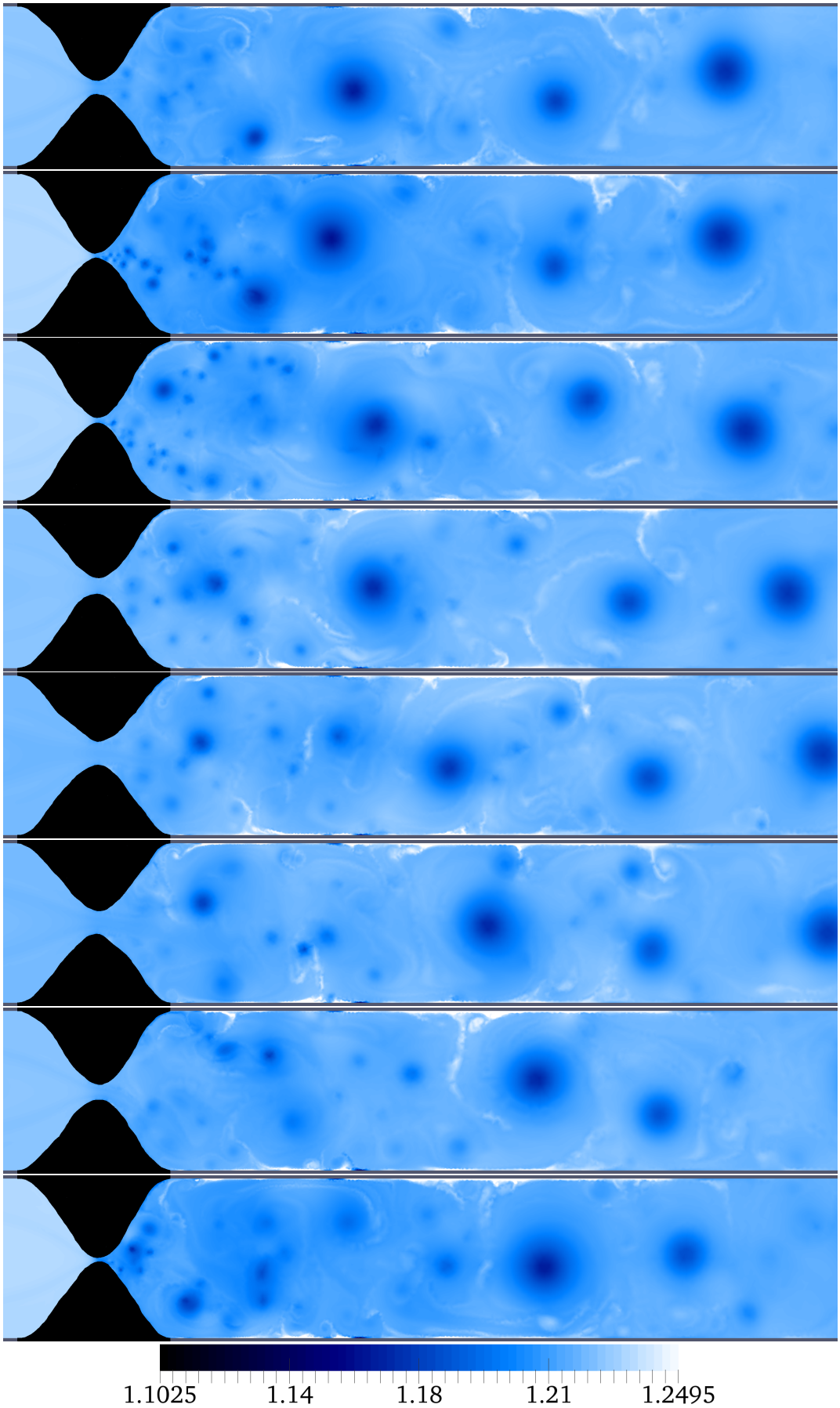

Figure 5.10: Distribution of the density and the displacement of the elastic body at time instants $0.0834, 0.0842, \ldots, 0.089$ s.

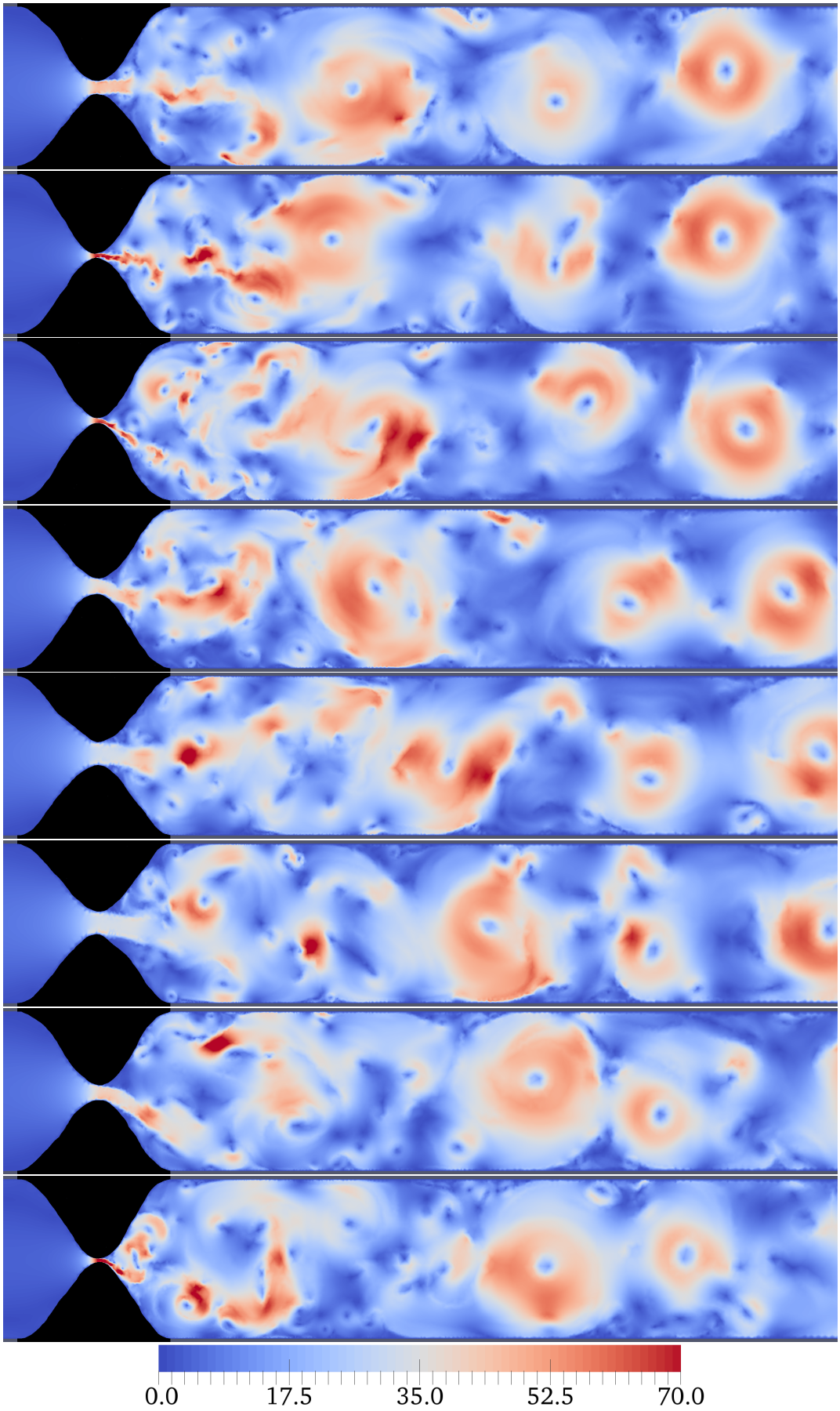

Figure 5.11: The magnitude of the velocity and the displacement of the elastic body at time instants $0.0834, 0.0842, \ldots, 0.089$ s.

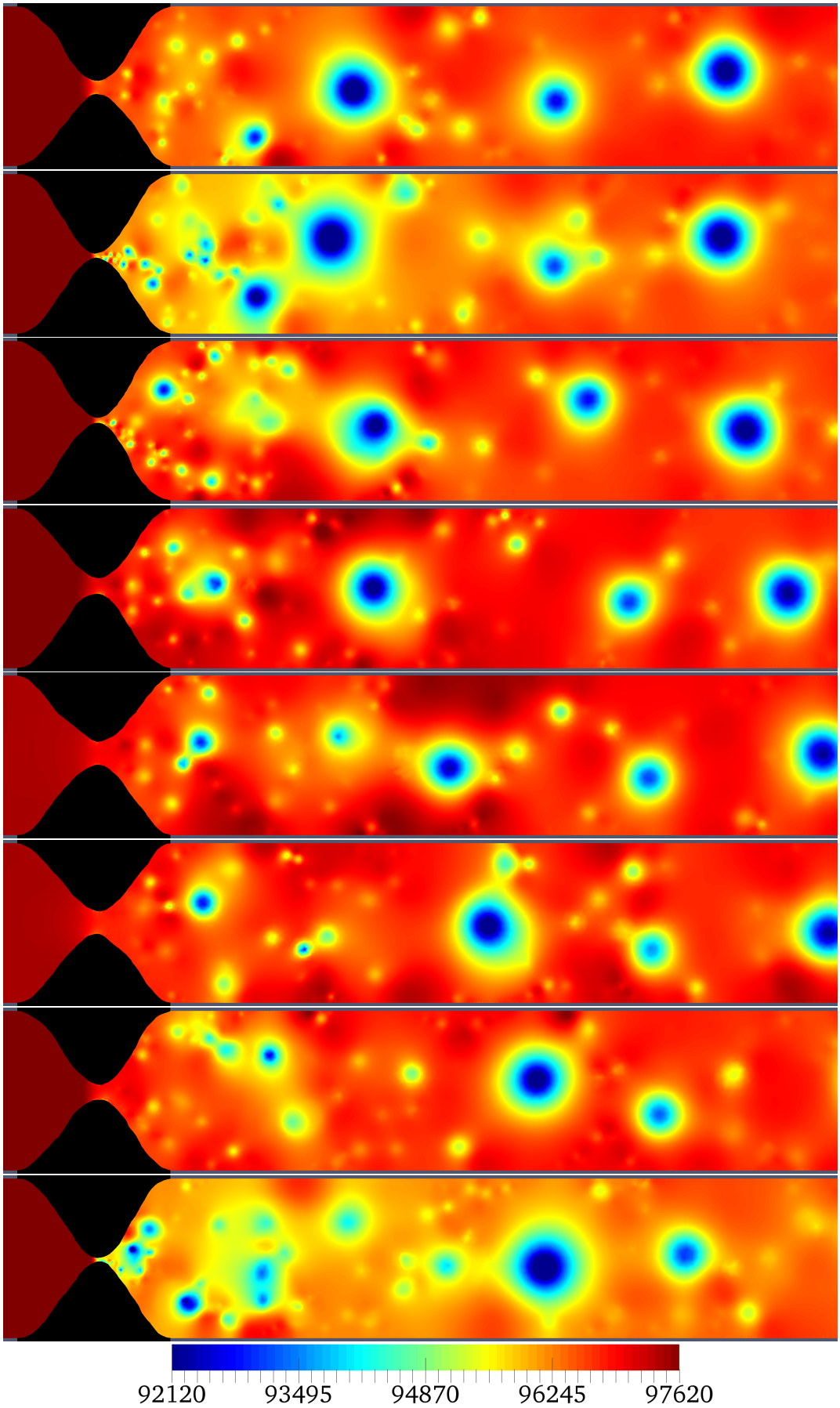

Figure 5.12: Distribution of the pressure and the displacement of the elastic body at time instants $0.0834, 0.0842, \ldots, 0.089$ s.

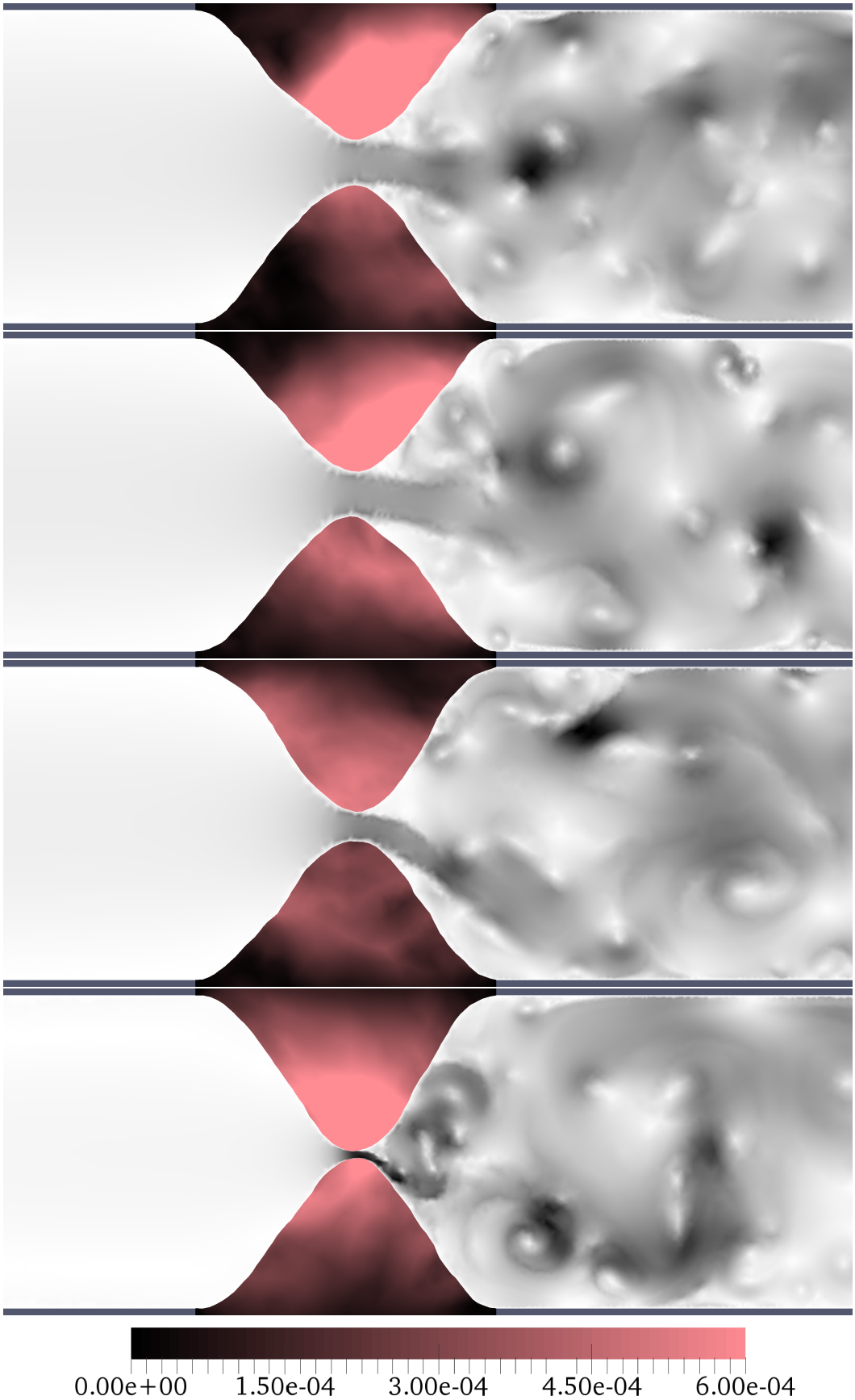

Figure 5.13: Magnitude of the displacement of the elastic body at time instants $0.0866, 0.0874, 0.0882, 0.089$ s.

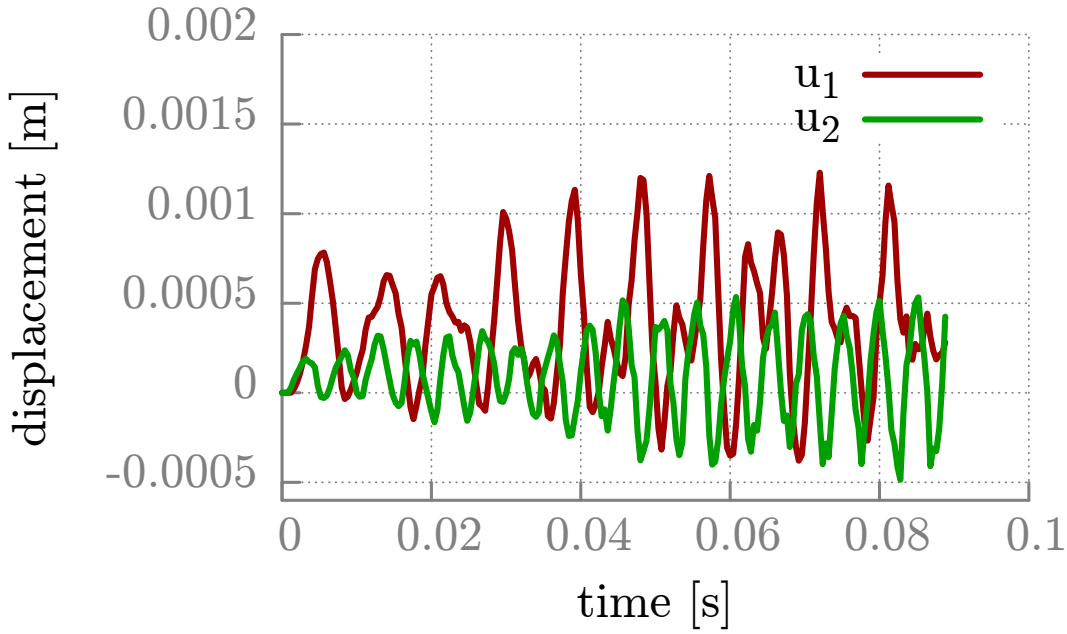

Figure 5.14: Cosine benchmark: The displacement at point [0.0077, -0.0008].

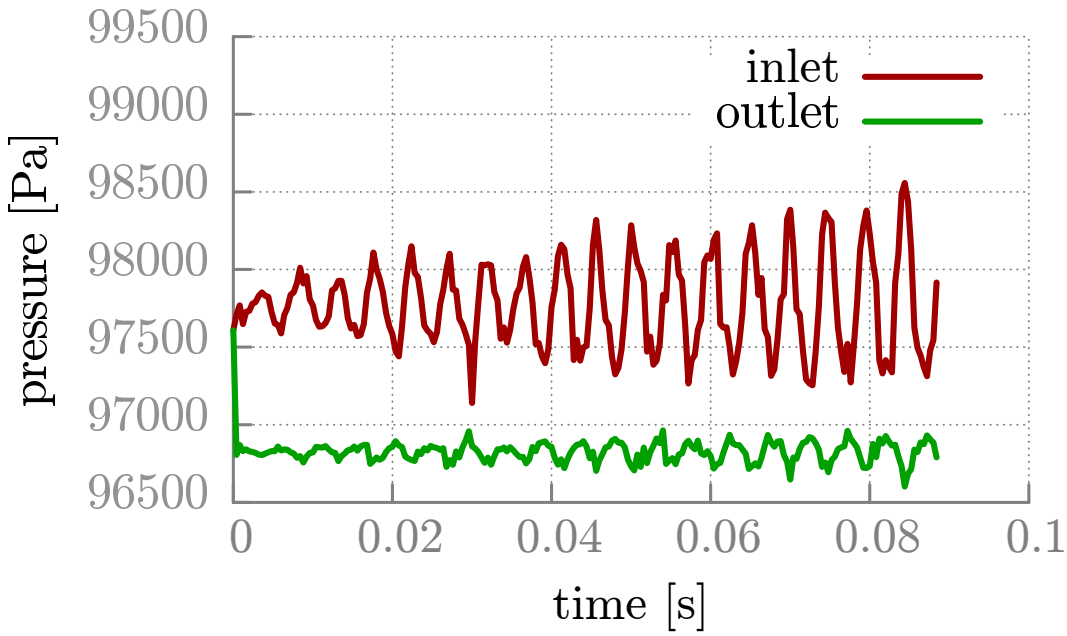

Figure 5.15: Cosine benchmark: The fluid average pressure fluctuation on the inlet and on the outlet.

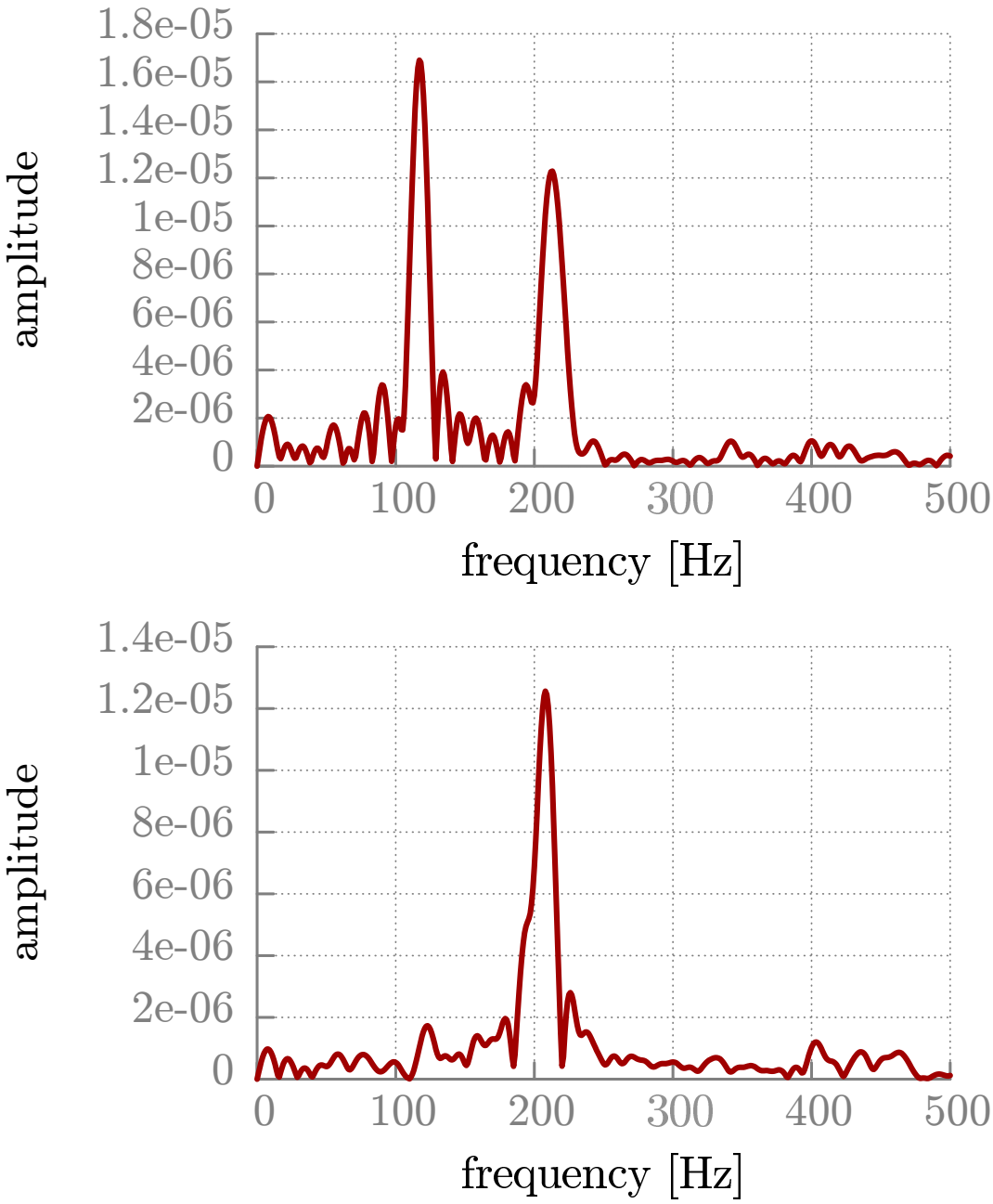

Figure 5.16: Cosine benchmark: Fourier analysis of the displacement u_1 (top) and u_2 (bottom) at point [0.0077, -0.0008].

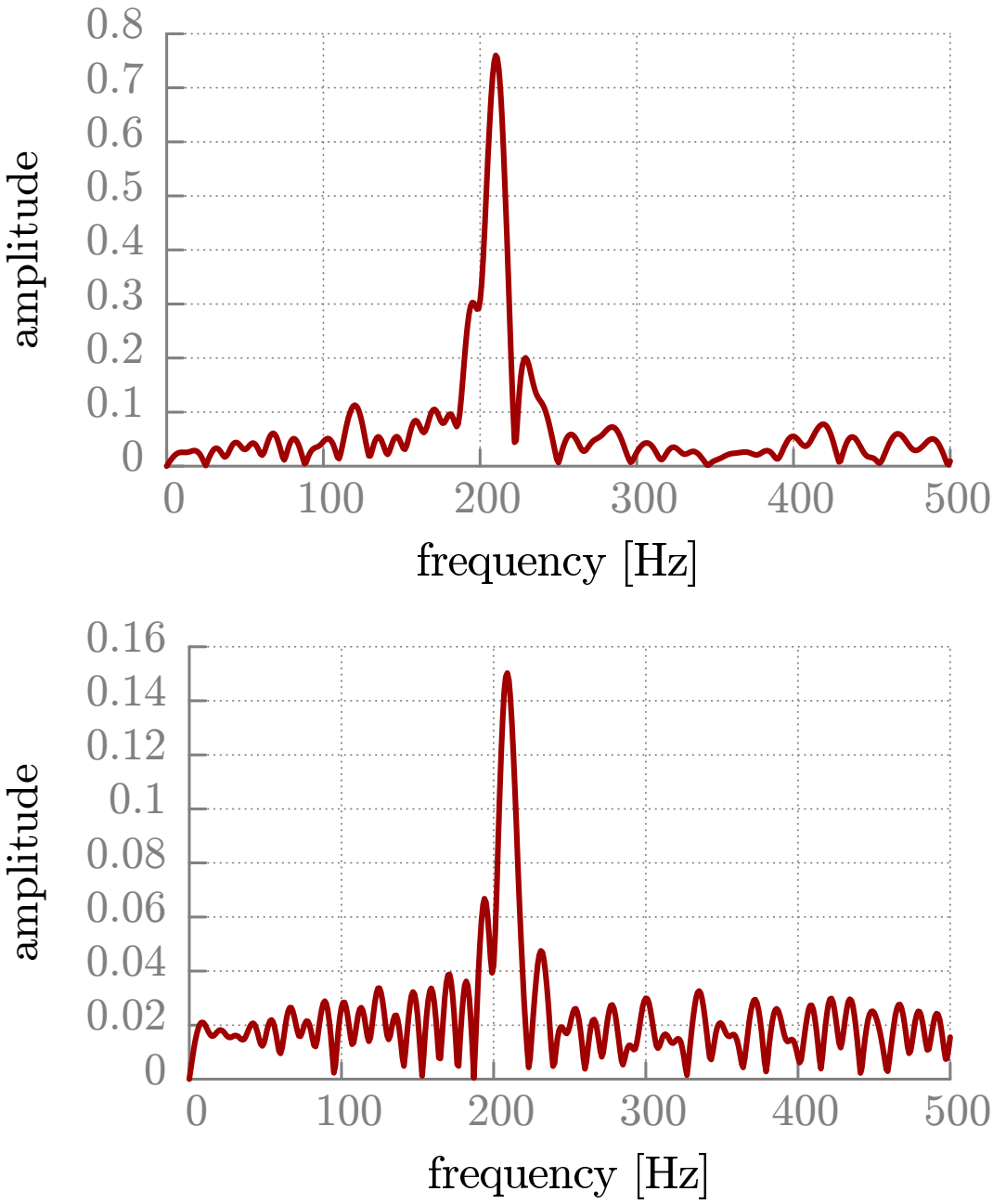

Figure 5.17: Cosine benchmark: Fourier analysis of the fluid average pressure fluctuation on the inlet (top) and on the outlet (bottom).

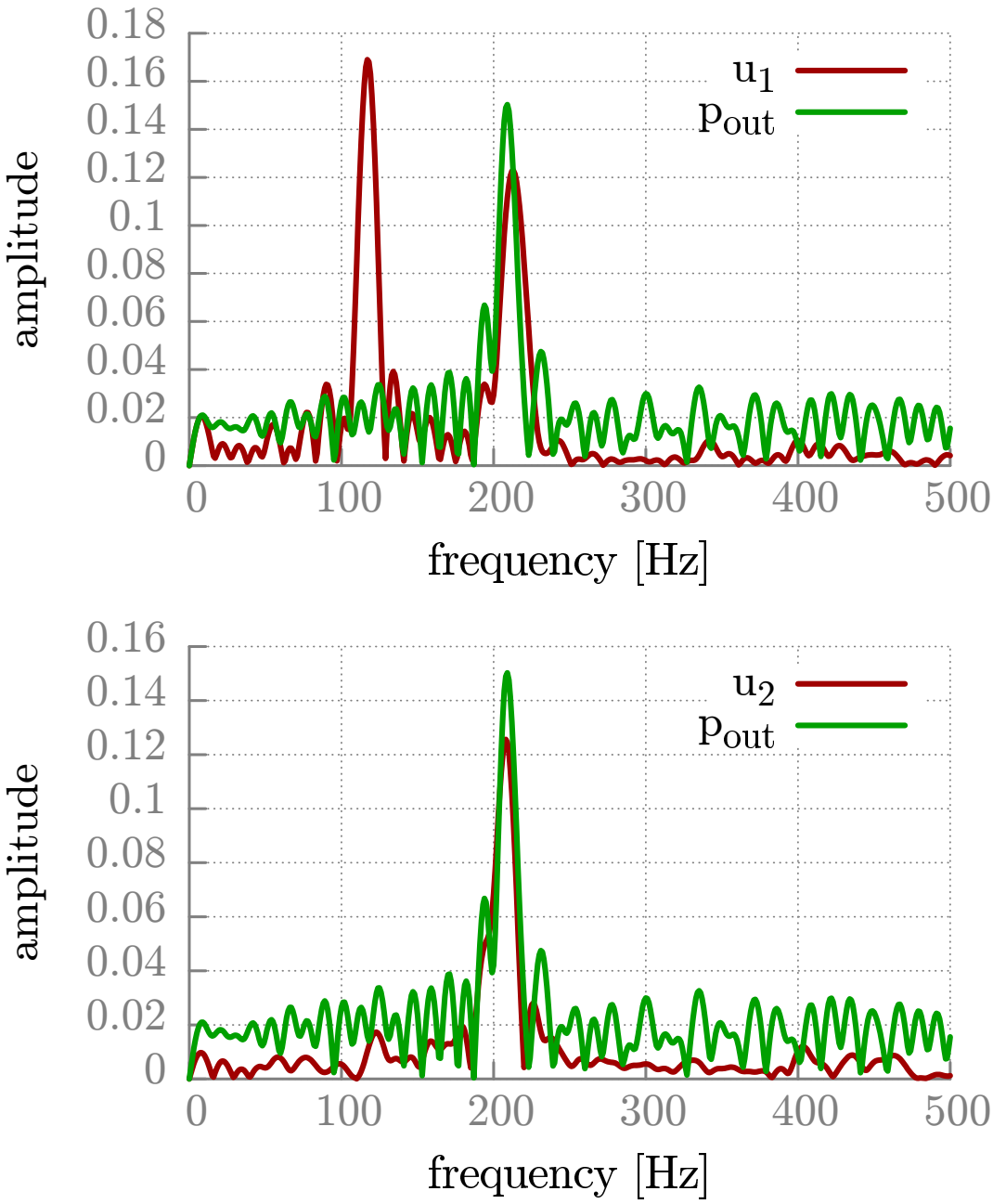

Figure 5.18: Cosine benchmark: Comparison of the Fourier analysis of the displacement u_1 (top) and u_2 (bottom) at point [0.0077, -0.0008] and the fluid average pressure fluctuation on the outlet.

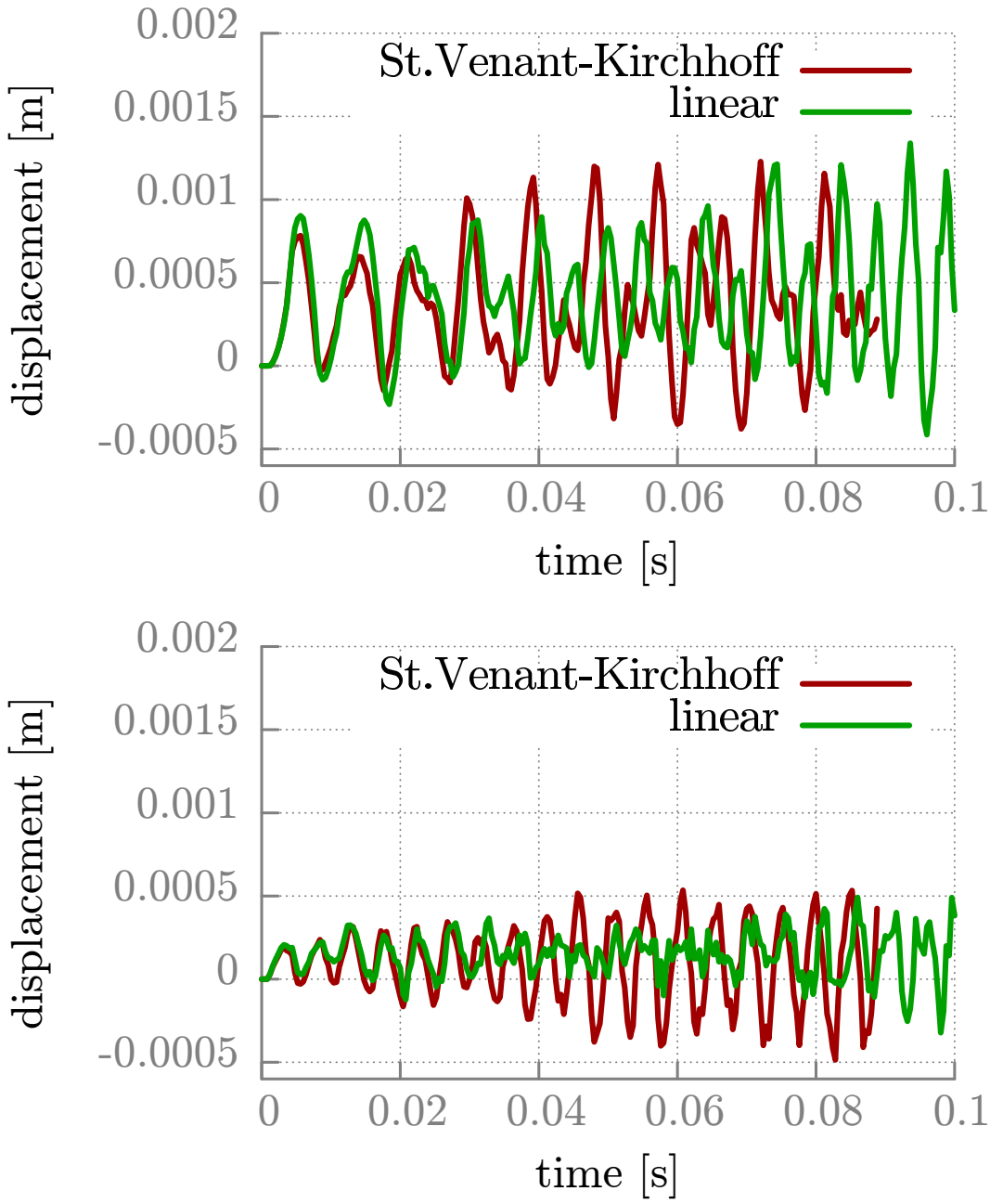

Figure 5.19: Cosine benchmark: Comparison of the displacement u_1 (top) and u_2 (bottom) at point [0.0077, -0.0008] using the linear elasticity model and the nonlinear St. Venant-Kirchhoff elasticity model.

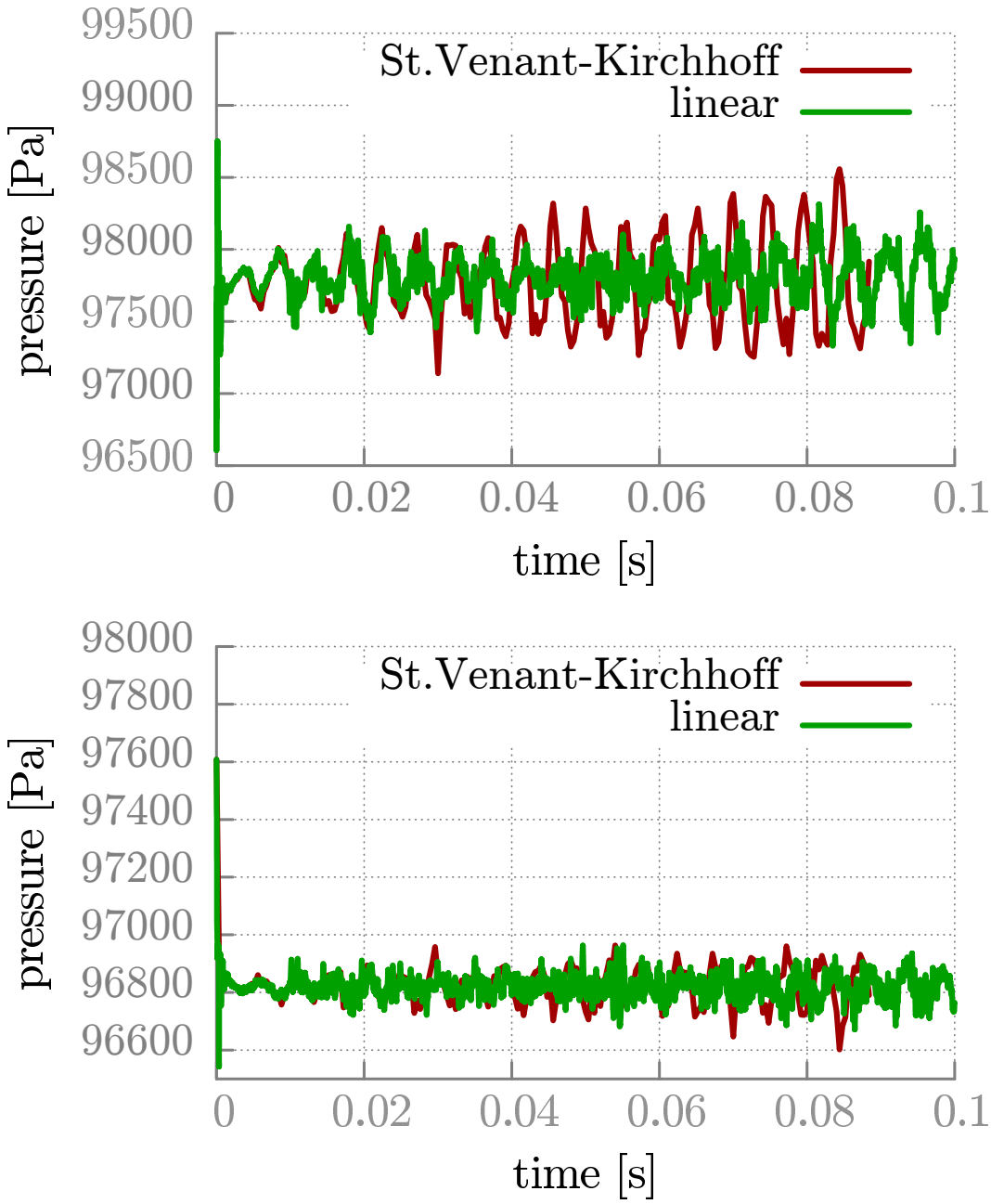

Figure 5.20: Cosine benchmark: Comparison of the fluid average pressure fluctuation on the inlet (top) and on the outlet (bottom) using the linear elasticity model and the nonlinear St. Venant-Kirchhoff elasticity model.

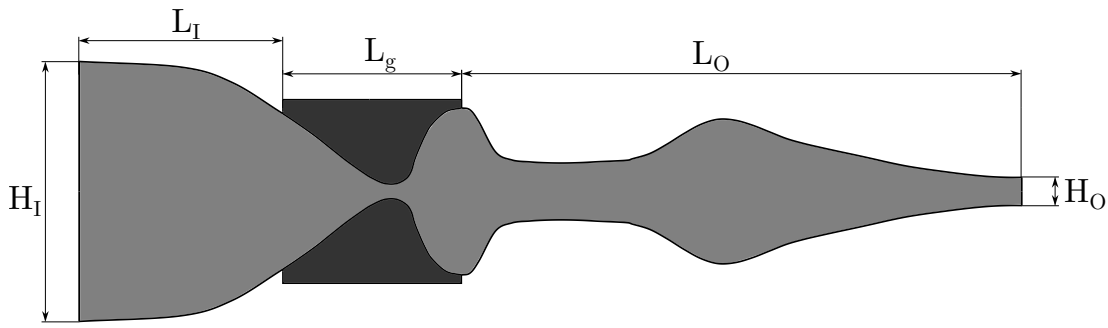

Figure 5.21: Geometry of the computational domain at time $t = 0$ and the description of its size: $L_I = 20.0$ mm, $L_g = 17.5$ mm, $L_O = 55.0$ mm, $H_I = 25.5$ mm, $H_O = 2.76$ mm.

5.4.2 Model of vocal tract

Here, we present the obtained numerical results for the more realistic model of vocal folds. The geometry of the domain occupied by the fluid is set according to the experiments described in [43, 60]. The description of its size is given in Figure 5.21. As in the previous case, we add to the geometry a semicircle subdomain with a radius 3.0 cm as an outlet.

The boundary conditions were set similarly as for the previous model. We prescribe the inlet boundary conditions on Γ_I (left part of the boundary), the outlet boundary conditions on Γ_O (the right part of the boundary, which is a semicircle), and we prescribe the boundary conditions for the impermeable walls that may move in dependence on time on Γ_{Wt} (the rest of the boundary of the domain including the vertical segments of the semicircle). The fluid flow problem is computed on the triangulation with 17652 elements. Further for the definition of the fluid flow problem the following data are used:

the magnitude of the inlet velocity	$v_{in} = 4$ m s^{-1},
the dynamic viscosity	$\mu = 1.80 \cdot 10^{-5}$ kg m^{-1} s^{-1},
the inlet density	$\rho_{in} = 1.225$ kg m^{-3},
the outlet pressure	$p_{out} = 97611$ Pa,
the Reynolds number	$Re = \rho_{in} v_{in} H_I / \mu = 6941.7$,
the heat conduction coefficient	$\kappa = 2.428 \cdot 10^{-2}$ kg m s^{-2} K^{-1},
the specific heat	$c_v = 721.428$ m^2 s^{-2} K^{-1},
the Poisson adiabatic constant	$\gamma = 1.4$.

For the fluid solver we use the STDGM with the polynomial approximation of degree 2 in space and degree 1 in time. We employ the IIPG variant of the DGM with the choice of the penalization constant $C_W^f = 500$ for inner faces and $C_W^f = 5000$ for boundary edges. The stabilization parameters ν_1 and ν_2 from (4.50) are set to 0.1. The time step τ is set to $1.0 \cdot 10^{-6}$ s. For the first 1000 time steps the fluid flow is computed with the fixed boundary and then we solve the FSI problem.

We assume that the elastic bodies motivated by a cut of vocal folds are defined as in Section 3.5.2, i.e. as bodies divided into a few regions with different material properties. They are considered as isotropic bodies with constant material

density $\rho^b = 1040$ kg m^{-3}. The division of the domain into 4 regions with different material characteristics is illustrated in Figure 3.35 by the Lamé parameters and the setting of the material characteristics is described in Table 3.14. The triangulation used for the solution of the structure problem has 5118 elements. We consider the neo-Hookean material. Further, the initial displacement and the initial velocity is set to be zero. On the bottom, right and left straight parts of the boundary we prescribe homogeneous Dirichlet boundary condition and on the curved part of the boundary we prescribe the Neumann boundary condition. The damping coefficient $C_M = 1.0$ s^{-1}. For the solution of the dynamic elasticity problem we employ the NIPG variant of the DGM, where the penalization constant is set to $C_W^b = 4 \cdot 10^6$, and the BDF method of order 2. The DGM is set to use piecewise linear approximation in space.

The ALE mapping is determined with the aid of the static linear elasticity problem as described in Section 5.3.2. We use the pseudo-elasticity model with $c_{\mathcal{A}} = 100$ and $\lambda_{\mathcal{A}}$, $\mu_{\mathcal{A}}$ as in (5.27). For the solution of the static elasticity problem we employ the NIPG variant of the DGM, where the penalization constant is set to $C_W^{\mathcal{A}} = 10^3$.

We use the strong coupling algorithm described in Section 5.2 with the prescribed tolerance 10^{-5} for the absolute variation and 10^{-6} for the relative variation. Further, we use 5 coupling subiterations as the maximum. However the prescribed tolerance was usually reached after 2 or 3 coupling subiterations. An example of the variations obtained during one iteration of the coupling process is in Table 5.1.

subiteration	absolute variation	relative variation	coupling condition
1	$1.76 \cdot 10^{-1}$	$5.01 \cdot 10^{-3}$	false
2	$1.18 \cdot 10^{-3}$	$3.38 \cdot 10^{-5}$	false
3	$1.61 \cdot 10^{-6}$	$4.50 \cdot 10^{-8}$	true

Table 5.1: Variation of the displacement obtained during one iteration of the coupling process at time 0.05 s.

Finally, we present the visualizations of the computed quantities and the deformation of the elastic bodies accordingly to the domain occupied by the fluid. Figure 5.22 shows the distribution of density and the displacement of the elastic body at time instants 0.013, $0.014, \ldots, 0.02$ s. Figure 5.23 shows the magnitude of the velocity and Figure 5.24 shows the distribution of the pressure. Finally, Figure 5.25 shows the displacement of the elastic body at time instants $0.017, 0.018, 0.019$ and 0.02 s with distinguished regions of different material characteristics. Further, in Figure 5.26 we show the evolution of the displacement at point $[0.0077, -0.0008]$ and in Figure 5.27 the fluid average pressure fluctuation at the inlet and at the outlet, which are computed as in (5.31). The obtained results show the applicability of the proposed method to the interaction of compressible viscous flow and a nonlinear elastic structure in 2D using the discontinuous Galerkin method (DGM).

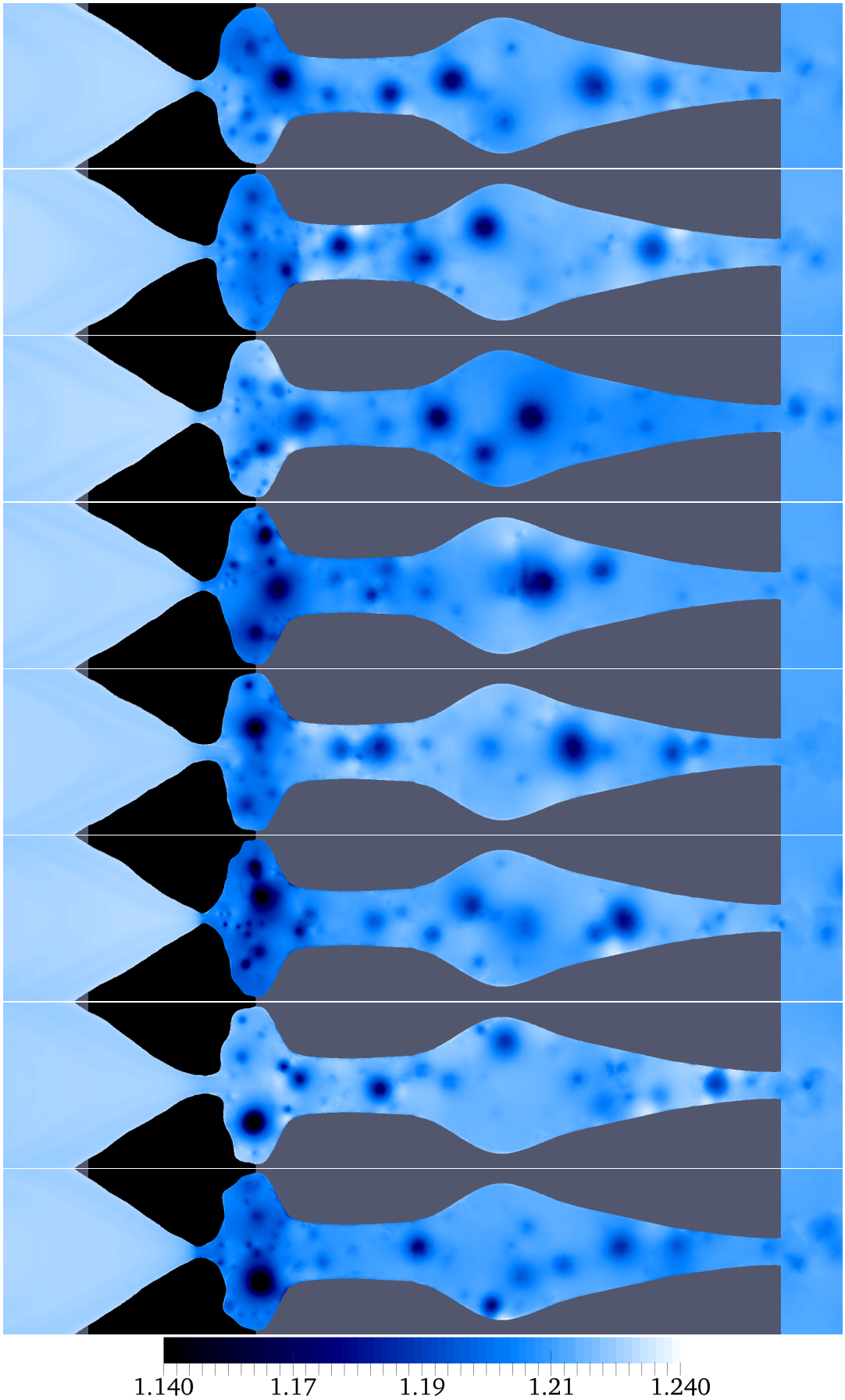

Figure 5.22: Distribution of the density and the displacement of the elastic body at time instants $0.013, 0.014, \ldots, 0.02$ s.

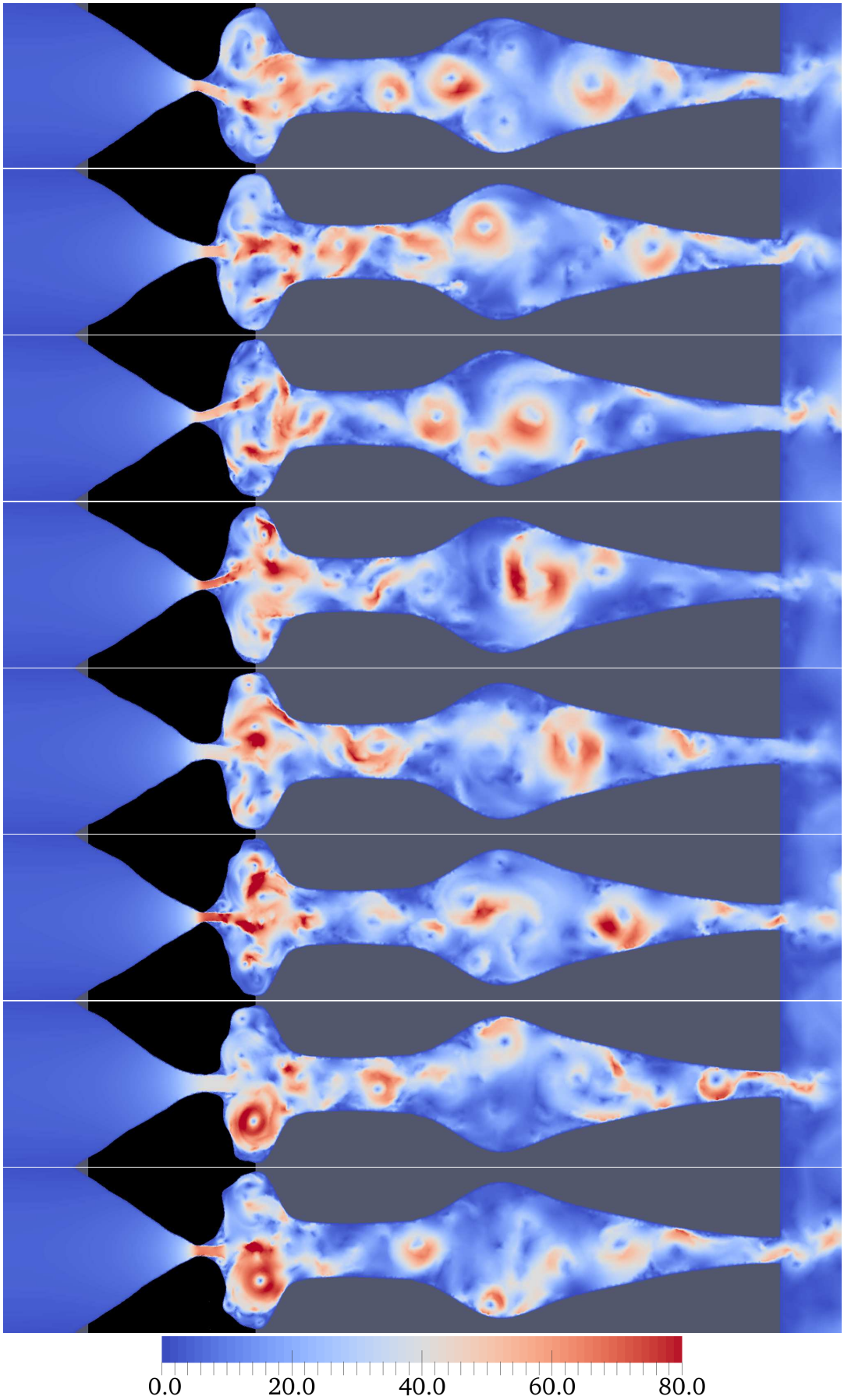

Figure 5.23: The magnitude of the velocity and the displacement of the elastic body at time instants $0.013, 0.014, \ldots, 0.02$ s.

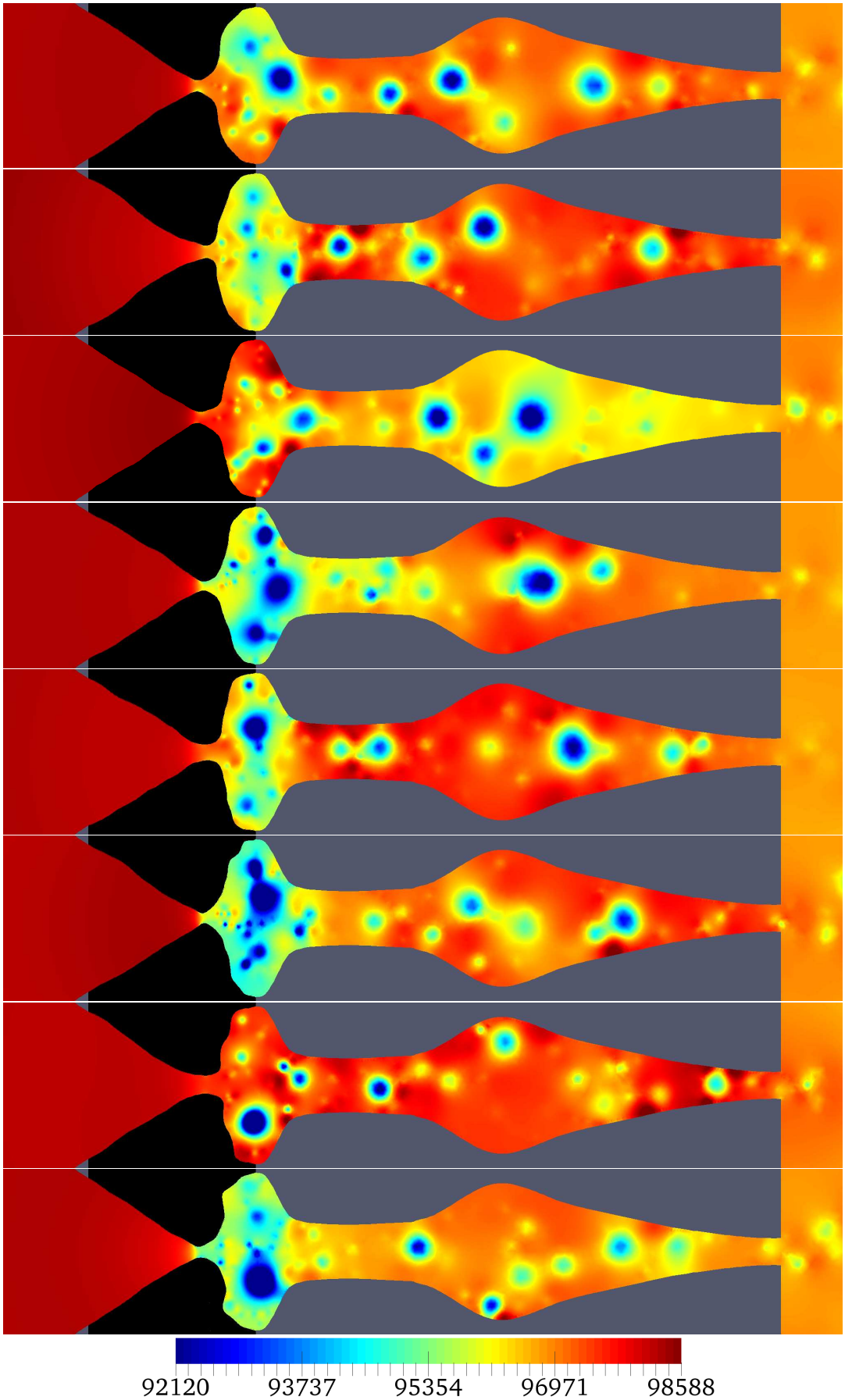

Figure 5.24: Distribution of the pressure and the displacement of the elastic body at time instants $0.013, 0.014, \ldots, 0.02$ s.

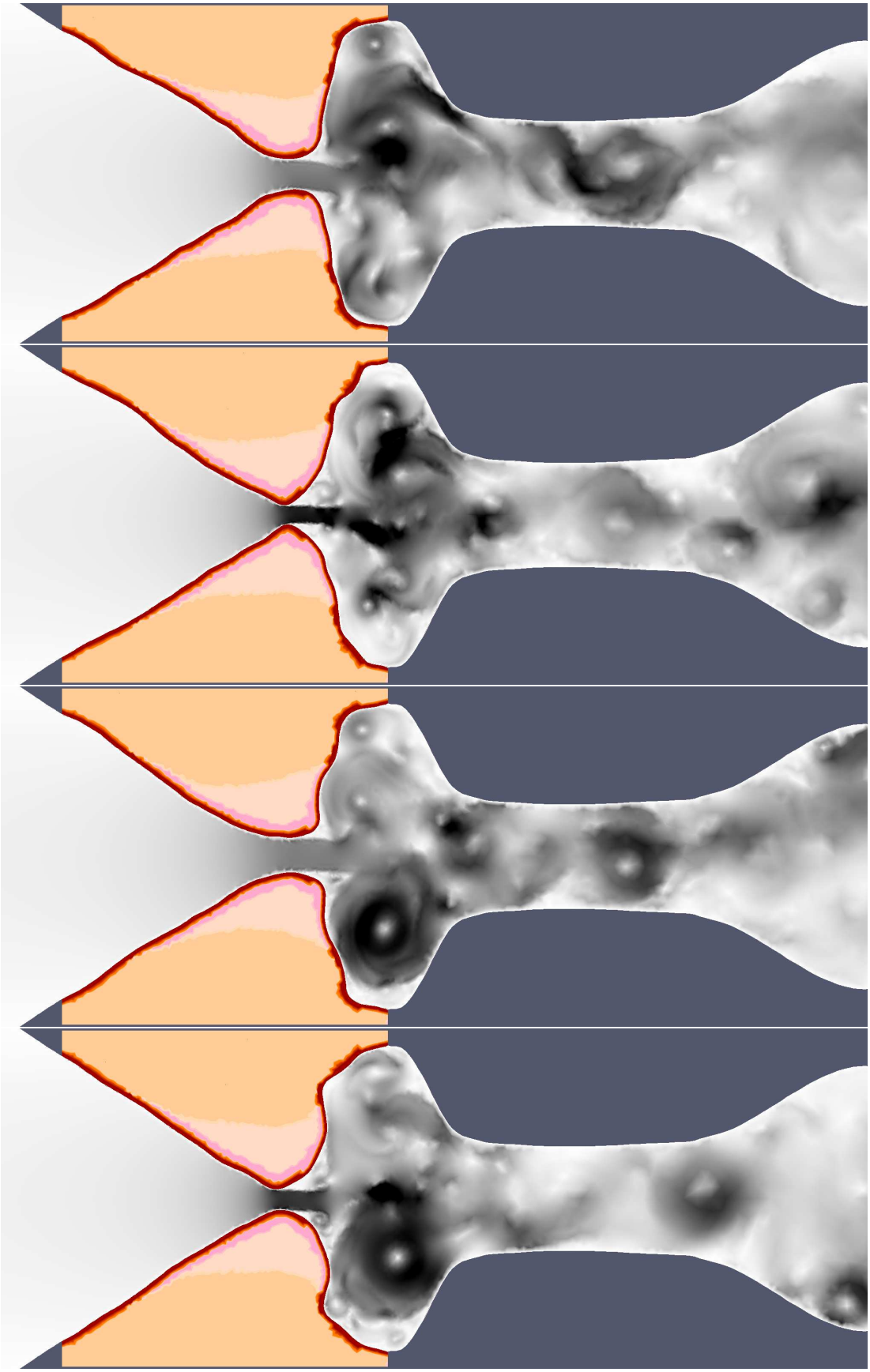

Figure 5.25: The displacement of the elastic body at time instants $0.017, 0.018, 0.019$ and 0.02 s. The colors distinguish the regions with different material characteristics.

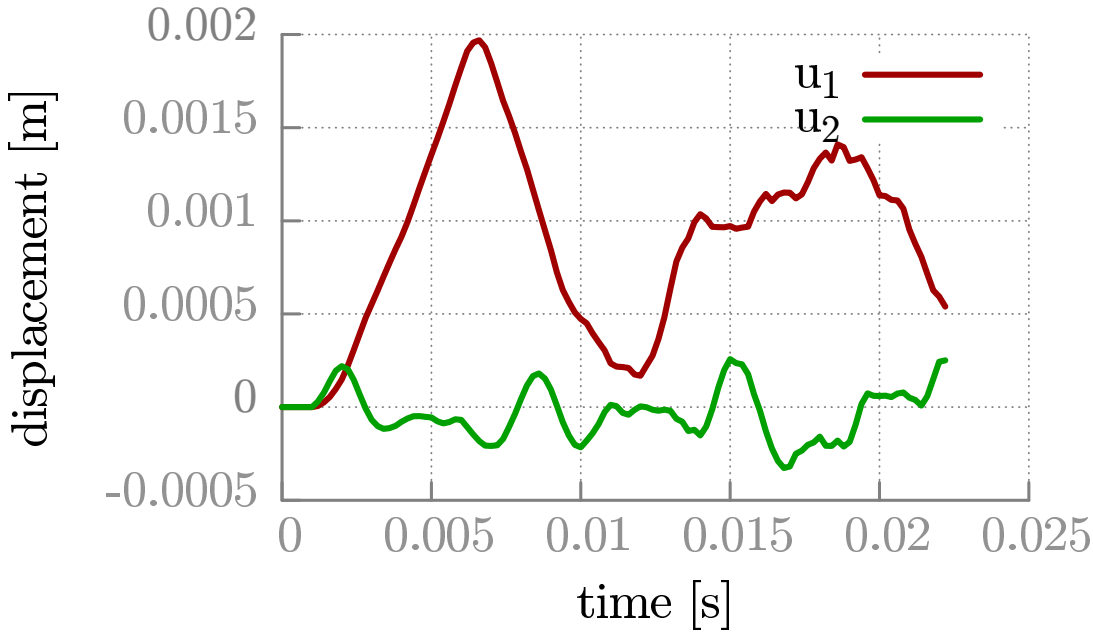

Figure 5.26: Vocal folds model: The displacement at point [0.0077, -0.0008].

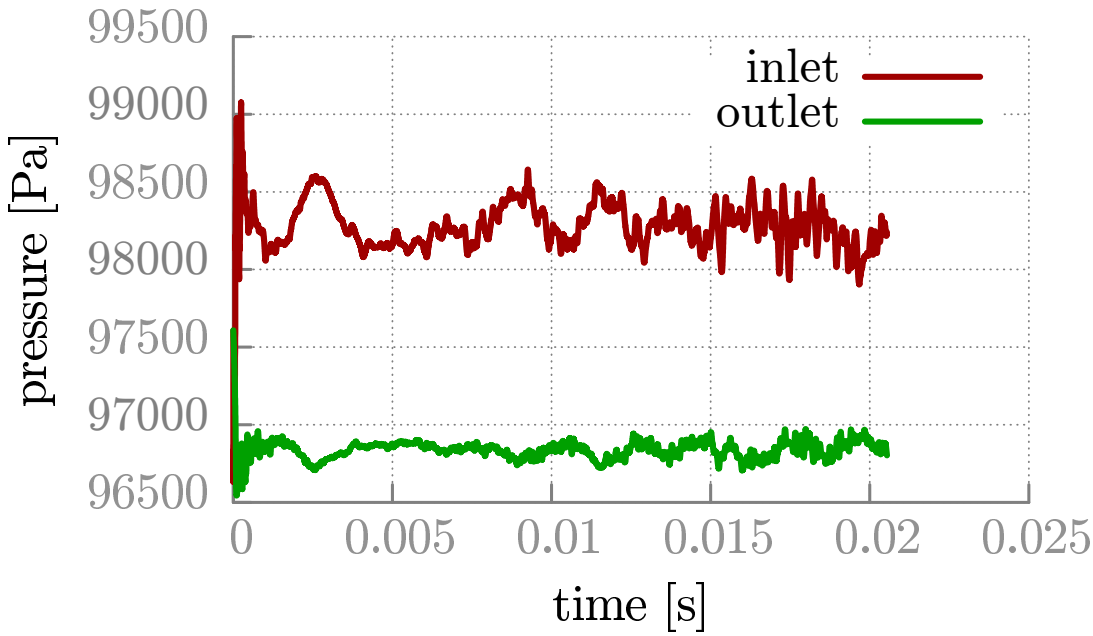

Figure 5.27: Vocal folds model: The fluid average pressure fluctuation on the inlet and on the outlet.

6. Implementation notes

In this chapter some technical details of the implementation and few remaining numerical topics as mesh generation and numerical integration are included.

6.1 Mesh generation

For the computations using the discontinuous Galerkin finite element method the construction of a triangulation in the computational domain is needed. In the current implementation we assume that a triangulation of a computational domain is given and provided as a separate file. There are two basic formats supported by the mesh generating software GMSH [34] and the anisotropic mesh generator ANGENER [17]. The latter one is used in the C library for the fluid flow problem in order to use the anisotropic mesh adaptation algorithm included in ANGENER. A drawback of ANGENER is the lack of graphical user interface, which would be useful in the creation of meshes for more complicated computational domains. This is not the case of GMSH, which is an open source software commonly used for the generation of meshes. It allows us also to create meshes with a common boundary for the FSI problems. As mentioned, in the current implementation both formats are supported, but the C-library for the fluid flow is accepting only the ANGENER format. Therefore, the computational mesh was created by the use of GMSH and for the solution of the fluid flow problem it was converted to the ANGENER format. In the case of the FSI problem the mesh for the fluid flow and the mesh for the elasticity problem have to share a common boundary and the edges on the common boundary have to belong to both the fluid triangulation and the structure triangulation. In order to obtain such triangulations, we prepare the geometry of both domains in GMSH and define there different regions. In this way we get two triangulations satisfying the assumed conditions.

Currently the mesh is expected to include just triangles and hanging nodes are not supported. On the given triangulation we obtain an approximate solution of the problem, where the number of the elements of the triangulation and their size play the role in the accuracy of the solution. On the other hand, the growth of the number of elements causes computations more complicated and more time-consuming. In the case of fluid-structure interaction problem we assume a common boundary of both triangulations for fluid and structure. Therefore the edges on the common part of the boundary belong always to one adjacent element of the triangulation $\mathcal{T}_h^b$ of the domain Ω_h^b of the structure and to one adjacent element of the triangulation $\mathcal{T}_{h0}^f$ of the domain Ω_{h0}^f occupied by the fluid.

6.2 Numerical integration

In this section we are concerned with the computation of the integrals determining the elements of the matrices of systems (2.40), (2.50), (2.119), or (4.59), and (4.63). Usually we are not able to compute these integrals exactly but with the

aid of the numerical quadratures. The choice of a sufficiently accurate quadrature is crucial in finite element methods. The list of implemented line quadrature rules on a reference interval $[-1, 1]$ is shown in Tables 6.1 and 6.2. The list of implemented triangle quadrature rules on a reference triangle $\hat{K}$ with vertices $[0, 0]$, $[1, 0]$ and $[0, 1]$ is shown in Tables 6.3, 6.4 and 6.5. In the second column we indicate the maximum polynomial degree for which the quadrature is exact. Theoretically our implementation allows arbitrary choice of the polynomial degree of the discretization by the DGM. However, this choice is limited by the available implemented quadrature rules. For the higher degree polynomial approximation the computation of the respective integrals would not be exact.

Quadrature type	Polynomial degree	Weights	Nodes
Trapezoid	1	1	-1
		1	1
Simpson	2	1/3	-1
		4/3	0
		1/3	1

Table 6.1: Simple quadrature rules on the reference interval $[-1, 1]$.

Q. type	P. degree	Weights	Nodes
Gauss	1	2	0
Gauss	3	1	-0.577350269189
		1	0.577350269189
Gauss	5	5/9	$-\sqrt{3/5}$
		8/9	0
		5/9	$\sqrt{3/5}$
Gauss	7	0.347854845137	-0.861136311594
		0.652145154862	-0.339981043584
		0.652145154862	0.339981043584
		0.347854845137	0.861136311594
Gauss	9	0.23692688505618908751426	-0.90617984593866399279762
		0.47862867049936646804 13	-0.53846931010568309109632
		0.56888888888888888888888	0
		0.47862867049936646804 13	0.53846931010568309109632
		0.23692688505618908751426	0.90617984593866399279762

Table 6.2: Gauss quadrature rules on the reference interval $[-1, 1]$ obtained from [59].

Q. type	P. degree	Weights	x-nodes	y-nodes
Trapezoid	1	1/6	0	0
		1/6	1	0
		1/6	0	1
Midpoint	2	1/6	0	0.5
		1/6	0.5	0
		1/6	0.5	0.5

Table 6.3: Simple quadrature rules on the reference triangle $\hat{K}$.

Q. type	P. degree	Weights	x-nodes	y-nodes
Gauss	5	0.112500000000000	0.333333333333333	0.333333333333333
		0.066197076394253	0.470142064105115	0.470142064105115
		0.066197076394253	0.470142064105115	0.059715871789769
		0.066197076394253	0.059715871789769	0.470142064105115
		0.0629695902724135	0.101286507323456	0.101286507323456
		0.0629695902724135	0.101286507323456	0.797426985353087
		0.0629695902724135	0.797426985353087	0.101286507323456
Gauss	7	-0.074785022233835	0.333333333333333	0.333333333333333
		0.087807628716602	0.260345966079038	0.260345966079038
		0.087807628716602	0.479308067841923	0.260345966079038
		0.087807628716602	0.260345966079038	0.479308067841923
		0.0266736178044195	0.065130102902216	0.869739794195568
		0.0266736178044195	0.869739794195568	0.065130102902216
		0.0266736178044195	0.065130102902216	0.065130102902216
		0.0385568804451285	0.638444188569809	0.312865496004875
		0.0385568804451285	0.312865496004875	0.638444188569809
		0.0385568804451285	0.638444188569809	0.048690315425316
		0.0385568804451285	0.048690315425316	0.638444188569809
		0.0385568804451285	0.312865496004875	0.048690315425316
		0.0385568804451285	0.048690315425316	0.312865496004875

Table 6.4: Gauss quadrature rules on the reference triangle $\hat{K}$ obtained from [11]]

Q. type	P. degree	Weights	x-nodes	y-nodes
Gauss	1	0.5	1/3	1/3
Gauss	2	1/6	2/3	1/6
		1/6	1/6	1/6
		1/6	1/6	2/3
Gauss	3	-0.281250000000	1/3	1/3
		0.260416666666	1/5	1/5
		0.260416666666	3/5	1/5
		0.260416666666	1/5	3/5
Gauss	4	0.1116907948390	0.108103018168	0.445948490915
		0.1116907948390	0.445948490915	0.445948490915
		0.1116907948390	0.445948490915	0.108103018168
		0.0549758718276	0.816847572980	0.091576213509
		0.0549758718276	0.091576213509	0.091576213509
		0.0549758718276	0.091576213509	0.816847572980
Gauss	5	0.112500000000	0.333333333333	0.333333333333
		0.062969590272	0.101286507323	0.101286507323
		0.062969590272	0.797426985353	0.101286507323
		0.062969590272	0.101286507323	0.797426985353
		0.066197076394	0.470142064105	0.470142064105
		0.066197076394	0.059715871789	0.470142064105
		0.066197076394	0.470142064105	0.059715871789
Gauss	6	0.058393137863	0.501426509658	0.249286745170
		0.058393137863	0.249286745170	0.249286745170
		0.058393137863	0.249286745170	0.501426509658
		0.025422453185	0.873821971016	0.063089014491
		0.025422453185	0.063089014491	0.063089014491
		0.025422453185	0.063089014491	0.873821971016
		0.041425537809	0.053145049844	0.310352451033
		0.041425537809	0.310352451033	0.053145049844
		0.041425537809	0.053145049844	0.636502499123
		0.041425537809	0.636502499123	0.053145049844
		0.041425537809	0.636502499123	0.310352451033
		0.041425537809	0.310352451033	0.636502499123
Gauss	7	-0.074785022233	0.333333333333	0.333333333333
		0.087807628716	0.479308067841	0.260345966079
		0.087807628716	0.260345966079	0.260345966079
		0.087807628716	0.260345966079	0.479308067841
		0.026673617804	0.869739794195	0.065130102902
		0.026673617804	0.065130102902	0.065130102902
		0.026673617804	0.065130102902	0.869739794195
		0.038556880445	0.048690315425	0.312865496004
		0.038556880445	0.312865496004	0.048690315425
		0.038556880445	0.048690315425	0.638444188569
		0.038556880445	0.638444188569	0.048690315425
		0.038556880445	0.638444188569	0.312865496004
		0.038556880445	0.312865496004	0.638444188569

Table 6.5: Gauss quadrature rules on the reference triangle $\hat{K}$ obtained from [59]

6.3 Description of the implementation

According to the proposed algorithmization we developed a `.NET` framework application that solves partial differential equations using the discontinuous Galerkin method (DGM). In Chapters 2 and 3 we presented the algorithmization standing behind the library dealing with elasticity problems. This library can be used for the numerical solution of the 2D dynamic linear and nonlinear elasticity problem with mixed boundary conditions. Further, for the numerical simulation of the fluid flow problem we modified the C library developed by Česenek, see [11], which was embedded in the `.NET` library for the numerical solution of the elasticity problem and used for the numerical solution of the FSI problem. The whole `.NET` framework application includes also the solvers of other partial differential equations, namely the Laplace equation, parabolic equations, and linear or nonlinear convection-diffusion equations.

The programme is written in `C#`, i.e. we need `.NET` framework for launching the application or its open-source equivalent `Mono`. The programme runs on `Windows`, `Linux` and `Mac OS X`. However, if we want to use it on `Linux`, we may need to compile the `UMFPACK` solver separately. This can be done easily, because most of the distributions have it as a precompiled library and the only thing we have to do is to link the shared object `libumfpack.so` to the `libs` directory in our `.NET` application installation.

Before starting the programme it is necessary to create a configuration file. Then, we can easily run the application from the command line by

```
DGMNET.exe config_file.xml
```

where as an argument we give the path to the created configuration file. In Attachment A.2 is an example of the XML configuration used for the numerical solution of the FSI problem.

Conclusion

In this thesis, the new implementation of the DGM to FSI problem is described. The FSI problem is defined by the model of compressible viscous flow coupled with the dynamic linear or nonlinear elasticity problem in 2D. Our motivation was to develop methods for the numerical simulation of the problem inspired by the model of self-oscillating human vocal folds. There were two main goals of the thesis: the application of the DGM to the linear and the nonlinear elasticity problem and the extension of the numerical solution of the viscous compressible fluid flow problem in a time-dependent domain.

In the first three chapters we were concerned with the numerical solution of the elasticity problem. At first the linear and nonlinear elasticity problem was defined. For the description of the deformation of the elastic structure we use the nonlinear St. Venant-Kirchhoff model and neo-Hookean model. Then, we introduced the discretization of both the linear and nonlinear static elasticity problem by the DGM. Further, we described the discretization of the dynamic problem by the DGM in space and by the BDF in time. On the basis of the theory of the DGM we developed a .NET library written in C# for the numerical solution of the 2D dynamic linear and nonlinear elasticity problem with mixed boundary conditions.

The first part on the elasticity is concluded by the presentation of several numerical experiments for the numerical simulation of the elasticity problem. We presented the numerical experiments for the static and dynamic elasticity problem considering the linear and nonlinear elasticity. Some of the numerical tests were devoted to the choice of the parameter of the DGM defined for every edge of the triangulation, which estimates the penalty weight in the interior and boundary penalty term. We also compare results of the numerical tests obtained by using the DGM and FEM with each other. Finally, we presented the applicability of the developed method to problems with nonhomogeneous elasticity material.

In the other part of the thesis we were concerned with the numerical solution of the fluid flow problem in a time-dependent domain and the FSI problem. The chapter on the fluid flow problem is related to the former work presented in [11]. We consider the compressible viscous flow in time-dependent domain and the DGM is again used for the discretization of the problem. In order to validate the method we present the results of the numerical simulation for the fluid flow problem on a fixed domain without any interaction.

Newly, we extended the fluid flow solver with the elastic deformation of the computational domain and coupled it with the solution of the linear and nonlinear elasticity problem. We introduced the scheme with the discretization in time by the BDF method and in space by the DGM and also the full space-time DGM scheme. The ALE mapping was introduced with the aid of an artificial static linear elasticity problem in the domain occupied by the fluid. We formulated the partitioned strongly coupled scheme. The results of numerical experiments demonstrate that the DGM can be successfully applied to all three problems involved in FSI: fluid flow, a large elastic material deformation and the ALE mapping construction.

In the second example we have presented a more realistic problem with geom-

etry and parameters better characterizing the properties of the tissue of human vocal folds. The elastic structure domain was split in four subdomains with the same material density, but with different material characteristics. Also the shape of the computational channel was more realistic. Even if there were large deformations of the structure causing creation of the massive vortices in the flow domain, no difficulties in the flow part were marked and the vortices were smoothly leaving the domain.

There are some possible extensions for the future work. It is a comparison of our compressible model with incompressible flow in FSI simulations. Moreover, the treatment of the complete closure of the channel between the vocal folds is important. This effect occurs during the phonation in human vocal folds and together with the acoustic resonances of the human vocal tract causes the creation of voice. Last but not least is the identification of the acoustic signal.

Bibliography

[1] F. Alipour, et al., Mathematical models and numerical schemes for the simulation of human phonation. Current Bioinformatics, (2011), 6.3: 323–343.

[2] M. Balázsová, M. Feistauer, M. Hadrava, A. Kosík, On the stability of the space-time discontinuous Galerkin method for the numerical solution of the nonstationary nonlinear convection-diffusion problems, J. Numer. Math. 23 (2015), No. 3: 211–233.

[3] F. Bassi, S. Rebay. A high-order accurate discontinuous finite element method for the numerical solution of the compressible Navier–Stokes equations. Journal of Computational Physics, (1997), 131.2: 267–279.

[4] F. Bassi, S. Rebay. A high order discontinuous Galerkin method for compressible turbulent flow. In B. Cockburn, G. E. Karniadakis, and C.-W. Shu, editors, Discontinuous Galerkin Method: Theory, Computations and Applications, Lecture Notes in Computational Science and Engineering 11, Springer-Verlag, (2000), 113–123.

[5] C. E. Baumann, J. T. Oden. A discontinuous hp finite element method for the Euler and Navier-Stokes equations. Int. J. Numer. Methods Fluids, (1999), 31(1):79–95.

[6] A. F. Bower, Applied mechanics of solids, CRC Press Taylor & Francis Group, Boca Raton, 2010.

[7] H.-J. Bungartz, M. Schäfer, Fluid-Structure Interaction. Modelling, Simulation, Optimisation. Lecture Notes in Computational Science and Engineering 53, Springer, 2006.

[8] H.-J. Bungartz, M. Schäfer, Fluid-Structure Interaction II. Modelling, Simulation, Optimisation. Lecture Notes in Computational Science and Engineering, Springer, 2010.

[9] A. Curnier, Computational Methods in Solid Mechanics, Kluwer Academic Publishing Group, Dordrecht, 1994.

[10] P. G. Ciarlet, Mathematical Elasticity, Volume I, Three-Dimensional Elasticity, Volume 20 of Studies in Mathematics and its Applications, Elsevier Science Publishers B.V., Amsterdam, 1988.

[11] J. Česenek, Discontinuous Galerkin Method for Solving Compressible Viscous Flow (in Czech). PhD thesis, Faculty of Mathematics and Physics, Charles University in Prague, 2011.

[12] J. Česenek, M. Feistauer, A. Kosík, DGFEM for the analysis of airfoil vibrations induced by compressible flow, Z. Angew. Math. Mech. 93 No. 6–7 (2013) 387–402.

[13] J. Česenek, M. Feistauer, J. Horáček, V. Kučera, J. Prokopová, Simulation of compressible viscous flow in time-dependent domains, Applied Mathematics and Computation 219 (2013) 7139–7150.

[14] T. A. Davis, I. S. Duff, An Unsymmetric-pattern multifrontal method for sparse LU factorization, SIAM Journal on Matrix Analysis and Applications 18 no. 1 (1997) 140–158.

[15] P. Deuflhard, Newton Methods for Nonlinear Problems, Affine Invariance and Adaptive Algorithms, Springer Series in Computational Mathematics 35, Springer, Berlin, 2004.

[16] L. T. Diosady, D. L. Darmofal. Preconditioning methods for discontinuous Galerkin solutions of the Navier-Stokes equations. J. Comput. Phys. 228 (2009) 3917–3935.

[17] V. Dolejší, Anisotropic mesh generator ANGENER V3.0, Faculty of Mathematics and Physics, Charles University in Prague. `http://www.karlin.mff.cuni.cz/~dolejsi/angen/angen.htm`

[18] V. Dolejší, M. Feistauer and C. Schwab, On some aspects of the discontinuous Galerkin finite element method for conservation laws, Math. Comput. Simul., **61** (2003) 333–346.

[19] V. Dolejší. On the discontinuous Galerkin method for the numerical solution of the Navier- Stokes equations. Int. J. Numer. Methods Fluids, (2004), 45:1083–1106.

[20] V. Dolejší. Discontinuous Galerkin method for the numerical simulation of unsteady compressible flow. WSEAS Transactions on Systems, (2006) 5(5):1083–1090.

[21] V. Dolejší, M. Vlasák, Analysis of a BDF-DGFE scheme for nonlinear convection–diffusion problems. Numerische Mathematik, (2008) 110.4: 405–447.

[22] V. Dolejší, Semi-implicit interior penalty discontinuous Galerkin methods for viscous compressible flows, Commun. Comput. Phys. 4 (2008) 231–274.

[23] E. H. Dowell (Ed.), R. Clark, D. Cox, H. C. Curtiss Jr., J. W. Edwards, K. C. Hall, D. A. Peters, R. Scanlan, E. Simiu, F. Sisto, T. W. Strganac, A modern course in aeroelasticity, Kluwer Academic Publishers, Springer, 2005.

[24] M. Dumbser and C.-D. Munz. Building blocks for arbitrary high-order discontinuous Galerkin methods. J. Sci. Comput. 27 (2006) 215–230.

[25] M. Dumbser. Arbitrary high order PNPM schemes on unstructured meshes for the compressible Navier-Stokes equations. Comput. Fluids (2010) 39(1):60–76.

[26] R. P. Dwight. Robust mesh deformation using the linear elasticity equations. Computational Fluid Dynamics 2006, Springer Berlin Heidelberg, (2009) 401–406.

[27] M. Feistauer, J. Felcman, I. Straškraba. Mathematical and computational methods for compressible flow. Oxford University Press, 2003.

[28] M. Feistauer, V. Kučera, On a robust discontinuous Galerkin technique for the solution of compressible flow. J. Comput. Phys., 224 (2007), 208–221.

[29] M. Feistauer, V. Dolejší, V. Kučera, On the discontinuous Galerkin method for the simulation of compressible flow with wide range of Mach numbers, Comput. Vis. Sci. 10 (2007) 17–27.

[30] M. Feistauer, J. Horáček, V. Kučera, J. Prokopová, On numerical solution of compressible flow in time-dependent domains. Mathematica Bohemica, 137 (2012) 1–16.

[31] M. Feistauer, J. Hasnedlová-Prokopová, J. Horáček, A. Kosík, V. Kučera, DGFEM for dynamical systems describing interaction of compressible fluid and structures, J. Comput. Appl. Math. 254 (2013) 17–30.

[32] M. Feistauer, P. Sváček, J. Horáček, Numerical simulation of fluid-structure interaction problems with applications to flow in vocal folds. Fluid-Structure Interaction and Biomedical Applications, T. Bodnár, G. P. Galdi, Š. Nečasová (eds.), Birkhäuser Springer, Basel, 2014.

[33] M. A. Fernandez, M. Moubachir, A Newton method using exact jacobians for solving fluid-structure coupling, Computers and Structures 83 (2005) 127–142.

[34] C. Geuzaine, J.-F. Remacle, Gmsh: a three-dimensional finite element mesh generator with built-in pre- and post-processing facilities. International Journal for Numerical Methods in Engineering 79(11) (2009) 1309–1331. `http://geuz.org/gmsh/`

[35] M. Hadrava, M. Feistauer, J. Horáček, A. Kosík, Discontinuous Galerkin method for the problem of linear elasticity with applications to the fluid-structure interaction in: Proc. of 11th International Conference of Numerical Analysis and Applied Mathematics 2013 (ICNAAM 2013). AIP Conf. Proc. 1558 (2013) 2348–2351.

[36] M. Hadrava, M. Feistauer, J. Horáček, A. Kosík, Space-time discontinuous Galerkin method for the problem of linear elasticity In Numerical Mathematics and Advanced Applications-ENUMATH 2013, Springer International Publishing (2015) 115–123.

[37] R. Hartmann and P. Houston. Adaptive discontinuous Galerkin finite element methods for the compressible Euler equations. J. Comput. Phys., 183(2) (2002) 508–532.

[38] R. Hartmann and P. Houston. Symmetric interior penalty DG methods for the compressible Navier-Stokes equations I: Method formulation. Int. J. Numer. Anal. Model. (2006) 1:1–20.

[39] R. Hartmann and P. Houston. Symmetric interior penalty DG methods for the compressible Navier-Stokes equations II: Goal-oriented a posteriori error estimation. Int. J. Numer. Anal. Model. (2006) 3:141–162.

[40] J. Hasnedlová, M. Feistauer, J. Horáček, A. Kosík, V. Kučera, Numerical simulation of fluid-structure interaction of compressible flow and elastic structure, Computing 95 (2013) 343-361

[41] J. Horáček, P. Šidlof, J. G. Švec, Numerical simulation of self-oscillations of human vocal folds with Hertz model of impact forces, J. Fluids Struct. 20 (2005) 853–869.

[42] J. Horáček, P. Šidlof, V. Uruba, J. Veselý, V. Radolf, V. Bula, Coherent structures in the flow inside a model of the human vocal tract with self-oscillating vocal folds., Acta technica ČSAV 55(4) (2010) 327–343.

[43] J. Horáček, V. Uruba, V. Radolf, J. Veselý, V. Bula, Airflow visualization in a model of human glottis near the self-oscillating vocal folds model. Applied and Computational Mechanics, 5(1) (2011).

[44] J. Jaffre, C. Johnson and A. Szepessy, Convergence of the discontinuous Galerkin finite element method for hyperbolic conservation laws. Math. Models Methods Appl. Sci., 5 (1995), 367–386.

[45] C. Johnson, J. Pitkäranta, An analysis of the discontinuous Galerkin method for a scalar hyperbolic equation, Math. Comp., 46 (1986) 1–26.

[46] C. M. Klaij, J. J. W. van der Vegt, H. Van der Ven. Pseudo-time stepping for space-time discontinuous Galerkin discretizations of the compressible Navier-Stokes equations. J. Comput. Phys., 219(2) (2006) 622–643 .

[47] C. M. Klaij, J.J.W. van der Vegt, and H. Van der Ven. Space-time discontinuous Galerkin method for the compressible Navier-Stokes equations. J. Comput. Phys., 217(2) (2006) 589–611.

[48] A. Kosík, M. Feistauer, J. Horáček, P. Sváček, Numerical Simulation of Interaction of Human Vocal Folds and Fluid Flow, Springer Proceedings in Physics 139 (2011) 765–771.

[49] A. Kosík, M. Feistauer, M. Hadrava, J. Horáček, Numerical simulation of the interaction between a nonlinear elastic structure and compressible flow by the discontinuous Galerkin method, Applied Mathematics and Computation 267 (2015) 382–396.

[50] P. Le Saint, P.-A. Raviart, On a finite element method for solving the neutron transport equation, In: de Boor, C. (ed.) Mathematical Aspects of Finite Elements in Parial Differential Equations, Academic Press, (1974) 89–145

[51] R. Mittal, B. D. Erath, M. W. Plesniak, Fluid dynamics of human phonation and speech, Annu. Rev. Fluid Mech. 45 (2013) 437–467.

[52] T. Nomura, T. J. R. Hughes, An arbitrary Lagrangian-Eulerian finite element method for interaction of fluid and a rigid body, Comput. Methods Appl. Mech. Engrg. 95 (1992), 115–138.

[53] R. W. Ogden, Non-linear Elastic Deformations, Dover Publications, 1997.

[54] M. P. Paidoussis, Fluid-Structure Interactions, Slender structures and axial flow, Academic Press, Elsevier 2nd Edition, 2013.

[55] P. Punčochářová-Pořízkovă, K. Kozel, J. Horáček, J. Fürst, Numerical simulation of unsteady compressible low Mach number flow in a channel. Engineering mechanics, 17(2-3), 83-97 (2010).

[56] P. Punčochářová-Pořízkovă, K. Kozel, J. Horáček, Simulation of unsteady compressible flow in a channel with vibrating walls-Influence of the frequency. Computers & Fluids 46.1 (2011): 404-410.

[57] W. H. Reed, T. R. Hill, Triangular mesh metod for the neutron transport equation. Technical Report LA-UR-73-479, Los Alamos Scientific Laboratory, 1973.

[58] T. Richter, Goal oriented error estimation for fluid-structure interaction problems, Computer Methods in Applied Mechanics and Engineering 223-224 (2012) 28–42.

[59] B. M. Rivière, Discontinuous Galerkin Methods for Solving Elliptic and Parabolic Equations: Theory and Implementation. Frontiers in Applied Mathematics, 2008.

[60] P. Šidlof, J. G. Švec, J. Horáček, J. Veselý, I. Klepáček, R. Havlík, Geometry of human vocal folds and glottal channel for mathematical and biomechanical modeling of voice production. Journal of Biomechanics, 41(5) (2008) 985-995.

[61] K. Stein, T. Tezduyar, and R. Benney, Mesh moving techniques for fluid-structure interactions with large displacements. Journal of Applied Mechanics 70.1 (2003): 58-63.

[62] A. Ten Eyck, A. Lew, Discontinuous Galerkin methods for non-linear elasticity, International Journal for Numerical Methods in Engineering 67.9 (2006): 1204–1243.

[63] F.-B. Tian, H. Dai, H. Luo, J. F. Doyle, B. Rousseau, Fluid structure interaction involving large deformations: 3D simulations and applications to biological systems, Journal of Computational Physics 258 (2014) 451–469.

[64] S. Turek, J. Hron, Proposal for numerical benchmarking of fluid–structure interaction between an elastic object and laminar incompressible flow, in: H. J. Bungartz, M. Schäfer (Eds.), Fluid-Structure Interaction: Modelling, Simulation, Optimisation, Springer–Verlag Berlin Heidelberg, Netherlands, (2006) 371–385.

[65] G. Vijayasundaram, Transonic flow simulation using upstream centered scheme of Godunov type in finite elements. J. Comput. Phys., 63 (1986) 416–433.

[66] M. Vlasák, V. Dolejší, J. Hájek, A priori error estimates of an extrapolated space-time discontinuous Galerkin method for nonlinear convection–diffusion problems. Numer. Methods Partial Differ. Equations 27, No. 6 (2011) 1456–1482.

[67] M. P. De Vries, H. K. Schutte, A. E. P. Veldman, G. J. Verkerke, Glottal flow through a two-mass model: comparison of Navier-Stokes solutions with simplified models, J. Acoust. Soc. Am. 111 (2011) 1874–1853.

[68] Z. Zhang, J. Neubauer, D. A. Berry, Physical mechanisms of phonation onset: A linear stability analysis of an aeroelastic continuum model of phonation, J. Acoust. Soc. Am. 122 (2007) 2279–2295.

List of Tables

A. Attachments

A.1 Nonhomogeneous model of vocal folds

Here, we show the .NET implementation of the model of vocal folds defined in Section 3.5.2. The boundaries of the subdomains of the model of vocal folds are given by spline interpolations.

```
public class VocalFoldsModel : LameParametersBase
{
    private const double MuscleLeftEdgeX = 0.0055;
    private const double MuscleRightEdgeX = 0.0133;
    private const double DeepLayerLeftEdgeX = 0.00319 + EPar;
    private const double DeepLayerRightEdgeX = 0.01394 - EPar;
    private const double EPar = 0.0002;
    private const double EPar2 = EPar * 1.41421;

    private double[] EpitheliumX = {
        0.0,
        0.00139 + EPar,
        0.00319 + EPar,
        0.00468 + EPar,
        0.00627 + EPar,
        0.00788 + EPar,
        0.00874 + EPar,
        0.00991 + EPar,
        0.01109,
        0.01206 - EPar,
        0.01257 - EPar2,
        0.01290 - EPar2,
        0.01330 - EPar2,
        0.01394 - EPar,
        0.01461 - EPar,
        0.016 - EPar,
        0.0175
    };

    private double[] EpitheliumY = {
        0.00763 + EPar2,
        0.00670 + EPar,
        0.00542 + EPar,
        0.00424 + EPar,
        0.00299 + EPar,
        0.00185 + EPar,
        0.00132 + EPar,
        0.00081 + EPar,
        0.00077 + EPar2,
        0.00125 + EPar,
```

```
    0.00197,
    0.00305,
    0.00408,
    0.00550 + EPar,
    0.00660 + EPar,
    0.00784 + EPar,
    0.0082 + EPar2
};
private readonly CubicSpline Epithelium;

private double[] DeepLayerX = {
    0.00319 + EPar,
    0.0055,
    0.0077,
    0.01,
    0.0124,
    0.0133,
    0.01394 - EPar
};
private double[] DeepLayerY = {
    0.00542 + EPar,
    0.0045,
    0.004,
    0.004,
    0.0045,
    0.0051,
    0.00550 + EPar
};
private readonly CubicSpline DeepLayer;

private double[] MuscleX = {
    0.0055,
    0.0091,
    0.0113,
    0.0124,
    0.0133
};
private double[] MuscleY = {
    0.0045,
    0.00204,
    0.00175,
    0.003,
    0.0051
};
private readonly CubicSpline MuscleLayer;

public readonly List<LameParametersTuple> Parameters;
public VocalFoldsModel2(List<LameParametersTuple> parameters)
```

```
    {
        if (parameters.Count != 4)
        {
            throw new ArgumentException(GetType().Name
                + ": expected 4 parameter tuples!");
        }

        Parameters = parameters;

        Epithelium = new CubicSpline(EpitheliumX, EpitheliumY);
        DeepLayer = new CubicSpline(DeepLayerX, DeepLayerY);
        MuscleLayer = new CubicSpline(MuscleX, MuscleY);
    }

    public LameParametersTuple GetLambdaMu(double x, double y)
    {
        if (Math.Abs(y) > Epithelium.ValueAt(x))
        {
            if ((x > DeepLayerLeftEdgeX)
                && (x < DeepLayerRightEdgeX)
                && Math.Abs(y) < DeepLayer.ValueAt(x))
            {

                if ((x > MuscleLeftEdgeX)
                      && (x < MuscleRightEdgeX)
                      && (Math.Abs(y) > MuscleLayer.ValueAt(x)))
                {
                    return Parameters[1];
                }
                else
                {
                    return Parameters[2];
                }
            }
            else
            {
                return Parameters[0];
            }
        }
        else
        {
            return Parameters[3];
        }
    }
}
```

A.2 XML configuration file

Here, we show an example of a XML configuration file used by the `.NET` framework application. It is the XML configuration used for the numerical solution of the FSI problem.

```
<?xml version="1.0" encoding="utf-8"?>
<XmlConfigurationFSI
    xmlns:xsi="http://www.w3.org/2001/XMLSchema-instance"
    xmlns:xsd="http://www.w3.org/2001/XMLSchema">
  <Version>STDGM</Version>
  <FluidConfiguration>
    <ProblemDataType>VOCAL_FOLDS</ProblemDataType>
    <FluidForceType>COMPLETE_WITH_COFACTOR</FluidForceType>
    <AmbientPressure>97611</AmbientPressure>
    <ComputeDragLift>false</ComputeDragLift>
    <DragLiftFluidForceType>COMPLETE</DragLiftFluidForceType>
    <EdgeQuadrature>DEGREE_3</EdgeQuadrature>
    <OverrideCesenekAlgebraicSolver>false
        </OverrideCesenekAlgebraicSolver>
    <AlgebraicSolver>UMFPACK_LIB_CSR</AlgebraicSolver>
  </FluidConfiguration>
  <CesenekConfiguration>
    <Parallelization>
      <IsEnabled>1</IsEnabled>
      <ThreadCount>8</ThreadCount>
    </Parallelization>
    <Control>
      <InitialTime>11.25</InitialTime>
      <Tau>0.0005</Tau>
      <TauMultiple>1</TauMultiple>
      <LastMultiplied>0</LastMultiplied>
      <MaxIteration>200000</MaxIteration>
      <MaxSubIteration>5</MaxSubIteration>
      <StartSubIteration>1</StartSubIteration>
      <SaveIteration>500</SaveIteration>
      <LogProfileHeightAndAngle>0</LogProfileHeightAndAngle>
    </Control>
    <Gmres>
      <MaxIteration>20</MaxIteration>
      <InnerIteration>30</InnerIteration>
      <Tolerance>1E-06</Tolerance>
      <Preconditioner>DIAG</Preconditioner>
    </Gmres>
    <PhysicalConstants>
      <Gamma>1.4</Gamma>
      <Viscosity>1</Viscosity>
      <HeatConductivity>1</HeatConductivity>
      <Reynolds>4335.6</Reynolds>
```

```
  <Prandtl>0.64</Prandtl>
  <ReferenceLength>0.016</ReferenceLength>
  <ReferenceProfileWidth>0.05</ReferenceProfileWidth>
  <ReferenceDensity>1.225</ReferenceDensity>
  <ReferenceVelocity>4</ReferenceVelocity>
 <Kappa>1.4</Kappa>
</PhysicalConstants>
<Method>
  <DgVariant>IIPG</DgVariant>
  <Cw>500</Cw>
  <Cww>5000</Cww>
  <StabEl>0.01</StabEl>
  <StabEd>0.01</StabEd>
  <BoundaryTypes>
    <Inlet>1</Inlet>
    <Outlet>2</Outlet>
    <Wall>4</Wall>
    <Isowall>3</Isowall>
  </BoundaryTypes>
  <TriangulationPath>
      triang/cosine_radius_27k/fluid_dimensionless.ang
  </TriangulationPath>
</Method>
<Profile>
  <InitialAngle>0</InitialAngle>
  <InitialDimensionlessShift>0</InitialDimensionlessShift>
</Profile>
<InitialConditions>
  <InitialConditionsPath>
      initialCondition.txt
  </InitialConditionsPath>
  <InitialConditionsType>FILE</InitialConditionsType>
  <ConstantConditions>
    <Density>1</Density>
    <VelocityX>1</VelocityX>
    <VelocityY>0</VelocityY>
    <Pressure>4980</Pressure>
  </ConstantConditions>
</InitialConditions>
<BoundaryConditionsInlet>
  <Density>1</Density>
  <VelocityX>1</VelocityX>
  <VelocityY>0</VelocityY>
  <Pressure>4980</Pressure>
</BoundaryConditionsInlet>
<BoundaryConditionsOutlet>
  <Density>1</Density>
  <VelocityX>1</VelocityX>
```

```
    <VelocityY>0</VelocityY>
    <Pressure>4980</Pressure>
  </BoundaryConditionsOutlet>
</CesenekConfiguration>
<SolutionConfiguration>
  <SaveEveryIter>100</SaveEveryIter>
  <LogAveragePressure>true</LogAveragePressure>
  <LogAveragePressureEachIter>true</LogAveragePressureEachIter>
  <LogStateVectorVertices>false</LogStateVectorVertices>
  <LogStateVectorHighOrder>false</LogStateVectorHighOrder>
  <LogFlowQuantitiesVertices>false</LogFlowQuantitiesVertices>
  <LogFlowQuantitiesHighOrder>false</LogFlowQuantitiesHighOrder>
  <LogVtp>true</LogVtp>
  <OutputFolder>log/Fluid</OutputFolder>
</SolutionConfiguration>
<AleDisplacementConfiguration>
  <AleProviderType>ELASTIC_MATERIAL</AleProviderType>
  <ElasticMaterialConfiguration>
    <SolverConfigurationFile>
        AleSolverConfiguration.xml
    </SolverConfigurationFile>
    <Lambda>-10</Lambda>
    <Mu>10</Mu>
    <InitialConditionFile>ALE_IC.csv</InitialConditionFile>
  </ElasticMaterialConfiguration>
</AleDisplacementConfiguration>
<InteractionConfiguration>
  <InteractionType>ELASTIC_MATERIAL</InteractionType>
  <PrescribedMotionConfiguration>
    <PrescribedMotionModelType>FIXED</PrescribedMotionModelType>
  </PrescribedMotionConfiguration>
  <ElasticMaterialConfiguration>
    <SolverConfigurationFile>
        ElasticitySolverConfiguration.xml
    </SolverConfigurationFile>
    <Lambda>17143</Lambda>
    <Mu>4285</Mu>
    <Rho>1040</Rho>
    <DampingMass>0.1</DampingMass>
    <DampingStiffness>0</DampingStiffness>
    <RelaxationParameter>0.8</RelaxationParameter>
    <SubiterationStopCriterionConfiguration>
      <AbsoluteTolerance>1E-05</AbsoluteTolerance>
      <RelativeTolerance>1E-06</RelativeTolerance>
      <MaxSubiteration>5</MaxSubiteration>
    </SubiterationStopCriterionConfiguration>
  </ElasticMaterialConfiguration>
</InteractionConfiguration>
```

```
  <Logger>
    <LogConfiguration>true</LogConfiguration>
    <LogTrace>true</LogTrace>
    <OutputFolder>log</OutputFolder>
  </Logger>
</XmlConfigurationFSI>
```